2012

Fabrication, analysis, application, and characterization of core-containing microparticles and hydrophilic microfluidic devices produced via the primary- and in situ tertiary-amine catalyzed Michael addition of multifunctional thiols to multifunctional acrylates

Christopher O. Bounds
Louisiana State University and Agricultural and Mechanical College

FABRICATION, ANALYSIS, APPLICATION, AND CHARACTERIZATION OF CORE-CONTAINING MICROPARTICLES AND HYDROPHILIC MICROFLUIDIC DEVICES PRODUCED VIA THE PRIMARY- AND IN SITU TERTIARY-AMINE CATALYZED MICHAEL ADDITION OF MULTIFUNCTIONAL THIOLS TO MULTIFUNCTIONAL ACRYLATES

A Dissertation

Submitted to the Graduate Faculty of the
Louisiana State University and
Agricultural and Mechanical College
In partial fulfillment of the
requirements for the degree of
Doctor of Philosophy

in

The Department of Chemistry

by
Christopher O. Bounds
B.S. The University of Southern Mississippi, 2007
December 2012

ACKNOWLEDGEMENTS

I would like to greatly thank all of my family, friends and advisors that have supported and guided me throughout my educational years. I would like to especially thank my parents, Dr. Jerry and Mrs. Vicki Bounds, for all of their love, support, and direction throughout my life and for the values that they instilled in me that have allowed me to succeed. I also really appreciate the guidance and strong educational influence bestowed upon me by the professors at Louisiana State University including Dr. John A. Pojman, Dr. David Spivak, Dr. Donghui Zhang, Dr. Paul Russo, Dr. Karl Knopf, Dr. Daniel Hayes, and Dr. Rafael Cueto. A sincere and special thanks goes to my major advisor, Dr. John A. Pojman, as I attribute much of my success to the knowledge gained from him and his unsurpassed and constant encouragement, inspiration, and guidance throughout my educational career.

TABLE OF CONTENTS

LIST OF ABBREVIATIONS

ACE	Activated Chain End
AM	Activated Monomer
BADGE	Bisphenol A Diglycidyl Ether
BCl_3-amine	Boron Trichloride- Amine Complex
BF_3-amine	Boron Trifluoride- Amine Complex
BPO	Benzoyl Peroxide
CA	Contact Angle
CNT	Carbon Nanotubes
$dBCl_3$	Dissolved BCl_3-amine
DEA	Diethylamine
DHFA	Dodecafluoroheptyl Acrylate
DMpT	N,N-Dimethyl-*para*-*T*oluidine
DSC	Differential Scanning Calibration
$eBCl_3$	Encapsulated BCl_3-amine
f	Functionality
FITC	Fluorescein Isothiocyanate
HFIPA	Hexafluoroisopropyl Acrylate
ID	Inside Diameter
LA	Lauryl Acrylate
LOC	Lab-on-a-Chip
µTAS	Micro Total Analysis System
OA	Octylamine
OD	Outside Diameter
ρ_c	Critical Conversion
PDMS	Polydimethylsiloxane
PEG	Poly(Ethylene Glycol)
PEGMEA	Poly(Ethylene Glycol) Methyl ether acrylate
PETA	Pentaerythritol Triacrylate
PG90	Polygloss 90 (kaolin clay)
PHR	Parts per Hundred Resin
PMMA	Poly(methyl methacrylate)

PS	Poly(styrene)
PVA	Poly(Vinyl Alcohol)
R_p	Rate of Polymerization
RPM	Revolutions Per Minute
SEM	Scanning Electron Microscope
SiO_2	Fumed Silica
T-A	Thiol-Acrylate
TAOTA	2,4,6-Triallyloxy-1,3,5-Triazine
TATATO	1,3,5-Triallyl-1,3,5-Trazine-2,4,6-Trione
TBP	Tert Butyl Peroxybenzoate
TEA	Triethylamine
T_g	Glass Transition Temperature
TGA	Thermal Gravitational Analysis
TMPeTA 692	Trimethylolpropane ethoxylate Tricrylate M_n=692
TMPeTA 912	Trimethylolpropane ethoxylate Tricrylate M_n=912
TMPDAE	Trimethylolpropane Diallyl Ether
TMPTA	Trimethylolpropane Triacrylate
TMPTGE	Trimethylolpropane Triglycidyl Ether
TMPTMP	Trimethylolpropane Tris(3-mercaptopropionate
UA	Urethane Acrylate CN929

ABSTRACT

The objective of this research was to investigate amine-catalyzed thiol-acrylate chemistry for various novel applications that could fully utilize the untapped potential of this useful and robust chemistry. The use of this chemistry in each application solved a problem, improved on a disadvantage of current technologies, and decreased the level of complexity in association with required time, cost, and/or preparation conditions. The first novel application conceived, applied, and analyzed was in the field of microencapsulation. A novel approach for the preparation of microparticles via a dispersion polymerization using the primary amine-catalyzed addition of a trithiol to a triacrylate was realized and investigated. Various core materials were microencapsulated via this technique and introduced into appropriate systems to improve the desired characteristics of the given system. In a specific case, microparticles containing a borontrichloride-amine complex were observed to prevent the interaction between the Lewis acid initiator and fumed silica, hence improving the rheological properties of an epoxy system containing the initiator while maintaining the strength of the resulting polymer. Another application involved a novel approach to prepare stable hydrophilic microfluidic devices. Hydrophilic thiol-acrylate materials were fabricated with native stable water contact angles of ~60˚ via a two-pot soft lithography technique at room temperature, very rapidly, and with little equipment. The material hydrophilicity was modified from 10-85˚ via bulk- or post-modification techniques. These materials were prepared via the Michael addition of a secondary amine to a multifunctional acrylate, producing a nonvolatile tertiary amine utilized in the catalysis of the Michael addition of a multifunctional thiol to the multifunctional acrylate. Because the

final chip was self-adhered via a chemical process utilizing the same chemistry, and it was naturally hydrophilic, there was no need for expensive equipment or methods to “activate” the surface. Also, due to the pre-synthesized monomer/catalyst molecule serving as the *in situ* catalyst, there was no need for post-processing removal of the catalyst as it was incorporated into the polymer network. Both novel applications facilitated great improvements by exploiting the major advantages of thiol-acrylate chemistry. The fabrication, analysis, application, and characterization of these novel amine-catalyzed thiol-acrylate microparticles and microfluidic devices are described.

CHAPTER 1. INTRODUCTION

1.1 Thiol-Ene Chemistry

The first recorded reaction of sulfur with nonactivated carbon-carbon double bonds came in 1844 with Charles Goodyear's patent on the vulcanization of natural rubber, poly(cis-isoprene). [1] More than half a century later, in 1905, Theodor Posner reported the addition of thiols to olefins and was given credit for discovering thiol-ene chemistry.[2] Since that time, a multitude of data has been collected that greatly explains the reaction mechanisms, kinetics, thermodynamics, and various uses of thiol-ene chemistry and its many branches.

A resurgence of thiol-ene based chemistry has been observed in recent years, with the majority of the research directed at the photopolymerization of such thiol-ene systems.[3-12] The photoinitiated polymerization of thiol-ene systems has been extensively studied, including the kinetics and the mechanical and physical properties.[4, 5, 11-14] There are many advantages to using photoinitiated thiol-ene systems. Many of the desired properties of acrylic photopolymerizations are exhibited by thiol-ene photopolymerizations. For example, like acrylic systems, thiol-ene photopolymerized products do not require solvent for processing and posses highly desired and useful optical and mechanical properties. [6, 15-17] Thiol-ene photopolymerized systems also add some unique and desirable properties that acrylic systems lack. Unlike acrylic photopolymerization processes, thiol-ene systems can be rapidly photopolymerized in the presence of oxygen, as peroxy radicals do not inhibit their mechanism. [6, 7, 11] The acidic proton of the thiol group effectively eliminates the terminating peroxy radicals. (Scheme 1-2) They can also undergo rapid photoinitiation

in the presence or absence of a photoinitiator due to the formation of a thiyl free radical. [5, 7, 10 , 11] In addition, thiol-ene photopolymerization systems exhibit delayed gelation due to the lack of the Trommsdorff effect [18], show very low shrinkage [4], illustrate high conversion [5], demonstrate uniform crosslink densities [11], and facilitate the free-radical photopolymerization of a wide assortment of thiol and vinyl functional groups. [6, 15, 19] The products of these photopolymerized thiol-ene reactions can also be very versatile and robust. Woods et al. [16] reported essentially no weight loss for films held at 200˚C in air for 40 minutes illustrating a resistance to water absorption and good oxidative stability. These thiol-ene materials are extremely stable in air due to the thioether group formed by the addition of a thiol group across an ene double bond, and thioether groups are well known to serve as antioxidant stabilizers. [20-22] The thermal decomposition of these thiol-ene products has been reported to be greater than 250˚C at a heating rate of 10˚C per minute.[16] In terms of long-term stability, literature from Norland Optical [23] has shown that some photopolymerizable thiol-ene electronic adhesives and optical materials experienced very little discoloration or loss in performance even when exposed to 50˚C conditions for 3 years, which would correspond to greater than 20 years at room temperature. Norland Optical [23] also noted that photopolymerizable thiol-ene networks were relatively stable in the presence of a wide range of chemicals, with only aqueous sodium hydroxide exposure resulting in film degradation after the 1 hour analysis period.

It is well known that thiol-ene photopolymerizations proceed via a free radical step-growth mechanism as shown in Scheme 1-1. [4, 6, 10, 11, 15, 24] This scheme illustrates initiation via the ultraviolet-induced production of a thiyl free radical in the

presence or absence of a photoinitiator. The initiation is followed by a two-step propagation regime, first involving the addition of a thiyl radical across a carbon-carbon double bond and then a subsequent hydrogen extraction from another acidic thiol group resulting in the regeneration of a free radical. [10] The mechanism is terminated by normal free radical recombination techniques.

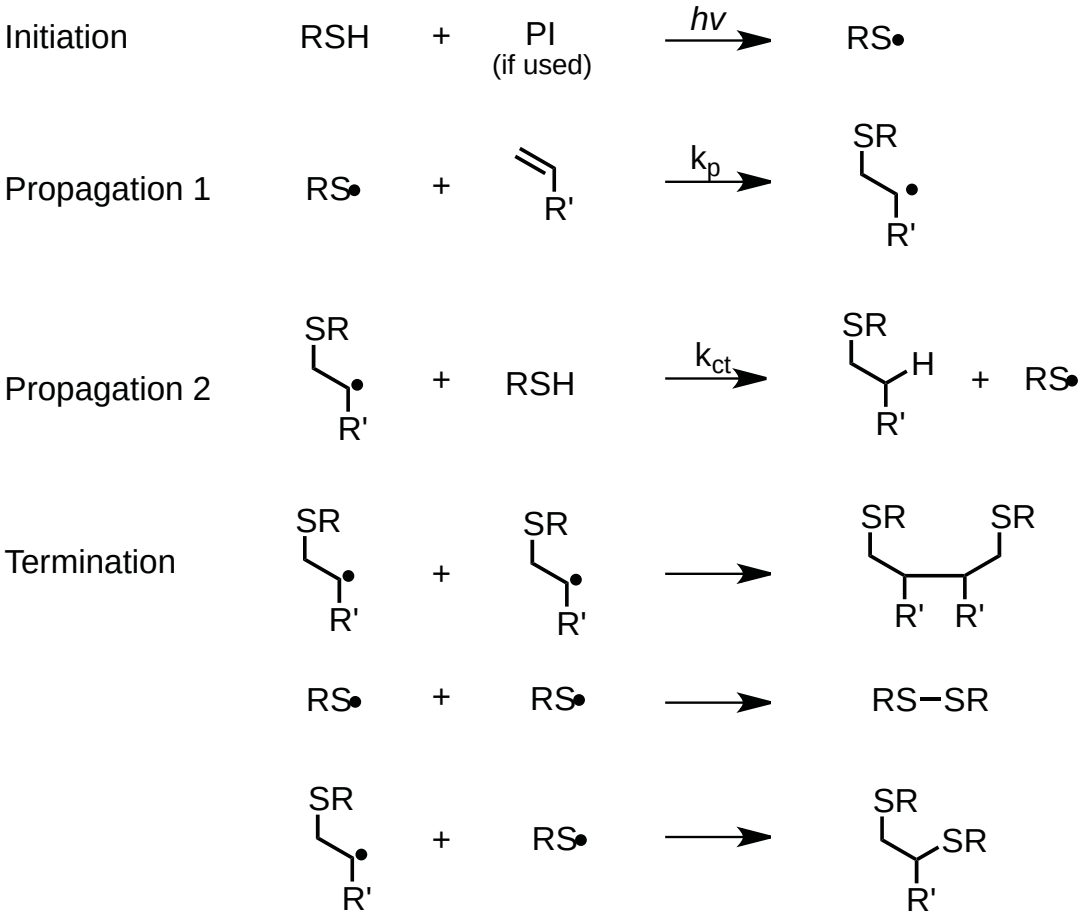

Scheme 1-1. General thiol-ene photoinitiated free-radical step growth mechanism.

This thiol-ene reaction could also be considered a chain growth mechanism with a continuous chain transfer (propagation 2) step following the free radical addition (propagation 1).[4] The chain transfer step has been found to be the rate-determining step. In this aspect, the thiol-ene mechanism operates in a chain growth manner with

first order kinetics governing the reaction, only depending on the thiol concentration [10] This differs from normal step growth mechanisms which are normally governed by second order kinetics with respect to both reactant concentrations such as with a simple condensation reaction. In terms of linear, branched, and network polymer formation, the thiol-ene photopolymerization systems proceed in a step growth fashion. Monofunctional monomers will not produce a polymer but only adducts, difunctional monomers lead to the formation of linear polymers, and the formation of polymer networks requires the use of a system with an average functionality greater than two. [10]

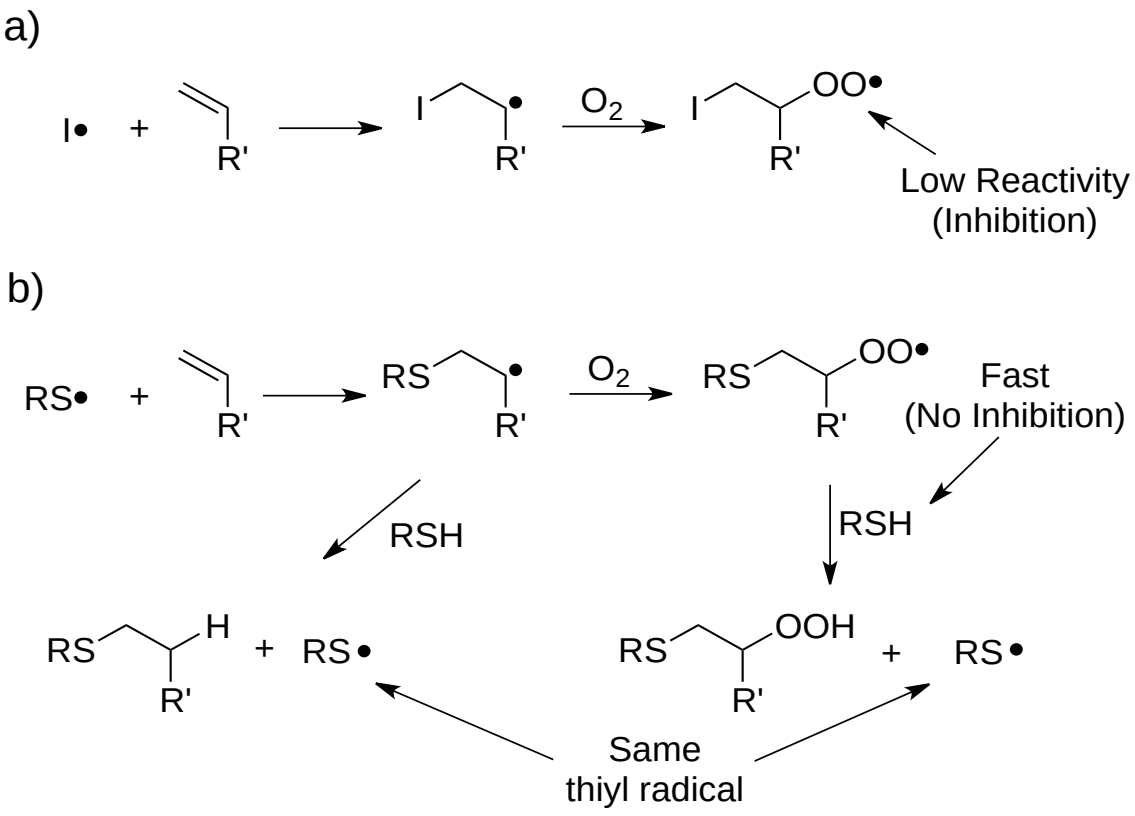

Scheme 1-2. Oxygen inhibition in normal free radical acrylic polymerization (a) and the lack of oxygen inhibition in free radical thiol-ene polymerization.

There have been many useful applications of photoinitiated thiol-ene chemistry in various areas including coatings, dental, optical, and photolithographic applications. Thiol-ene photopolymerizable coating applications extend back to the work of Morgan, Ketley, and coworkers [15, 17, 25] in the mid 1970's at W. R. Grace that lead to the fabrication of relief printing plates and conformal coatings on electronics. This work then lead a collaborator, Armstrong, to develop wear layers for floor tiles based on thiol-ene photopolymerization.[4] Since the mid 1970s there have been many attempts at commercializing thiol-ene photoinitiated systems, notably Norland Products has produced and marketed thiol-ene based photopolymerizable electronic and optical adhesives for many years. [23] In more recent thiol-ene photoinitiated applications, the focus has shifted toward click-type reactions. [5] Easy surface modifications can be accomplished via thiol-ene photochemistry both in a grafting-from approach [26-28] and a grafting-to approach [29, 30]. Due to its many useful properties and lack of- or disproved disadvantages, photopolymerized thiol-ene systems have been and will continue to be used in critical, high performance applications.

1.2 Thiol-Acrylate Photoinitiated Chemistry

Extremely useful properties can be realized when acrylates are incorporated into a photoinitiated thiol-ene copolymer as the ene portion, however some mechanistic complexities are added as are shown in Scheme 1-3. The thiol-acrylate photopolymerization mechanism involves a dual process comprised of the thiol copolymerizing with the acrylate upon the hydrogen abstraction from the thiol followed by the addition of the thiyl across the double bond of the acrylate and the homopolymerization of the acrylate.[17] This homopolymerization occurs only when

electron deficient enes such as acrylates are used, as normal electron-rich enes cannot homopolymerize.

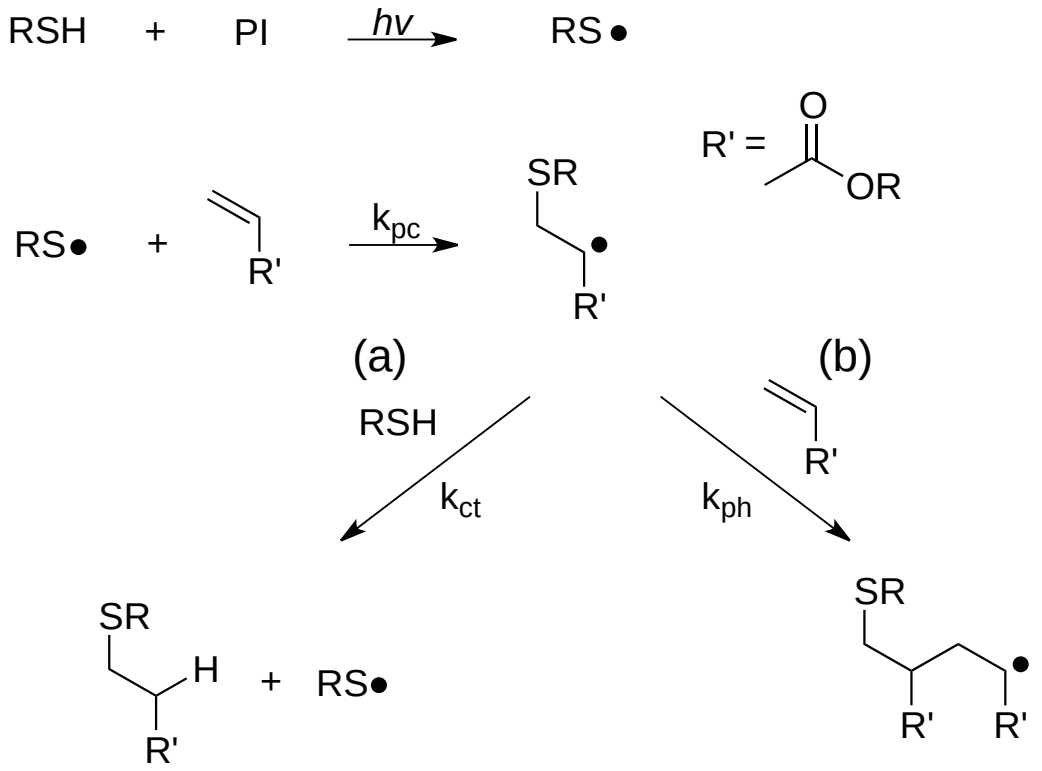

Scheme 1-3. Photoinitiated free radical polymerization of a thiol-acrylate system illustrating the dual process including a) thiol-acrylate copolymerization and b) acrylate homopolymerization.

Cramer and Bowman[10] compared the glass transition of a homopolymerized diacrylate system to that of a diacrylate system to which tetrathiol had been added. It was observed that the addition of the tetrathiol caused a lower and narrower glass transition.[10] There is a great increase in the uniformity of the network produced when as little as 15 mol% of a multifunctional thiol is integrated into an acrylate network. This allows for the manipulation of both the physical and mechanical properties of a photopolymerized acrylate system by the addition of multifunctional thiols.[4] While preparing thiol-methacrylate dendrimer networks, Nilsson et al. demonstrated the use of

excess thiol to obtain 100% conversion of methacrylate groups with residual thiol content available for further surface modification. This allowed for the production of highly functional dendrimer films with adjustable physical properties.[31] A collaborative study done by Koo et al. reported that radical thiol-ene chemistry is not a straightforward method for polymer-polymer conjugation. The two groups concluded that head-to-head coupling interrupted the propagation cycle of the radical thiol-ene process. [32]

There is an inherent shelf life issue associated with all thiol-acrylate systems. Base impurities can cause the Michael Addition of thiols to acrylic carbon-carbon double bonds (discussed later). Spontaneous free radical impurities can cause the premature polymerization of thiol-acrylate systems. As discussed previously, the presence of hydroperoxides (peroxy radicals) can cause a hydrogen abstraction and subsequent initiation of thiol-acrylate polymerization. The shelf-life stability of an acrylate thiol mixture is inversely proportional to the average functionality. Therefore multifunctional thiol-acrylate systems are much more likely to undergo spontaneous premature polymerization. It has been reported that as little as 5 pph trithiol can reduce the shelf life of an acrylate monomer system from more than 30 days to about 12 hours. [4, 33]

1.3 Amine-Catalyzed Thiol-Acrylate Chemistry

A thiol-ene system can undergo an ionic Michael addition polymerization mechanism utilizing a base catalyst, however this type of reaction is limited to electron-deficient unsaturated enes, such as acrylates (Scheme 1-4). [3, 5, 34, 35] Although thiols are nucleophilic (generally more nucleophilic than amines), bases are used to deprotonate them because of their relatively high acidity. The thiolate anion is the active species formed by the thiol deprotonation that subsequently adds to an activated

olefin such as an acrylate. [36] The rate of the thiol Michael addition increases with pH due to an increase in the thiolate anion concentration [37] The rate is also dependent on the pKa of the thiol with a more acidic thiol being more favorable. These acid-base reactions are thermodynamically controlled reactions that can occur spontaneously and can proceed to high conversation with an appropriate choice of thiol and catalyst. [38] Hu et al. used the predictable rise in pH facilitated by the formaldehyde-sulfite clock reaction to trigger the time-lapse Michael addition of a trithiol to a triacrylate. [39]

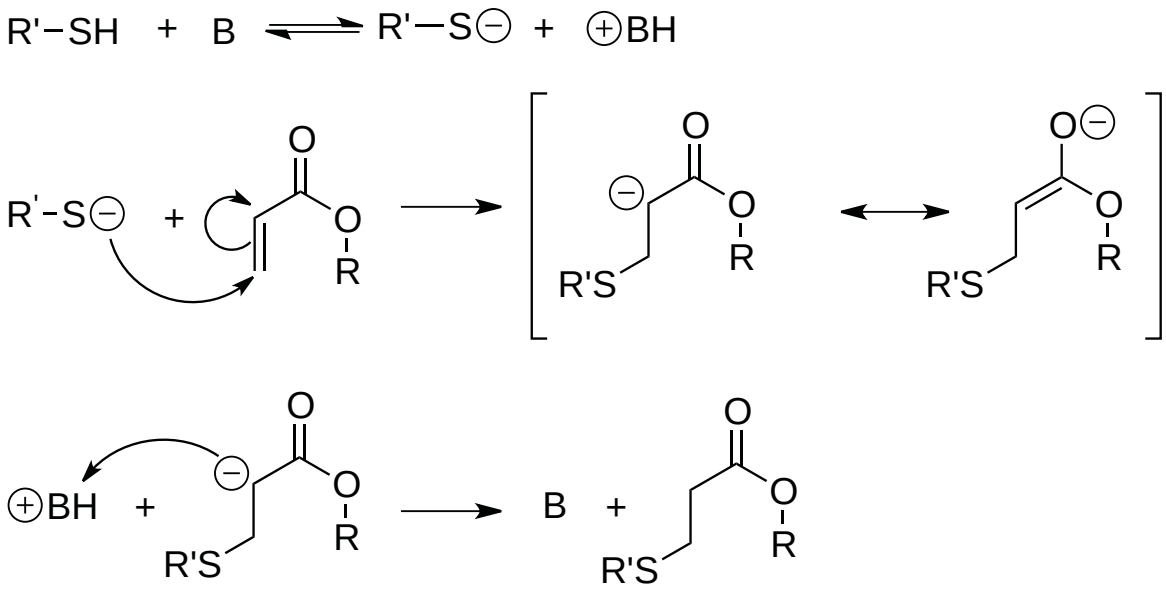

Scheme 1-4. Base catalyzed thiol-acrylate reaction scheme.

Thiol-acrylate systems can be catalyzed using tertiary amines, which function as base catalysts (Scheme 1-5). The tertiary amine functions to deprotonate the thiol, forming thiolate anions that can add across acrylate double bonds to form the thiol-ene bond. However, these tertiary amine catalysts are relatively inefficient in the formation of such thiolate anions. [3, 40]

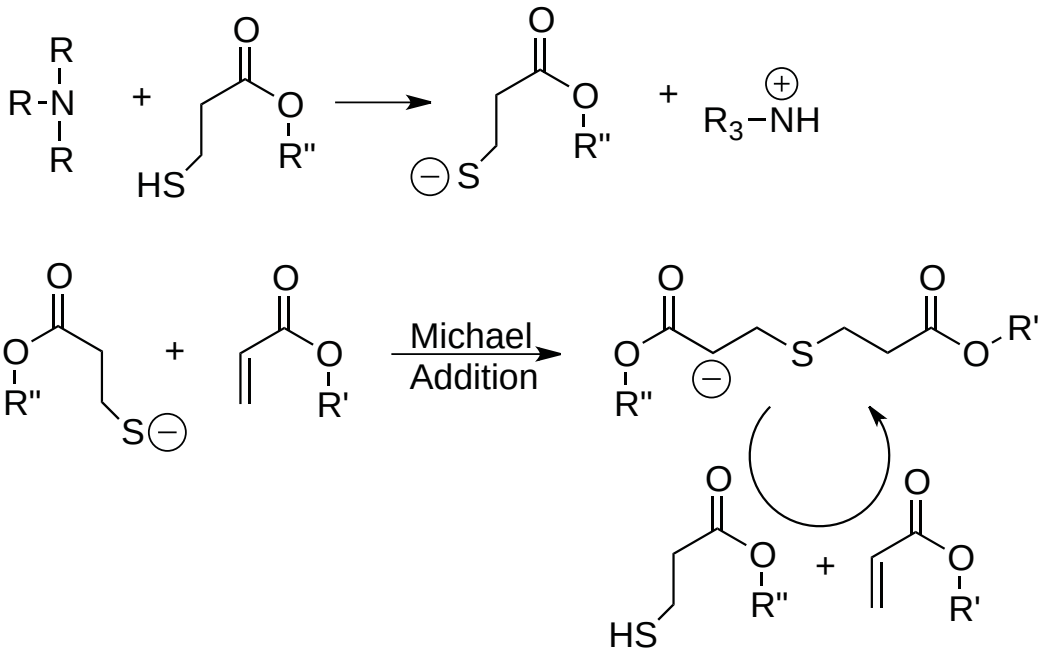

Scheme 1-5. Tertiary amine catalyzed thiol-acrylate reaction scheme.

Much more effective and efficient catalysts for the reaction between thiols and electron-deficient enes include primary amines[3, 40], secondary amines[40-46], or nucleophilic alkyl phosphine catalysts.[43, 45] Lee et al. used a secondary amine to catalyze the Michael addition of thiols to acrylates to produce novel vinyl ester monomers for photopolymerization kinetic studies.[41] Matsushima et al. produced tunable hybrid thiol-isocyanate-acrylate systems via the amalgamation of thiol-isocyanate coupling, thiol-acrylate Michael addition, and acrylate homopolymerization using a phosphine catalyst system coupled with photolysis.[47] Chan et al. reported producing a 1:1 reaction of thiol and acrylate to >95% conversion in less than 3 minutes in the presence of <2% primary or secondary amine.[3] Akzo Nobel reported in a series of patents that a primary amine catalyzed the Michael addition of a thiol faster than did a tertiary amine.[48] While attaching acrylate groups to a thiol-containing surface, Khire et al. determined that the thiol-acrylate reaction proceeds much faster when using

ethylenediamine (almost instantaneously) compared to triethylamine (several hours) or diethylamine (a few minutes).[40] Chan et al. has recently examined the major properties and kinetics of the primary amine-catalyzed Michael reaction with various multifunctional thiols and acrylates.[3]

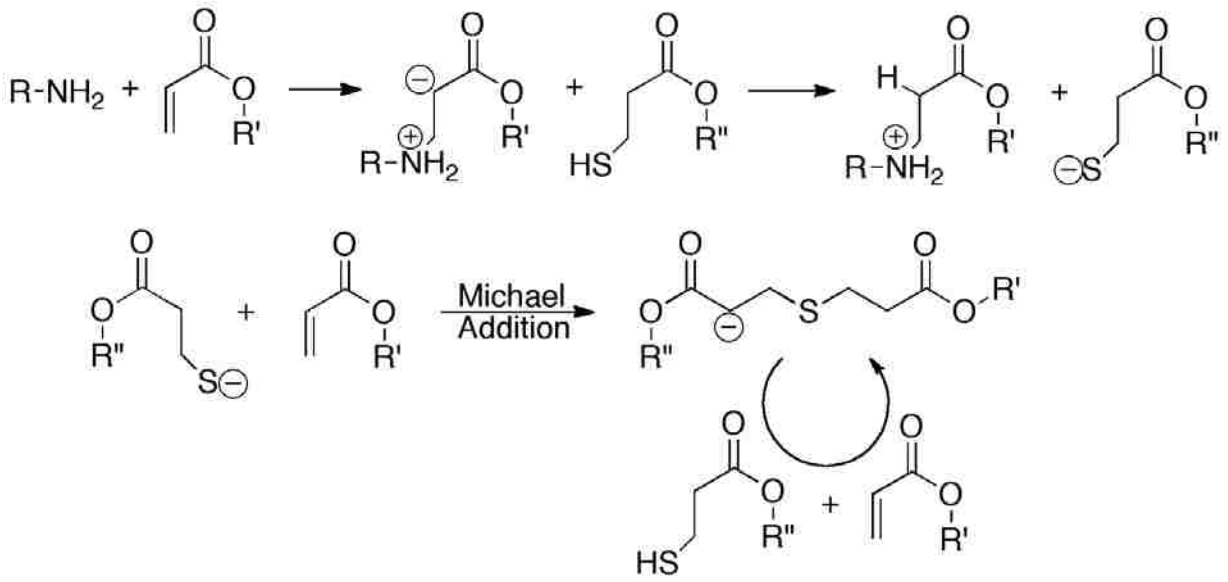

Scheme 1-6. General primary amine-initiated thiol-acrylate anionic mechanism.

The primary amine initiated thiol-acrylate anionic chain reaction is shown in Scheme 1-6. The reaction proceeds by the addition of the catalyst to the electron-deficient ene and the successive abstraction of the thiol proton to form a thiolate anion allowing for the Michael addition across the acrylate double bond. Unlike the free-radical thiol-ene mechanism, once initiated, termination is not facilitated by the combination of two growing chains. Unlike tertiary amine base catalysts, the use of these nucleophilic catalysts produces systems that reach high conversion at room temperature in minutes or even seconds.[5] This fast reaction time has been reported from multiple sources[3, 5, 40, 48, 49] and makes this process extremely useful for many applications that have not been previously explored.

CHAPTER 2. CORE-CONTAINING THIOL-ACRYLATE MICROPARTICLES*

2.1 Chapter Summary

This chapter encompasses a novel approach to prepare microparticles via a dispersion polymerization using the primary amine-catalyzed addition of a trithiol to a triacrylate. Unlike most microcapsules that have a thin shell containing a liquid core, these microparticles were composed of a solid matrix enveloping pockets of core material. This method of microencapsulation has multiple advantages over other methods of microencapsulation using various materials, as these microparticles were prepared with a minimum number of components in less than one hour at room temperature and at ambient pressure. The chemistry used to prepare these microparticles is very versatile in that a multitude of different monomers can be incorporated to prepare microparticles with varying properties. Also, the reaction used to prepare these microparticles can be initiated using various sources, which allows for variations if necessary. Microparticles loaded with various core materials were produced and applied in various systems to improve the desired characteristics of the given system. It was determined that this type of microparticles could be used as either a stimulated release or controlled release mechanism depending on core material.

* Portions of this chapter originally appeared in: Bounds, C. O., R. Goetter, et al. (2012). "Preparation and Application of Microparticles Prepared Via the Primary Amine-catalyzed Michael Addition of a Trithiol to a Triacrylate." J. Polym. Sci. Part A: Polym. Chem. **50**: 409–422. Reprinted via a limited license agreement.

The preparation and application of microparticles containing one initiator in particular, a boron trichloride-amine complex, was extensively studied. These microparticles were observed to prevent the interaction between the Lewis acid initiator and fumed silica by separating the two components, hence improving the rheological properties of an epoxy system containing the initiator while maintaining the strength of the resulting polymer. Benzoyl peroxide, Dimethyl-para-toluidine, a boron trifluoride-amine complex, and carbon nanotubes were also microencapsulated using this primary amine-catalyzed thiol-acrylate method and analyzed in various capacities.

2.2 Introduction/Background

Microencapsulation is a process in which a substance is enclosed in a material that affects its transfer to the surroundings.[50, 51] Microencapsulation is used in many applications such as pesticides,[52, 53] medications[54] and scratch-n-sniff materials.[55, 56] Some of the other common applications in which it is used include cosmetics[57], as food preservatives[58], and in carbonless copy paper, where ink contained in microcapsules is released when pressure is applied.[59]

Microencapsulation is often used to achieve the controlled release of a substance. This controlled release can be brought about in several different ways, depending on the type of microcapsules used and the application. For example, many prescription and non-prescription medications that are taken orally are described as “time-released”. The medication does not release from the carrier until a certain time, usually when the carrier reaches the stomach.[54] In other cases, it is desirable to keep a constant concentration of drug in the system, which can be achieved with a

biodegradable encapsulation material or by diffusion of the drug through an interfacial barrier.[60]

An example of a different controlled release mechanism is that of self-healing polymer composites, in which microcapsules are ruptured mechanically when the material cracks.[61-63] Dicyclopentadiene is normally the core material that is released when a crack reaches the capsules, and it polymerizes upon contact with Grubbs catalyst in the matrix, repairing the crack.

There are a multitude of encapsulation methods that employ different polymer shell materials such as complex coacervation using gum arabic and gelatin[59], interfacial polymerization using polyurea[64-69], polyurethane[70], polyurea-polyurethane dual shells[71], and *in situ* polymerization producing poly (urea formaldehyde).[72] Porous methacrylate microparticles have been produced via the copolymerization of 2,3-epoxypropoxybenene and trimethylolpropane trimethacrylate.[73] Berkel et al. prepared composite polymer-metal nanoparticles via the miniemulsion polymerization of AIBN-initiated divinylbenzene. The surfaces of the resulting nanoparticles were post modified via thiol-ene chemistry facilitated by excess surface divinylbenzene.[74] Highly bioactive microparticles were produced by Gu et al. via AIBN-initiated free radical polymerization of a diacrylate followed by thiol-ene surface modification.[75] Costoyas et al. prepared core-shell hybrid silica/polystyrene composite nanoparticles via potassium persulfate initiated miniemulsion polymerization of styrene.[76] Each of these methods have disadvantages, including the need for a multitude of components, the necessity for elevated temperatures, non-ambient conditions, and lengthy reaction times. We sought to produce the same quality microparticles with

minimum complexities using a primary amine-catalyzed Michael addition of a thiol to an electron-deficient ene. The procedure used in this research only requires a small number of components, can be done in less than 1 hour and proceeds at room temperature and ambient pressure.

2.3 Primary-Amine Catalyzed Thiol Acrylate Reaction Scheme

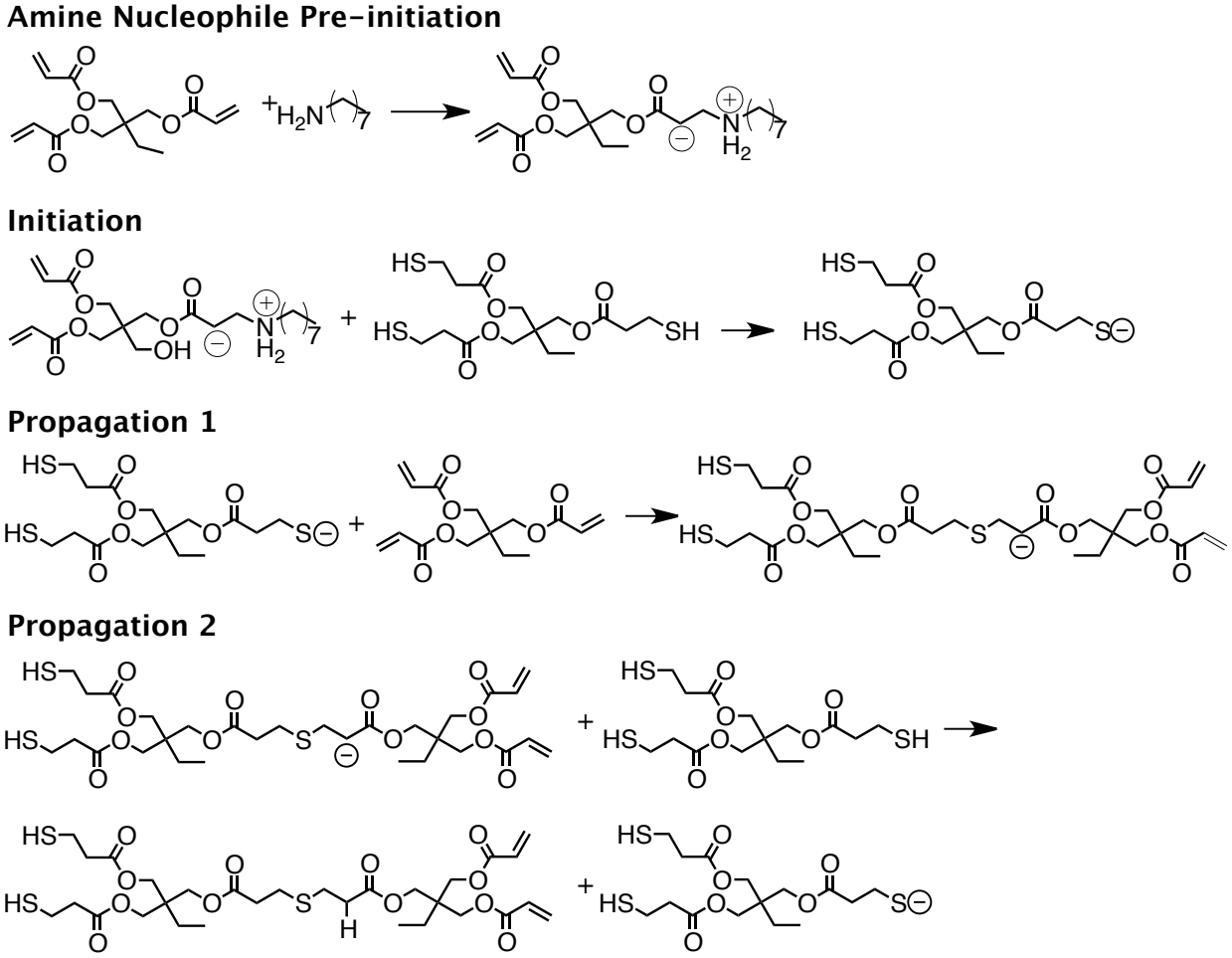

Scheme 2-1. Reaction scheme for the primary amine-catalyzed Michael addition of trimethylolpropane tris (3-mercaptopropionate) to trimethylolpropane triacrylate. This reaction is used to produce the microparticle matrix material.

The primary-amine catalyzed thiol acrylate reaction is illustrated in Scheme 2-1. The reaction proceeded via a pre-initiation step involving the nucleophilic addition of the primary octylamine catalyst to the electron-deficient ene. The resulting carbanion

abstracted an acidic thiol proton to form a thiolate anion, resulting in the initiation of an anionic step-growth polymerization mechanism. Two separate propagation steps then followed. The first propagation step involved the Michael Addition of the deprotonated thiyl anion to the electron-deficient ene group. Next, a hydrogen transfer occurred between another thiol and the newly formed carbon anion. This second propagation step resulted in a chain transfer and another deprotonated thiol that was activated for another Michael Addition. This dual propagation mechanism is why this reaction is considered to be a step growth polymerization, however it is essentially a chain growth mechanism with a continuously sequential chain transfer step (propagation 2).

2.4 Generic Procedure

Scheme 2-2 illustrates a generic procedure used in the formation of the thiol-acrylate microparticles. The procedure was a modified interfacial polymerization method where a core organic solution was dispersed in an immiscible aqueous solution and polymerized via a molecule containing a hydrophilic amino head and a hydrophobic hydrocarbon tail.

The general procedure consisted of the dispersion of a solution containing a core material dissolved in a stoichiometrically equivalent solution of trimethylolpropane triacrylate and trimethylolpropane tris(3-mercaptopropionate) in a 1.28% poly(vinyl alcohol) aqueous solution. This core solution was dispersed using various amounts and sources of energy depending on the size of microparticles (or nanoparticles) desired. Once the droplet size was adequate, ~3% by volume of octyl amine was added to the dispersion to catalyze the thiol-acrylate reaction. The microparticles were harvested via vacuum filtration and dried overnight under ambient conditions. Depending on the

contained core material, various solvents were used to wash the excess core material from the exterior of the microparticles prior to their testing and incorporation into a given system.

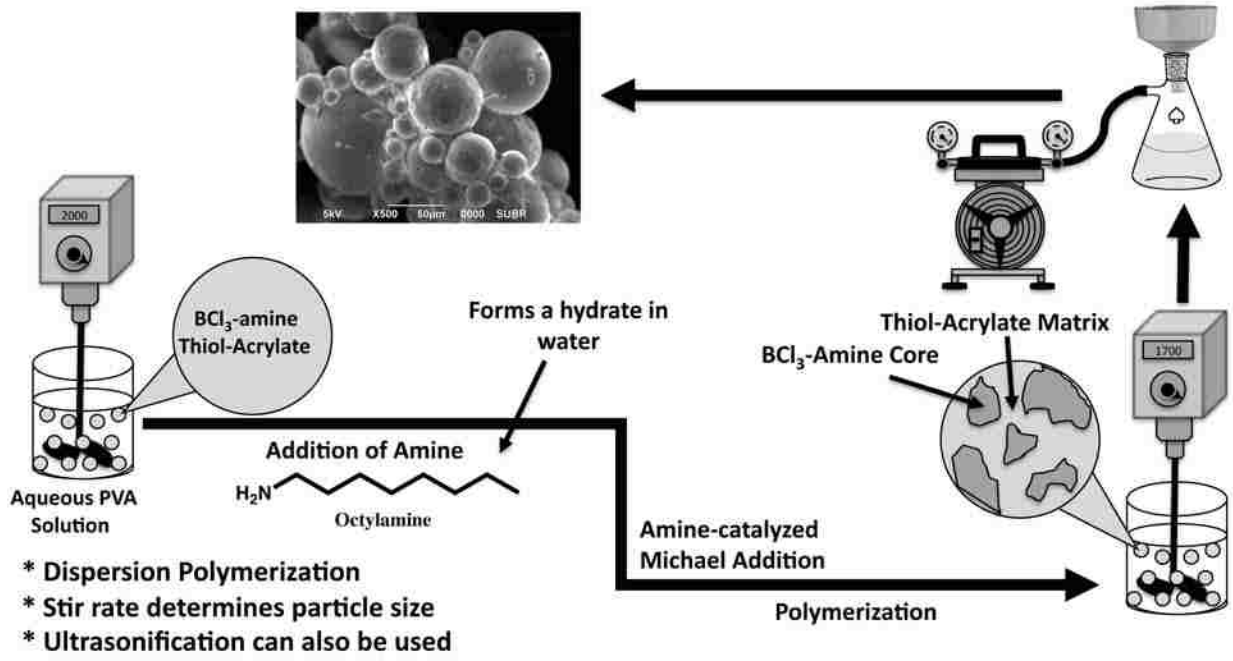

Scheme 2-2. Basic process for encapsulating a core material in a thiol-acrylate matrix. Small deviations from this process are needed in a few cases.
resins.

2.4.1 Materials

All materials were used as received without further purification. Borontrichloride-amine (BCl_3-amine) was obtained from Huntsman under the name Accelerator DY9577. Borontrifluoride-amine (BF_3-amine) was obtained from Leepoxy Plastics, Inc under the name Leepoxy leecure B-612. *Tert*-butyl peroxybenzoate was obtained from Ashland with 98% reported purity. Trimethylolpropane triacrylate (TMTPA) technical grade, trimethylolpropane tris(3-mercaptopropionate) (TMPTMP), octylamine 99%, poly(vinyl alcohol) (PVA) 87-89% hydrolyzed, N,N-Dimethyl-p-toluidine 99%, Trimethylolpropane triglycidyl ether (TMPTGE), and Bisphenol A diglycidyl ether (BADGE) (epoxy

equivalent weight of 172-176) were obtained from Sigma-Aldrich. Fumed silica ≥99.8% was obtained from US composites under the name of Aerosil-Cabosil or Aerosil® 200 with a specific surface area (BET) of 200±25 m^2/g and an average primary particle size of 12 nm. Structures for notable chemicals are illustrated in Figure 2-1.

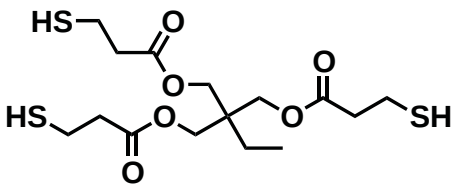

Trimethylolpropane tris(3-mercaptopropionate)

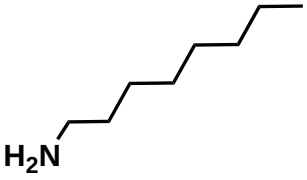

octyl amine

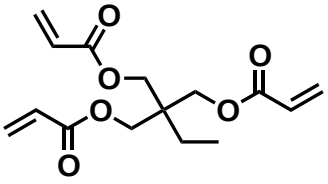

trimethylolpropane triacrylate

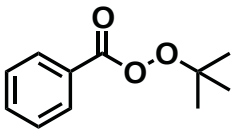

tert-butyl peroxybenzoate

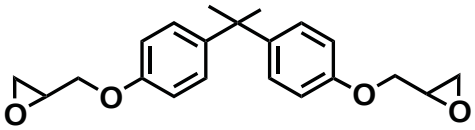

Bisphenol A diglycidyl ether

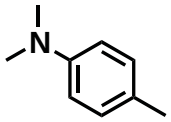

N,N-dimethyl-para-toluidine

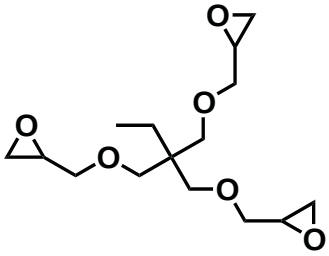

Trimethylolpropane triglycidyl ether

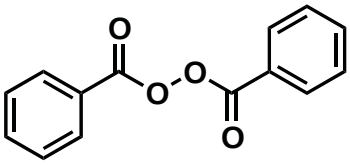

Benzoyl Peroxide

Figure 2-1: Notable structures of shell forming monomers, core materials, and epoxies

2.4.2 Equipment

The agitation reactor used for dispersing the mobile phase consisted of an IKA RW 20 DS1 digital overhead stirrer equipped with a 3-blade low shear propeller with a

diameter of 54 cm. The sonicator used was a Branson Sonifier 450 with a maximum output of 400 Watts. All rheological measurements were obtained from a TA AR1000 equipped with parallel plates. All strength data were obtained using a 3-point bending method with an INSTRON 5582 and Bluehill software. Optical microscopy was performed using a phase contrast Nikon ECLIPSE 50*i* microscope equipped with a Nikon Digital Sight DS-Fi1 camera. The optical microscopy measurements were made using calibrated NIS-Elements BR 3.0 software. The differential scanning calorimetry data were obtained using a TA Instruments 2920 modulated DSC.

2.5 Size Analysis of Control/Blank Microparticles

Microparticles containing no core material were prepared at different stir rates to determine the ease of manipulation of the microparticle size. The relative sizes of the microparticles were determined via optical microscopy and size analysis software. The particle size distributions at different stir rates are illustrated in Figure 2-2, 2-3, and 2-4. Figure 2-5 and Table 2-1 illustrate the collected average particle size at different stir rates using the data from Figures 2-2, 2-3, and 2-4.

Figure 2-2 illustrates the particle size distribution data for control microparticles containing no core material stirred at 500 RPM. These data indicate that the average particle size was 267.8±109.9 µm when agitated at 500 RPM for 1 hour. The maximum and minimum microparticle diameters were measured at 583.4 µm and 34.3 µm, respectively at this low stir rate. These data demonstrate a nearly symmetrical bell-type distribution with 83% of the microparticles measuring between 100-400 µm.

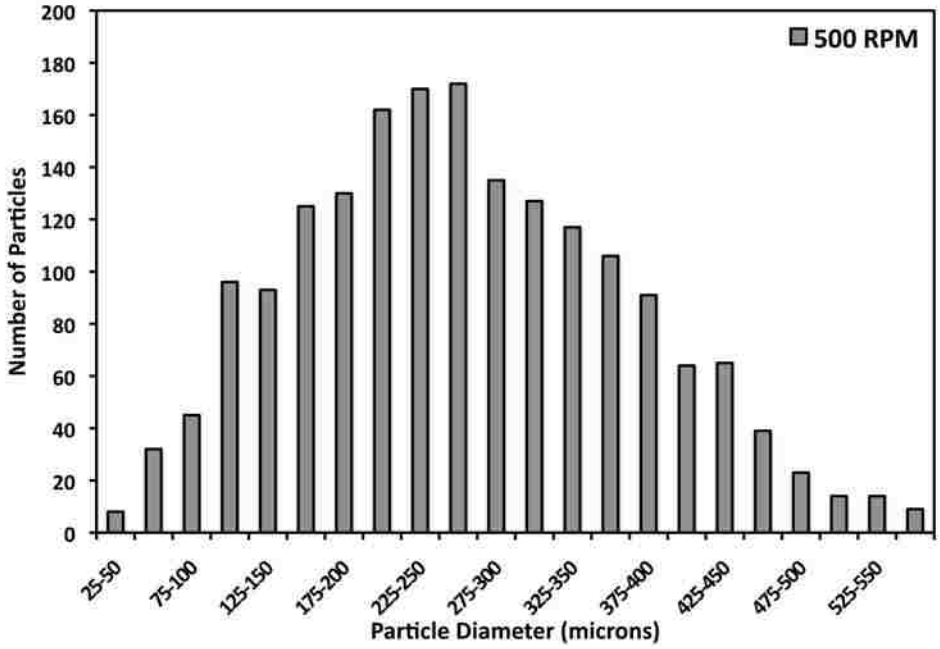

Figure 2-2: Particle size distribution data for solid microparticles (no core component) at 500 RPM. All particle size data were collected via optical microscopy and particle size analysis software.

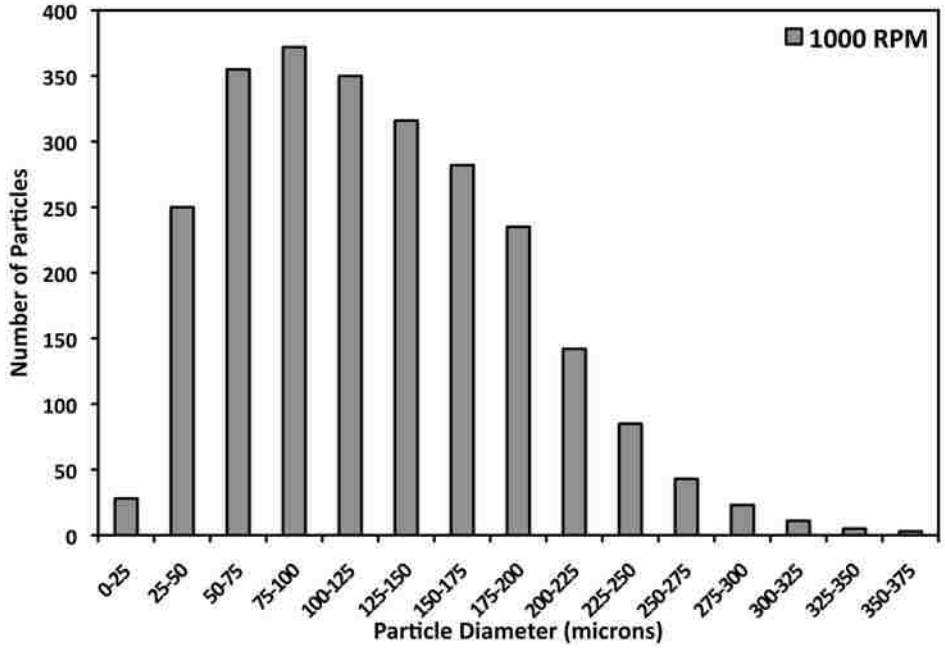

Figure 2-3: Particle size distribution data for solid microparticles (no core component) at 1000 RPM. All particle size data were collected via optical microscopy and particle size analysis software.

Figure 2-3 shows the particle size distribution data for control microparticles containing no core material agitated at 1000 RPM. These data indicate that the average particle size was 125.1±62.8 µm at a stir rate of 1000 RPM. The maximum microparticle size was found to be 369.8 µm, while the minimum microparticle diameter was measured at 122.4 µm at this medium stir rate. These data illustrated a less symmetrical distribution, semi-weighted to the smaller particle size, with 76.4% of the microparticle diameters measured in the range of 50-200 µm.

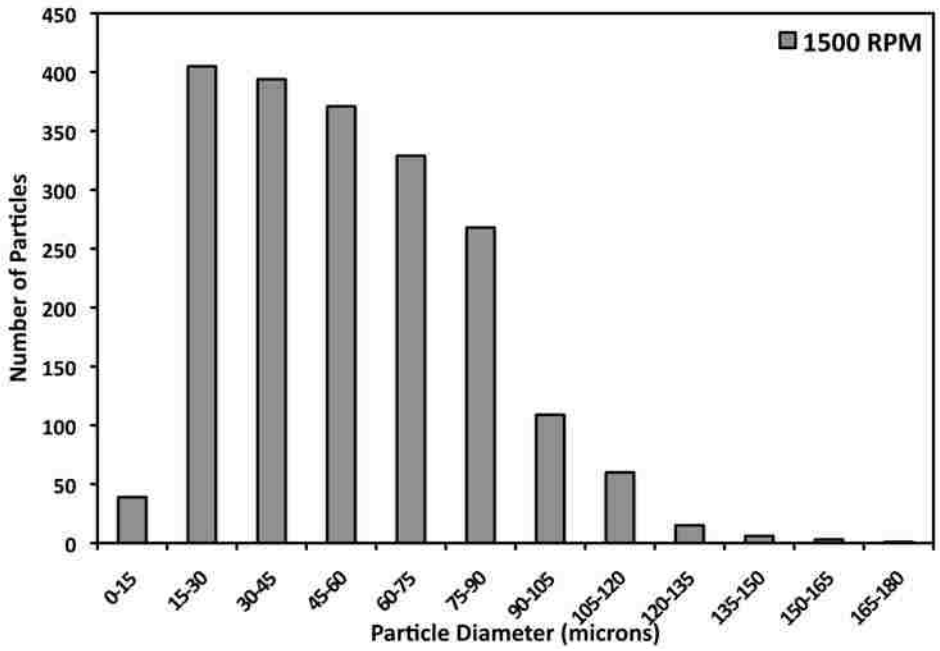

Figure 2-4: Particle size distribution data for solid microparticles (no core component) at 1500 RPM. All particle size data were collected via optical microscopy and particle size analysis software.

Figure 2-4 illustrates the particle size distribution data for control microparticles containing no core material stirred at 1500 RPM. These data indicate a much smaller average particle size of 54.5±6.0 µm when agitated at 1500 RPM for 1 hour. The maximum and minimum microparticle diameters were measured at 171.3 µm and 6.0 µm, respectively at this relatively high stir rate. These data demonstrated an

unsymmetrical distribution, weighted heavily to the smaller particle size, with 88.4% of the microparticles being 20-80 µm in diameter.

Figure 2-5 and Table 2-1 condense all of the data from the particle size distribution analysis for the control microparticles containing no core material. As can be observed in Figure 2-5 and Table 2-1, as the stir rate was increased from 500 RPM to 1000 RPM to 1500 RPM, the mean particle diameter decreased. Also, as more energy was applied, the distribution became narrower, as was proven by the decrease in the values of standard deviation. Both the maximum and the minimum measured microparticle diameters were also observed to decrease as a function of increasing stir rate. Because these particles in were prepared with no core component, the exact size values could not necessarily be used to forecast the average particle diameter of any given system. However, the trend could be applied to any system containing any core material.

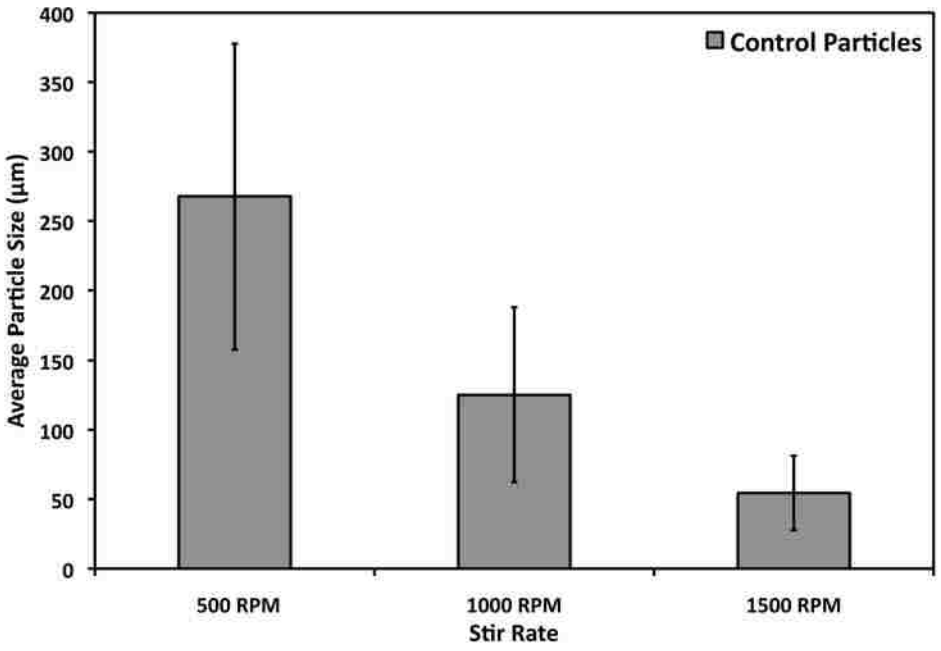

Figure 2-5: Particle size distribution for solid microparticles (no core component) as a function of stir rate. All particle size data were collected via optical microscopy and particle size analysis software.

Table 2-1. Control (empty) thiol-acrylate microparticles statistics as a function of stir rate.

RPM	Mean Diameter (um)	Standard Deviation (um)	Maximum Diameter (um)	Minimum Diameter (um)
500	267.8	109.9	583.4	34.3
1000	125.1	62.8	369.8	12.4
1500	54.5	26.8	171.3	6.0

Figure 2-6 illustrates the microparticles via SEM microscopy. This figure provides some visual conformation for the difference in the size of the microparticles at different stir rates. The images shown are both at the same magnification and it is obvious that the microparticles in the left image (stirred at 500 RPM) are visibly much larger than the microparticles on the right (stirred at 1000 RPM).

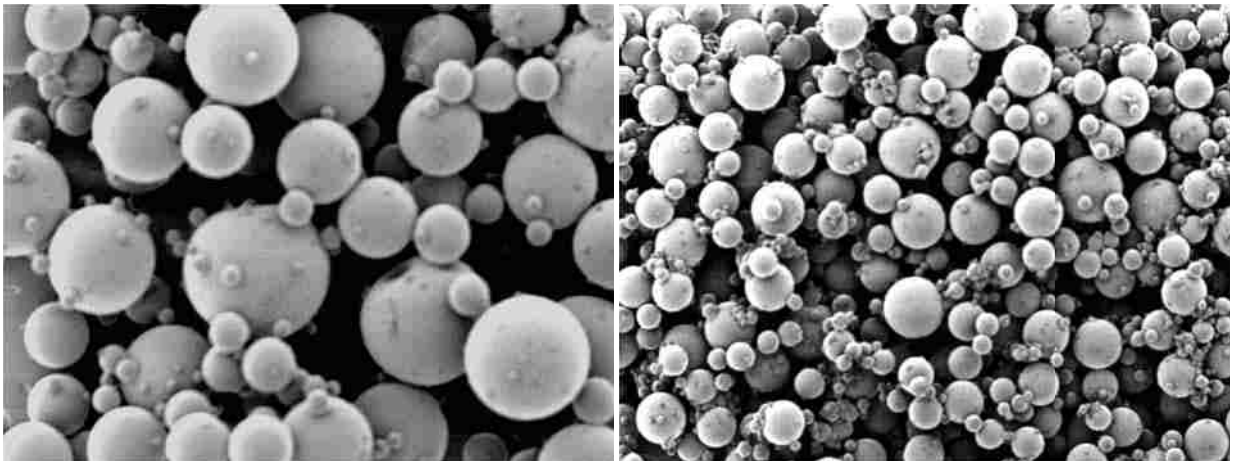

Figure 2-6: Scanning electron microscopy images showing visual difference in control microparticles containing no core component agitated at 500 RPM (left) and 1000 RPM (right). These images were taken at X50 magnification.

2.6 Dimethyl-para-Toluidine Microparticles

2.6.1 Introduction and Rationale for Microencapsulation

Dimethyl-*para*-toluidine (DMpT) is a tertiary aromatic amine that accelerates the decomposition of organic peroxides such as benzoyl peroxide (BPO) at room temperature.[77, 78] Tertiary amines like dimethylaniline (DMA) (differing in structure

from DMpT only by the absence of a *para* methyl group) have been used in various accounts in the presence of benzoyl peroxide as redox initiating systems to polymerize vinyl monomers such as vinyl chloride [79] styrene [80, 81], and methyl methacrylate [80, 82]. Imoto and Takemoto reported the solution polymerization of acrylonitrile via a substituted benzoyl peroxide-dimethylaniline redox initiator system. [83] O'Driscoll and McArdle reported the bulk polymerization of styrene at various temperatures via a benzoyl peroxide-dimethylaniline redox initiation system [84, 85] and the bulk polymerization of styrene using substituted diethylaniline and benzoyl peroxide as redox initiators. [86] The decomposition of acyl peroxides (like BPO) is much more rapid in the presence of amines as opposed to thermal decomposition. [87] Walling and Indictor reported an apparent rate constant of 2.3×10^{-4} sec^{-1} for a system containing benzoyl peroxide and dimethylaniline in styrene or chloroform at 0˚C. [80] The high reactivity of these tertiary amine-acyl peroxide systems are very useful for the room temperature curing of vinyl monomers and widely utilized unsaturated polyester resins. Although these monomer and prepolymer systems can be cured in the absence of tertiary amine accelerators such as DMpT via thermal decomposition, it is desirable from an economical viewpoint to cure these systems at room temperature. However, there lies an inherent tradeoff between room temperature curing and pot life. In order to achieve room temperature curing, the pot life of the system much be sacrificed due to an increase in reactivity. [88] Here, it was hypothesized that the tertiary amine accelerator (DMpT) could be separated from the acyl peroxide initiator (BPO) via microencapsulation of the DMpT in a thiol-acrylate matrix. If separated by this matrix,

the pot life of a system could be greatly increased by the production of a highly stable latent accelerator system for vinyl monomers and unsaturated polyester resins.

2.6.2 Experimental Procedure

Microparticles containing dimethy-*para*-toluidine (DMpT) as the core component were prepared with a matrix comprised of trimethylolpropane triacrylate (TMPTA) and trimethylolpropane tris(3-mercaptopropionate) (TMPTMP) catalyzed by octylamine. A solution of stoichiometrically equivalent TMPTMP and TMPTA was prepared containing 15.94 grams and 11.85 grams, respectively. The core DMpT (20 g) was dissolved in the trithiol/triacrylate solution. This solution was then emulsified in 500 mL of a 1.28% poly(vinyl alcohol) aqueous solution with a stir motor equipped with a 3-bladed propeller. The mixture was agitated for 30 minutes at 2100 RPM. Once the desired droplet size range was achieved, 3% by volume (~0.9 mL) of octylamine was added to the mixture to catalyze the polymerization, and the stir rate was decreased to 1700 RPM. The mixture was allowed to react for 1 hour at room temperature and ambient temperature with continuous mixing at 1700 RPM. The microparticles were recovered by vacuum filtration and dried overnight. Any unencapsulated material was washed from the exterior of the shells using cyclohexane or hexane before the microparticles were used.

2.6.3 Scanning Electron Microscopy Analysis

Dimethyl-*para*-toluidine (DMpT) was microencapsulated in a thiol-acrylate matrix and SEM images were obtained (figures 2-7a and b). From these SEM images, it can be observed that most of these microparticles are symmetrical spheres with

diameters of less than 50 microns. Also, a significant amount of unencapsulated core DMpT could be observed on the exterior of the microparticles.

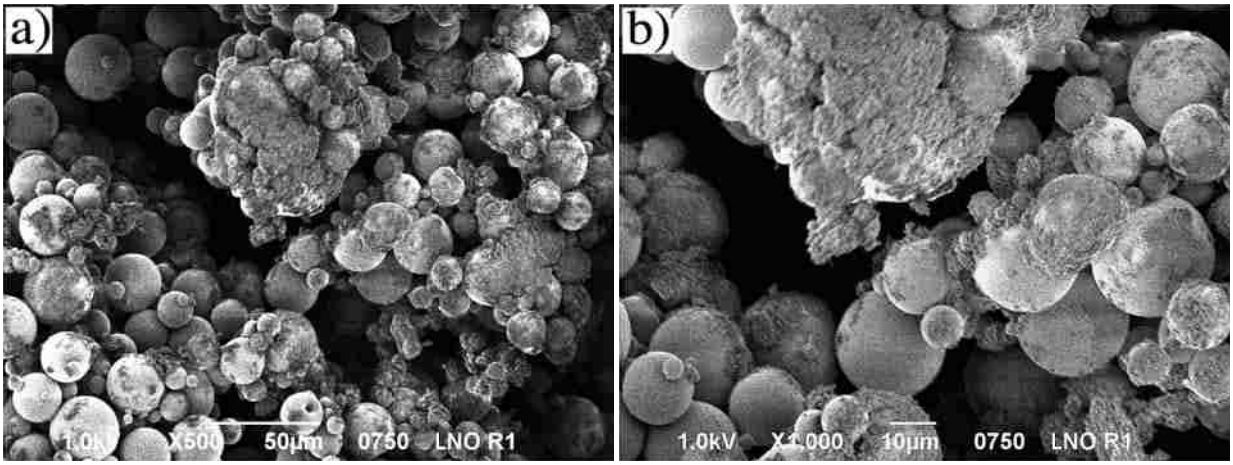

Figure 2-7: SEM images of microparticles containing dimethyl-para-toluidine (DMpT). a) X500 magnification b) X1000 magnification.

2.6.4 Particle Size Analysis

Particle size analysis was performed on the resulting DMpT-containing thiol-acrylate microparticles. The microparticle sizes were determined via optical microscopy and size analysis software. The microparticle size distribution data are illustrated in Figure 2-8. A 2005 microparticle population was used to collect these data. These microparticles were agitated initially at 2100 RPM for 30 minutes and then 1700 RPM after the octyl amine was added to the reaction vessel. These data illustrate that the average particle size was 28.3±11.8µm. Figure 2-8 also shows a relatively narrow distribution where the smallest measured microparticle was 2.7µm and the largest measured microparticle was 75.5µm. These data agreed well with the SEM images as 96.7% of the microparticles were found to be <50 microns using the microparticle size distribution analysis.

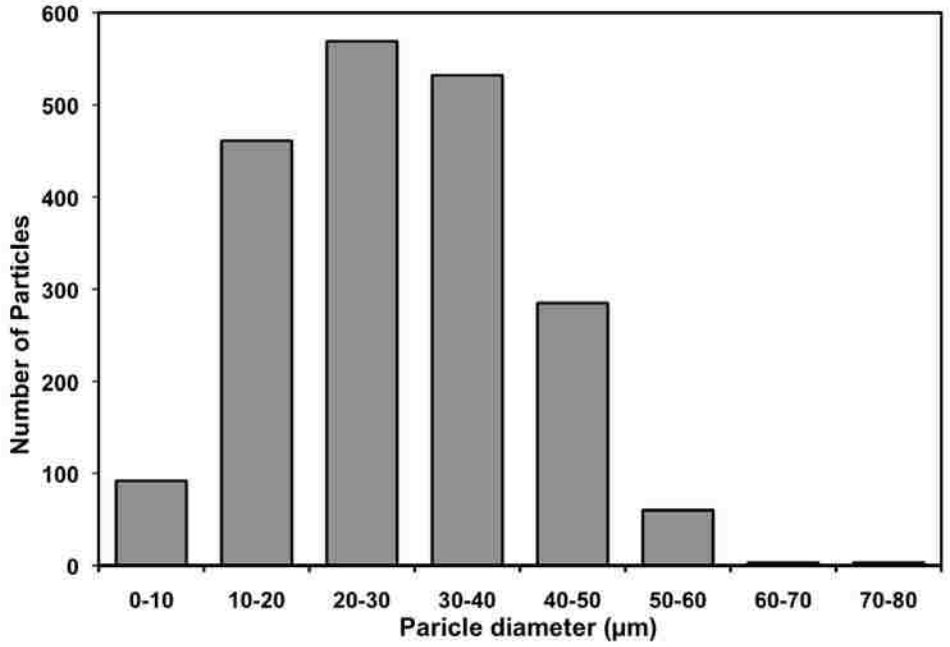

Figure 2-8: Particle size distribution data for DMpT-containing thiol-acrylate microparticles stirred initially at 2100 RPM and then1700 RPM after catalyst addition. All particle size data were collected via optical microscopy and particle size analysis software.

2.6.5 Conclusions and Discussion

As was shown by the SEM analysis (Figure 2-7), there was a large amount of unencapsulated DMpT surrounding the exterior of the microparticles. This unencapsulated core material caused the particles to agglomerate and be inefficient as a mechanism for separating the core material from its surroundings. This excess core material could be washed away via a cyclohexane-washing step; however, the DMpT would eventually diffuse through the matrix material and again be present on the surface of the microparticles. Because of this leaching problem this was found to be an inefficient method for microencapsulating this particular tertiary aromatic amine. However, this result did provide some potential new pathways for the use of thiol-acrylate microparticles as control release vessels with the ability to release core

material slowly and constantly over time as would be necessary to maintain a constant level of core material in the surroundings.

2.7 Benzoyl Peroxide Microencapsulation

2.7.1 Introduction and Rationale for Microencapsulation

Benzoyl peroxide (BPO) is an organic acyl peroxide with a multitude of uses. It is widely used as thermal initiator for free-radical polymerizations. [89-91] Benzoyl peroxide is also commonly used in cosmetic applications such as an acne treatment because of its antimicrobial properties that can destroy surface and ductal bacterial organisms and yeasts. [92-94] Due both to its many uses and unstable nature [94, 95], the microencapsulation of benzoyl peroxide provides enormous benefits. Benzoyl peroxide has been successfully microencapsulated using various techniques. Jelvehgari et al. produced and analyzed benzoyl peroxide microparticles via an emulsion solvent diffusion method. [96, 97] Fuchigami et al. microencapsulated benzoyl peroxide (BPO) with polyethyl methacrylate (PEMA) via a drying-in-liquid method with an efficiency of over 90%. [98] Wilson et al. prepared benzoyl peroxide microcapsules for a self-healing bone cement application via a urea-formaldehyde technique. [99] Although these references illustrate the availability of valid techniques for the microencapsulation of benzoyl peroxide, many of them still suffer from potentially solvable disadvantages. In order to address these disadvantages, benzoyl peroxide microparticles were prepared using this thiol-acrylate technique via a relatively inexpensive dispersion technique in less than one hour at room temperature and under ambient conditions.

2.7.2 Neat Microencapsulation

2.7.2a Experimental Procedure

Microparticles containing benzoyl peroxide (BPO) as the core component were prepared with a matrix comprised of trimethylolpropane triacrylate (TMPTA) and trimethylolpropane tris(3-mercaptopropionate) (TMPTMP) catalyzed by octyl amine. A solution of stoichiometrically equivalent TMPTMP and TMPTA was prepared containing 11.98 grams and 9.33 grams, respectively. The BPO (5 g) was dissolved in the trithiol/triacrylate solution. This solution was then emulsified in 250 mL of a 1.28% poly(vinyl alcohol) aqueous solution with a stir motor equipped with a 3-bladed propeller. The mixture was agitated for 30 minutes at 2000 RPM. Once the desired droplet size range was achieved (determined via optical microscopy), ~3mL of octylamine was added to the mixture to catalyze the polymerization. The mixture was allowed to react for 1 hour at room temperature and ambient pressure with continuous mixing at 1700 RPM. The microparticles were recovered by vacuum filtration and dried.

2.7.2b Scanning electron microscopy

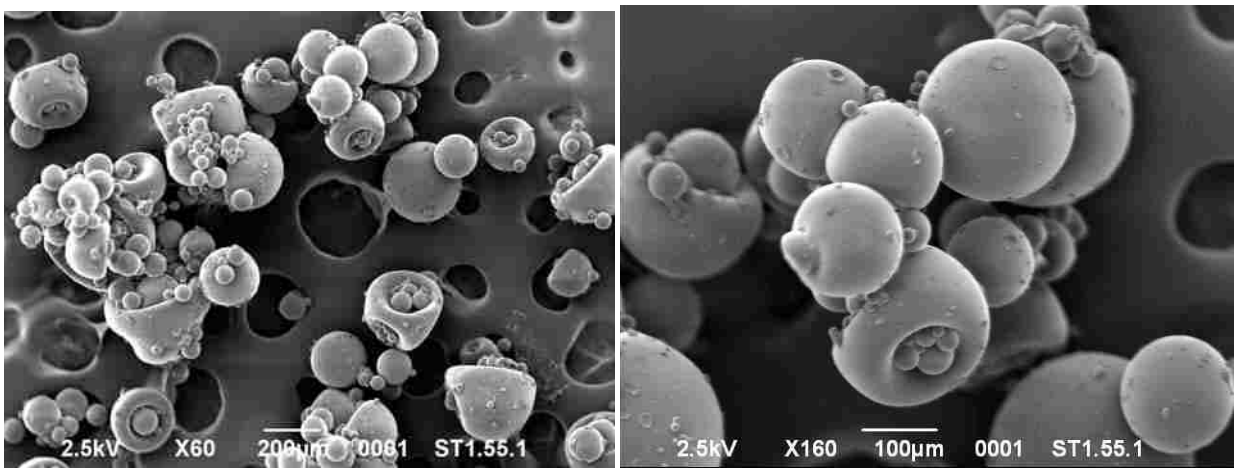

Figure 2-9: Scanning electron microscopy of neat BPO microparticles at X60 magnification (left) and X160 magnification (right).

Benzoyl peroxide was microencapsulated in a thiol-acrylate matrix and SEM images were obtained (Figure 2-9). The microparticles produced using this neat technique were observed to have a caved doughnut appearance as shown by the SEM images. This morphology could not completely be explained, however it was likely linked to the phase separation and precipitation of the BPO from the thiol acrylate matrix upon polymerization of the shell material. Nonetheless, this artifact generated the illusion if not the fact that these microparticles were empty and contained no core material, perhaps caused by some interaction between the thiol-acrylate copolymerization mechanism and the free radical initiator, resulting in the incorporation of the core material into the thiol-acrylate network.

2.7.2c Particle Size Distribution

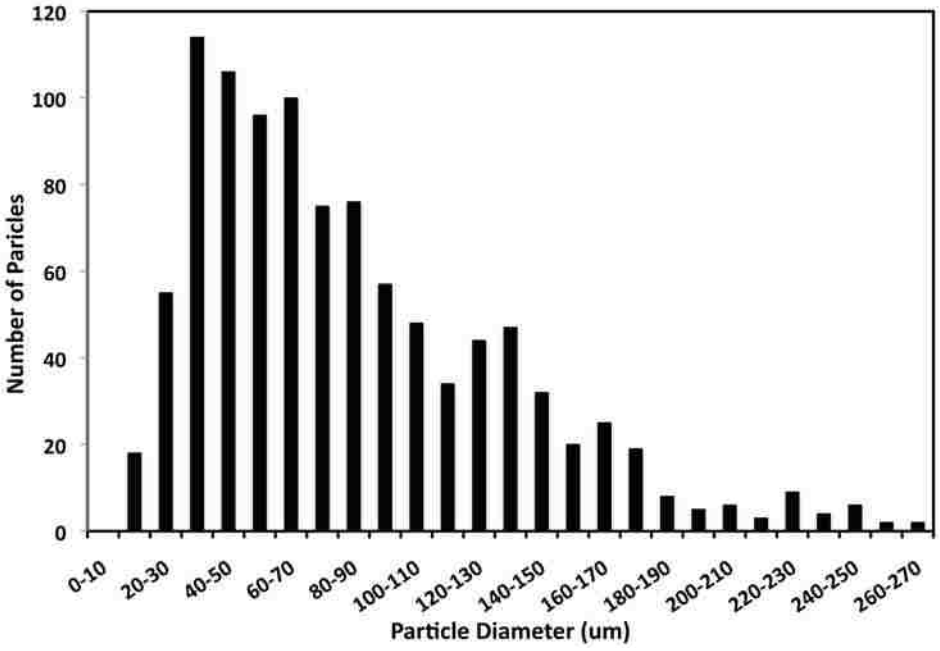

Figure 2-10: Particle size distribution data for neat benzoyl peroxide microparticles agitated at 2000 RPM.

Particle size analysis was performed on the resulting neat BPO thiol-acrylate microparticles via optical microscopy and size analysis software. The microparticle size

distribution data are illustrated in Figure 2-10. A 1011 microparticle population was used to collect these data. These microparticles were agitated at 2000 RPM throughout the entire microencapsulation process. These data illustrate that the average particle size was 85.83±52.08µm. A relatively broad distribution was observed where the smallest measured microparticle was 13.5 µm and the largest measured microparticle was 349 µm.

2.7.2d Core Loading Percent

It was vital to know the percentage of core material contained within the microparticle matrix, as this would determine its usefulness as a potential initiator or cosmetic antimicrobial. Due to the low solubility of benzoyl peroxide in the thiol-acrylate monomers, a large core loading percent was not expected using this neat technique. The following formula was used to estimate the core loading percentage.

$$\textbf{Core Loading \%} = \frac{\textbf{Core}}{\textbf{Core + Monomer 1 + Monomer 2}}$$

In this formula, the Core, Monomer 1, and Monomer 2 values corresponded to the amount of BPO, TMPTMP, and TMPTA in grams, respectively. Using this equation, the theoretical core loading percent for the neat BPO microparticles was calculated to be 19%. Because the above formula technically provides only the theoretical core loading if all of the components in the system were *completely* immiscible in water, thermal gravitational analysis was performed on microparticles containing BPO (Figure 2-11) to validate this method of estimating the core loading percent.

From the TGA data in Figure 2-11a, the core loading percent was found to be ~3.5% when the material was heated at a rate of 10˚C/min. The decomposition of the benzoyl peroxide began at ~150˚C and the weight decreased by 3.5% after which it

remained constant until ~325˚C at which point the thiol-acrylate matrix began to degrade. To determine the weight loss under isothermal conditions, another TGA analysis was performed where the neat microparticles were heated to 150˚C and held for >1hr (Figure 2-11b).

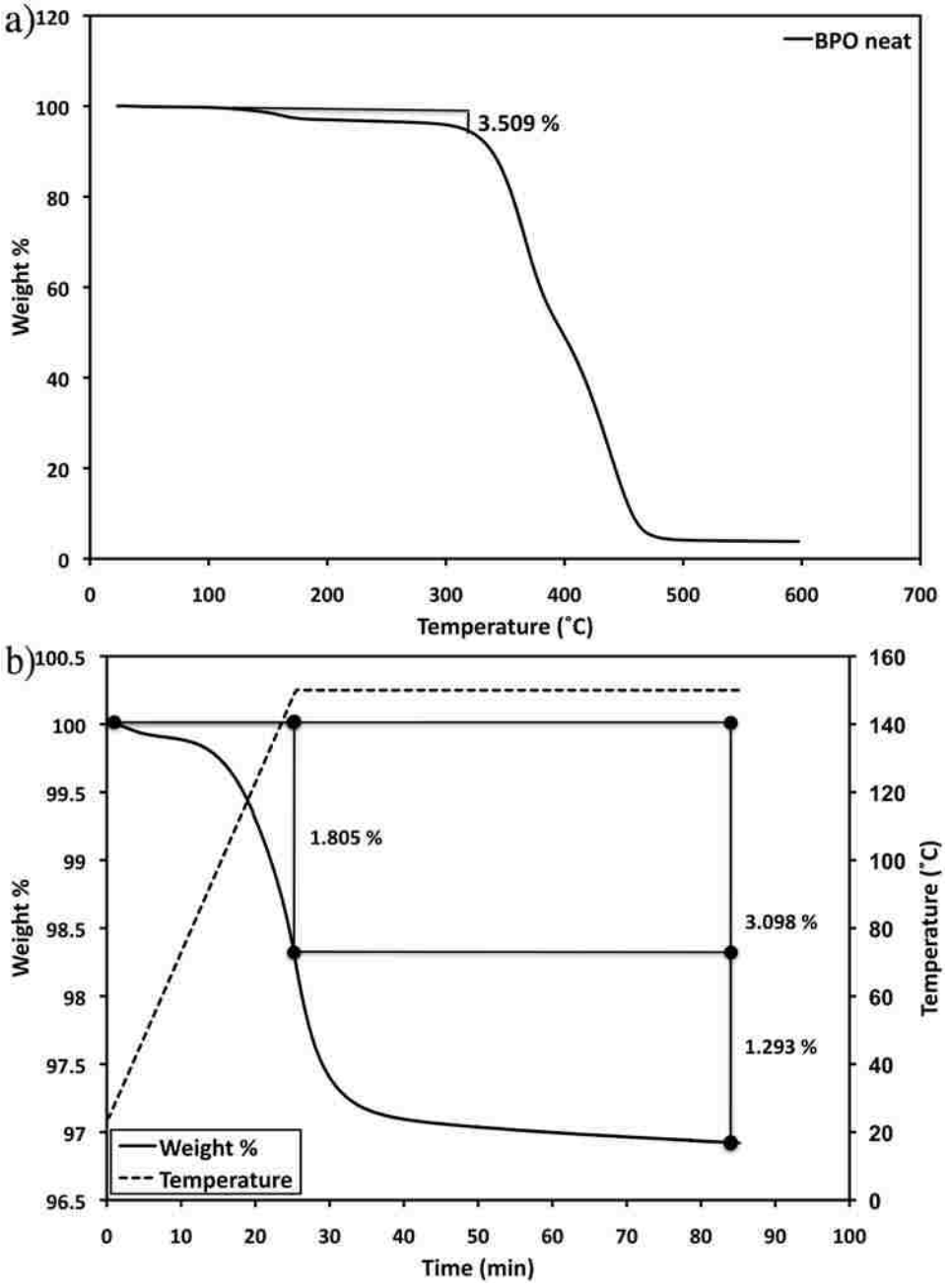

Figure 2-11: Thermal gravimetric analysis of neat BPO microparticles a) ramped at 10 ˚C/min to 600˚C b) ramp and hold at 150˚C for 1 hr.

Figure 2-11b illustrates the weight loss information in more detail. During the ramp to 150˚C, 1.8% of the weight was loss which could be attributed not only to the loss of BPO but also to the loss of water at ~100˚C. After reaching 150˚C, the remaining weight loss of 1.3% was observed after about 45 minutes. From this TGA data, it was determined that the theoretical formula for determining the core loading percent of these neat BPO microparticles was not an accurate method for estimating the value. This indicated that there was a loss in the core BPO at some time during the microparticle synthesis process. This was likely due to the consumption of the BPO in the form of a free radical initiator for the polymerization of the acrylate monomer during the thiol-acrylate matrix forming mechanism.

2.7.3 Solvent Microencapsulation

2.7.3a BPO in Toluene

Experimental Procedure

Microparticles containing benzoyl peroxide (BPO) dissolved in toluene as the core component were prepared with a matrix comprised of trimethylolpropane triacrylate (TMPTA) and trimethylolpropane tris(3-mercaptopropionate) (TMPTMP) catalyzed by octyl amine. A solution of stoichiometrically equivalent TMPTMP and TMPTA was prepared containing 11.98 grams and 9.33 grams, respectively. The core BPO (5 g) was dissolved in 40 grams of toluene. The trithiol/triacrylate solution was then dissolved in the BPO/toluene solution. This core/matrix solution was then emulsified in 250 mL of a 1.28% poly(vinyl alcohol) aqueous solution with a stir motor equipped with a 3-bladed propeller. The mixture was agitated for 30 minutes at 1700 RPM. Once the desired droplet size range was achieved, ~3mL of octylamine was added to the mixture to

catalyze the polymerization. The mixture was allowed to react for 1 hour at room temperature and ambient pressure with continuous mixing at 1700 RPM. The microparticles were recovered by vacuum filtration and dried.

Scanning Electron Microscopy

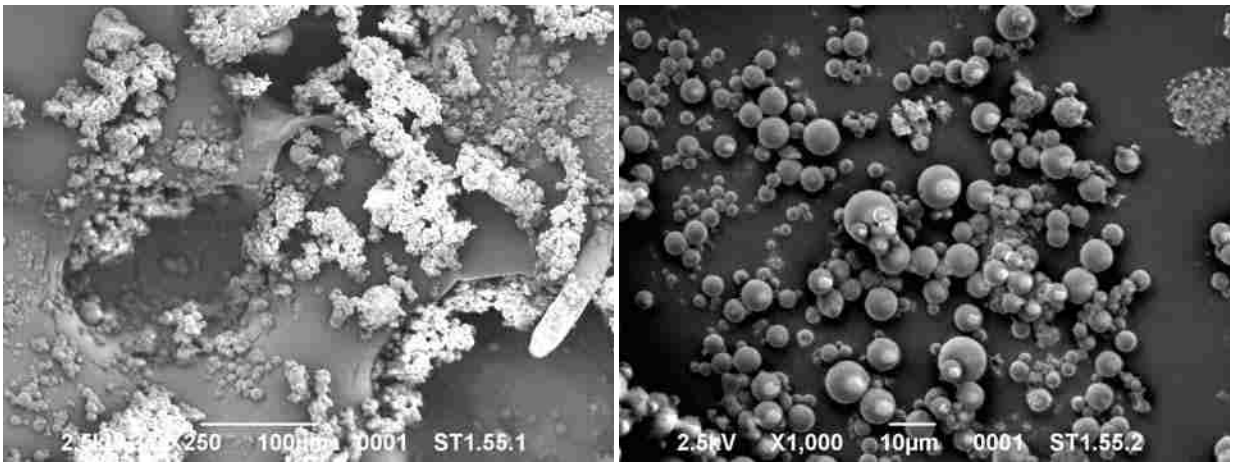

Figure 2-12: Scanning electron microscopy of microparticles containing BPO dissolved in toluene shown at X250 magnification (left) and X1000 magnification (right).

Benzoyl peroxide was dissolved in toluene, microencapsulated in a thiol-acrylate matrix, and SEM images were obtained (Figure 2-12). The SEM images illustrate that the microparticles formed were symmetrical in shape forming nearly flawless spheres as opposed to the doughnut, concave motif that was observed with the neat BPO microparticles. The microparticles produced using this toluene technique were very small relative to the microparticles prepared in a neat fashion as shown by the SEM images. The image on the left illustrates the microparticles at X250 with a 100µm scale bar, which does not give a good representation of the size of the particles and visual particle size distribution. These aspects were much more obvious at higher magnification of X1000 (right image). The majority of these microparticles were found to

be <10 microns and a they possessed a relatively narrow visual particle size distribution as can be seen in Figure 2-12.

Particle Size Distribution

Optical microscopy and size analysis software was used to determine the particle size distribution of the resulting thiol-acrylate microparticles containing benzoyl peroxide dissolved in toluene. The microparticle size distribution data are illustrated in Figure 2-13. A 2015 microparticle population was used to collect these data. These microparticles were agitated at 1700 RPM throughout the entire microencapsulation process. These data illustrate that the average particle size was 5.5±2.0µm. A relatively narrow distribution was observed where the smallest measured microparticle was 1.6µm and the largest measured microparticle was 16.3µm.

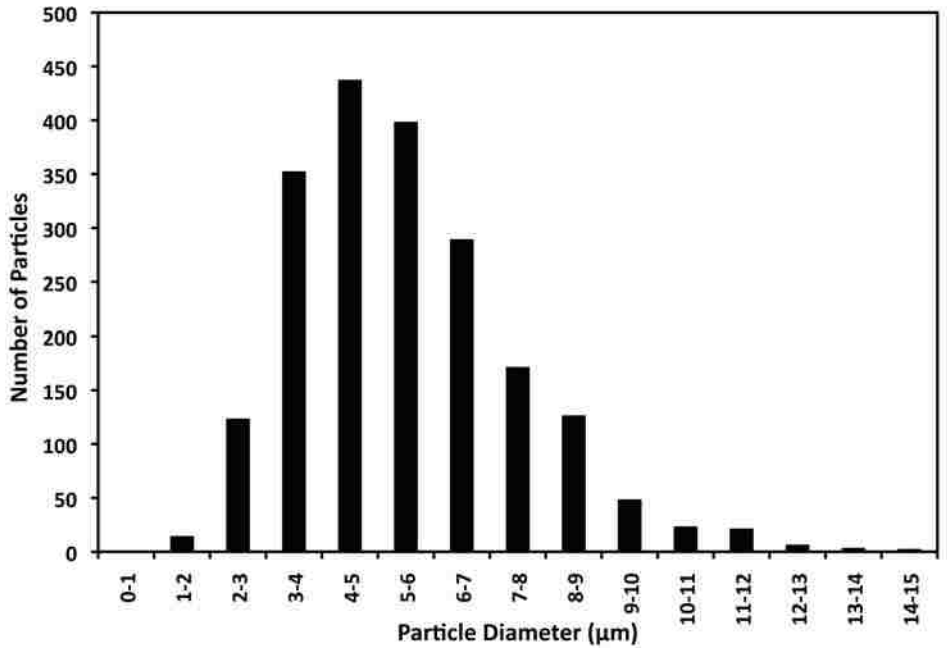

Figure 2-13: Particle size distribution data for microparticles containing benzoyl dissolved in toluene and agitated at 1700 RPM.

Core Loading Percentage

As stated earlier, it was vital to know the percentage of core material contained within the microparticle matrix. Again, due to low solubility, a large core loading percent was not expected using this solvent technique. The theoretical core loading percentages were calculated, and it was found that theoretically the entire system, including the solvent, was composed of 7.5% BPO. There was a calculated 68% by weight of solvent + BPO relative to the entire system. If it was assumed that all of the solvent was lost during the microencapsulation process, then the calculated BPO weight percent relative only to the polymer matrix was 19%. Again to determine the real or experimental core loading percent, TGA analysis was performed. (Figure 2-14)

From the TGA data in Figure 2-14a, the core loading percent was found to be 18% when the material was heated at a rate of 10˚C/min showing some similarities between the theoretical core loading and the experimental core loading. The decomposition of the benzoyl peroxide and potentially the loss of solvent was evident near ~100˚C at the onset of weight loss. At ~320˚C the thiol-acrylate matrix began to degrade. To determine the weight loss under isothermal conditions, another TGA analysis was performed where the microparticles were heated to 150˚C and held for >1 hr (Figure 2-14b).

Figure 2-14b illustrates the weight loss information in more detail. During the ramp to 150˚C, 7.5% of the weight was loss, which could be attributed not only to the loss of BPO but also to the loss of toluene at 110˚C. After reaching 150˚C, a weight loss of 5.2% was observed. The slow loss in weight after the immediate loss during ramp is indicative of the loss of core BPO, as it was more difficult for it to escape from

the thiol-acrylate matrix due to its solid form as opposed to the liquid toluene. As with the neat microparticles, some of the core BPO was likely lost in the form of a free radical initiator for the homopolymerization of the acrylate used during to form the matrix material.

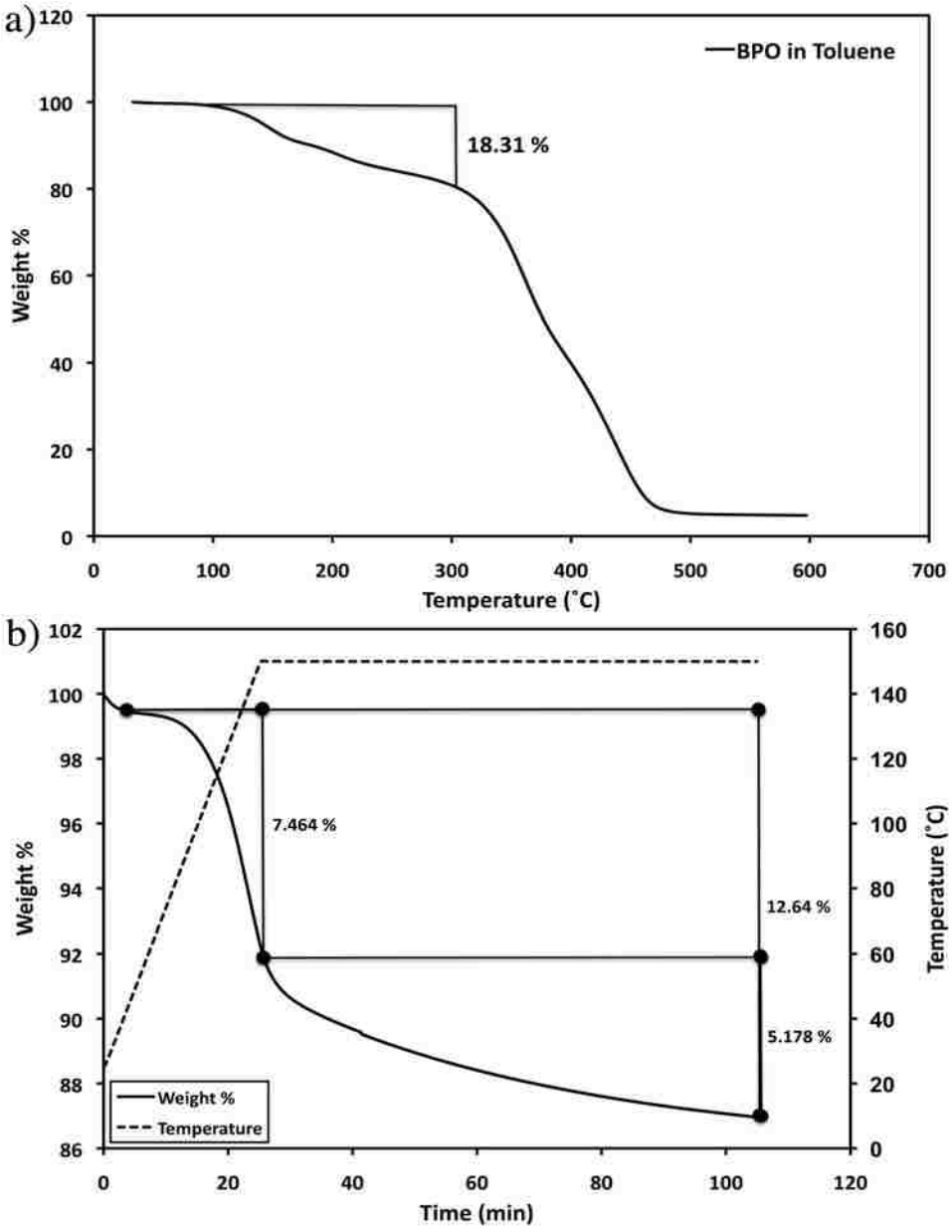

Figure 2-14: Thermal gravimetric analysis for microparticles containing BPO dissolved in toluene a) ramped at 10 ˚C/min to 600˚C b) ramp and hold at 150˚C for 1 hr.

2.7.3b BPO in Benzene

Experimental Procedure

Microparticles containing benzoyl peroxide (BPO) dissolved in benzene as the core component were prepared with a matrix comprised of trimethylolpropane triacrylate (TMPTA) and trimethylolpropane tris(3-mercaptopropionate) (TMPTMP) catalyzed by octyl amine. A solution of stoichiometrically equivalent TMPTMP and TMPTA was prepared containing 11.98 grams and 9.33 grams, respectively. The core BPO (5 g) was dissolved in 30 grams of benzene. The trithiol/triacrylate solution was then dissolved in the BPO/toluene solution. This core/matrix solution was then emulsified in 250 mL of a 1.28% poly(vinyl alcohol) aqueous solution with a stir motor equipped with a 3-bladed propeller. The mixture was agitated for 30 minutes at 1700 RPM. Once the desired droplet size range was achieved, ~3mL of octylamine was added to the mixture to catalyze the polymerization. The mixture was allowed to react for 1 hour at room temperature and ambient pressure with continuous mixing at 1500 RPM. The microparticles were recovered by vacuum filtration and dried.

Scanning Electron Microscopy Analysis

Benzoyl Peroxide was dissolved in benzene, microencapsulated in a thiol-acrylate matrix, and SEM images were obtained (Figure 2-15). As with the toluene/BPO microparticles, the SEM images illustrate that the microparticles formed were symmetrical in shape forming nearly flawless. Also like the toluene/BPO particles, these microparticles were very small as shown by the SEM images. The image on the left illustrates the microparticles at X500 with a 50μm scale bar, which does not give a good representation of the size of the particles and visual particle size distribution.

These aspects were much more obvious at higher magnification of X1000 (right image). The majority of these microparticles were found to be <10 microns as with the toluene method. These microparticles were observed to have a relatively narrow visual particle size distribution compared to that of the neat microparticles.

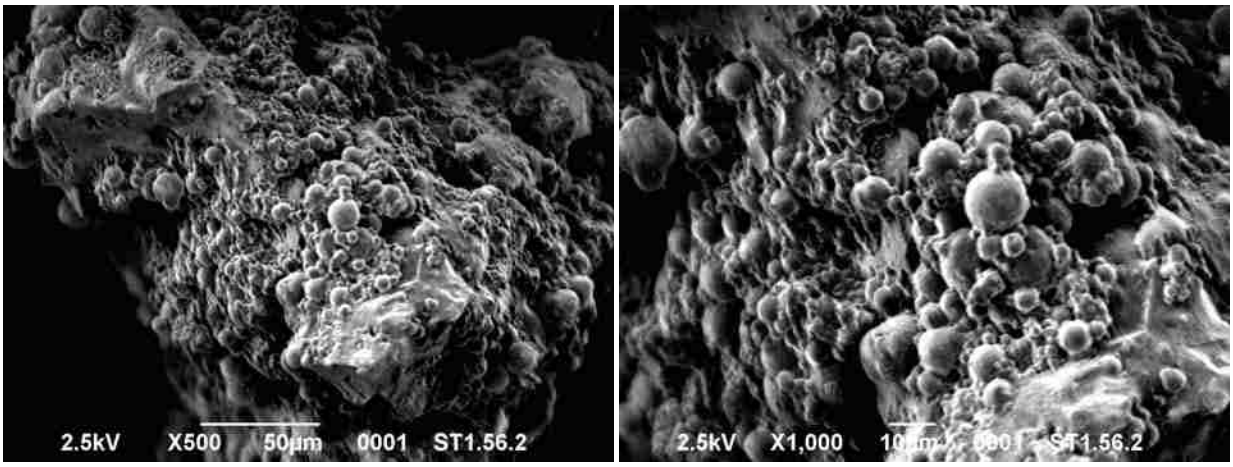

Figure 2-15: Scanning electron microscopy of microparticles containing BPO dissolved in benzene shown at X500 magnification (left) and X1000 magnification (right).

Core Loading Percentage of BPO in Benzene

The calculated solvent+BPO core loading percent was found to be 62% by weight. The BPO weight percent of 9% relative to everything else was calculated to be a little higher than the toluene/BPO microparticles as less solvent was used in this benzene technique. Because the BPO core-loading relative only to the polymer matrix was independent of the solvent content, that theoretical weight percent remained the same at 19%, again if it was assumed that all of the solvent was lost during the microencapsulation process. The experimental core loading percent data were determined using TGA, and these data are illustrated in Figure 2-16.

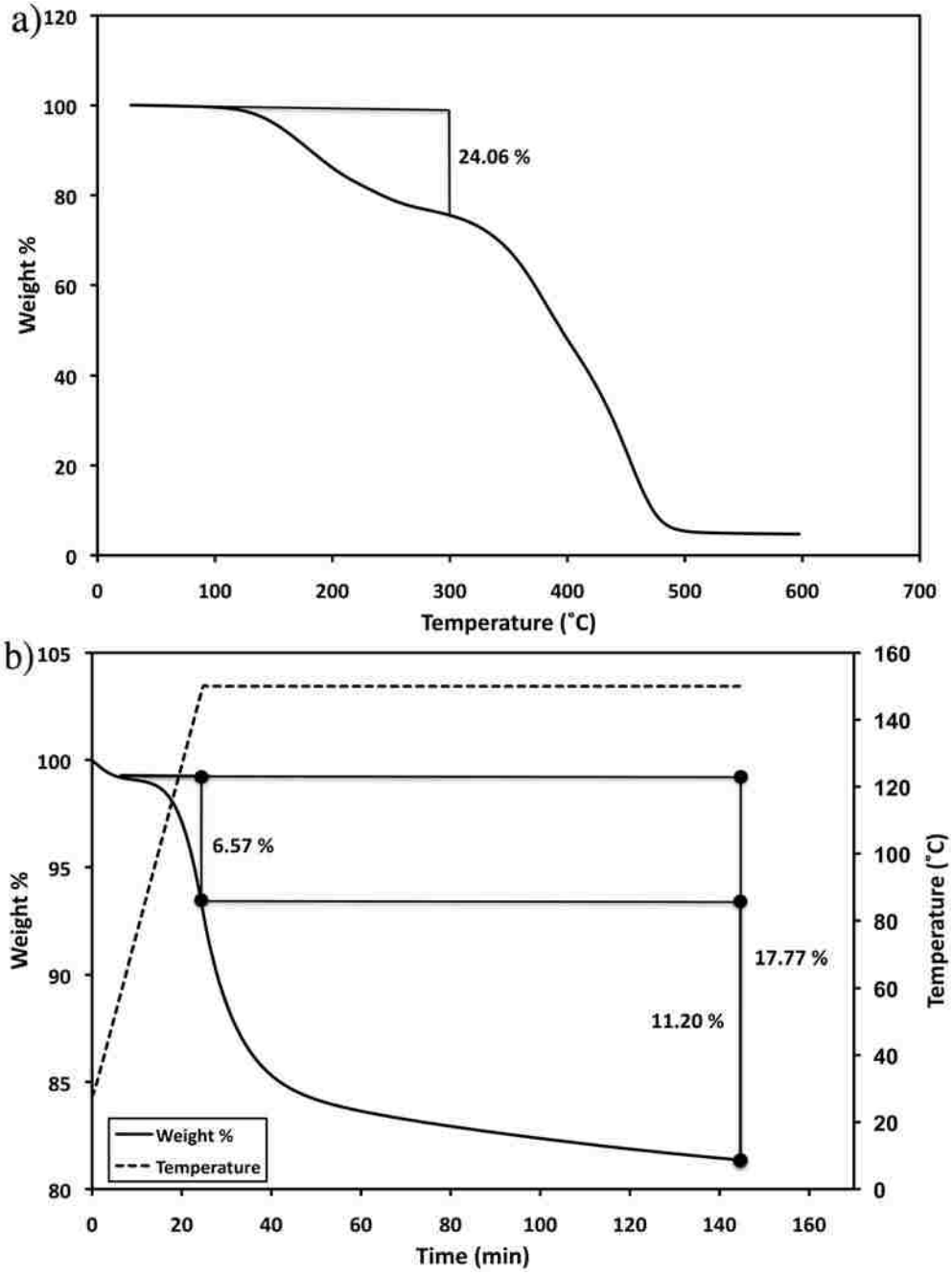

Figure 2-16: Thermal gravimetric analysis for microparticles containing BPO dissolved in benzene a) ramped at 10 ˚C/min to 600˚C b) ramp and hold at 150˚C for 1 hr.

The TGA ramp data are shown in Figure 2-16a. The core loading percentage was found to be 24% when the material was heated at a rate of 10˚C/min implying that there was a higher overall core loading for these microparticles compared to both the

neat BPO microparticles and the BPO/toluene microparticles. Again, at ~325˚C the thiol-acrylate matrix began to degrade. To determine the weight loss under isothermal conditions, another TGA analysis was performed where the microparticles were heated to 150˚C and held for >1 hr (Figure 2-16b).

Figure 2-16b illustrates the weight loss information in more detail. During the ramp to 150˚C, 6.6% of the weight was loss, which could be attributed not only to the loss of BPO but also to the loss of benzene at 80˚C. After reaching 150˚C, a weight loss of 11.2% was observed. The increase in the weight loss for the isothermal plot after 150˚C for the benzene/BPO microparticles compared to the toluene/BPO microparticles, implies once more that the BPO concentration was higher in these microparticles because the slow loss in weight after the immediate loss during ramp is indicative of the loss of core BPO.

2.7.4 Conclusions and Discussion

For all three of these BPO methods, the thiol-acrylate matrix was observed to separate the core material from its surroundings and increase the pot life of an acrylate system containing the microparticles and a small amount of the accelerator DMpT. However, the polymerization of an acrylic monomer was not attained using these microparticles with or without an accelerator. There could have been very little or no benzoyl peroxide encapsulated within the polymer matrix. All of the BPO core could have been consumed via a free radical homopolymerization mechanism. Another possibility could be that the microparticles did contain encapsulated BPO, but the BPO was trapped into the matrix material in such low concentrations or the release was too slow to allow for the polymerization of an acrylic monomer system.

The experimental core loading percent, determined via TGA, was much higher when a solvent method was utilized; however, this increase in core loading did not cause an increase in the reactivity or usefulness of the microparticles. This implies that the majority of the core material was simply the solvent or a solvent solution containing a very low concentration of BPO.

2.8 Caron Nanotubes Microparticles

2.8.1 Introduction and Rationale for Microencapsulation

Carbon nanotubes have the potential to improve many properties of composite materials including mechanical [100, 101] and electrical [102-104] properties. A normal problem associated with the use of carbon nanotubes is that unmodified CNTs aggregate due to van der Waals interactions among the nanotubes.[105, 106] This thiol-acrylate matrix could be useful in preventing CNTs from agglomerating when dispersed in a medium. These were the first thiol-acrylate microparticles (or nanoparticles) to be prepared using this method via ultrasonication.

2.8.2 Experimental Procedure

Microparticles containing 1% carbon nanotubes (CNTs) as the core component were prepared with a matrix comprised of trimethylolpropane triacrylate (TMPTA) and trimethylolpropane tris(3-mercaptopropionate) (TT1) catalyzed by octyl amine. A solution of stoichiometrically equivalent TT1 and TMPTA was prepared containing 0.81 grams and 0.60 grams respectively. The core, CNTs (0.0140 grams), was dispersed in the trithiol/triacrylate solution via a magnetic stirrer for 20 minutes. This solution was then emulsified in 25 mL of a 1.28% poly(vinyl alcohol) aqueous solution in an ice bath (to keep the temperature low) with a Branson sonifier 450 at constant 45% output. The

mixture was emulsified for 30 minutes with this constant sonification. Once the mixture was efficiently emulsified, ~3% by volume (0.05 mL) of octylamine was added to the mixture to catalyze the polymerization. The mixture was allowed to react for 1 hour at room temperature with continuous sonication. The micro/nanoparticles were recovered by vacuum filtration and dried overnight.

2.8.3 Scanning Electron Microscopy Analysis

Microparticles containing carbon nanotubes (CNTs) were prepared using the general thiol-acrylate microencapsulation procedure with a few small deviations, and SEM analysis was performed (Figures 2-17a and b). These particles were prepared with a smaller average particle size via the use of ultrasonication during the dispersion and polymerization process. The particles were observed to have a large particle size distribution ranging from 120 µm (Figure 2-17a) to <75 nm (Figure 2-17b).

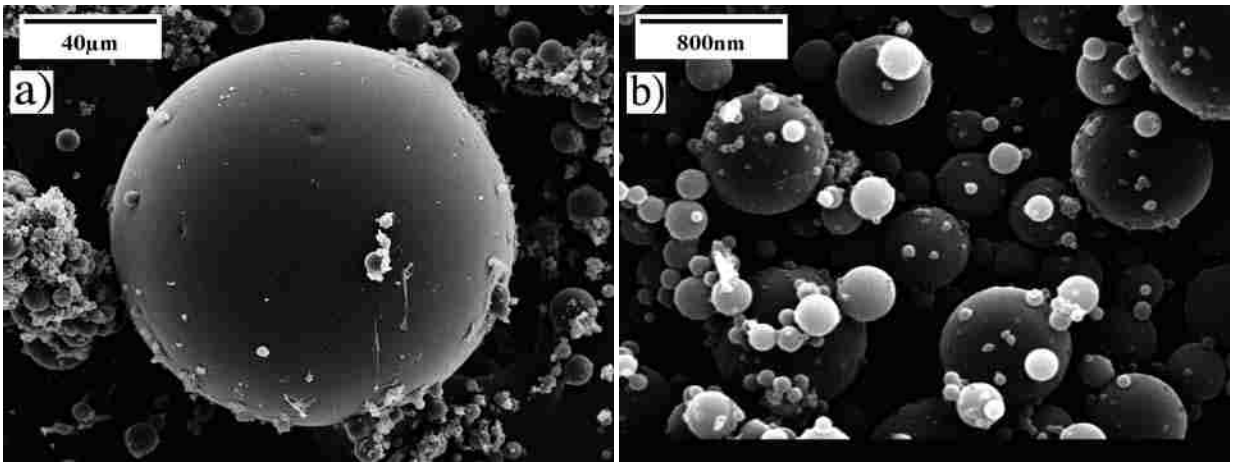

Figure 2-17: SEM images of microparticles containing carbon nanotubes. The majority of the particles were observed to be <1 micron (figure b) but a few of the particles were relatively large (figure b).

2.8.4 Results and Discussion

These results illustrated the capacity to produce very small microparticles and even nanoparticles using this thiol-acrylate encapsulation method coupled with

ultrasonification. Although very small particles were produced containing carbon nanotubes, they were observed to agglomerate inside the particles. Optical microscopy analysis (Figure 2-18) illustrates dark agglomerates inside the transparent microparticles. This optical microscopy analysis does provide evidence of the encapsulation of the CNTs. However, the agglomeration would still inhibit an adequate distribution of the carbon nanotubes in a composite material, as the thiol acrylate matrix would only separate large agglomerations of CNTs and not individual nanotubes. It would be necessary to adequately disperse the CNTs in the thiol-acrylate monomer system prior to the addition of the catalyst in order to solve this agglomeration problem. Although these results indicate the lack of success in separating carbon nanotubes in a composite material via microencapsulation, this indicates the potential for the production of much smaller thiol-acrylate particles, even nanoparticles via ultrasonification.

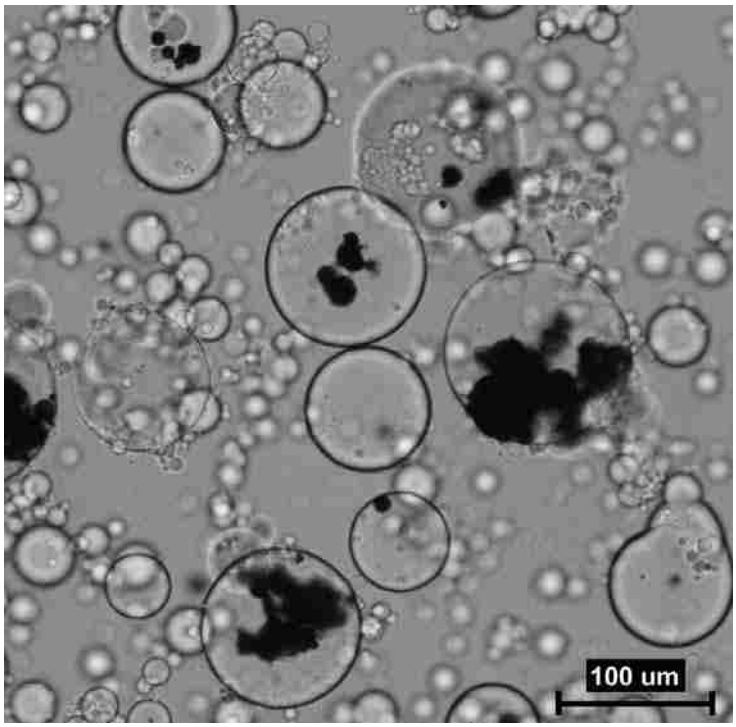

Figure 2-18: Optical microscopy image of thiol-acrylate microparticles containing carbon nanotubes.

2.9 Boron Trifluoride-Amine Microparticles

2.9.1 Rationale for Microencapsulation

Formation of Initiator/Catalyst **X = F or Cl**

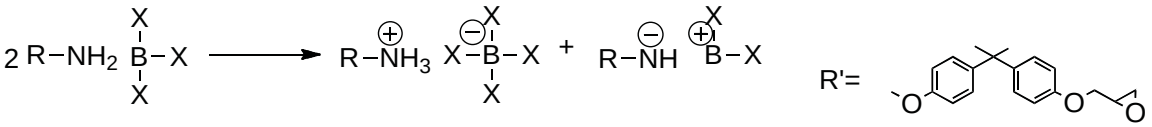

Preinitiation

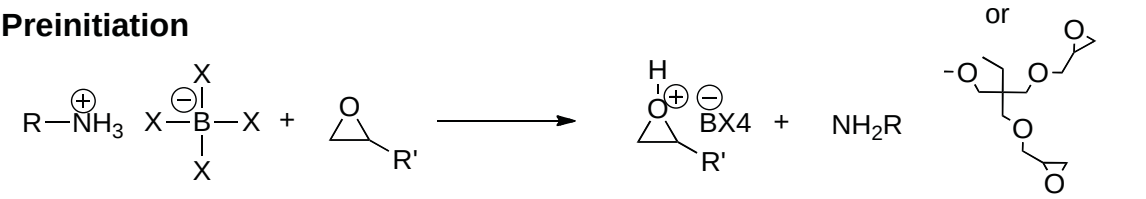

Activated Chain End (ACE)

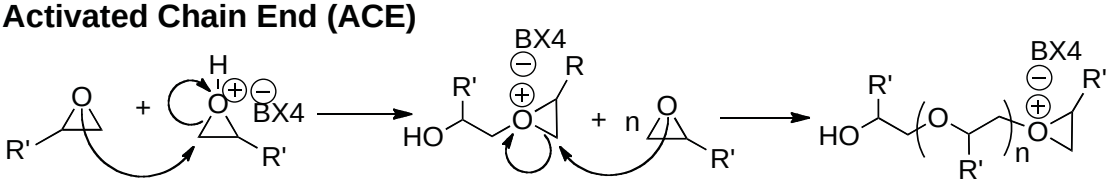

Activated Monomer (AM)

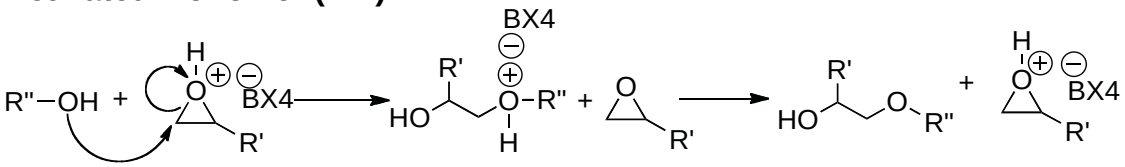

Chain Transfer

Intermolecular

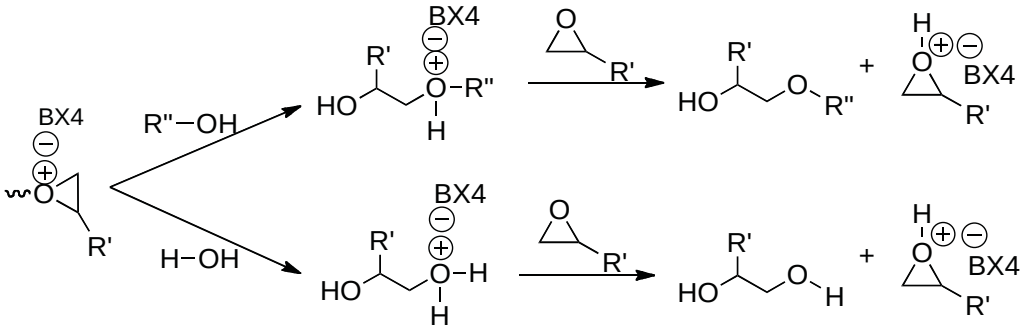

Intramolecular

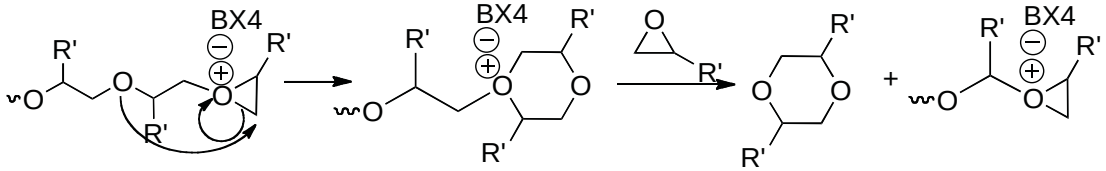

Scheme 2-3: Basic Lewis acid initiated epoxy reaction scheme including the activated chain end (ACE) and activated monomer (AM) propagation mechanisms. X represents either Cl or F, and R' indicates the pendent group (Upper: BADGE and lower TMPTGE).

Epoxy resins can be cationically polymerized via Lewis acid initiators.[107, 108] Lewis acids complex with amines allowing for low reactivity at room temperature but rapid curing at elevated temperatures because the acid – base complex dissociates at high temperatures.[109] Depending on the basicity of the associated amine, the reactivities of these complexes can vary.[110] At elevated temperatures, Lewis acid complexes dissociate into RNH_3^+ and BX_4^- (X being either Cl or F halogens), which activate an epoxy monomer by forming an oxonium ion. The propagation of this cationic polymerization proceeds by two competing mechanisms, the activated chain end (ACE) and the activated monomer (AM) mechanisms. The Lewis-acid-initiated epoxy reaction scheme, including the ACE and AM mechanisms is shown in Scheme 2-3.[111] The ACE mechanism predominates at the beginning of the reaction until a sufficient number of polymer chains are formed, causing an increase in hydroxyl groups due to the polymer chain ends at which time the AM mechanism begins to become more favorable.[111]

Borontriflouride-amine Lewis acid initiators can cause the polymerization of epoxy reins in as little as 20 seconds at room temperature. The rapid pot lives of these BF_3-amine/Epoxy systems were found in literature [112] and confirmed experimentally. Figure 2-19 illustrates the pot life as a function of various commercially available BF_3-amine complexes given in literature, analyzed using a difunctional epoxy resin (diglycidyl either of bisphenol A (BADGE)) and analyzed using a trifunctional epoxy resin (trimethylolpropane triglycidyl ether (TMPTGE)). The pot life data did not precisely match the data found in literature, and there was some variations depending on the functionality of the epoxy, however the trend between the various types of BF_3-

amine complexes remained constant regardless of the epoxy used. The average pot lives, combining the literature, BADGE systems, and TMPTGE systems, were found to be ~18 min, ~9 min, ~2 min, and ~15 sec for Leepoxy Resins B-1310, B-614, B-612, B-610, respectively. (Figure 2-19)

A highly reactive Lewis acid complex initiator was sought; therefore, B-612 was selected for the microencapsulation experiments based on the data in Figure 2-19. The microencapsulation of this Lewis acid initiator (BF_3-amine complex) would facilitate its separation from the epoxy resin until acted upon by an external force (e.g. elevated temperature), resulting in a highly reactive latent initiator for epoxy resins. This would be especially useful in a frontally-polymerizable system because high reactivity and heat release are necessary to sustain a front of polymerization.

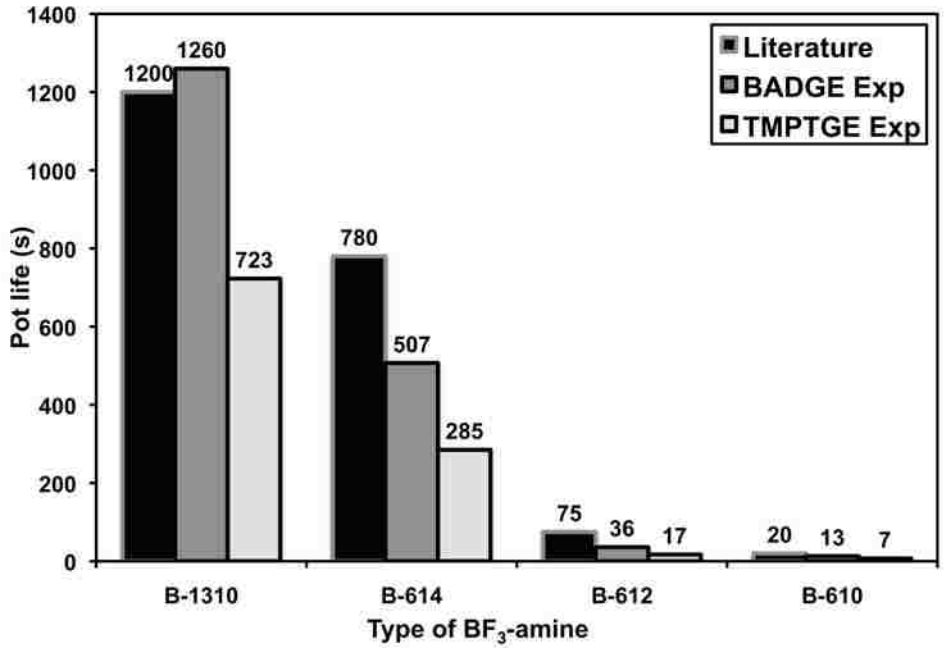

Figure 2-19: Pot life as a function of borontrifluoride-amine complex type found in literature and experimentally tested in BADGE and TMPTGE.

2.9.2 Experimental Procedure

Microparticles containing borontrifluoride-amine (BF_3) complex as the core component were prepared with a matrix comprised of trimethylolpropane triacrylate (TMPTA) and trimethylolpropane tris(3-mercaptopropionate) (TMPTMP) catalyzed by octyl amine. A solution of core material was prepared by dissolving 40 mL of a borontrifloride-amine complex (612) in a stoichiometrically equivalent solution of trimethylolpropane triacrylate (11.85 g) and trimethylolpropane tris(3-mercaptoproionate) (15.94g). Approximately 10% relative to the BF_3-amine complex of *tert*-butyl peroxybenzoate was added to the core material as a rupturing component. The core solution was then emulsified using a stir motor equipped with a three-blade propeller in 500 mL of a 0.4% Span 80 mineral oil solution contained in a water bath at 50˚C (heat necessary only to keep the viscosity of oil relatively low). The mixture was agitated for 10 minutes at 2000 RPM. Once the desired droplet size range was achieved, 2 mL of octyl amine (~7% relative to the trithiol/triacrylate content) was added, and the stir rate was decreased to 1700 RPM. The mixture was allowed to react for 1 hour at 50 °C with continuous mixing at 1700 RPM. After 1 hour, the microcapsules were recovered by vacuum filtration. In order to remove the remaining viscous mineral oil from the system, the microcapsules were washed with cyclohexane.

2.9.3. Scanning Electron Microscopy Analysis

Boron trifluoride-amine 612 is a highly reactive Lewis acid-amine complex capable of initiating the polymerization of a bisphenol A difunctional epoxy resin in ~2 minutes at room temperature with only 8-12 phr of the initiator present.[112] This Lewis acid initiator was microencapsulated using a thiol-acrylate matrix via an oil-in-oil

dispersion polymerization and SEM analysis was preformed on the resulting microparticles (Figures 2-20a and b).

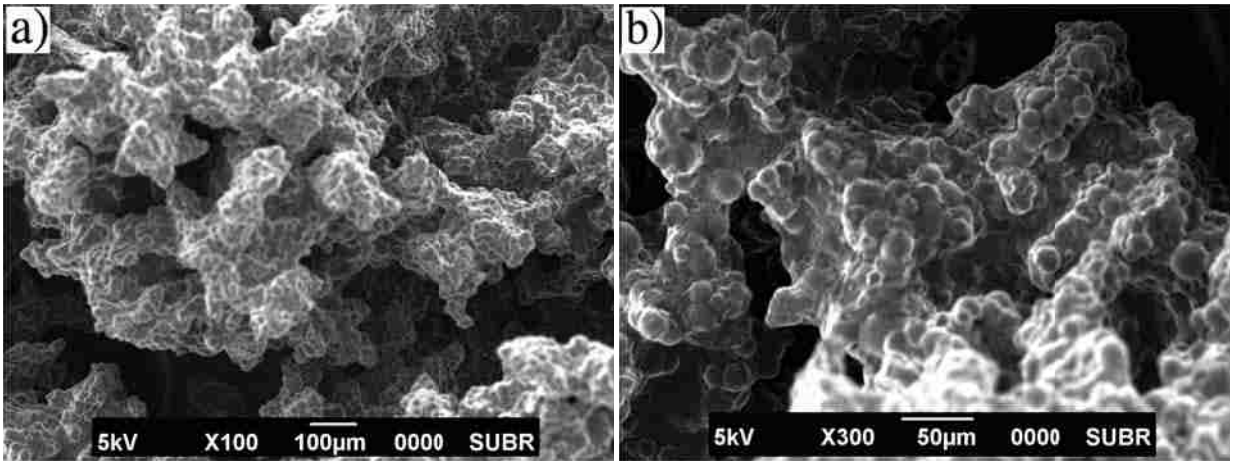

Figure 2-20: SEM images of microparticles containing boron trifluoride amine complex. a) X100 magnification b) X300 magnification

These microparticles had an overall agglomerated, sponge-like consistency that could be a result of multiple factors associated with the process. Figure 2-20a (low magnification) illustrates this overall agglomerated appearance; however, upon higher magnification (Figure 2-20b), it can be observed that small particles can be distinguished from the agglomeration. They were simply fixed together by some material between each particle.

2.9.4 Results and Discussion

The limiting factor for the success of the BF_3-amine thiol acrylate microparticles was agglomeration of the microparticles. There are a few possible causes for this high level of agglomeration. Because these microparticles were prepared via an oil-in-oil dispersion as opposed to an oil-in-water dispersion, an adequate and stable dispersion of the droplets could have been more difficult as a result of the higher interfacial tension

within the system, the more viscous continuous oil phase, and the large density difference between the continuous phase and mobile phase.

Another possible problem could be associated with the use of the thermal initiator, *tert*-butyl peroxybenzoate (TBP), as a rupturing agent. The TMPTMP (trithiol) could act as an accelerator to decompose the TBP causing the homopolymerization of the TMPTA (triacrylate) via a free-radical chain growth mechanism. This could leave excess, unreacted, viscous TMPTMP causing a high level of agglomeration. There are a few possible solutions to these agglomeration issues. The viscosity of the continuous mineral oil phase could be decreased by the addition of a less viscous oil such as cyclohexane. The microparticles could be prepared using an alternate rupturing agent or possibly no rupturing agent, and the density of the continuous phase could be increased. Another complication of the process was the miscibility of the amine catalyst in the mineral oil continuous phase. This forced the use of excess amine that could undergo an exchange reaction with the BF_3-amine complex, changing the associated amine thereby changing the reactivity of the initiator. One approach to preventing this problem and possibly achieving microparticles with different properties could include utilizing a true thiol-ene reaction instead of the thiol-acrylate reaction. A multifunctional electron-rich ene such as 2,4,6-triallyloxy-1,3,5-triazine or 1,3,5-triallyl-1,3,5-trazine-2,4,6-trione could be photopolymerized with the TMPTMP producing a copolymer composed of the simple ene rather that the acrylate.[5] Alternatively, this reaction could also be initiated by the TBP since it can be decomposed at room temperature in the presence of a thiol, and the electron-rich ene could not homopolymerize. This would

produce microparticles with similar properties while reducing the problems associated with catalyst miscibility.

The application of these microparticles indicated limited and some level of somewhat inexplicable success. Due to the high agglomeration of the product, the BF_3-amine microparticles were very difficult to disperse in an epoxy system. In some cases the microparticles were observed to greatly increase the pot-life of the highly reactive BF_3-amine/epoxy system and still be somewhat reactive upon heating the system. The true cause of the increase in the pot-life of the system is still not completely understood. There was a possibility as mentioned above that the Lewis acid initiator underwent an exchange reaction with the amine catalyst used to produce the microparticles, thereby reducing the reactivity of the initiator and causing an increase in pot life.

2.10 Boron Trichloride-Amine Microparticles

2.10.1 Rationale for Microencapsulation

The boron Trichloride amine (BCl_3-amine) complex used here was a latent, heat-activated initiator for epoxy systems with a nearly infinite pot life.[109] This Lewis acid initiator proceeds via the same mechanism as was illustrated for the BF_3-amine initiator (Scheme 2-3) In batch applications, a borontrichloride-amine Lewis acid initiator can be used to produce systems with a longer pot life at elevated temperatures, shorter full cure times, and a product that is much less brittle compared to BF_3-amine initiators.[109] Also, BCl_3-amine complexes show much better hydrolytic stability.[109] In some applications, BCl_3-amine complexes interfere with the desirable thixotropic properties of an epoxy system. The purpose for microencapsulating this initiator was unlike the other research performed in this work. The goal was to microencapsulate

the BCl_3-amine complex in a sphere or shell from which it could be released at the desired curing temperature of 170 ˚C. There was some interaction between BCl_3-amine and fumed silica, which is normally added to epoxy systems as a thixotropic agent. This interaction caused an undesirable loss in the rheological properties of the epoxy monomer solution. By microencapsulating this initiator, the matrix material was observed to prevent this unwanted interaction by separating the initiator from the silica until heated, allowing the rheological properties to be preserved until the desired reaction took place.

2.10.2 Experimental Procedure

Microparticles containing borontrichloride-amine (BCl_3) complex as the core component were prepared with a matrix comprised of trimethylolpropane triacrylate (TMPTA) and trimethylolpropane tris(3-mercaptopropionate) (TMPTMP) catalyzed by octyl amine. A solution of stoichiometrically equivalent TMPTMP and TMPTA was prepared containing 15.94 grams and 11.85 grams, respectively. The core BCl_3-amine (60 g) was dissolved in the trithiol/triacrylate solution. This solution was then emulsified in 500 mL of a 1.28% poly(vinyl alcohol) aqueous solution with a stir motor equipped with a 3-bladed propeller. The mixture was agitated for 30 minutes at 2000 RPM. Once the desired droplet size range was achieved, 3% by volume (~0.9 mL) of octylamine was added to the mixture to catalyze the polymerization, and the stir rate was decreased to 1700 RPM. The mixture was allowed to react for 1 hour at room temperature and ambient pressure with continuous mixing at 1700 RPM. The microparticles were recovered by vacuum filtration and dried overnight.

2.10.3. Scanning Electron Microscopy Analysis

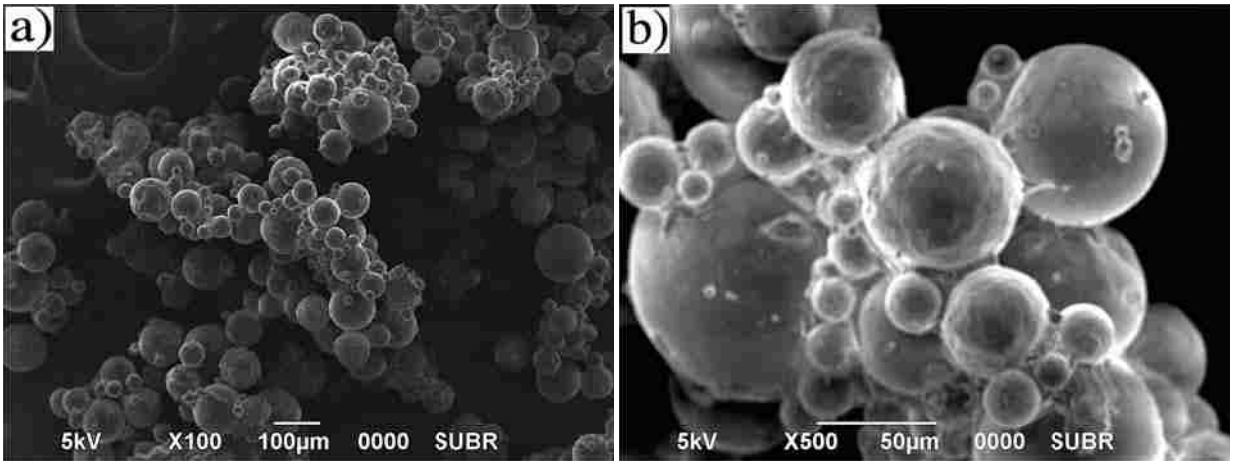

Figure 2-21: SEM images of BCl_3-amine microparticles. a) X100 magnification b) X500 magnification

Another Lewis acid-amine complex, boron trichloride-amine (BCl_3-amine) was microencapsulated using a thiol-acrylate matrix and SEM analysis was preformed on the resulting microparticles (Figures 2-21a and b). From these SEM images, it can be observed that these microparticles were symmetrical in shape, free of agglomeration, did not contain any unencapsulated material around the exterior of the shells, and had a relatively narrow particle size distribution. For these and other reasons, these microparticles were the main focus of the research, and more extensive results were obtained regarding these microparticles relative to the other particles prepared.

2.10.4 Size Analysis

Particle size analysis was performed on the resulting BCl_3-amine thiol-acrylate microparticles. The microparticle size distribution data were collected via optical microscopy and size analysis software. The size distribution data are illustrated in Figure 2-22 and tabulated in Table 2-1. A 1059 microparticle population and a 1562

microparticle population was used to collect the data for the microparticles initially stirred at 2000 RPM and the microparticles initially stirred at 900 RPM, respectively.

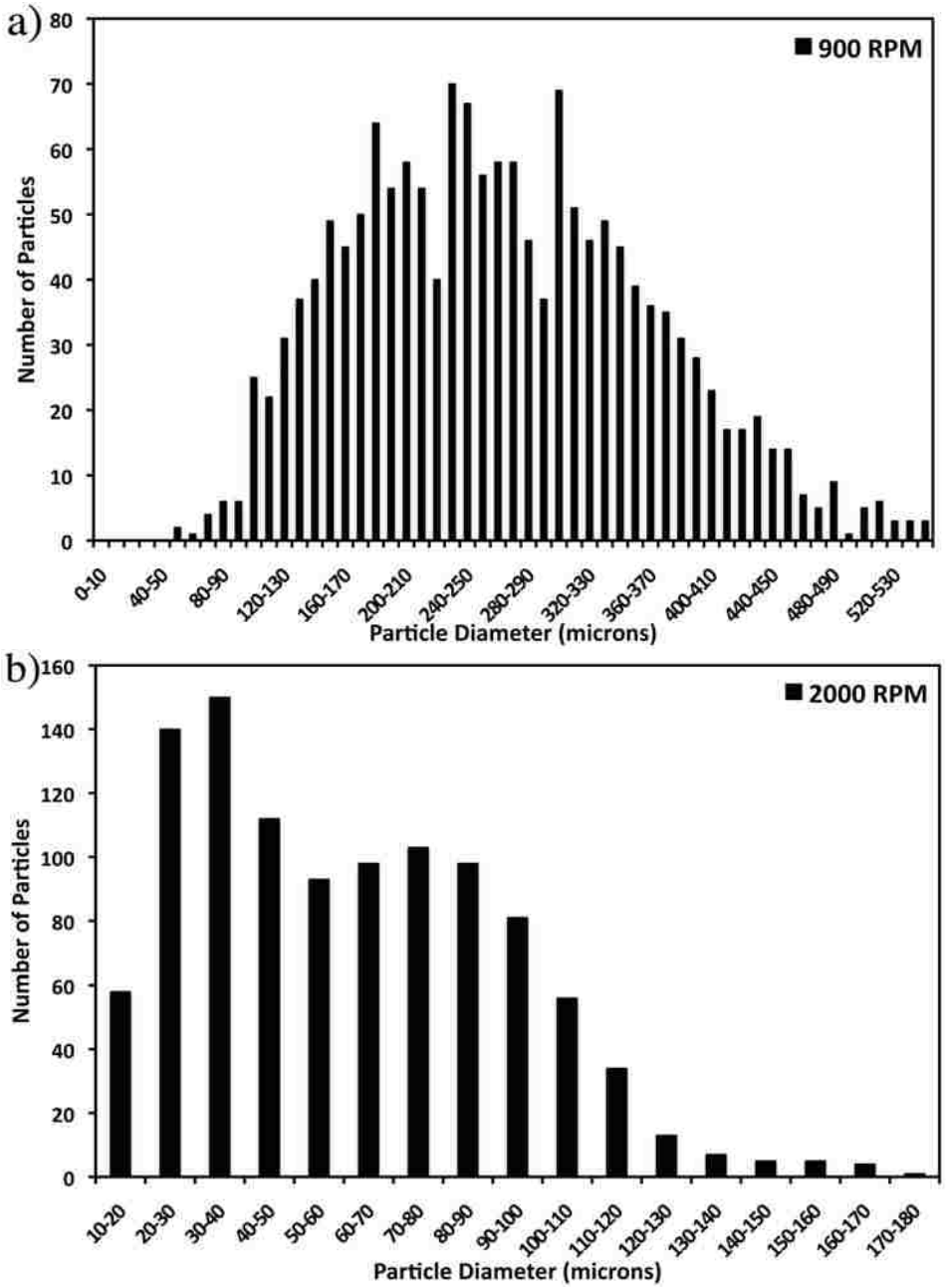

Figure 2-22: Particle size distribution for solid BCl_3-amine microparticles at a) 900 RPM and b) 2000 RPM. All particle size data were collected via optical microscopy and particle size analysis software.

Figure 2-22a illustrates the particle size distribution data for BCl_3-amine microparticles stirred initially at 900 RPM. These data illustrate that the average particle

size was 268.3±98.2µm for this stir rate. Figure 2-22a also shows a relatively broad and sporadic distribution where the smallest measured microparticle was 57.7µm and the largest measured microparticle was 646 µm. These data indicated that 89% of the microparticles were between 100-400 µm when agitated at initially at 900 RPM.

Figure 2-22b illustrates the particle size distribution data for BCl_3-amine microparticles stirred initially at 2000 RPM. These data illustrate that the average particle size was 62.4±31.5µm for this stir rate. Figure 2-22a also shows a somewhat weighted distribution where the smallest measured microparticle was 13.0µm and the largest measured microparticle was 179.2µm. These data showed that 83% of the microparticles were between 200-100 µm when agitated at initially at 2000 RPM.

Table 2-1. BCl_3-amine thiol-acrylate microparticles statistics as a function of stir rate.

RPM	Mean Diameter (um)	Standard Deviation (um)	Maximum Diameter (um)	Minimum Diameter (um)
900	268.3	98.2	645.5	57.7
2000	62.4	31.5	179.2	13.0

Figure 2-23 compares the BCl_3-amine microparticle size distribution data to the control (empty) microparticles size data. The average particle size data for the BCl_3-amine microparticles did not fall into the size range indicated by the data for the empty microparticles; however, the same trends regarding the stir rate, mean diameter, and standard deviation were observed. As the stir rate was increased, regardless of core component, the average particle size decreased as well as the corresponding standard deviation. Control microparticles with an average particle size near 250µm could be prepared with a stir rate of 500 RPM, whereas a higher energy input (900 RPM) was required to obtain BCl_3-amine microparticles with the same average diameter (Figure 2-23). Depending on the core component used, different amounts of applied energy

resulted in different average particle sizes and standard deviations due to the differences in the interfacial tensions between the continuous phase and the mobile phase of the given dispersion polymerization.

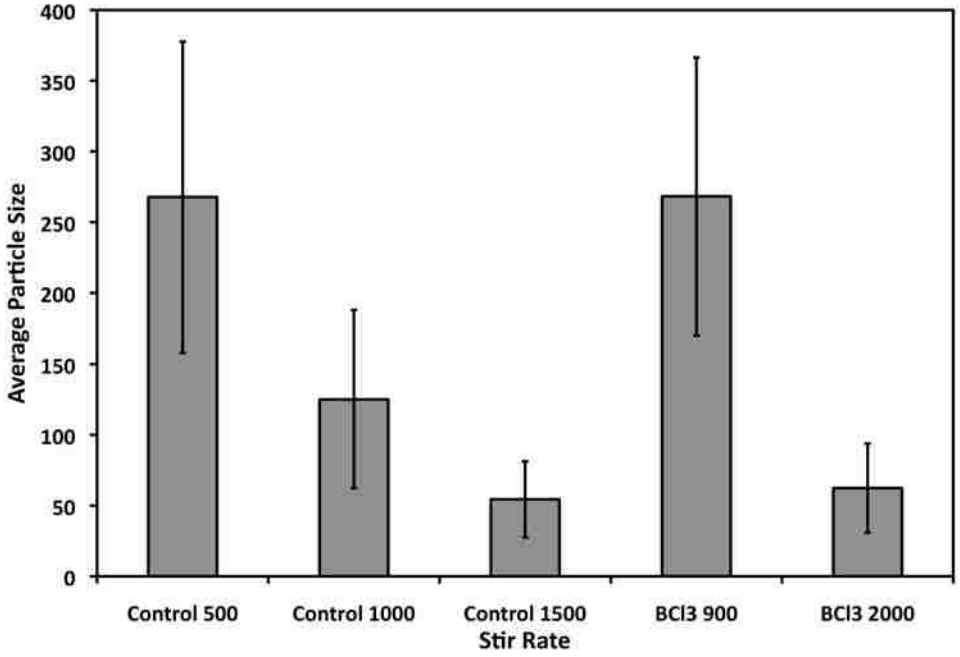

Figure 2-23: The BCl_3-amine microparticles were agitated at 2000 RPM initially and reduced to 1700 RPM once the primary amine catalyst was added.

2.10.5 Core-Loading Percentage

It was vital to know the percentage of core material contained within the microparticle matrix before a valid comparison to be made between systems containing the core in either the dissolved or microencapsulated form. The following formula was used to estimate the core loading percentage.

$$\textbf{Core Loading \%} = \frac{\textbf{Core}}{\textbf{Core + Monomer 1 + Monomer 2}}$$

In this formula, for the BCl_3-amine system, the Core, Monomer 1, and Monomer 2 values corresponded to the amount of BCl_3-amine, TMPTMP, and TMPTA in grams,

respectively. Using this equation, the core loading percent for the BCl_3-amine microparticles was calculated to be 68%.

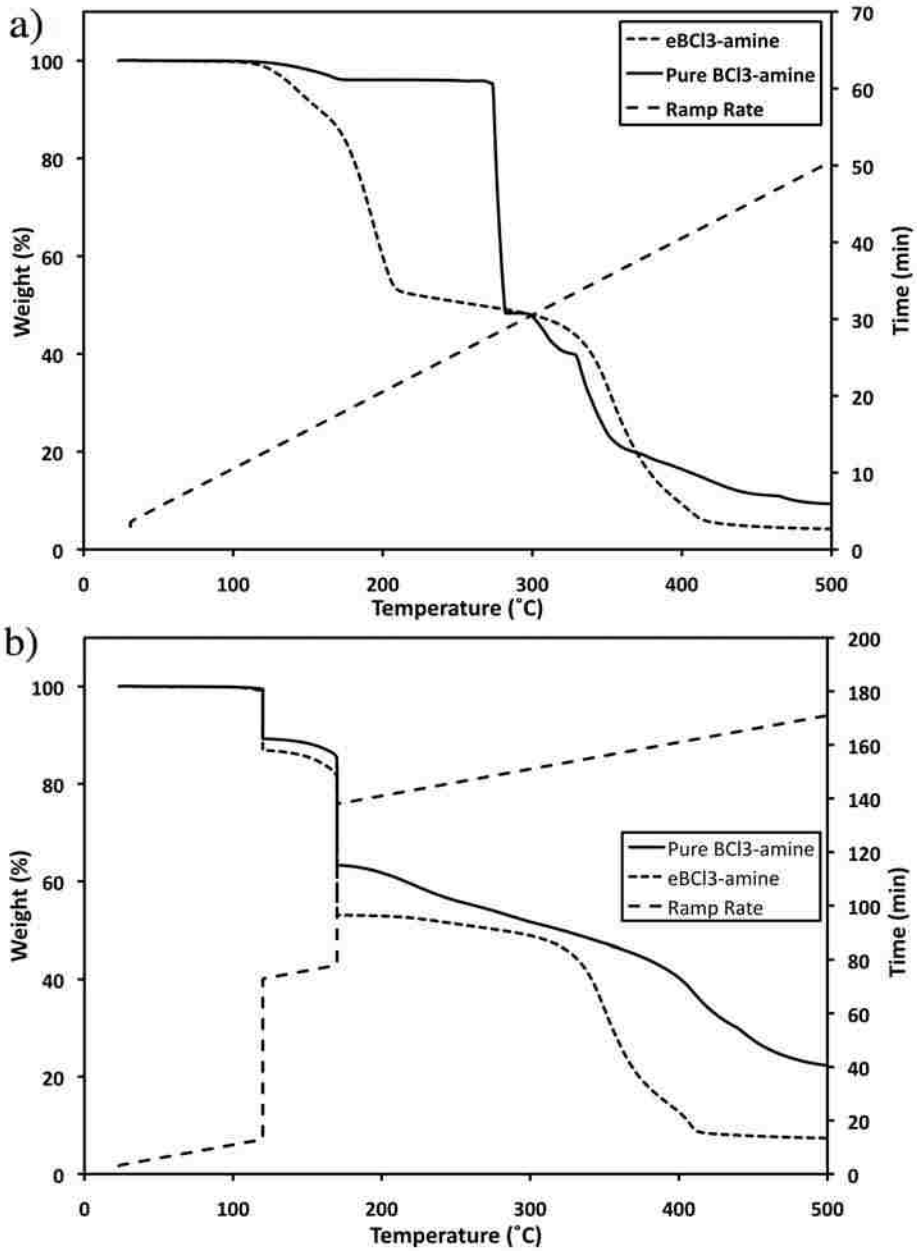

Figure 2-24: Thermal Gravitational Analysis data for BCl_3-amine thiol-acrylate microparticles. a) Encapsulated BCl_3-amine ($eBCl_3$-amine) and pure BCl_3-amine heated at a rate of 10˚C/min with initial weights of 3.403 mg and 7.776 mg, respectively. b) Encapsulated BCl_3-amine ($eBCl_3$-amine) and pure BCl_3-amine heated at a rate of 10˚C/min and held at 120˚C for one hour and again at 170˚C for one hour with initial weights of 7.497 mg and 7.595 mg, respectively. The heating rate is also added to show correlation between the heat and the weight loss.

The theoretical formula was assumed to be reliable if all of the components used in the process were immiscible in the continuous aqueous phase because any excess materials, either unencapsulated core or unreacted monomer, would be easily observed due to the formation of a separate layer from the filtered aqueous phase in which they would be immiscible. The fact that the thiol-acrylate reaction is known to reach high conversion, as explained above, also adds confidence to this method of estimating the core loading percentage. However, because the above formula technically provides only the theoretical core loading if all of the components in the system were *completely* immiscible in water, thermal gravitational analysis was performed on microparticles containing BCl_3-amine (Figure 2-24) to validate this method of estimating the core loading percent.

From the TGA data in Figure 2-24, the core loading percent appeared to be ~50%. This indicated that the theoretical equation was reasonably close to the experimental result. The lower core loading percent indicated by the TGA could be attributed to the slow release of the core component over time. Some of the core BCl_3-amine could have been trapped within the polymer matrix preventing its volatilization even at the elevated temperature. In order to confirm that the weight loss can be attributed only to the loss of the core material, the TGA data in figure 2-24b illustrate both the pure and microencapsulated BCl_3-amine heated and held at both 120˚C and 170˚C for 1 hour each. These temperatures were chosen to insure that the microparticles were free of water and because BCl_3-amine complex completely dissociates below 170˚C.[113] At the 170˚C point it can be observed that there was a steady loss of weight followed by relatively no weight loss until about 350 ˚C at which

time the polymer matrix began to decompose. Both the data received from the TGA and the theoretical equation were considered when determining the core loading percent, and from these data, it was concluded that the core loading percent for the BCl_3-amine microparticles was ~60%.

2.10.6 Improvement of Rheological Properties

Once the core loading percentage was determined, the BCl_3-amine microparticles were applied to two epoxy systems in an attempt to improve the rheological properties of the resulting systems prior to polymerization. The rheological data obtained can be observed in Figures 2-25 and 2-26. In can be deduced from these figures that the microencapsulation of the BCl_3-amine complex in a thiol-acrylate matrix was successful.

2.10.6a Trimethylolpropane Triglycidyl Ether

Preparation of TMPTGE Samples for Rheology Testing

Trimethylolpropane triglycidyl ether samples containing silica and dissolved BCl_3-amine, microencapsulated BCl_3-amine or no BCl_3-amine were prepared to examine the rheological benefit associated with separating the silica and BCl_3-amine via microencapsulation. Initially, 10 grams of TMPTGE was placed in a vial and heated in a water bath at 50°C for 20 minutes to decrease the viscosity. Next, 7.5 phr (parts per hundred resin) silica (Aerosil 200) was dispersed in the TMPTGE. The mixture was then returned to the water bath for an additional 10 minutes, periodically removing and stirring. The mixture was then removed and 10 phr BCl_3-amine was dissolved or dispersed (1 g dissolved or 1.54 g microparticles to compensate for matrix material). The vials were then capped and stored for varying periods of time. Viscosity as a

function shear rate was determined at a constant temperature of 25°C with the rheometer gap set at 500 μm.

TMPTGE Rheological Properties

Depending on the concentration of the fumed silica in a given system, different rheological properties (shear thickening, shear thinning or even thixotropic) can be observed. High concentrations of fumed silica can cause shear thickening to occur.[114] In the case illustrated in Figure 2-25 where trimethylolpropane triglycidyl ether (TMPTGE) was the epoxy resin used, a higher concentration of fumed silica was used than would normally be incorporated into a commercial formulation. This was done in order to amplify the effect of the interaction between the BCl_3-amine and the fumed silica. The curves in Figure 2-25a therefore present a shear thickening effect.

It can be noted in Figure 2-25 that the curves corresponding to the system containing encapsulated BCl_3-amine were much more similar to the control system (no BCl_3-amine) than those corresponding to the systems containing the dissolved BCl_3-amine. As the rotational velocity was increased on the control systems (no BCl_3-amine), the viscosity was observed to display a shear thickening effect after ~3 RPM. The systems containing the microencapsulated BCl_3-amine followed a very similar shear thickening trend with a less intense increase in the viscosity after ~3 RPM of rotational velocity. The systems containing the dissolved BCl_3-amine were observed to act initially with a similar trend until ~3 RPM. At this point, instead of the shear thickening effect, the system stabilized with a constant viscosity well below that of the control or microparticle systems. The lack of the shear thickening effect of the system containing dissolved BCl_3-amine was caused by the interaction between the fumed

silica and the BCl_3-amine. This interaction rendered the silica useless as an agent to improve the rheological properties of the system.

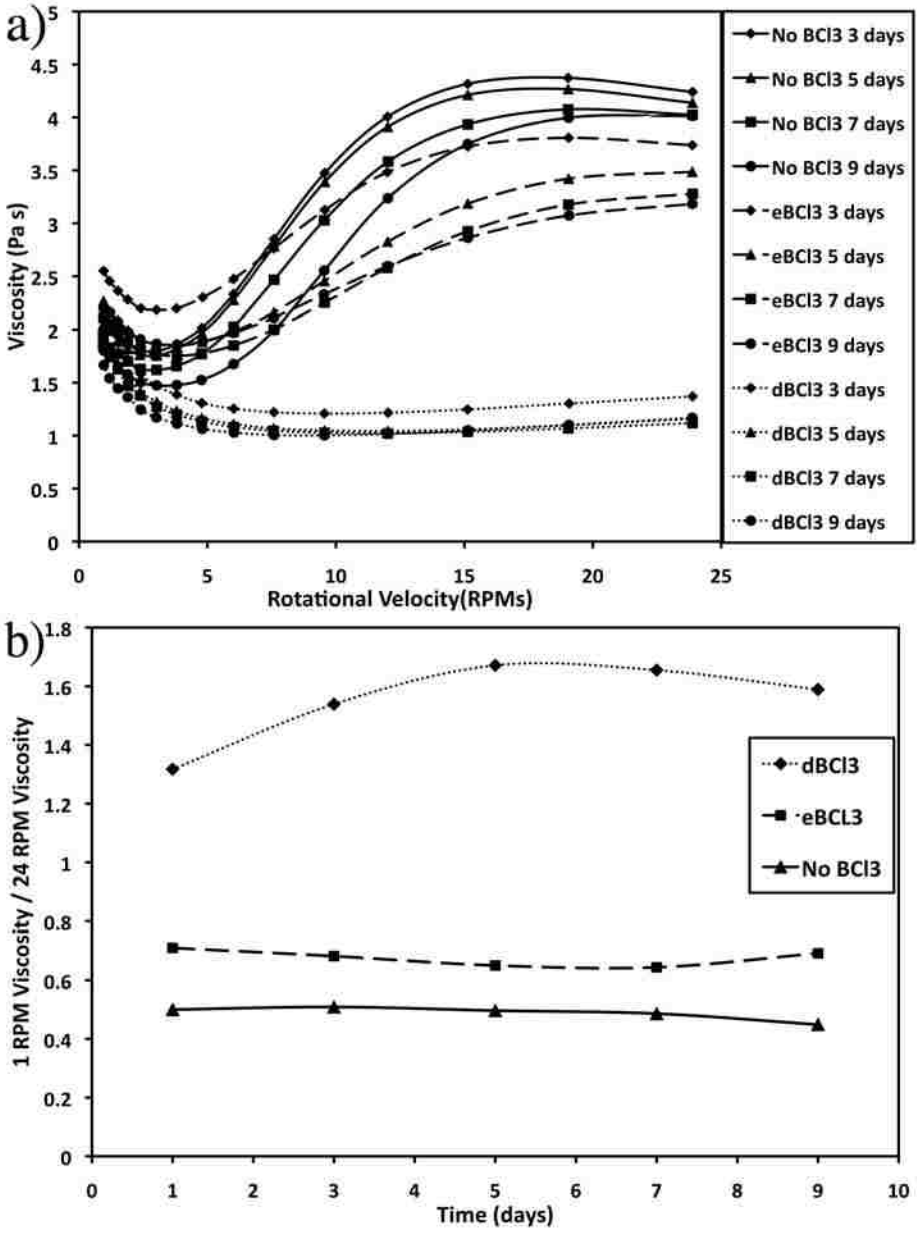

Figure 2-25: Rheology data for TMPTGE systems containing BCl_3-amine complex and fumed silica. Each TMPTGE sample contained 7.5 phr fumed silica and either no BCl_3-amine, 10 phr dissolved BCl_3-amine, or 10 phr microencapsulated BCl_3-amine (calculated based on core-loading). Figure a) illustrates the raw rheometer data of viscosity (Pa s) as a function of rotational velocity (converted to RPM) for different samples over a period of 9 days. Figure b) illustrates the ratio of low viscosity to high viscosity as a function of time for three different types of samples.

The large difference in the rheological properties of the system containing the dissolved BCl_3-amine and the system containing the microencapsulated BCl_3-amine, as well as the similarities between the properties of the latter and the control system indicated that the polymeric matrix prevented the interaction of the BCl_3-amine complex with the fumed silica, allowing for the preservation of the rheological properties of the monomer solution.

2.10.6b Bisphenol A Diglycidyl Ether

Preparation of BADGE Samples for Rheology Testing

Bisphenol A diglycidyl ether samples containing Polygloss 90 (kaolin clay), silica and dissolved BCl_3-amine, microencapsulated BCl_3-amine or no BCl_3-amine were prepared to examine the rheological benefit associated with separating the silica and BCl_3-amine via microencapsulation. Initially, 10 grams of BADGE was placed in a vial and heated in a water bath at 50°C for 20 minutes to decrease the viscosity. Next, 1.5 phr silica (Aerosil 200) and 1.5 phr Polygloss 90 were dispersed in the BADGE. The mixture was then returned to the water bath for an additional 10 minutes, periodically removing and stirring. The mixture was then removed and 3 phr BCl_3-amine was dissolved or dispersed (0.3 g dissolved or 0.5 g microparticles to compensate for matrix material). The vials were then capped and stored for varying periods of time. Viscosity as a function shear rate was determined at a constant temperature of 25°C with the rheometer gap set at 750 μm.

BADGE Rheological Properties

In order to test the effectiveness of these microparticles in a real world setting, the rheology of a commercially useful bisphenol A diglycidyl ether (BADGE) system was

studied. In this system kaolin clay was also incorporated as additional filler, along with fumed silica (functioned mainly as a thixotropic agent).

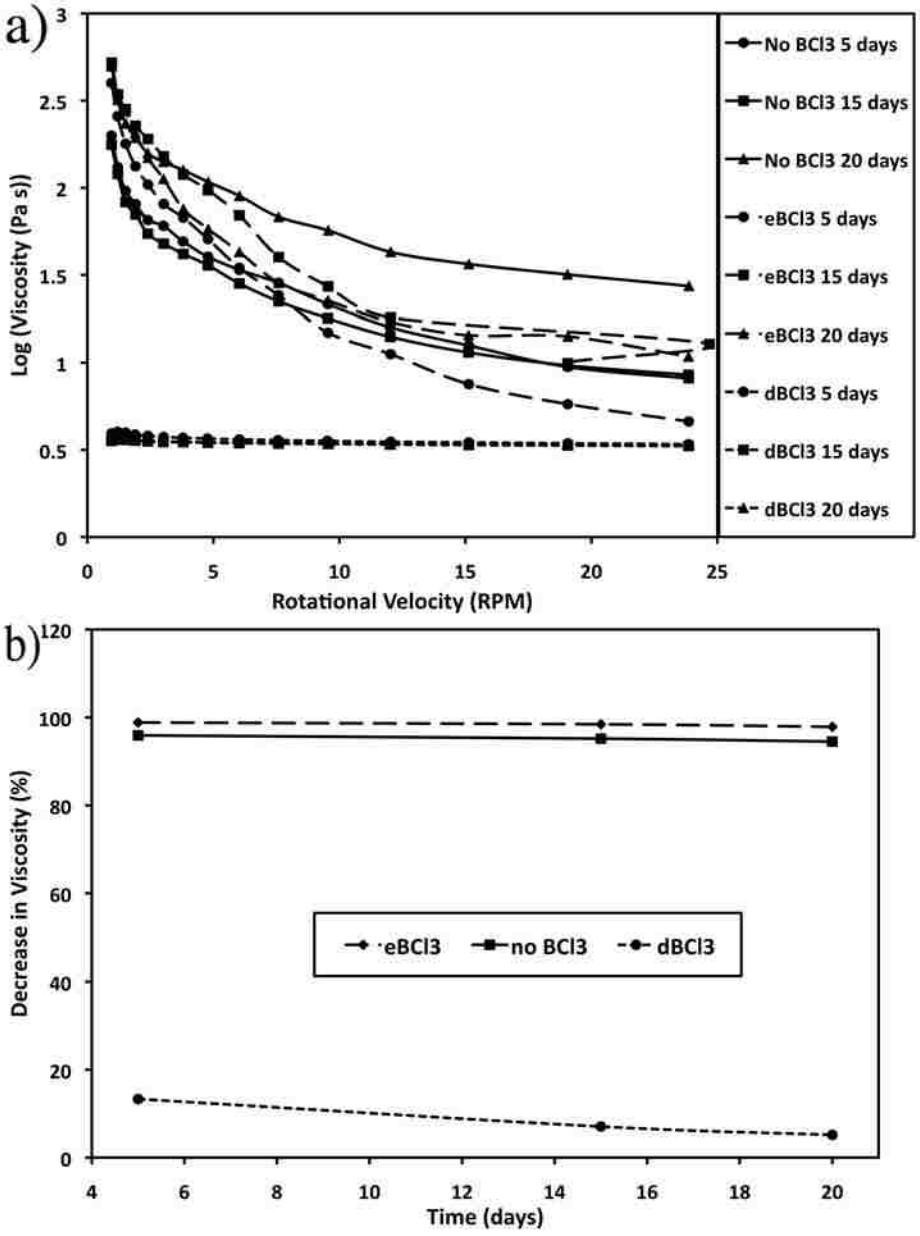

Figure 2-26: Rheology data for BADGE systems containing BCl_3-amine complex, fumed silica, and kayolin clay. Each BADGE sample contained 1.5 phr fumed silica, 1.5 phr Polygloss 90. and either no BCl_3-amine, 10 phr dissolved BCl_3-amine, or 10 phr microencapsulated BCl_3-amine (calculated based on core-loading). Figure a) illustrates the raw rheometer data of viscosity (Pa s) as a function of rotational velocity (converted to RPM) for different samples over a period of 20 days. Figure b) illustrates a comparison of the decrease in viscosity from 1 to 20 RPM as a function of time for the three different types of samples.

Figure 2-26 illustrates the results obtained from this study, and further proves the success of the microparticle systems. Both the control systems (no BCl_3-amine) and the systems containing the microencapsulated BCl_3-amine exhibit a shear thinning effect as a function of rotational velocity and follow almost identical trends (Figure 2-26a). The systems containing the dissolved BCl_3-amine that was available to interact with the fumed silica displayed no signs of a shear thinning effect. Figure 2-26b further proves this point by illustrating the decrease in viscosity from 1 RPM to 20 RPM rotational velocity as a function of time. It can be noted from the curve corresponding to the dissolved BCl_3-amine system in Figure 8b that the interaction became more prominent with time from 5 to 20 days as the percent decrease approached zero. From these studies of the rheology of the two epoxy systems, it was concluded that the thiol-acrylate matrix was successful in separating the core BCl_3-amine from the fumed silica, preventing the undesirable loss in the rheological properties of the monomer systems.

2.10.7 Mechanical Analysis of Epoxy Samples

2.10.7a Preparation of TMPTGE Samples for Instron Testing

Trimethylolpropane triglycidyl ether (TMPTGE) samples containing dissolved BCl_3-amine or microencapsulated BCl_3-amine were prepared to test the relative strength of the sample if BCl_3-amine microparticles were used instead of dissolved BCl_3-amine. The epoxy bars were 7.5 x 2.3 x 1.0 cm. Initially, 20 grams of trimethylolpropane triglycidyl ether (TMPTGE) was placed in an 80 mL beaker and heated in a water bath at 50°C for 20 minutes to decrease the viscosity. After the viscosity was acceptable, 2.5 phr (parts per hundred resin) fumed silica (Cabosil) was dispersed in the TMPTGE. The mixture was then returned to the water bath for an additional 10 minutes,

periodically removing and stirring. The mixture was then removed and 5 phr BCl_3-amine was dissolved or dispersed (1g dissolved or 1.54 g microparticles to compensate for shell material). The mixture was then placed under vacuum to remove the air introduced when stirred. Once the majority of the air had been removed, the mixture was poured into a poly(tetrafluoroethylene) mold and cured in an oven at 170 °C for 1 hour. The epoxy bars were then subjected to Instron strength testing.

2.10.7b Strength Testing of TMPTGE Systems

After determining that the rheological properties of an epoxy system could be maintained via microencapsulation, it was vital to determine if comparable strength data could be obtained using the microparticle systems. The strength of two TMPTGE systems differencing only in the method by which the BCl_3-amine initiator was introduced into the system (ether microencapsulated or dissolved) were compared. Mechanical analysis was performed on epoxy block samples with the same dimensions utilizing the different types of introduction methods. The resulting data are plotted in figure 2-27. In both of the plots in figure 2-27, the systems containing the microencapsulated BCl_3-amine complex on average demonstrated an increase in the respective measurement. The maximum flexure of the systems containing the microencapsulated BCl_3-amine was observed to increase by 23%, and the Young's modulus increased by 16%. The increase in the strength of the samples when BCl_3-amine microparticles were used as opposed to the sample containing the dissolved initiator could be due in part to the matrix material of the microparticles strengthening the material. In order to obtain a substantial increase in the strength of the material, a

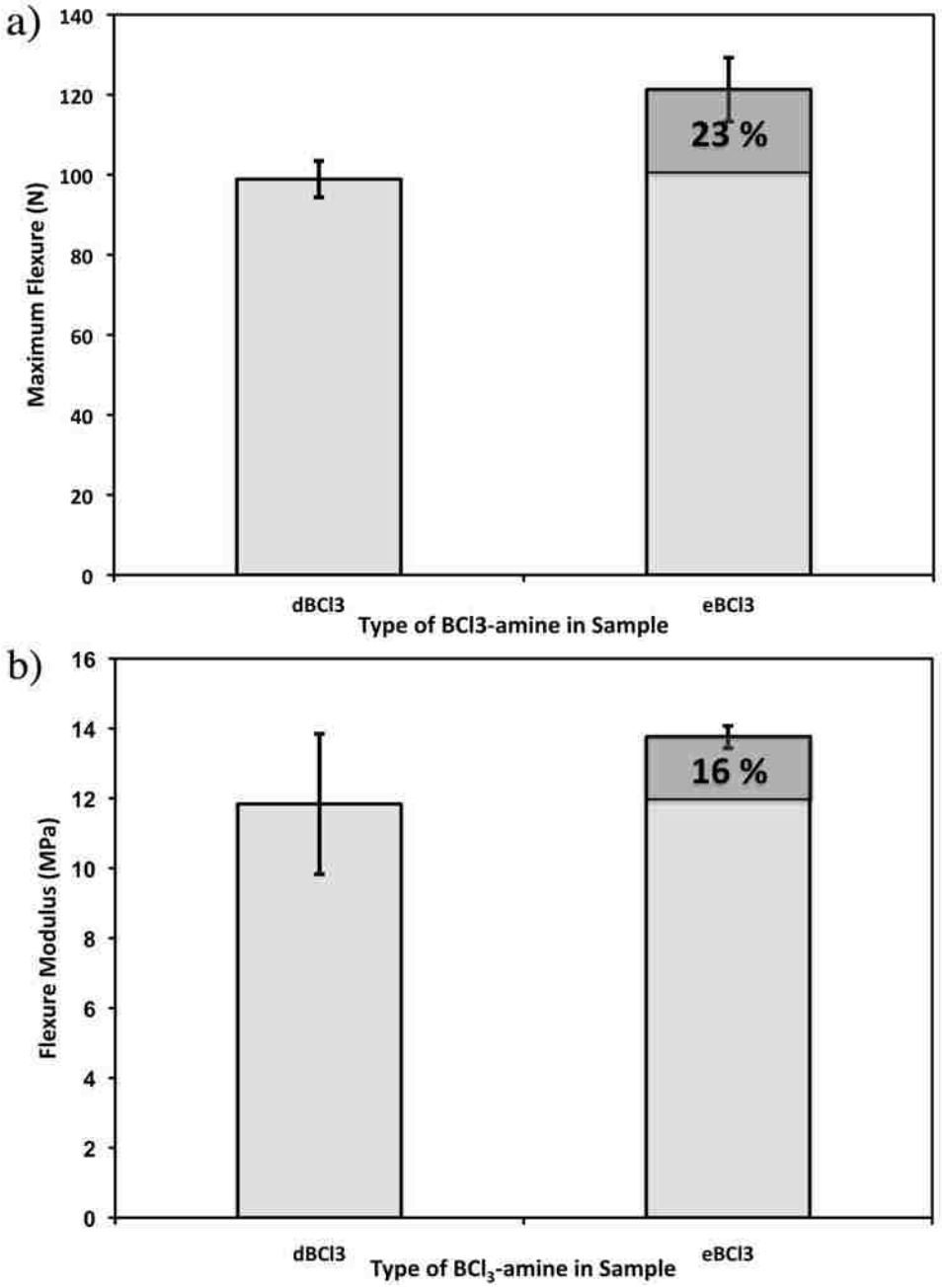

Figure 2-27: Strength data for TMPTGE systems containing BCl_3-amine complex and fumed silica. Each TMPTGE sample contained 2.5 phr fumed silica and 5 phr dissolved BCl_3-amine ($dBCl_3$), or 5 phr (calculated based on core-loading) microencapsulated BCl_3-amine ($eBCl_3$). The figures illustrate (a) the maximum flexure in Newtons and (b) the Young's modulus (MPa) .

sufficiently strong interaction between the microparticles (filler material) and the epoxy matrix would needs to be present[115]. The free thiol groups present on the surface of

the crosslinked polymer matrix due to steric hindrance preventing full conversion could explain this strong interaction. Thiols are known to react with epoxy resins via either a nucleophilic displacement or base-catalyzed addition reaction.[116] If this interaction was occurring, then the microparticles served a dual purpose in separating the initiator from the monomer, thereby preventing undesirable rheological effects, and acting as a strengthening agent to produce a composite material with a thiol-acrylate matrix material as filler. From these data, it was determined that the strength of the epoxy polymer was not negatively affected by the incorporation of the BCl_3-amine in the microparticle form.

2.11 Conclusions

A novel approach to prepare microparticles via a dispersion polymerization using the primary amine-catalyzed addition of a trithiol to a triacrylate has been reported here. Unlike most microcapsules composed of a thin shell containing a liquid core, these microparticles were composed of a solid matrix enveloping pockets of core material. There are many advantages to using nucleophilic primary amine-catalyzed thiol-acrylate chemistry as a microencapsulation method. First, the thiol-acrylate reaction is not affected by oxygen entrained into the system via mixing [5]. Secondly, because the primary-amine catalyzes the Michael addition of a thiol to an acrylate very rapidly[40], this process has an advantage over many other types of microencapsulation techniques as it can be completed in less than one hour, as opposed to many hours or even days. Thirdly, this method can proceed at room temperature[5] as opposed to other microencapsulation techniques that require a reaction temperature of 50 ˚C or higher. Fourthly, as with other microencapsulation procedures and general dispersion

polymerizations, the size of the droplets (mobile phase) can be easily manipulated by the surfactant concentration or agitation rate. Also, the chemistry used to prepare these microparticles is very versatile in that a multitude of different monomers could be incorporated to prepare microparticles with various tunable properties. Finally, the reaction used to prepare these microparticles can be initiated using various sources, which allows for variations in initiation techniques if necessary.

The size of these microparticles was easily manipulated depending on the amount of energy applied to the system. It was determined that this type of microparticles could be used as either a stimulated release or controlled release mechanism depending on core material. These thiol-acrylate microparticles have been prepared containing different initiators and activators including dimethyl-*para*-toluidine, benzoyl peroxide, a borontrifluoride-amine complex, a borontrichloride-amine complex, and carbon nanotubes. Scanning electron microscopy analysis was preformed on the microparticles containing different core materials to determine the effectiveness of the microencapsulation technique relative to the core material. It was concluded that the DMPT microparticles were insufficient due to the leaching of the core material from the microparticle matrix. The BPO microparticles suffered from a lack of sufficient core material or from a lack of effective release of trapped core material. The BF_3-amine microparticles were observed to increase the stability of a highly reactive epoxy-Lewis acid system, however a high level of agglomeration prevented an even dispersion of the microparticles in an epoxy resin. The thiol-acrylate micro- or nanoparticles containing carbon nanotubes require further investigation in order to determine the full benefit of using this method of encapsulation with this particular core. The preparation and

application of microparticles containing one initiator in particular, a borontrichloride-amine complex, was extensively studied. These microparticles were observed to prevent the interaction between the Lewis acid initiator and fumed silica by separating the two components, hence improving the rheological properties of an epoxy system containing the initiator while maintaining the strength of the resulting polymer product.

CHAPTER 3. THIOL-ACRYLATE STABLE HYDROPHILIC MICROFLUIDIC DEVICES

3.1 Chapter Summary

This portion of the document will focus mainly on a novel approach to prepare stable hydrophilic surfaces for possible microfluidic applications where low water contact angles are desirable. Hydrophilic polymer films have been produced with native water contact angles ranging from 10-85˚. The hydrophilicities of these films were tuned depending on the formulation of the sample. These films were prepared via the Michael addition of a secondary amine to a multifunctional acrylate producing a nonvolatile tertiary amine utilized in the catalysis of the Michael addition of a multifunctional thiol to the multifunctional acrylate. There are many advantages of using amine-catalyzed thiol-acrylate chemistry as a method of microfluidic device fabrication. These thiol-acrylate materials can be prepared via a soft lithography method at room temperature, very rapidly, and with little equipment. As discussed previously, thiol-acrylate chemistry is useful because of the wide array of molecules that can easily be attached to- or incorporated into the material to change final properties of the material. This allows for a plethora of post- and bulk-modifications of the material to alter the surface chemistry, including the hydrophilicity. The native thiol-acrylate material is much more hydrophilic than the normally employed PDMS thermoset material, and the surface energy is very stable compared to PMDS. [117, 118] Because the final chip can be self-adhered via a chemical process utilizing the same chemistry, and it is naturally hydrophilic, there is also no need for an expensive oxygen plasma generator or any other equipment or methods to “activate” the surface. Finally, due to the pre-synthesized monomer/catalyst molecule serving as the *in situ* catalyst, there is no need

for post-processing removal of the catalyst as it is incorporated into the polymer network. The material can be prepared using a two-pot system that is easily mixed to prepare the final solution, has a controllable gel time as low as 20 minutes, and tunable mechanical properties.

3.2 Introduction/Background

Microfluidics is a science associated with the processing and manipulation of small amounts of fluids via channels that range from tens to hundreds of micrometers. [119] Entire analytical protocols that have conventionally been executed in full-scale laboratories can be accomplished via miniaturized microfluidic systems. [120] Microfluidic devices, also referred to as micro total analysis systems (μTAS) or labs-on-a-chip (LOC), have recently found applications in areas such as DNA analysis [121-123], protein assays [124, 125], air and water quality evaluations [126], and clinical diagnostics [127, 128]. Some of the obvious benefits of using microfluidic devices are their abilities to use microliter amounts of sample and reagents, their short reaction times, their minuscule analytical footprints, and their small, portable nature which all contribute to their high cost efficiency. [119, 129] Other less obvious characteristics associated with μTAS include their high resolution and sensitivity, better reliability and functionality, a reduced risk of contamination, lower power consumption, laminar flow, and their capabilities of controlling concentrations of molecular species in both space and time. [119, 120] Current technologies allow for a multitude of functions such as pretreatment, sample and reagent transport, reaction, separation, detection, and product collections to be implemented on a single μTAS. [120]

Microfluidic devices are typically prepared using silicon, glass, or polymeric materials. Each of these materials has its advantages and disadvantages. Due to its long history in the semiconductor industry, the highly evolved silicon fabrication technology allows for the production for virtually any geometrical microstructure with high precision and the physical and chemical properties of silicon are well characterized. Silicon microfluidic devices have their limitations, however, due to the poor optical properties of silicon. Silicon is not optically transparent in the UV/visible region, which severely limits its functionality as most bioanalyses are performed in this wavelength range. The commercialization of silicon is also hindered due to the costly fabrication of silicon microchips. [130] Glass improves on the optical properties of silicon, as glass has excellent optical properties in the biomolecule detection range. However, the fabrication of glass microchips via isotropic wet etching is also extremely expensive. [130] Polymers are extremely beneficial microfluidic device materials as many of the chemical, physical, electrical, and optical properties can be manipulated depending on the specific type of material employed. In terms of relative fabrication costs, time, and labor, polymers have become very attractive for use in μTAS. In terms of technological pathways of fabrication, polymeric materials used for microfabrication can be divided into 3 main classes. Thermoset materials are three-dimensional chemically-crosslinked polymer networks. [89] The most discernable aspects of thermosets with respect to microfluidic device fabrication are that thermoset materials do not formally melt but instead burn at elevated temperatures and typically have high glass transition temperatures near the decomposition temperature of the material. Once a thermoset device or material is heated and crosslinked, the materials can no longer

be reshaped upon heating, differentiating them from other microfluidic device materials.[131] Typical thermoset materials used in microfluidic device fabrication are polyesters [132, 133], polyimides [134, 135], and various types of photoresist materials [136]. The second type of microfluidic device material is thermoplastics. Thermoplastic materials are not chemically crosslinked and typically consist of long polymer chain entanglements of amorphous portions and crystalline portions. [89] Unlike thermosets, thermoplastics can be melted and reshaped at elevated temperatures. Thermoplastics show significant and distinct softening at their glass transition temperatures allowing them to be processed near this temperature. Their glass transition temperatures are typically far from their decomposition temperatures allowing for a large processing temperature range. [137] Thermoplastics are likely the most diverse family of materials used for microfluidic device fabrication. Typical thermoplastic materials used in microchip fabrication include poly(propylene)[138], poly(vinyl chloride) [139] poly(styrene) [138], poly(carbonate) [138, 140, 141], poly(methyl methacrylate) [140, 142-147], and cycloolefin polymers/copolymers [148, 149]. The third class of microfluidic polymeric materials is elastomers. Elastomers could be classified in the thermoset microfluidic material category as they are typically crosslinked and cannot be reshaped via temperature treatments. [137] They are in a different class due to their physical and mechanical properties. Elastomers are used above their glass transition temperatures (T_g below room temperature) and demonstrate a viscoelastic property, typically with a low Young's modulus and high yield strain. [89] If an external force acts upon an elastomer, it will deform due to the disentanglement of the polymer chains and reform once the external force is removed demonstrating an elastic-type motion. [137]

The most widely used elastomeric microfluidic material is poly(dimethylsiloxane) [117, 150-156]. Elastomers have become the most common materials used for low-volume manufacturing of microfluidic devices due to their low cost and ease of handing. [137]

Like the traditional glass and quartz substrates, the original fabrication techniques employed to produce microfluidic devices were borrowed from the microelectronics field. [137] Techniques such isotropic wet etching [157, 158], plasma etching [159-161], and laser ablation [162-164] can be extremely expensive especially when coupled with the relatively high cost of substrates such as glass or quartz. Mass production and disposability are therefore not conceivable using these traditional glass or silicon substrate-fabrication technique combinations. Inexpensive polymer substrates and their inexpensive fabrication requirements have become the solution to this high-cost microfluidic device challenge. Photodefinable polymer technologies are commonly used in the fabrication of polymeric microfluidic devices. [137] These processes involve a constructive or destructive reaction of a polymer with light. Photolithography entails a constructive reaction via photopolymerization of a liquid resin in the presence of a photomask resulting in a crosslinked solid thermoset polymer network containing microchannels where the photomask obstructed the UV light from initiating polymerization. [165, 166] One of the most commonly used photolithography materials, SU-8 [167-172], is a liquid photoresist composed of eight epoxy groups that can undergo photoinitiated cationic crosslinking. Limitations of this technique include low structural heights due to physical parameters such as viscosity and limited device throughput due to long preparation times of the resin and other process steps involved. [137] Laser ablation is a form of destructive photodefinable polymer fabrication where a

high-intensity laser beam is used to evaporate material at a focal point. Movement of either the laser beam or the substrate in the x and y direction or the use of a photomask produces the desired microchannel geometry. [162, 173-175] The most economically feasible and broadest microfluidic device fabrication methodology is based on replication methods. [137] The basis for these methods revolves around the replication of a master mold or structure, which is the geometrical inverse of the desired structure. [176] There are a many different methods readily available for the production of a master mold, including silicon etching or photoresist polymerization followed by electroplating [172, 177] and ultraprecision-machined stainless steel masters [172, 178]. Regardless of the technique chosen to prepare the master mold, certain aspects of the mold are necessary as the geometry of the microfluidic device can only be as good as the geometry of the master mold. The mold must be constructed from a material that can be easily removed from the replication material, the surface of the master must be as smooth as possible, and there must be no surface chemistries or exchanges taking place between the mold and the material being replicated. [137] Hot embossing [179-184] is one of the most common replication fabrication techniques used in both academia and industrial applications. Hot embossing involves the heating of both the master mold and the polymer substrate under vacuum to a temperature slightly above the glass transition temperature of the polymer material. The master mold structure is pressed into the polymer substrate with high force at the elevated temperature, and the master and replicated substrate are cooled isothermally to slightly below the glass transition temperature and separated. [179] The process results in the replication of the microstructures from the master mold to the polymer substrate. Microthermoforming

[185-189] is another type of microchannel replication in a polymer substrate. The process involves clamping and sealing of a thin polymer film (usually less than 50 μm thick) into a mold with the microstructures on one side. The film is heated to 10˚C above its glass transition temperature followed by the introduction of compressed gas into the sealed container, forcing the thin polymer film into the master microstructures. The polymer is then cooled to 20˚C below the glass transition temperature and removed, resulting in the replication of the master microstructures onto the polymer substrate film. [190] Another method that is likely the most widespread commercial fabrication process for polymer microfluidic devices is injection molding [156, 191-196]. Because this process requires a comparatively high level of equipment and a complicated process, injection molding is rather limited in the academic world. [192] Granulated polymer material is fed into a hopper that leads to a heated screw transporter where the material is melted and injected under high pressure into a mold containing the microstructures. The mold is then cooled and opened resulting in the rapid replication of the master mold onto the polymer substrate. [192] The injection molding process has the capacity to provide three-dimensional structures, which allow for microartifacts such as fluidic interconnects or through-holes. [156, 197, 198] Injection molding is limited due to the process complexity and the necessity for mechanically complicated molding tools with high-temperature and high mechanical precision capabilities. [137] Casting of elastomeric materials [137, 156, 199, 200] is perhaps the simplest way of replicating microstructures from a mold onto a polymer substrate. This technique, commonly referred to as soft lithography [201-207], is most relevant as the work presented here utilizes this technique. Soft lithography involves

the pouring of a monomer solution (usually an elastomeric-forming monomer and a crosslinker) over a master mold, degassing he solution, polymerizing (curing) at elevated temperatures, peeling the material from the mold, activating the surface, and adhering it to a flat surface, resulting in the final replicated microfluidic device. [137] This method can be used to prepare three-dimensional structures such as mixers [208], valves [209], and pumps [210, 211]. This technique has many advantages including method simplicity, low cost, and replication accuracy. All of the aforementioned techniques are very useful and prominent in the microfluidic fabrication technological field. In terms of industrially pertinent methods, hot embossing and injection molding are the frontrunners, while in academics, elastomer casting (soft lithography) is the principal method. [137]

Soft lithography of PDMS is likely the dominant polymeric material-fabrication technique combination in the field of microfluidics. [212] This is due in part to the many useful properties of PDMS including its elastomeric nature, biocompatibility, gas permeability, optical transparency (down to 230 nm), moldability to submicrometer features, ability to be bonded to itself or glass, chemical inertness, and low cost of manufacturing. [120, 213, 214] Although PDMS has many advantages, it has a natively hydrophobic surface that expresses a water contact angle of ~105˚. [118] This hydrophobicity leads to many limitations especially in the field of biology where the majority of microfluidics is targeted. Cells avoid the hydrophobic surface of PDMS making it very difficult to analyze cellular phenomenon. [215] Proteins adsorb to the surface in a non-specific manner making the native PDMS useless as a method of biomolecular separation assays. [216-218] From an obvious and practical standpoint,

the hydrophobic surface of a PMDS also makes the introduction of aqueous solutions into small microchannels extremely difficult. [212] PMDS, again due to its hydrophobicity, has a tendency to swell in some organic solvents causing difficulty in the analysis of various organic materials. [219] The surface of PDMS can be activated (oxidized) by oxygen plasma or ultraviolet treatments converting the hydrophobic silane-methyl groups to hydrophilic silane-hydroxyl groups. This hydrophilicity is only transient, however, as hydrophobic recovery is observed in as little as a few hours or days.[117, 118] Improvements to the surface of PMDS have recently been realized via a multitude of surface modification techniques [220-227] resulting in stable hydrophilic surfaces. However, a natively hydrophilic material with similar properties to that of PDMS that could be used in a simple and inexpensive soft lithography process could be very useful as no modifications would be necessary to obtain the high energy surfaces achieved via modified PDMS materials.

The need and benefits of thiol-ene chemistry have been realized in the field of microfluidics but have been limited only to photopolymerizable systems. The unique aspects of the thiol-ene step-growth reaction make it superlative for photolithography and microfluidic device fabrication. More distinct photolithographic features can be obtained due to the delay in gel point associated with thiol-ene chemistry. The network uniformity as well as the low shrinkage and shrinkage stress add some homogeneity and thus reproducibility to the final product. The lack of oxygen inhibition facilitated by the thiol provides a less complex procedure where ambient conditions are acceptable. [5] Photoinitiated thiol-ene systems have been used to fabricate microfluidic devices [228-233], modify the surface of microdevices [30], and control the material properties of

microfluidic devices [234, 235]. Good et al used photoinitiated thiol-ene chemistry to prepare a flexible membrane removable lid for a gas tight microfluidic device to separate an effervescent reaction from a sample. [232] Ashley et al prepared microfluidic devices with a range of shapes and aspect ratios via a soft lithography process using photoinitiated thiol-ene and thiol-acrylate chemistries. [233] To prevent the normal instabilities of microfluidic devices in aliphatic and aromatic organic solvents, Cygan et al fabricated organic solvent-resistant microfluidic devices using thiol-ene based resins via a rapid prototyping photolithography technique and quantified and explained their solvent resistance. [229] Natalie et al prepared multilayer thiol-ene microfluidic devices by direct photolithographic patterning and transfer lamination avoiding the necessity for intermediate master molds and stamps. [230] For the work described here, a method of using thiol-ene chemistry is described where all of the advantages associated with photoinduced thiol-ene chemistry were maintained, but the necessity for UV initiation was eliminated. A catalyst/commoner molecule was initially formed via the Michael addition of a secondary amine to a trifunctional acrylate. This resulting molecule was used as an *in situ* tertiary amine catalyst for the Michael addition of a multifunctional thiol to a multifunctional acrylate. By using this *in situ* catalyst pathway, further advantages were added to the already highly advantageous thiol-ene chemistry, especially in terms of biological systems and thus microfluidics. Amine catalyzed thiol-acrylate chemistry was used to prepare stable hydrophilic microfluidic devices in a simple fashion, in less time, and with out the need for expensive materials or instrumentation.

3.3 Materials and Structures

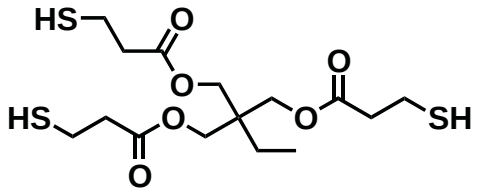

Trimethylolpropane tris(3-mercaptopropionate)

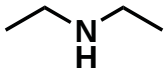

Diethylamine

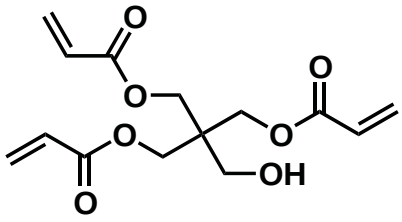

Pentaerythritol triacrylate

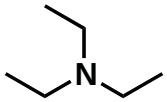

Trimethylamine

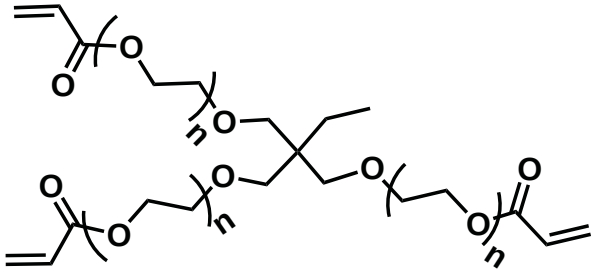

Trimethylolpropane ethoxylated triacrylate

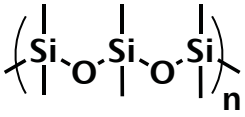

Polydimethylsiloxane

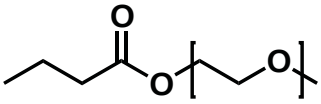

Poly(ethylene glycol) methyl ether acrylate

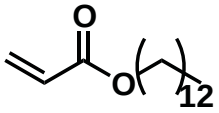

Lauryl Acrylate

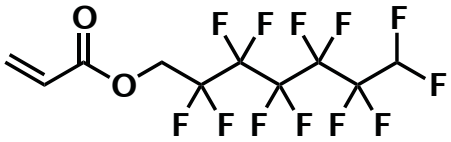

Dodecafluoroheptyl acrylate

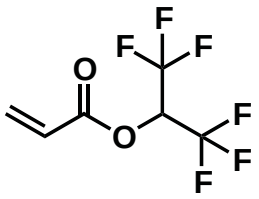

Hexafluoroisopropyl Acrylate

Scheme 3-1: Notable chemical structures for microfluidic device fabrication

All materials were used as received without further purification. Pentaerythritol triacrylate (PETA) was obtained from Sartomer and Sigma Aldrich. The urethane

acrylate (UA) utilized was obtained from Sartomer under the trade name CN929. Trimethylolpropane tris(3-mercaptopropionate) (TMPTMP), diethylamine (DEA), triethylamine (TEA), trimethylolpropane ethoxylated triacrylate 692 (TMPeTA 692), trimethylolpropane ethoxylated triacrylate 912 (TMPeTA 912), poly(ethylene glycol) methyl ether acrylate (PEGMEA), lauryl acrylate (LA), dodecafluoroheptyl acrylate (DFHA), and hexafluoroisopropyl acrylate (HFIPA) were obtained from Sigma-Aldrich. Polydimethylsiloxane was obtained from Dow Corning under the trade name Sylard 184. Structures for notable chemicals are illustrated in Scheme 3-1.

3.4 Generic Soft Lithography Fabrication Process

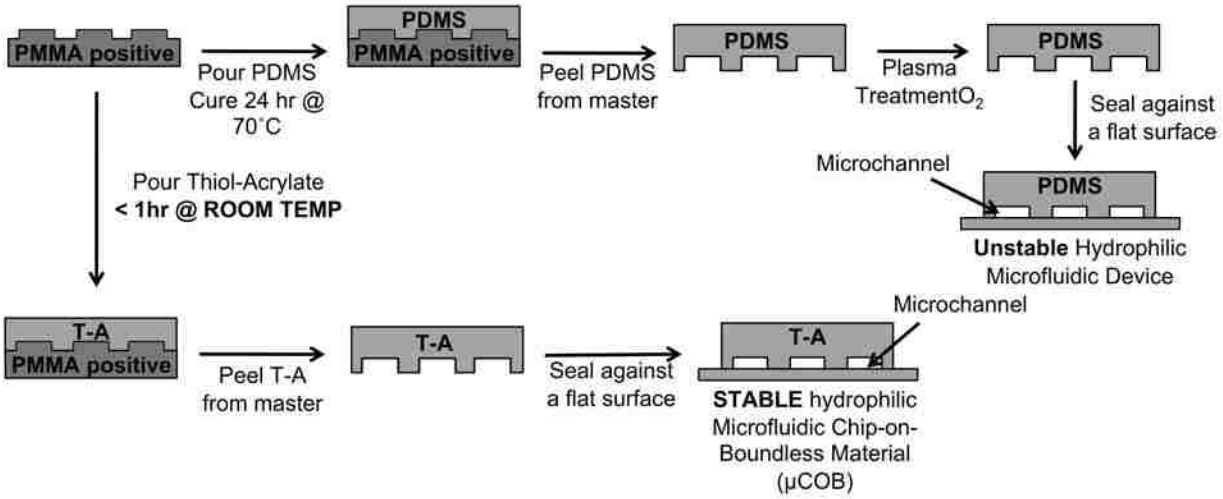

Scheme 3-2: Basic process for soft lithography production of PETA-co-TMPTMP Boundless microfluidic device

Scheme 3-2 illustrates the soft lithography fabrication method used to prepare the thiol-acrylate Boundless microfluidic devices. Also shown here is a diagram for the soft lithography fabrication of a polydimethylsiloxane (PDMS) microfluidic device for comparison purposes [137, 200]. As with PDMS soft lithography, the T-A method is initiated by pouring the liquid thiol-acrylate/catalyst solution onto a poly(methyl methacrylate) (PMMA) positive mold. Unlike the PDMS method that must be heated to

achieve rapid curing (1 hour), the thiol-acrylate method gels in less than 1 hour at room temperature. Next, both the PDMS and the T-A material can be peeled from the PMMA mold to yield a polymer negative. The surface of the PDMS material must then be modified via oxygen plasma for the adhering step and to produce a hydrophilic surface. The Boundless T-A material does not require any further surface modifications due to its native hydrophilicity and its ability to be adhered via the thiol-acrylate polymerization at the interface of the two materials.

3.5 PETA-co-TMPTMP

3.5.1 Experimental Procedures

In Situ Catalyst/Comonomer Preparation

The comonomer/*in situ* tertiary amine catalyst molecule was prepared via the addition of diethylamine (DEA) to Pentaerythritol triacrylate (PETA) in a glass jar or vial containing a stir bar. The jar was then capped, inverted multiple times in a rapid manner, and vigorously stirred on a magnetic stir plate for at least 3 hours prior to use.

Sample Preparation for Contact Angle Measurements

Thiol-acrylate thick film polymer samples were prepared via an *in-situ* base-catalyzed Michael addition of a multifunctional thiol to a multifunctional acrylate. The comonomer/catalyst was added to a stoichiometrically equivalent amount of trimethylolpropane tris(3-mercaptopropionate), taking into account the loss of acrylate functional groups from the initial reaction of the secondary amine and the triacrylate. The mixture was then lightly stirred with a glass stir rod as to not introduce any air bubbles. Once completely mixed to form one homogeneous solution, 5 grams of the solution was poured into a 60 x 15 mm polystyrene petri dish. The system was allowed

to react for 24 hours at room temperature. Once fully reacted, the films were peeled from the petri dishes and the contact angles measured. A 1 µL drop of nanopure water was allowed to equilibrate on the surface for 1 minute prior to measuring the contact angle. Three contact angle measurements at different places on the surface were measured per sample per day to insure homogeneity of the surface and statistical precision. After the measurement, the material was placed back in the petri dish and stored in a lab cabinet.

Sample Preparation for Experimental Gel Time as a Function of Amine Concentration

To determine the gel time as a function of amine concentration, comonomer/catalyst solutions were prepared with varying amounts of DEA. The comonomer/catalyst was then added to a vial containing a stoichiometrically equivalent amount of trimethylolpropane tris(3-mercaptopropionate), taking into account the loss of acrylate functional groups from the initial reaction of the secondary amine and the triacrylate. The mixture was shaken or stirred vigorously for 1 minute. The homogeneous solution was then placed in an inverted syringe attached to anther syringe, which was connected to an air source. Air was bubbled through the solution at a slow rate, and the gel time was determined and documented as the time at which a bubble could no longer travel through the solution (i.e. in the gel state).

Sample Preparation for Experimental Gel Time as a Function of Amine/Acrylate Reaction Time

To determine the gel time as a function of DEA/PETA reaction time, a comonomer/catalyst solution was prepared with a given amount of DEA and vigorously shaken and allowed to stir undisturbed constantly. Periodically, an aliquot was removed

and added to a vial containing a stoichiometrically equivalent amount of thiol, again taking into account the loss of acrylate functional groups. The mixture was shaken or stirred vigorously for 1 minute. The homogeneous solution was then placed in an inverted syringe attached to anther syringe, which was connected to an air source. Air was bubbled through the solution at a slow rate, and the gel time was determined and documented as the time at which a bubble could no longer travel through the solution (i.e. in the gel state).

Sample Preparation for Post-modification

Thiol-acrylate thick film polymer samples were prepared containing a calculated and known excess amount of thiol (e.g. 50% excess thiol) via an *in-situ* base-catalyzed Michael addition of a multifunctional thiol to a multifunctional acrylate. The comonomer/catalyst was added to the calculated amount of trimethylolpropane tris(3-mercaptopropionate) to result in the excess thiol, taking into account the loss of acrylate functional groups from the initial reaction of the secondary amine and the triacrylate. The mixture was then lightly stirred with a glass stir rod as to not introduce any air bubbles. Once completely mixed to form one homogeneous solution, the solution was poured into a mold or petri dish and allowed to react for 24 hours at room temperature. Once prepared, the films were weighed and then fully submerged in a liquid monofunctional acrylate solution containing 1.96 wt% triethylamine. The films remained in the solution for various amounts of time depending on desired result and analysis. After a given amount of time the films were removed, dabbed dry with a clean cloth, and weighed. Further analysis was then applied to the post-modified films.

Sample Preparation for Bulk Modification

Various amounts of monofunctional modifier were added to a vial containing stoichiometrically equivalent amounts of trimethylolpropane tris(3-mercaptopropionate), taking into account the loss of acrylate functional groups from the initial reaction of the secondary amine and the triacrylate as well as the amount of acrylate present from the monofunctional acrylate modifier. The percent of monofunctional small molecule modifier added and documented was calculated based solely on the acrylate content (by functionality). The TMPTMP and monofunctional acrylate were lightly stirred with a glass stir rod until a homogeneous solution resulted. The acrylate comonomer/catalyst was then added at the end and again stirred with a glass stir rod until a homogeneous solution resulted, taking care not to introduce any air bubbles into the sample. The sample was poured into a mold or petri dish and allowed to polymerize for ~24 hours prior to analysis.

Sample Preparation for 3-point Bending

The comonomer/catalyst was added to a stoichiometrically equivalent amount of trimethylolpropane tris(3-mercaptopropionate), taking into account the loss of acrylate functional groups from the initial reaction of the secondary amine and the triacrylate. The mixture was then lightly stirred with a glass stir rod as to not introduce any air bubbles. Once completely mixed to form one homogeneous solution, the solution was poured into a 4 cm x 16.5 cm x 0.55 cm collapsible mold constructed using wood, wax paper, PMMA blocks, and metal screws. The strengths of the samples were then analyzed via a 3-point bending method obtaining the flexure strength and modulus of elasticity.

Sample Preparation for Orthogonal Force Delamination Analysis

Two thiol-acrylate thick film polymer samples were prepared, one containing a calculated and known excess amount of thiol and the other containing a the same known and calculated excess amount of acrylate (e.g. 50% excess thiol or acrylate). The comonomer/catalyst was added to the calculated amount of trimethylolpropane tris(3-mercaptopropionate) to result in the appropriate amounts of excess thiol or acrylate, taking into account the loss of acrylate functional groups from the initial reaction of the secondary amine and the triacrylate. The mixture was then lightly stirred with a glass stir rod as to not introduce any air bubbles. Once completely mixed to form one homogeneous solution, the solution was poured into a 60 x 15 mm polystyrene petri dish and allowed to react for 1 hour at room temperature. After one hour the two films were removed from their respective petri dishes, cut into 2 cm circular disks using a cork borer, and immediately pressed together. A 6 lb weight was applied on top of the adhered samples and remained atop the samples for 24 hours. Once prepared, the adhered samples were fixed between two metal plates via a 5-minute epoxy adhesive. The metal plates were then attached to an instron, and a force was applied at a 90˚ angle to the adhered surface. The stress required for delamination of the adhered thiol-acrylate films was determined.

Sample Preparation for Real-Time Fourier Transform Infrared Spectroscopy

Thiol-acrylate samples containing various concentrations of amine were prepared via the addition of the catalyst/comonomer to a vial containing a stoichiometrically equivalent amount of trimethylolpropane tris(3-mercaptopropionate). The mixture was shaken vigorously for 2 minutes. An aliquot of the homogeneous

solution was then pipetted between two 25 mm x 2 mm Potassium Bromide salt plates and placed in the FTIR sample holder. The instrument was programmed to run a scan at given time intervals (e.g. scan every 2 minutes) until at least 24 hours of reaction time had passed.

3.5.2 Material Dependence on Urethane Acrylate Component

A multifunctional acrylate system was desired for the hydrophilic films and ultimately the microfluidic devices because a product of comparable strength to the presently available products would be essential. Pentaerythritol triacrylate was chosen as the major acrylate monomer because it was hydrophilic enough to produce a hydrophilic product, but not hydrophilic enough to result in a high-swelling hydrogel-type product. Trimethylolpropane tris(3-mercaptopropionate) was chosen because the Michael addition using this trithiol was well investigated by the Pojman Research Team [39, 236, 237] as well as other groups [4, 5, 238, 239]. Also, this trithiol was known to be mostly insoluble in water further preventing the swelling of the resulting product. A trifunctional aliphatic polyester urethane acrylate (CN929) was also incorporated into the initial formulations. This monomer was added originally in an attempt to improve the strength and flexibility of the of the resulting polymer product via the urethane linkage as the PETA product was assumed to be too brittle. The urethane acrylate being used (CN929) was a proprietary compound, thus the true molecular weight was not known from literature. This lack of known molecular weight made it nearly impossible to facilitate the 1:1 molar ratio of acrylate functional groups to thiol functional groups, which was a very important aspect for the success of this chemistry, especially for this particular microfluidic application. Also, the urethane acrylate was highly viscous,

causing problems with mixing as well as with the removal of air from the samples before the gel time, trapping bubbles within the polymer. Because of the associated problems with the urethane acrylate, the true dependence of the hydrophilic polymer materials on the urethane acrylate component was investigated.

The first dependence studied was that of the hydrophilicity of the polymer surfaces. Samples were prepared containing different concentrations of urethane acrylate, including a control sample containing no urethane acrylate. The water contact angles were determined for each of the corresponding samples and the data are illustrated in Figure 3-1.

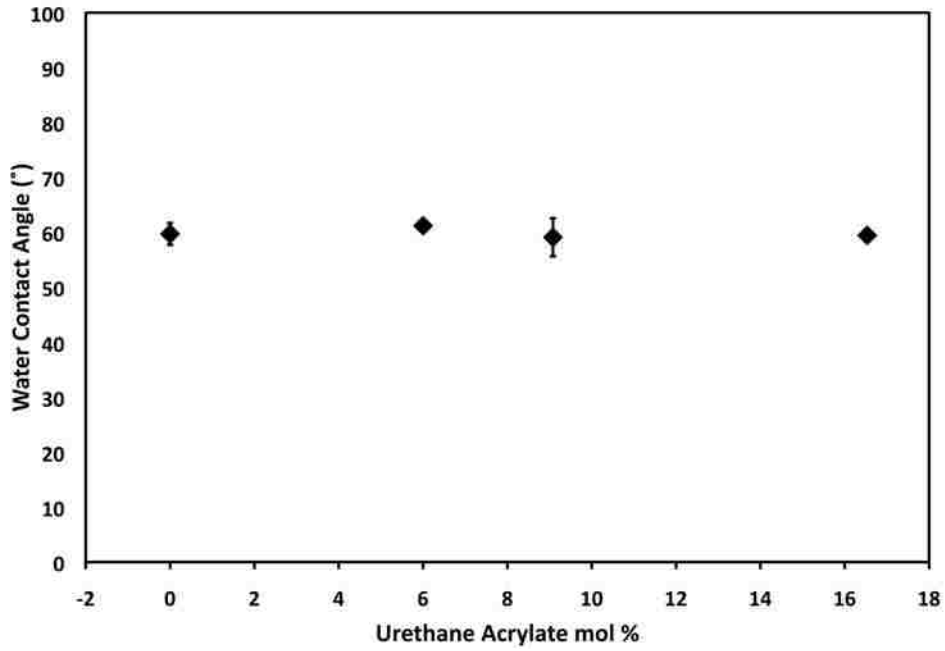

Figure 3-1: Water contact angle as a function of urethane acrylate concentration.

There was no real change in the water contact angle as the concentration of the urethan acrylate component was increased from no urethane acruylate to as much as 17 mol% urethane acrylate. The average water contact angle of the neat PETA-co-TMPTMP material (no urethane acrylate) was found to be 59.7±1.99˚. The material with

the highest studied urethane acrylate concentration (~17 mol%) had an average water contact angle of 59.4±0.60˚. The aveage water contact angles were observed to vary less than 1˚ amoung the 4 different urethane acrylate concentrations analyzed. This result indicated that the urethane acrylate had no affect on the hydrophilicity of the polymer surfaces.

Next, the strength of the thiol-acrylate samples (the original reason for adding urethane acrylate) was tested as a function of urethane acrylate. This was done by preparing samples with varying concentrations of urethane acrylate, and preforming tensile strength analysis. The results of this analysis are shown in Figures 3-2 through 3-4.

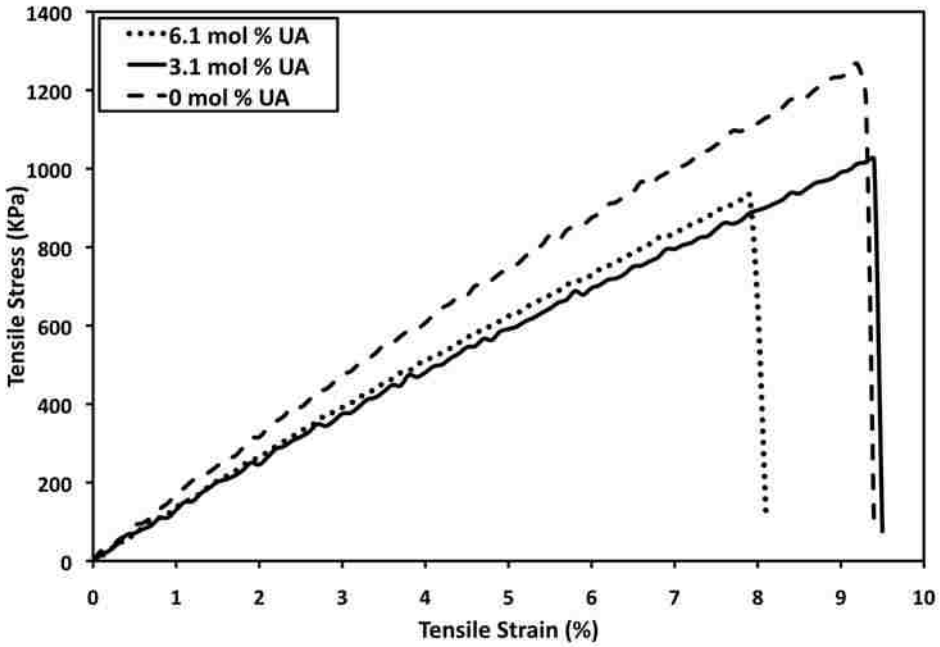

Figure 3-2: Stress strain curve as a function of urethane acrylate molar concentration.

Figure 3-2 illustrates the stress-strain curves for the different samples contianing various amounts of urethane acrylate. At first glance, the sample containing no urethane acrylate appeared to be the strongest as it could handle a higher stress and

appeared to strain comparibly well to the sample containing 3.1 mol% urethane acrylate. However, to confirm this, the actual values for the maximum stress and maximum strain at the breaking point as well as the modulus of elasticity were compared as shown in Figures 3-3 and 3-4.

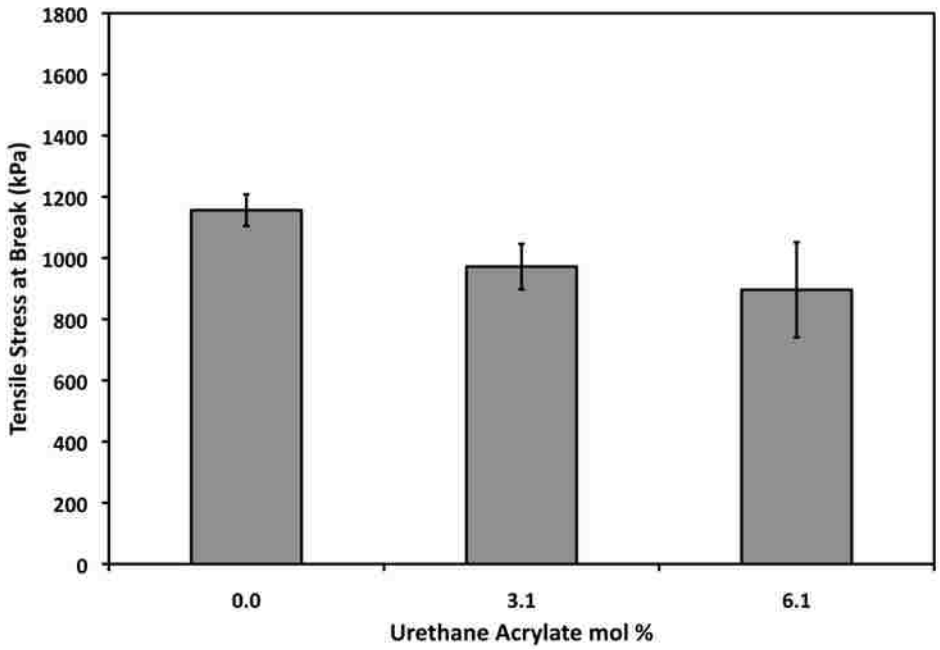

Figure 3-3: The maximum tensile stress at the breaking point as a function of urethane acrylate molar concentration.

Figure 3-3 illustrates the amount of stress that the samples could endure before failure. The samples containing no urethane acrylate were observed to be the strongest in terms of maximum stress. In fact, the maximum stress was observed to be indirectly related to the urethane acrylate concentration. The average tensile stress at break for the neat samples containing no urethane acrylate was found to be 1150±156 kPa. The materials containing 6.1 mol% UA were found to have an average tensile stress at break of 896±51.7. As the urethane acrylate molar concentration was increased, the maximum stress at the breaking point was observed to decrease.

The next comparison involved the modulus of elasticity. As can be observed in Figure 3-4, both of the samples containing urethane acrylate boasted average moduli of elasticity less than that of the sample containging only PETA. The neat PETA-co-TMPTMP samples containing no UA had a measured average tensile modulus of 16000±310 kPa. The samples containing 3.1 mol% UA and 6.1 mol% UA were found to have average tensile moduli of 12500±425 kPa and 12700±1330 kPa, respectively.

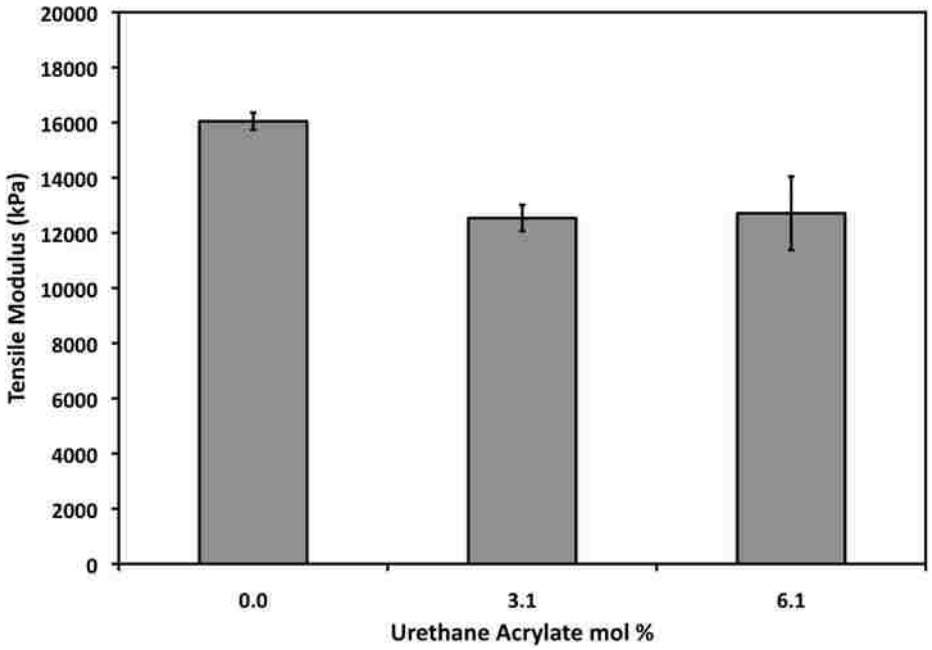

Figure 3-4: Modulus of Elasticity as a function of urethane acrylate molar concentration.

Although the urethane acrylate did reduce the stiffness of the materials to some degree, this was only a small benefit and not enough to justify its use when compared to the larger problematic issues associated with the urethane acrylate. From the strength data, it was concluded that the materials were all very similar in terms of their strengths, and not enough structural benefit was found to justify the use urethane acrylate in the formulation.

The next aspect that was observed in association with the use of urethane acrylate was its effect on the unstirred experimental gel times. The unstirred experimental gel times associated with samples contianing urethane acrylate and samples containing only PETA were compared. The data are illustrated in Figure 3-5.

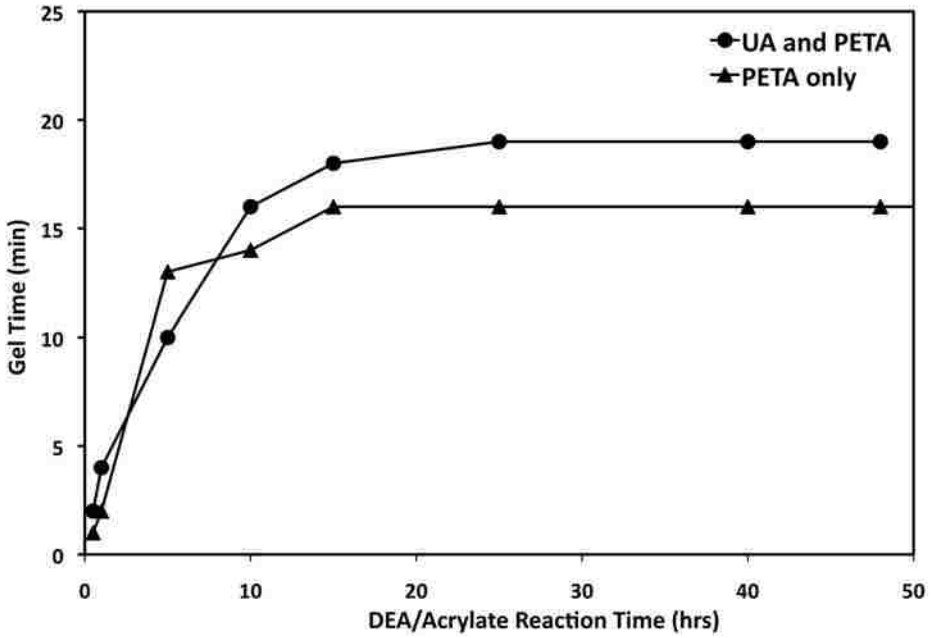

Figure 3-5: A comparison of the gel times as a function of DEA/Acrylate Reaction time for sample with and without urethane acrylte. Both systems contained 15 PHR diethylamine.

The same gel time trend was observed for both systems with or without the urethane acrylate component. The gel time increased as the reaction between the DEA/acrylate approached completion. Also, at this given concentration (15 phr), the final reaction times (after the completion of the intial reaction) for both samples were similar. The final constant reaction times differed by less than 4 minutes. This indicated that the urethane acrylate did not significantly alter the gel time, again showing the lack of necessity for the troublesome component.

Finally, the glass transition temperatures were determined as a function of the urethane acrylate concentration. Figure 3-6 illustrates these data.

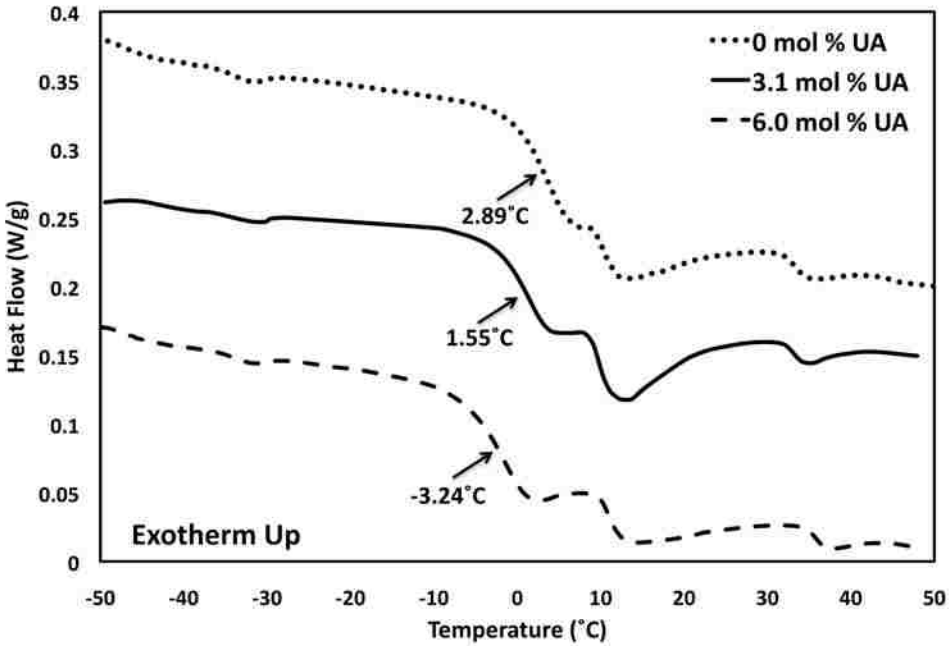

Figure 3-6: DSC showing the major Tg as a function of urethane acrylate.

The glass transition temperatures for the polymer materials were found to all be near zero and differ only by ~6˚C. This result shows that the glass transition temperature did not significantly depend on the composition of the sample with respect to the urethane acrylate component. This DSC data also provide the working temperatures associated with the use of thess polymer materials. These materials could be used at any temperature above 3˚C without performing as a glass.

The high viscosity and the proprietary nature of the urethane acrylate component caused very difficult handling, additional degassing steps, and potentially low conversion products due to stoichiometric issues. The tensile strength analysis illustrated that the urethane acrylate component slightly increased the flexibility of the final product as was expected. However, all other comparative analyses done here and

discussed above showed no benefits in the addition of the urethane acrylate component. From the hydrophilicity analysis, the strength analysis, the gel time analysis, and the thermal analysis, it was concluded that the complexity added by the urethane acrylate component outweighed the small benefits associated with the flexibility of the final product.

3.5.3 Michael Addition to Produce In Situ Bound Catalyst

It was concluded that the complexity added by the urethane acrylate component outweighed the small benefits associated with the flexibility of the final product. It was ideal for the applications of this polymeric material that it be easily produced under ambient conditions. Original samples were prepared using the simple tertiary amine, triethylamine. It was known and well studied [3] that tertiary amines such as triethylamine could act as a base catalyst for the thiol-acrylate reaction as shown in Scheme 1-5. However, original thiol-acrylate film samples prepared using this highly volatile triethylamine had tacky surfaces when allowed to react open to the environment. It was hypothesized that the tacky nature was caused by the evaporation of the small molecular weight and highly volatile triethylamine resulting in low conversion at the surface of the film. To eliminate this problem, a less volatile tertiary amine that would not affect the hydrophilic nature of the product was sought. A secondary amine can act as a strong nucleophile in a Michael Addition reaction with an electron-deficient acrylate. [36] Thus, a secondary amine, diethylamine, was attached to the high molecular weight acrylate (PETA) via a Michael addition resulting in a molecule that could function both as a nonvolatile catalyst and a comonomer containing available

functionality to be crosslinked with the trithiol. Scheme 3-3 illustrates the simple Michael addition reaction scheme.

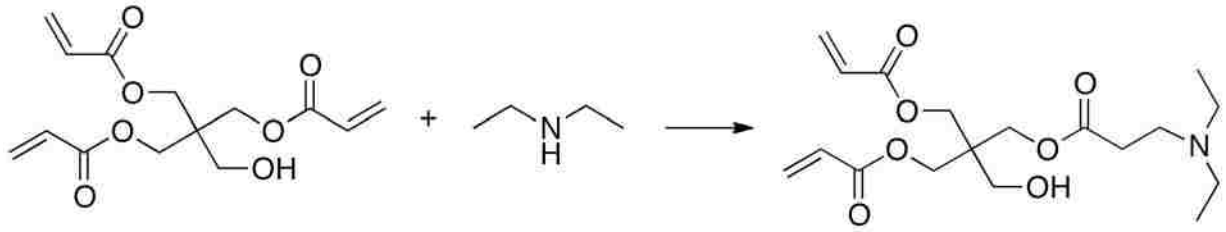

Scheme 3-3: Formation of *in situ* comonomer/catalyst molecule via the Michael addition of a secondary amine to a trifunctional acrylate.

It was important to note that each addition of the secondary amine (DEA) to the trifunctional acrylate (PETA) caused a decrease in the average functionality of the comonomer thiol-acrylate system. With each addition, a trifunctional acrylate molecule became a difunctional acrylate molecule. Because this reaction proceeds via a step-growth mechanism, an average functionality greater than two was required to achieve a crosslinked network. It was therefore imperative that he DEA concentration not reach an upper limit that would result in the decrease of the average monomer functionality to below two.

In order to confirm this reaction and determine the simple reaction kinetics, the reaction conversion was studied as a function of time. The decrease in the acrylate peak of PETA was monitored via NMR analysis. The results are shown in Figure 3-7. Figure 3-7a illustrates the NMR spectrum of PETA alone, while Figure 3-7b shows the spectrum of a mixture of PETA and 20 mol% DEA after 3 hours. The peaks corresponding to the acrylate groups (boxed in Figure 3-7) decreased by ~20% upon the reaction of PETA and DEA for 3 hours. This suggested quantitative conversion of the secondary amine to a tertiary amine catalyst/comonomer molecule via the Michael

addition of diethylamine to the electron deficient acrylate. Virtually all of the secondary amine was converted to a tertiary amine in 3 hours. Because of this result, the diethylamine and PETA were allowed to react for at least 3 hours prior the addition of the trithiol (TMPTMP) and the completion of the final product.

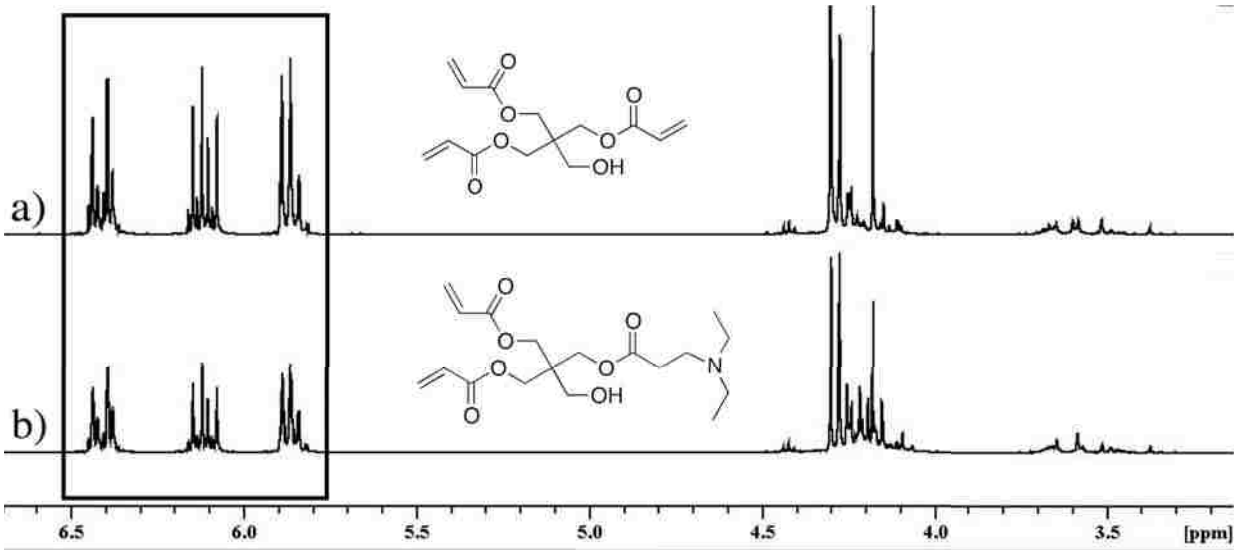

Figure 3-7: NMR spectra showing the loss of acrylate functional groups after 3 hours of reaction time. Spectrum a) represents PETA alone (t_0) and spectrum b) represents PETA containing 19.3 mol% after 3 hours (t_{3hr}) of reaction time. The boxed peaks, corresponding to the acrylate functional groups, decreased by ~20% from spectrum a) to spectrum b).

3.5.4 Addition of the Comonomer/Catalyst to the Multifunctional Thiol

Once the *in situ* catalyst was produced, it was added to the trithiol (TMPTMP) in a stoichiometric 1:1 molar ratio of thiol to acrylate functional groups. This molar ratio accounted for the amount of acrylate groups consumed during the initial Michael reaction with the secondary amine. Thus, the final amount of thiol added to the reaction mixture was not based on the initial amount of acrylate groups incorporated, and the amine concentrations are all given with respect only to the acrylate functional groups and not to the total mixture.

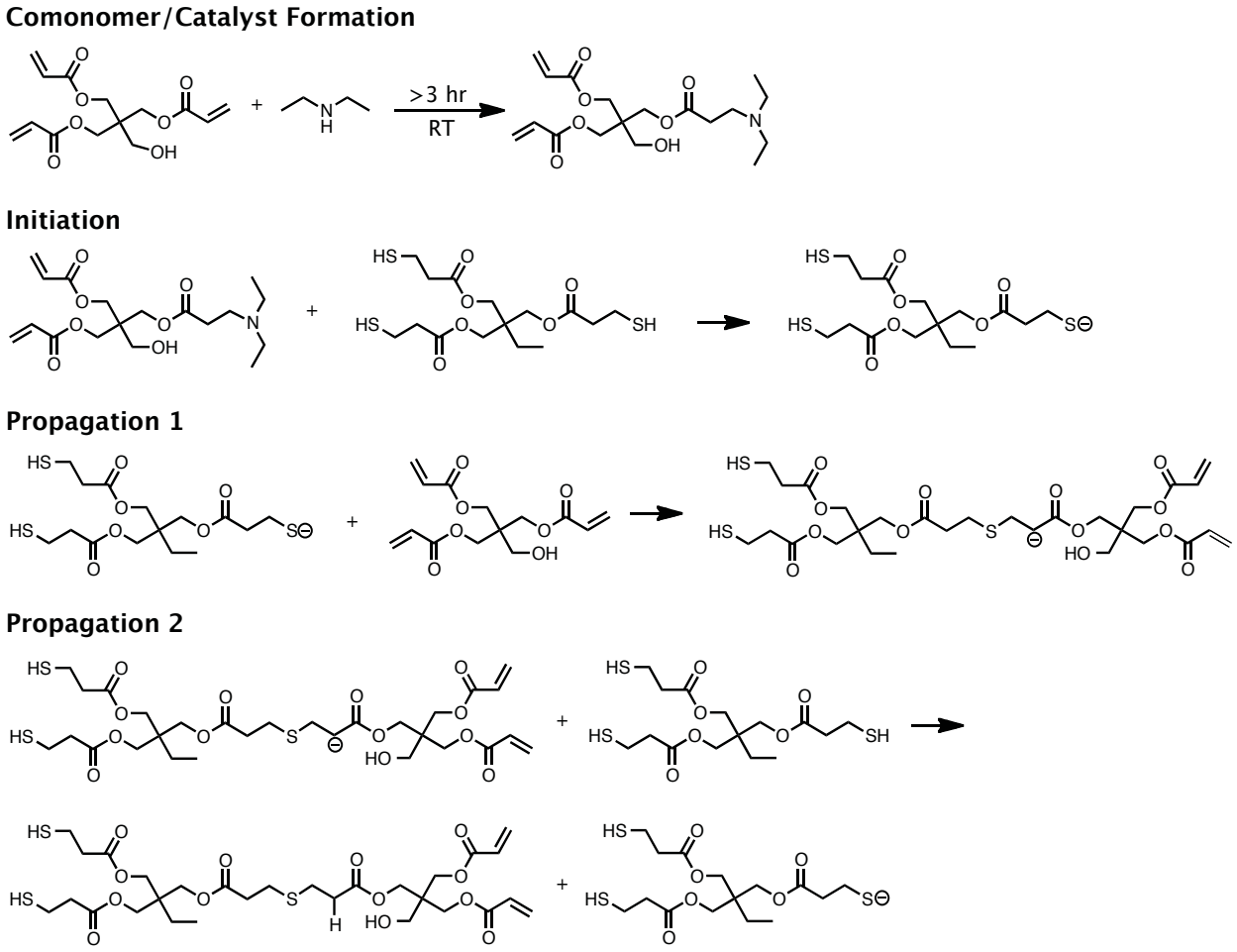

Scheme 3-4: Reaction scheme illustrating the production of the comonomer/catalyst molecule followed by the initiation and two propagation steps of the thiol-acrylate Michael addition.

Scheme 3-4 illustrates the suspected reaction from the initial Michael reaction producing the high molecular weight, non-volatile tertiary amine catalyst to the initiation and propagation of the thiol-acrylate polymerization. The tertiary amine catalyst functioned as a strong base to deprotonate the thiol, resulting in the initiation of the anionic step-growth polymerization mechanism. Two separate propagation steps then followed. The first propagation step involved the Michael Addition of the deprotonated thiyl anion to the electron-deficient ene group. Next, a hydrogen transfer occurred between another thiol and the newly formed carbon anion. This second propagation

step resulted in a chain transfer and another deprotonated thiol that was activated for another Michael Addition. This dual propagation mechanism is the reason that this reaction is considered a step growth polymerization, however it is essentially a chain growth mechanism with a continuously sequential chain transfer step (propagation 2).

3.5.5 Gel Times as a Function of DEA-PETA Reaction Time

The thiol-acrylate experimental gel times were determined as a function of DEA/PETA reaction time. This was necessary to determine the time required to reach high conversion of the nonvolatile tertiary amine prior to the addition of the trithiol. The experimental gel times were in agreement with the NMR data. Figure 3-8 illustrates the gel time curve.

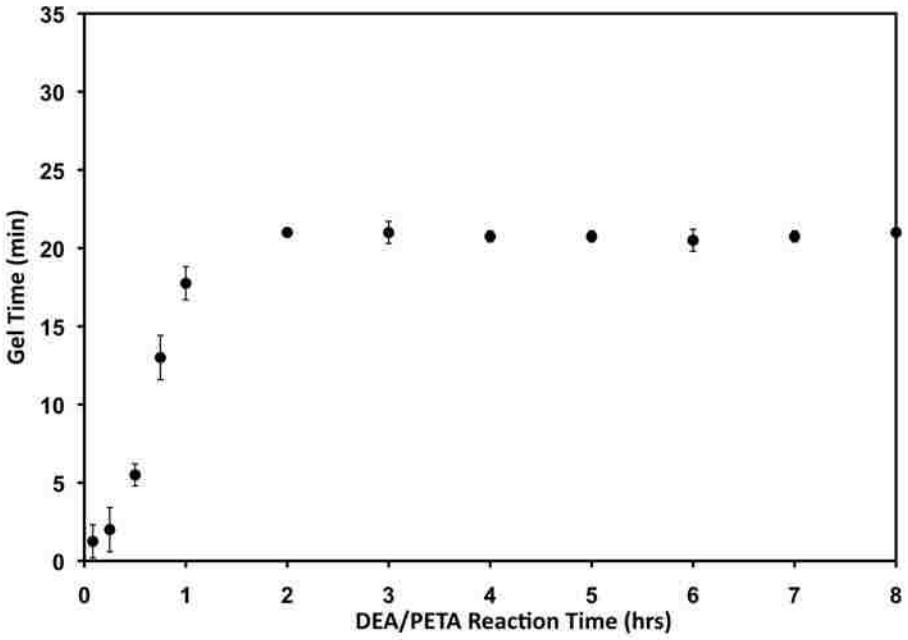

Figure 3-8: Thiol-acrylate gel time as a function of DEA/PETA reaction time. The reaction contained 16.1 mol% DEA relative the PETA functional groups.

Figure 3-8 illustrates the experimental gel time for the thiol-acrylate Boundless material as a function of the elapsed reaction time associated with the initial amine-acrylate Michael addition. The experimental gel time was defined as the point at which

an air bubble could no longer travel through the material via buoyancy-driven force. The gel time increased as a function of the amine-acrylate reaction time until a point after which the gel time stabilized. The increase in the gel time as a function of DEA/PETA reaction time is due to the differences in the catalytic abilities of tertiary and secondary amines [42]. Chan et al have shown that a primary amine or a secondary amine can function as a nucleophilic- and more efficient catalyst for the thiol-acrylate reaction as opposed to a tertiary amine base catalyst.[3] The increase in the thiol-acrylate gel time as a function of time is indicative of a conversion of a secondary amine to a tertiary amine. As the secondary amine was converted to a tertiary amine, the catalyst mechanism shifted from a nucleophilic catalysis to a less efficient base catalysis. Once the gel time reached a steady state, all of the nucleophilic secondary amine had been converted to a tertiary amine base catalyst. According to the experimental gel times, the DEA/PETA reaction was complete in ~2 hours as indicated by the constant gel times reached beyond 2 hours. This further proved, along with NMR data in Figure 3-7, that the initial amine-acrylate Michael reaction did occur, and reached completion in 2-3 hours. Because of the experimental gel time data and the NMR data, each DEA/PETA reaction was allowed to proceed for at least 3 hours under constant stirring prior to the addition of the trithiol.

3.5.6 Manipulation of Gel Times

The thiol-acrylate gel time could be manipulated by varying the concentration of DEA incorporated into the initial Michael reaction. Figure 3-9 illustrates the gel time as a function of initial amine concentration. The manipulated gel times ranged from ~2 hours to <20 minutes within the amine concentration array examined in this study.

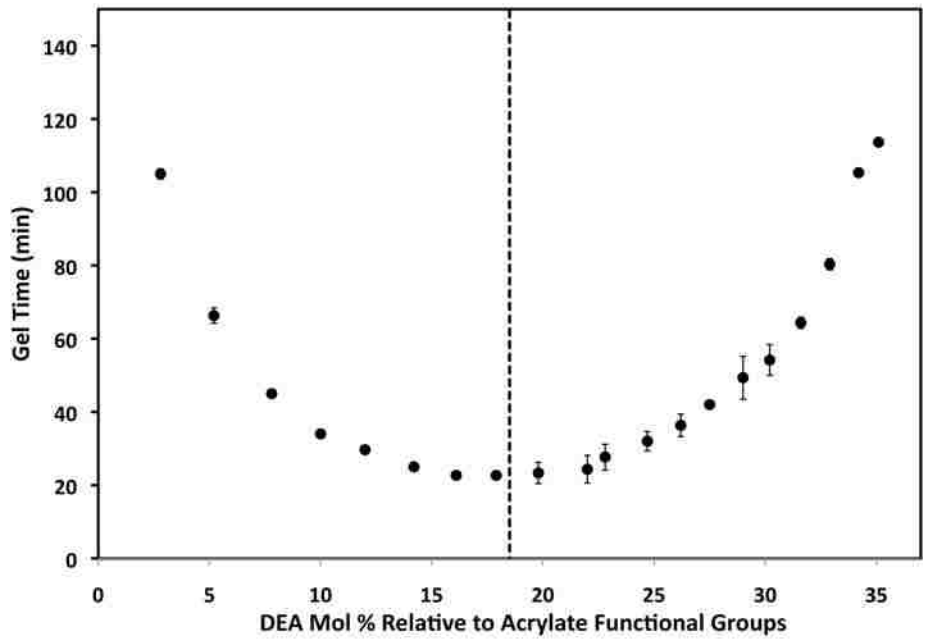

Figure 3-9: Experimental gel time as a function of diethyl amine concentration. DEA concentrations are with respect to the acrylate functional groups only.

The left half of Figure 3-9 conforms to the normally accepted catalyst concentration trend. As the concentration of catalyst was increased, the reaction rate increased causing a decrease in the gel time. However, beyond ~17 mol% DEA, the gel time began to increase, which would apparently indicate an uncommon decrease in the rate of polymerization with an increase in catalyst concentration. It could be argued that this was simply due to a dilution effect; declaring that at some point the catalyst diluted the acrylate and thiol functional groups causing a decrease in the rate of polymerization. It could also be argued that the loss of acrylate functional groups associated with the first Michael addition caused a decrease in the rate of polymerization with an increase in the amine concentration. When the decrease in monomer concentration outweighed the increase in the rate constant caused by an increase in catalyst concentration, the overall rate of polymerization decreased.

However, both of these arguments were falsified via FTIR analysis, and the conversion kinetics of this *in situ* thiol-acrylate polymerization reaction were determined.

3.5.7 Thiol-Acrylate Reaction Conversion and Kinetics

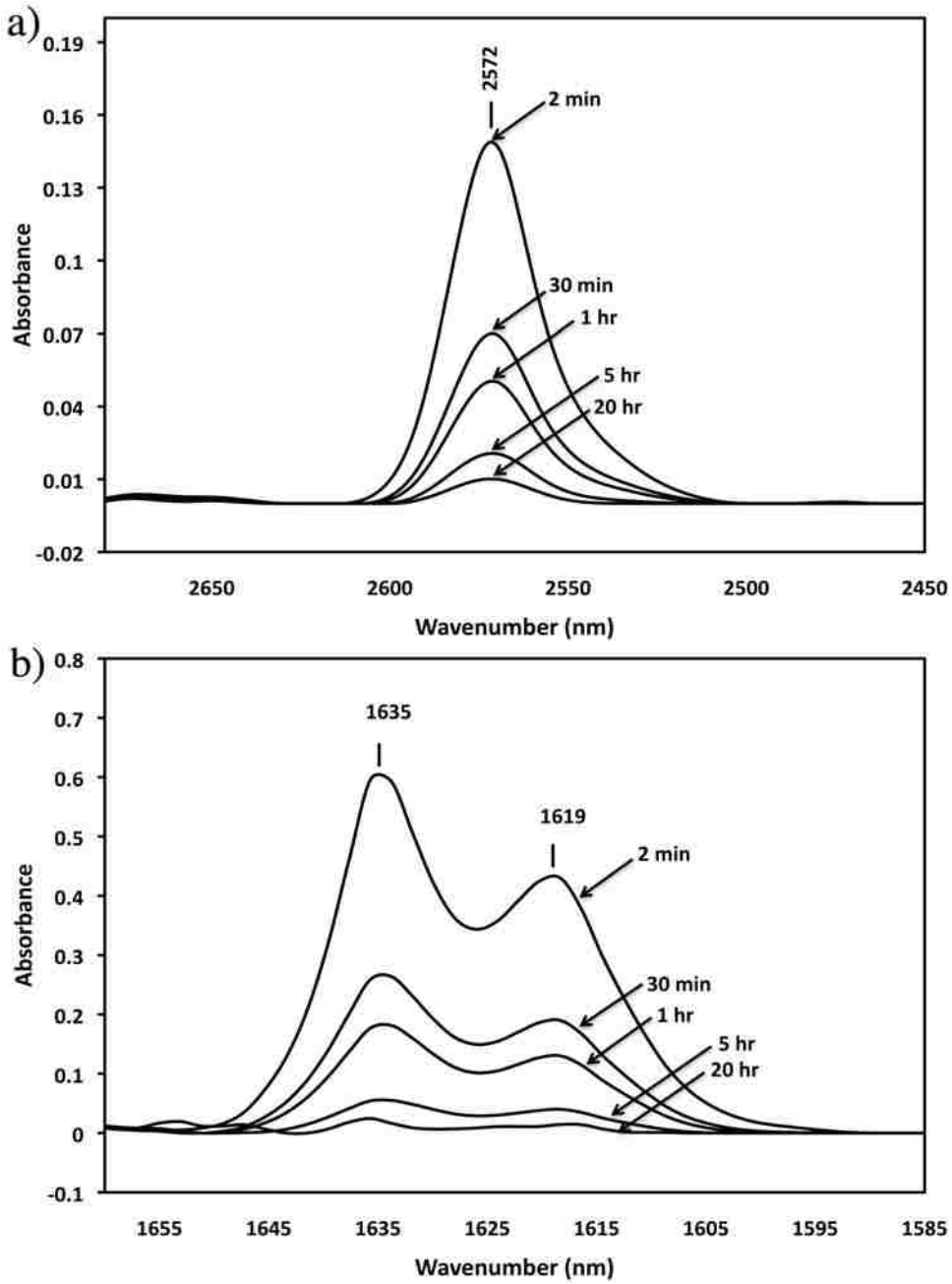

Figure 3-10: The loss in peak area as a function of time for the thiol peak (a) at 2572 nm and the loss in peak areas as a function of time for the acrylate peaks (b) at 1635 and 1619 nm. This system contained 16.1 mol% DEA relative only to acrylate functional groups.

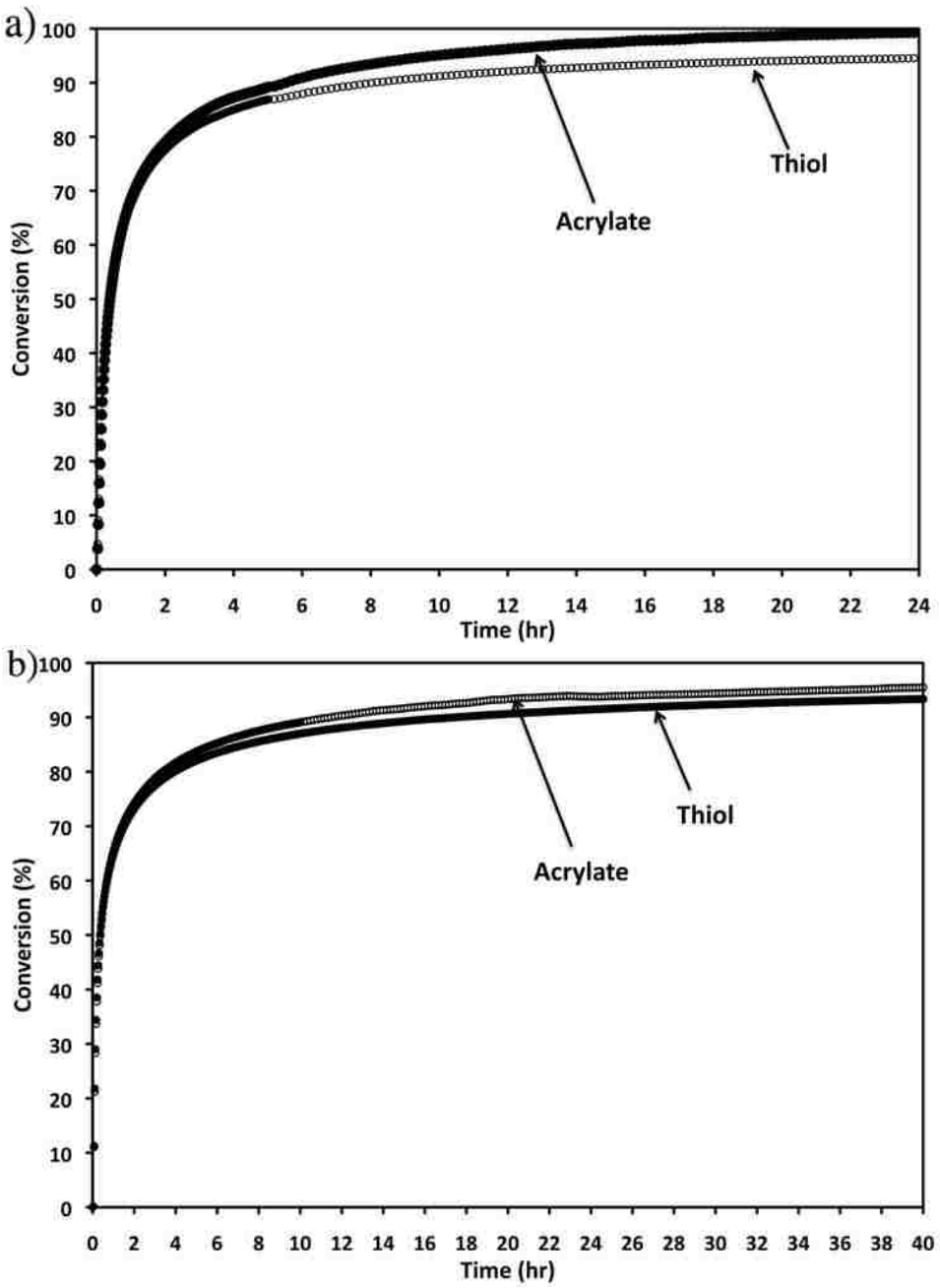

Figure 3-11: Conversion as a function of time for both the thiol (2572 nm) and the acrylate (1635 and 1619 nm) functional groups. a) 16.1 mol% b) 2.8 mol% relative to the acrylate functional groups.

The percent conversion and polymerization kinetics associated with the second Michael addition reaction (thiol to acrylate) were determined via FTIR analysis as a function of real time. Two distinct peaks were monitored as a function of time. The peak at 2572 nm [40, 240] was associated with the thiol functional groups, and the

peaks at 1635 and 1619 nm [40, 240] corresponded to the acrylate functional groups. The decrease in these peak areas as a function of time is shown in Figure 3-10.

The loss in both peaks as a function of time is obvious from Figure 3-10. The percent conversions of the thiol and acrylate groups were determined by monitoring the loss in the peak areas as a function of real time. The thiol-acrylate reaction was allowed to proceed between two salt plates fitted in an FTIR sample receptacle. A spectrum was obtained periodically (~2 min) during the polymerization, and the losses in peak areas were used to calculate the percent conversion. Figure 3-11 illustrates sample conversion data.

When 16.1 mol% DEA was used (Figure 3-11a), both the acrylate and thiol functional groups reached high conversion (>90%) in less than 24 hours. Although more time was required, the system containing only 2.8 mol% DEA (Figure 3-11b) also reached >90% conversion. The actual conversion was likely higher than indicated by Figure 3-11 as a "true" initial peak areas could not be adequately determined due to the time lost from mixing the thiol and acrylate and preparing the sample between the salt plates prior to the first scan. High conversion is a typical and very important property of these cationic thiol-acrylate reactions due in part to the lack of a termination step.[5] This high conversion is useful for any biological application (such as microfluidics) as there is no need to remove excess and potentially harmful monomer impurities from the final product.

3.5.8 Gel Time Analysis Via FTIR

To address the unusual gel time observation as a function of DEA concentration previously addressed (Figure 3-9), the thiol-acrylate kinetics were studied as a function

of amine catalyst concentration. Thus, FTIR studies were performed as a function of real time using systems with various concentrations of amine catalyst. Figure 3-12a illustrates these data.

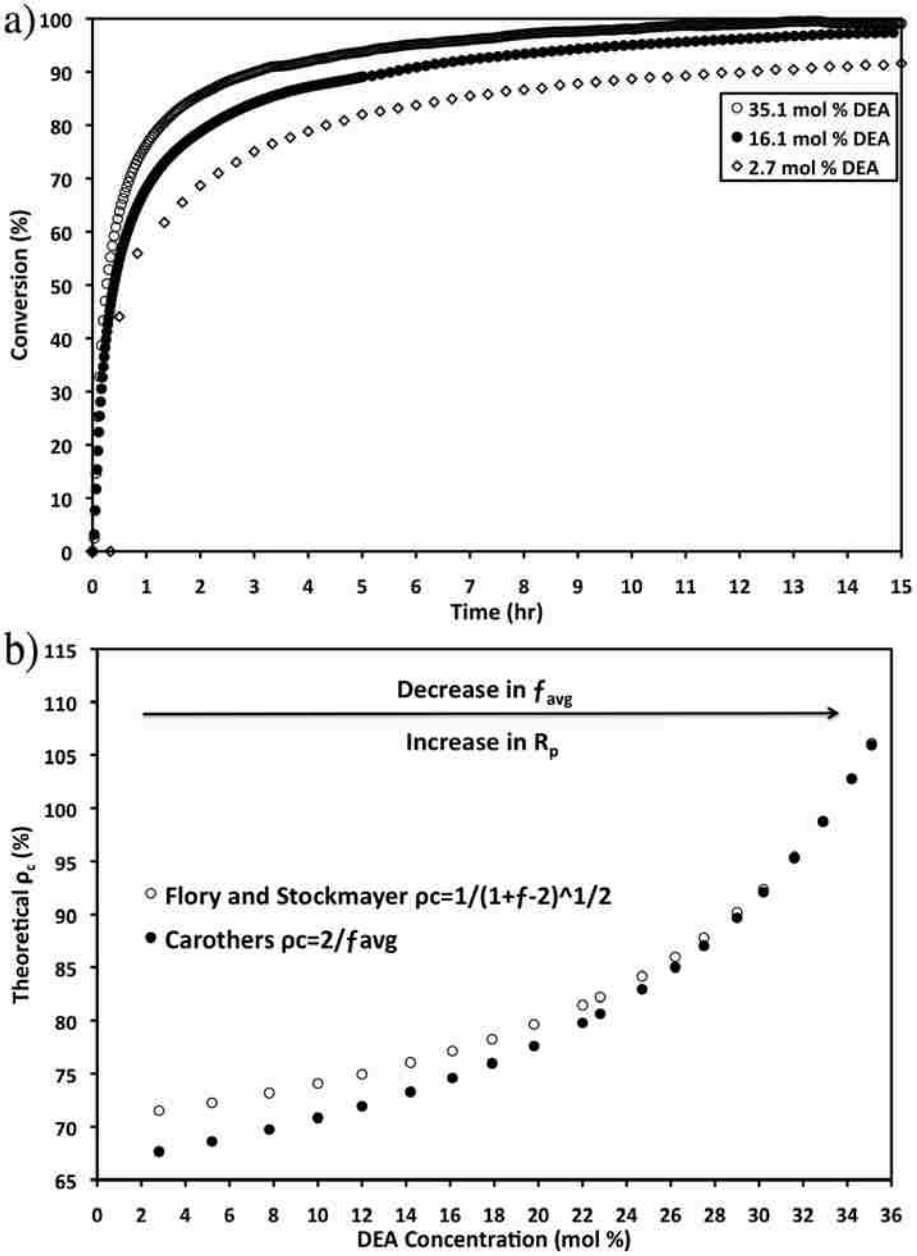

Figure 3-12: Conversion data as a function of amine concentration. Figure a) illustrates the real-time conversion of acrylate functional groups monitored via FTIR as a function of amine catalyst concentration. Figure b) illustrates the theoretical critical conversion value as a function of the fraction of acrylate groups previously reaction (DEA concentration) using both the Flory and Stockmayer estimation and the Carothers estimation.

The data in Figure 3-12a show that the rate of polymerization increased as a function of DEA concentration disproving the arguments discussed previously. Therefore, a different explanation was hypothesized where the average functionality of the monomer/catalyst molecule was the determining factor of the unusual gel times. The critical conversion required to reach gelation (ρ_c) can be estimated based on two different theories, the Carothers theory and the Flory and Stockmayer theory, both equations shown below:

$$\rho_c = 2/f_{avg} \qquad \textbf{(Carothers) [89]}$$

$$\rho_c = 1/(1+f-2)^{1/2} \qquad \textbf{(Flory and Stockmayer) [89]}$$

These theories assume equal reactivity of all functional groups of the same type regardless of the size of the molecule and that there are no intramolecular reactions between functional groups on the same molecule. [89] Because of this assumption, the theoretical numbers may not exactly match the experimental data, but the overall trend should. As shown in Figure 3-12a, the rate (R_p) of loss of monomer increased with an increase in the concentration of amine, however the gel time (Figure 3-9) increased with an increase in the concentration of amine. In this case, the increase in the gel time with extremely high amine concentration was associated with a change in the critical percent conversion (ρ_c). As the concentration of the amine was increased, the functionality of the acrylate was decreased due to the initial Michael reaction, causing ρ_c to increase greatly thereby preventing gelation until later in the reaction. This was the cause of the decrease in the gel time as a function of the increase in catalyst concentration at high concentration and the parabola-type curve shown in Figure 3-9. This resulted in the illusion of a decrease in the rate of polymerization. The physical gel times of these

particular thiol-acrylate reactions could be manipulated to a point, but a lower limit did exist due to the use of an *in situ* catalyst that inherently caused a decrease in the average functionality of the system.

3.5.9 Glass Transition Measurements

Differential scanning calorimetry was performed on these thiol-acrylate Boundless materials to determine their glass transition temperatures. Figure 3-13 illustrates the glass transition temperatures at different amine catalyst concentrations. Figure 3-13a shows the raw DSC data of heat flow as a function of temperature. The second-order transition temperatures are easily observed where the heat flow decreased at a given temperature without recovering back to the original baseline. Figure 3-13b illustrates the measured glass transition temperature as function of amine concentration. The DSC data provided the working temperatures associated with these thiol-acrylate materials via the determination of the glass transition temperatures (T_g). These materials can be used at a wide range of temperatures without performing as glass-like materials. Furthermore, the useable-temperature of the material could be manipulated based on the concentration of the *in situ* amine catalyst. All of the combinations observed in Figure 3-13 showed glass transition temperatures of less than 0˚C. The change in the glass transition temperature as a function of DEA concentration (Figure 3-13b) was attributed to the decrease in the crosslink density with an increase in the DEA concentration. An increase in the DEA concentration resulted in a decrease in the average functionality of the system by decreasing the functionality of the acrylate monomer. This decrease in the functionality led to a decrease in the material cross-link density, allowing for an increase in segmental mobility of the network thus causing a

decrease in the glass transition temperature. From a microfluidic standpoint, the natively low and manipulatable T_g of these materials is advantageous as it allows for a wide analyte temperature range to be employed during analysis.

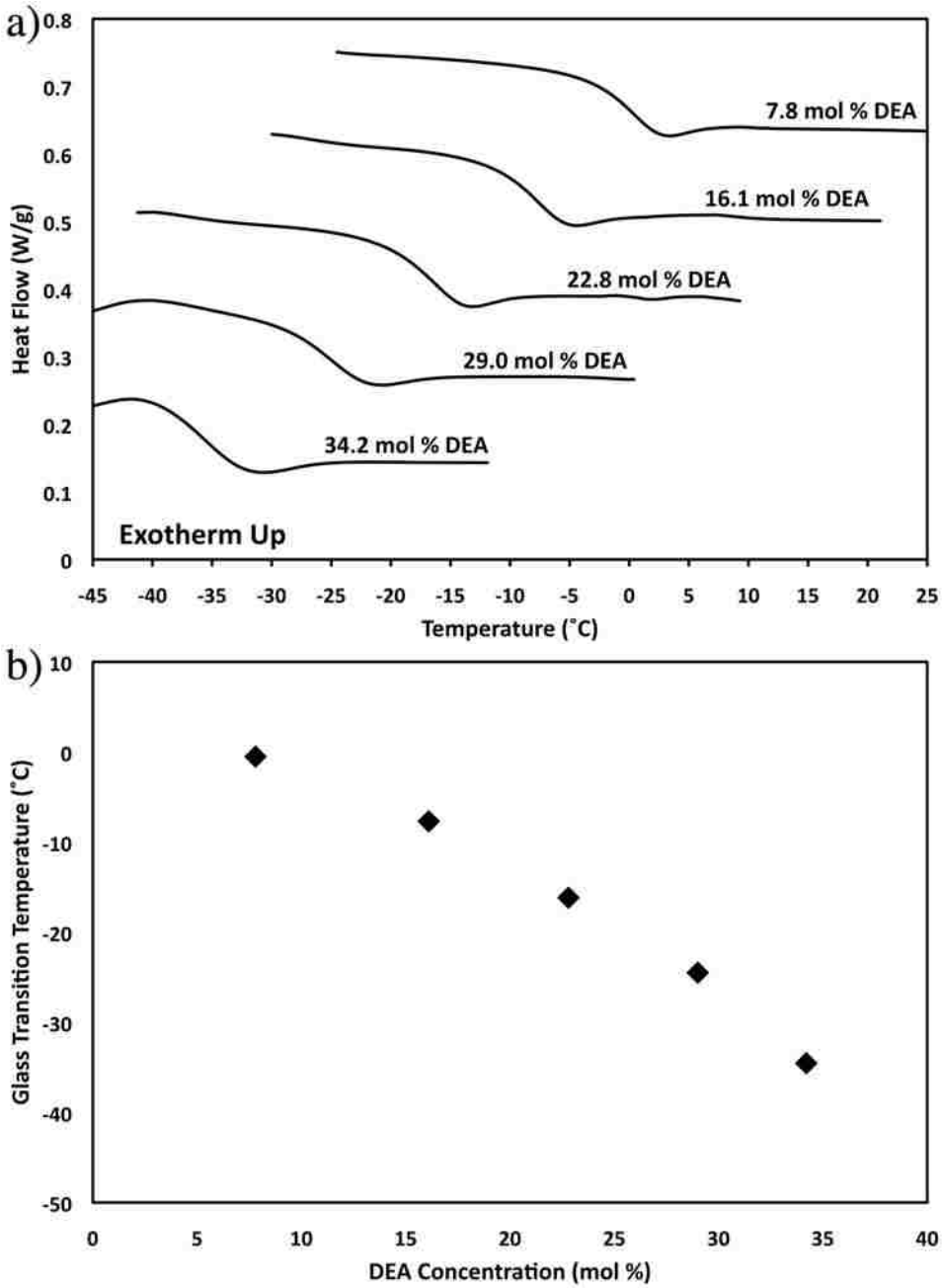

Figure 3-13: Differential scanning calorimetry data showing glass transition temperatures (T_g) for Boundless materials. Figure a) illustrates the heat flow as a function of temperature at varying DEA concentrations. Figure b) illustrates the glass transition temperature as a function of DEA concentration.

3.5.10 Flexure Strength

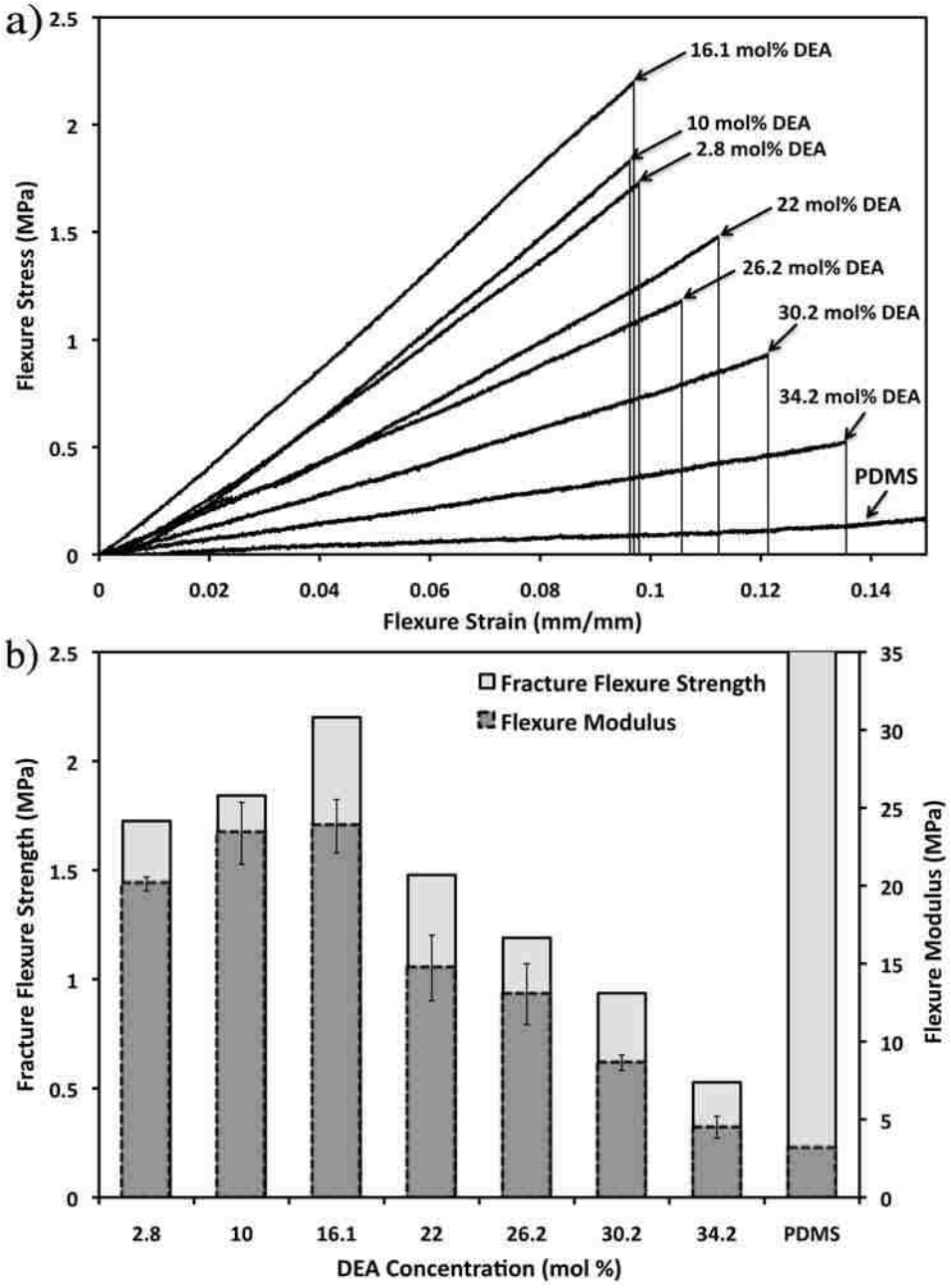

Figure 3-14: 3-point bending analysis results. a) Stress strain curve as a function of DEA concentration, b) fracture flexure strength and flexure modulus as a function of DEA concentration. All samples were tested after 24 hours.

The flexure strengths of these thiol-acrylate materials were determined using a 3-point bending method. Samples containing various amine concentrations were

analyzed and their mechanical aspects compared along with PDMS. The mechanical properties of the material were manipulated as shown in Figure 3-14. Beyond 16.1 mol% DEA, the flexure strength of the material (Figure 3-14b) decreased and the flexibility (Figure 3-14b) increased with an increase in the DEA concentration. The increase in flexibility and the decrease in flexure strength originated from the decrease in the crosslink density facilitated by the increase in the concentration of the amine. Again, due to the first Michael addition, an increase in the amine concentration caused a decrease in the functionality of the trifunctional acrylate, resulting in a decrease in the overall functionality and thus the crosslink opportunities. The material with the highest flexure strength and modulus was that containing 16.1 mol% DEA. Since there was a slight decrease in the flexure strength and modulus of materials containing less than 16.1 mol% DEA, the reaction conversion also likely played a role in the strength of the material. All of the samples used in the analysis were allowed to react for 24 hours prior to being tested. The material with the highest strength and modulus was also the material with the fastest gel time (gel time figure 3-9). This potentially implied that the polymerization kinetics played a role in the strength of the final material.

As a comparison tool, PDMS samples of the same dimensions were also analyzed using this 3-point bending technique. The data for these silicone samples are shown in Figure 3-14. The PDMS materials were found to have much higher flexure fracture strength. Because the 3-point bending technique employed was not successful in fracturing the samples, Figure 3-14a illustrates the continuation of the stress strain curve infinitely along the x-axis, and Figure 3-14b illustrates the continuation of the corresponding strength data bar beyond the scope of the measurement along the y-

axis. The PDMS samples also boasted a very low flexure modulus only attainable via a PETA-co-TMPTMP sample with very low flexure strength. These data indicated that, in terms of material strength, PDMS was much stronger and much more flexible than the PETA-co-TMPTMP samples. This material weakness compared to PDMS was not a strong disadvantage however, as the field of microfluidics does not require extremely tough and rugged materials for biological assays. The many advantages associated with the use of these novel thiol-acrylate materials greatly overpowered the small sacrifice in material strength.

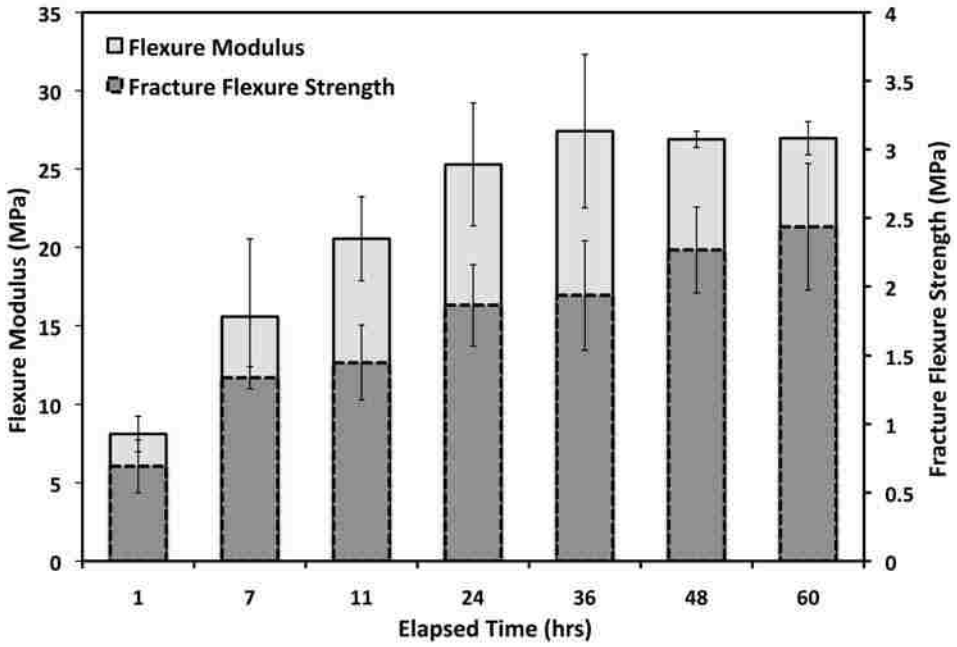

Figure 3-15: 3-point bending analysis results illustrating the flexure modulus and the flexure strength as a function of elapsed time after polymerization.

To determine if there was a kinetic aspect in correlation with the mechanical strength of the material, the mechanical properties were analyzed as a function of elapsed time beyond polymerization. These data are shown in Figure 3-15. Both the strength and stiffness of the material increased as a function of elapsed time from 1 to 24 hours. Beyond 24 hours the strength and flexibility of the material remained

constant, indicating that the full strength of the material could be obtained after 24 hours of reaction time. This was in full agreement with the kinetic data (Figure 3-11), as the reaction was observed to reach >95% conversion after a 24 hour time period.

3.5.11 Annealing Via Partial Polymerization/Excess Monomer Technique

Two thiol-acrylate films could be annealed using the same chemistry without the need for surface activation, which required expensive instrumentation. This eliminated a costly and time-consuming step in the final production of the microfluidic device. The adhesion was facilitated via a partial polymerization method involving excess functional groups on opposing surfaces. Scheme 3-4 illustrates the Bondless microfluidic device annealing mechanism.

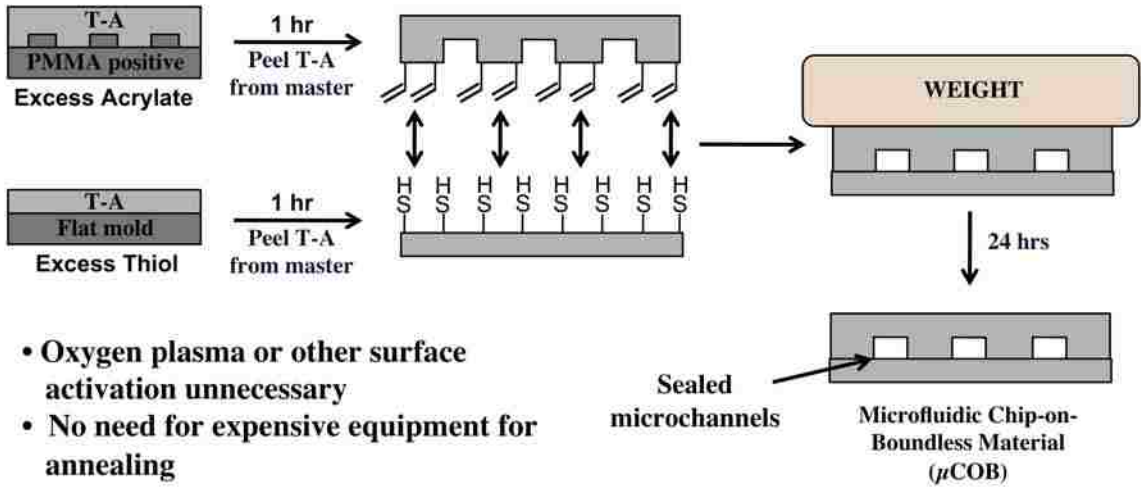

Scheme 3-4: Annealing of thiol acrylate microfluidic device via a partial polymerization and excess monomer method.

The adhesion between the two surfaces was attributed to the extremely high conversion associated with thiol-acrylate chemistry as well as the use of a step growth mechanism where the gel time was rapid, but the full conversion was relatively slow. The excess acrylate on one surface and excess thiol on the other resulted in a net 1:1 molar ratio of thiol to acrylate functional groups between the two surfaces. This then

allowed for the same Michael addition of thiol to acrylate, again catalyzed by the *in situ* tertiary amine previously incorporated into the network. The covalent thiol-carbon bond produced a strong adhesion between the surfaces resulting in sealed microfluidic channels down which water could confidently be pumped.

In order to determine the strength of the bond formed using this partial polymerization method, the orthogonal delamination force necessary to delaminate the annealed surfaces was determined. These data are shown in Figure 3-16.

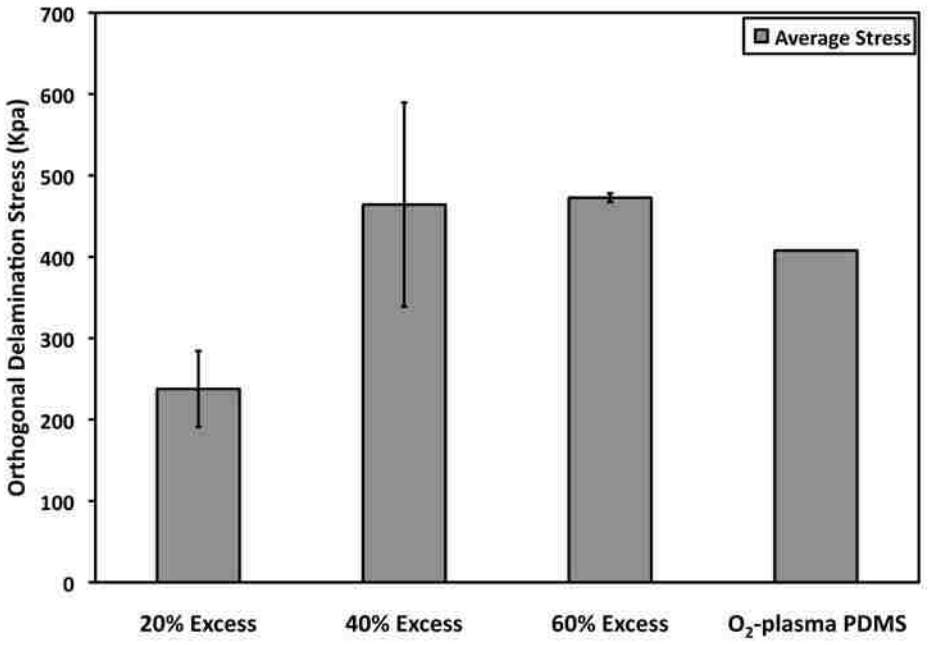

Figure 3-16: Adhesive bond strength as a function of excess monomer (thiol and acrylate) compared to the adhesive bond strength of oxygen plasma activated PDMS.

Flat samples were employed here for ease of comparison. Samples containing various amounts of excess monomers on opposing sides were analyzed using an orthogonal delamination analysis method. Figure 3-16 illustrates an increase in the average required delamination force as a function of increasing excess monomer concentration from 20% excess monomer to 40% excess monomer. There was little difference in the average strength of the annealing bond above 40% excess monomer.

This was attributed to the different types of failures experienced by the polymer samples. Two annealed samples could be delaminated at the surface of the material via an adhesive failure (Scheme 3-5a) where the strength of the bond was dependent on the strength of the adherence at the interface of the two materials. Samples could also fail in a cohesive manner (Scheme 3-5b) where the adhesive surface bond was stronger than the material being adhered.

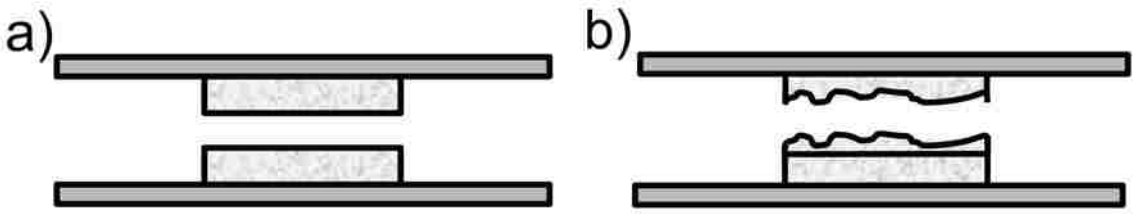

Scheme 3-5: Graphical illustrations of potential orthogonal delamination failure types, a) adhesive failure and b) cohesive failure.

The samples containing only 20% excess monomer (Figure 3-17a) suffered adhesive failure, while both the samples containing 40% (Figure 3-17b) and 60% excess monomer (Figure 3-17c) experienced cohesive failure.

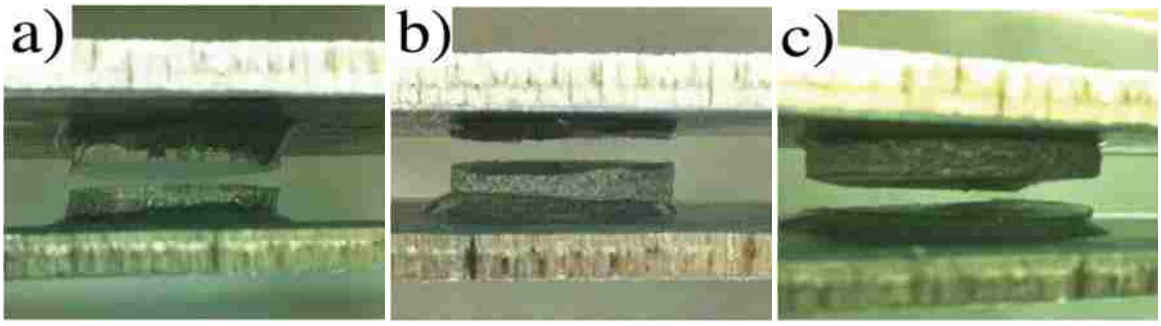

Figure 3-17: Photographic illustrations of experimental orthogonal delamination failure results, a) 20% excess monomer, b) 40% excess monomer, and c) 60% excess monomer.

At excess monomer concentrations below 40% the fewer number of covalent bonds between the two films limited the strength of the annealing process. Beyond

40% excess monomer, the strength of the annealing process was limited only by the mechanical strength of the material, thus no change in the average stress was observed from 40% to 60% excess monomer. There was, however, an apparent increase in the reliability of the annealing bond at 60% excess monomer, as the standard deviation was lower when 60% excess monomer was utilized (Figure 3-16).

Again for comparison purposes, annealed PDMS samples were exploited via the same orthogonal delamination analysis. Both PDMS pieces were first exposed to an oxygen plasma generator for 30 seconds to activate the surface for annealing. The PDMS materials were then pressed together and placed in an incubator oven for 24 hours at 37˚C. The average annealing strength of the thiol-acrylate materials containing 40% and 60% excess monomer were comparable to that of two PDMS materials annealed using the expensive oxygen plasma treatment. Therefore, a thiol-acrylate microfluidic device could be prepared with the same annealing integrity as that of a PDMS device without the need for expensive instrumentation such as an oxygen plasma generator.

3.5.12 Native Contact Angles

One of the most useful properties of this copolymer material in terms of microfluidic applications is its stable hydrophilic surface. Hydrophilicity is a very useful and sometimes necessary property of microfluidic devices for a multitude of reasons[212, 215-218]. One obvious advantage is the wetability of the surface. A hydrophilic surface allows for the passage of aqueous materials down small microchannels (or nanochannels) with little force as opposed to small hydrophobic channels.[212] Some polymer materials used in microfluidics can be modified to allow

for lower contact angles, such as oxygen plasma treatment to PDMS [117], which results in drastic decreases in the water contact angle. However, the surface of these oxygen plasma treated samples are not stable beyond a few days and eventually resume back to their hydrophobic state. [117] Therefore, a stable microfluidic device is a highly desirable novelty, as this would facilitate a prolonged shelf life. The water contact angles of these native thiol-acrylate copolymers were observed to range from ~60-65˚ regardless of the time elapsed after polymerization or the trithiol concentration. Figure 3-18a and 3-18b visually illustrate a water droplet on a native PDMS surface and on a native PETA-co-TMPTMP surface, respectively.

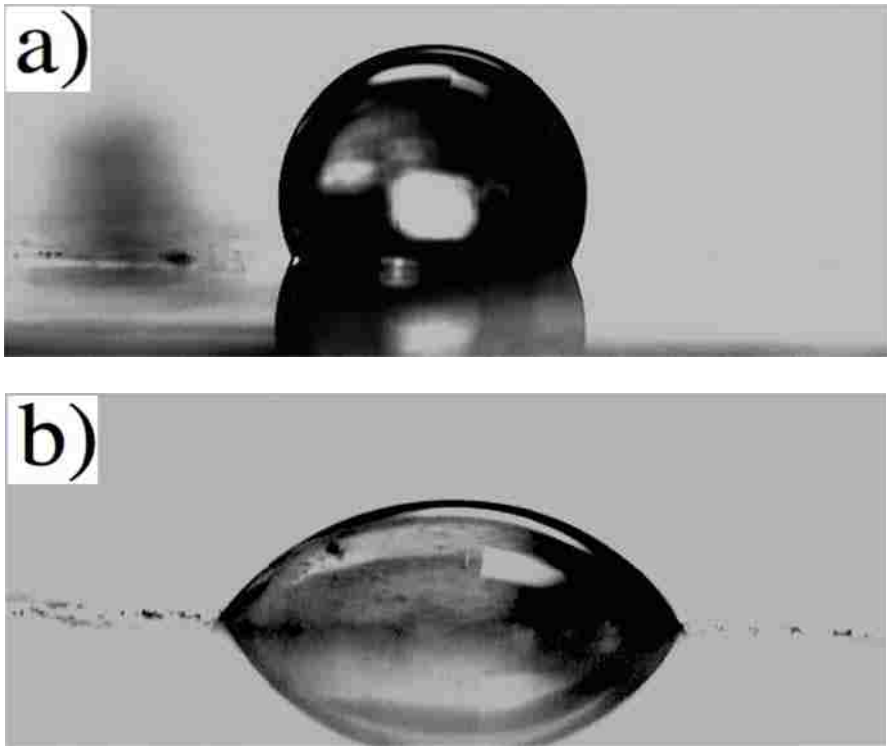

Figure 3-18: Photographic illustrations of water contact angles on polymer substrates, a) Native PDMS and b) Native PETA-co-TMPTMP.

It was obvious from these optical microscopy images that the thiol-acrylate surface was much more hydrophilic (wetable) compared to the PDMS substrate. The

native PDMS surface had a hydrophobic water contact angle of ~115˚ as opposed to the hydrophilic thiol-acrylate native contact angle of ~60˚. Figure 3-19 illustrates the water contact angles of native PDMS, oxygen plasma treated PDMS, and PETA-co-TMPTMP as a function of recovery time. Native PDMS had a hydrophobic surface with a water contact angle of ~115˚ that remained constant for 2 weeks (Figure 3-19a). A PDMS sample exposed to oxygen plasma for 30 seconds showed initial hydrophilicity, having a water contact angle of <20˚ immediately following the oxygen plasma treatment. This hydrophilicity was only transient, however, as the surface quickly recovered back to its hydrophobic state with a contact angle of ~70˚ after 1 day, >90˚ after 2 days, >100˚ after 1 week, and >107˚ after two weeks (Figure 3-19a). The PETA-co-TMPTMP sample, on the other hand, boasted a stable hydrophilic surface with an initial water contact angle of ~60˚ that remained constant within 6˚ over the same two week time period (Figure 3-19a). This result illustrated a significant increase in the surface stability of the thiol-acrylate material as opposed to the transient nature of the oxygen plasma-treated PDMS in maintaining a hydrophilic surface.

The surface of the native PETA-co-TMPTMP material was monitored for ~2.5 months to determine the longevity of its stable surface (Figure 3-19b). Throughout the extended study, the water contact angle remained constant within 6˚ for 2.5 months. The initial average water contact angle on day 1 was 61.23˚ and the final average water contact angle on day 77 was 60.07˚. Therefore, it was proven that this native thiol-acrylate microfluidic material could have a shelf life of at least 2.5 months, and there was little reason to expect any variations in the surface for even longer periods of time.

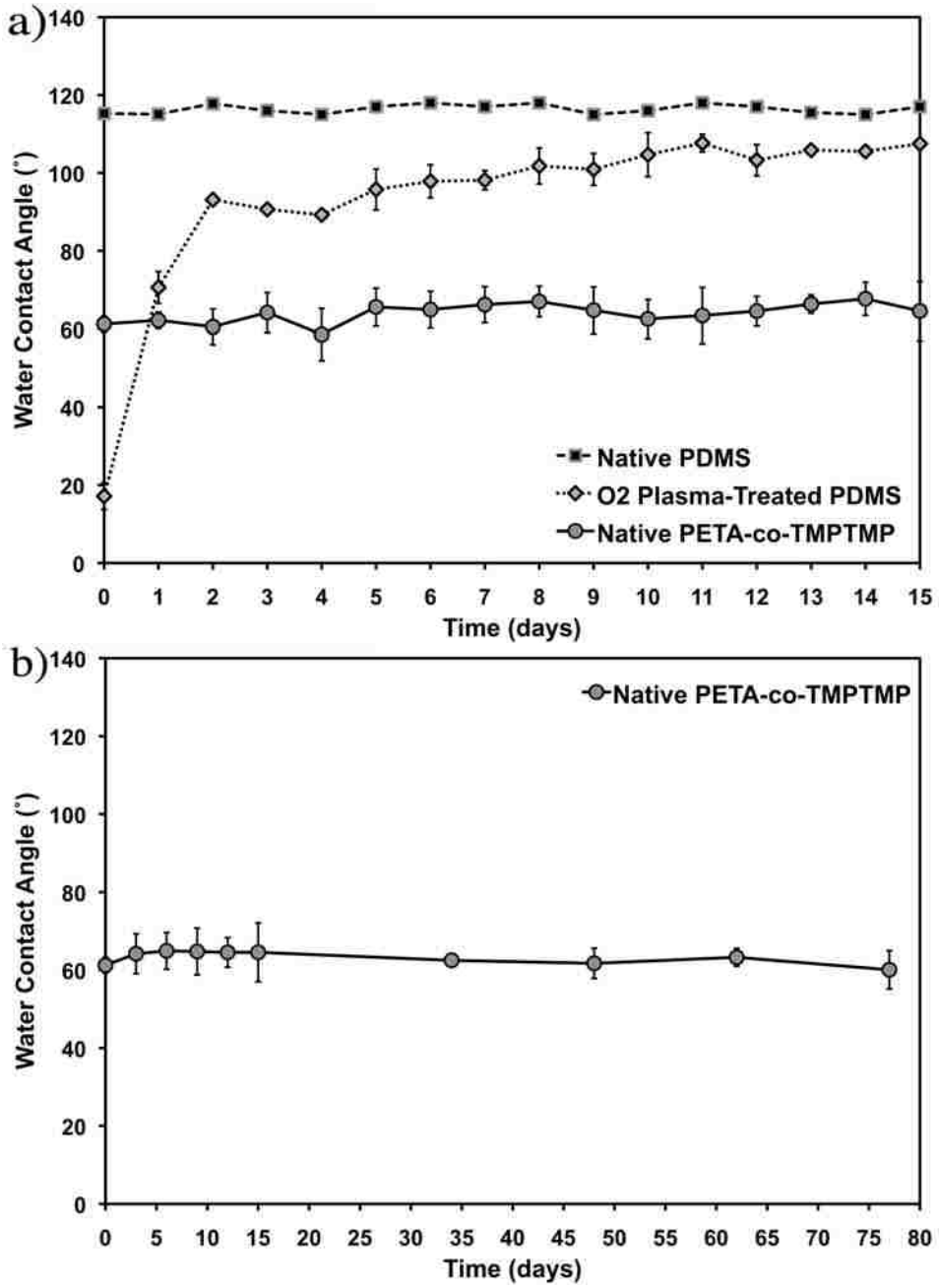

Figure 3-19: Water contact angle as a function of time for a) 2 weeks illustrating native PETA-co-TMPTMP, native PDMS, and PDMS exposed to oxygen plasma for 30 seconds and b) 2.5 months showing only native PETA-co-TMPTMP

The native water contact angles were also determined as a function of monomer concentration. This was a crucial factor in correlation with the annealing of the material. Because the materials were annealed using an excess monomer method, in was

important to know the effect of the monomer concentration on the surface properties of the material. Figure 3-20 shows that the contact angle is independent of the concentration of trithiol incorporated. This proved that the method used to anneal the two surfaces did not negatively affect the surface properties of the material in terms of hydrophilicity.

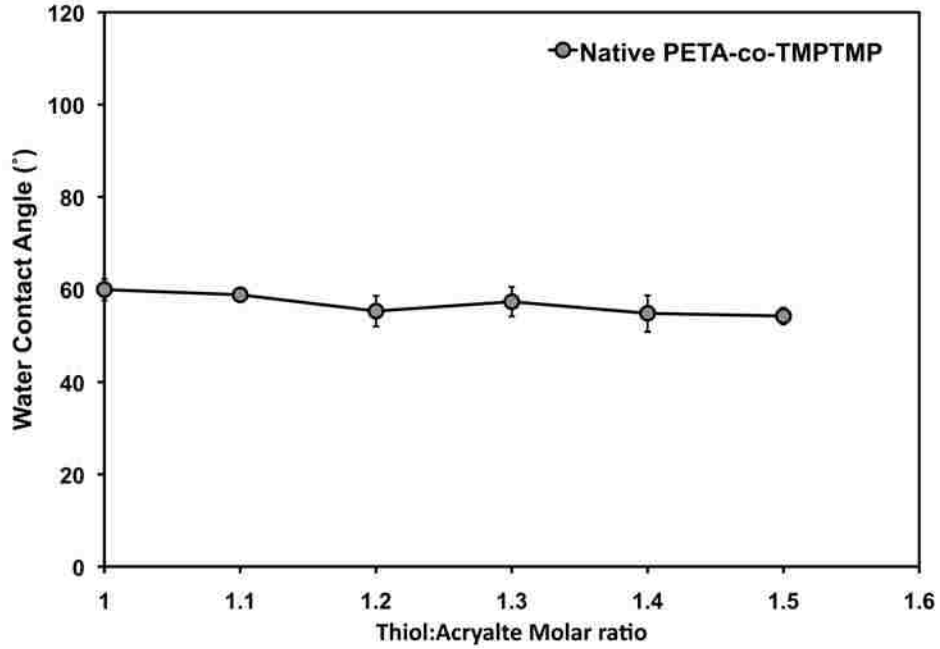

Figure 3-20: Water contact angle as a function of Trimethylolpropane tris(3-mercaptopropionate molar concentration.

3.5.13 Water Mass Uptake of Native PETA-co-TMPTMP Materials

Due to the hydrophilic nature of these native thiol-acrylate materials, some water mass uptake was expected over time. It was important to determine the water mass uptake as this could alter the size of the microchannels over time using this material. This “swelling” could also be very beneficial as smaller dimensions could be obtained via shrinkage of the microchannels to produce even nanodimensions via a post-processing swelling technique. The water mass uptake at various time intervals and different amine catalyst concentrations are illustrated in Figure 3-21. The native thiol-

acrylate samples were completely submerged in distilled water, removed and weighed periodically, and again submerged repeatedly for a lengthy 4-month study. For samples containing 1.35 mol% DEA, after 30 minutes of water exposure time, an average mass increase was documented at 0.19%. From there, the percent mass uptake increased over time to 0.80%, 1.0%, 1.5%, and 3.1% after 1 day, 2 days, 12 days, and 4 months, respectively when 1.35 mol% DEA was used. Because normal microfluidic applications involve only short transient interactions with aqueous solutions, only the water mass uptake at relatively low water exposure times were relevant. It was concluded that the water mass increases associated with these native thiol-acrylate materials were negligible as the material absorbs ≤1% of its mass after 2 days fully submerged in an aqueous environment.

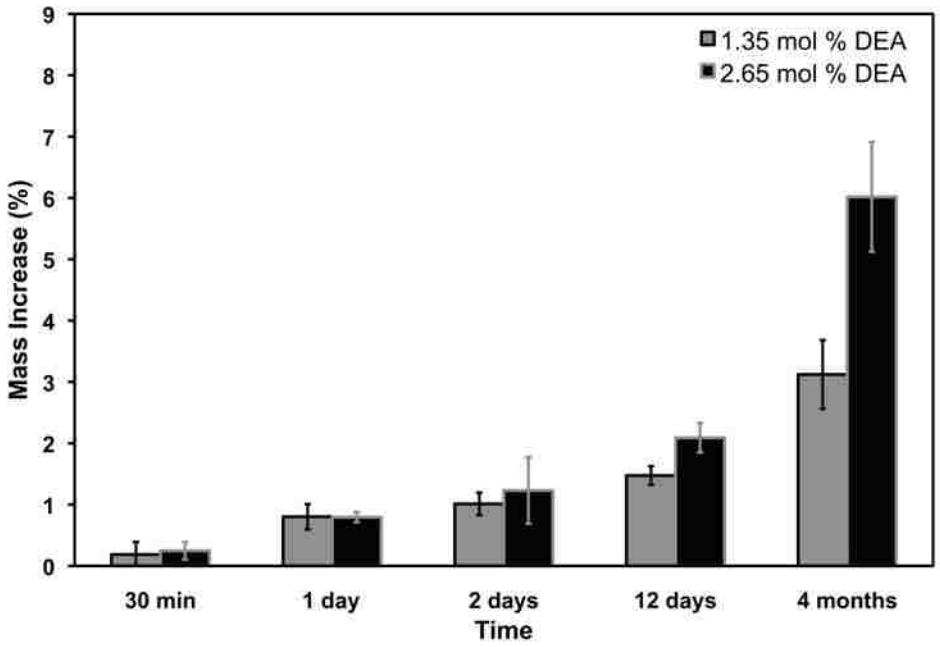

Figure 3-21: Water mass increase as a function of water submersion time.

There was a correlation between the water mass uptake and the concentration of the amine catalyst at long submersion times. No change in the mass uptake was observed, within the standard deviation, of samples containing different concentrations

of amine when submerged in water for 2 days or less. However, at submersion times ≥12 days, there was an increase in the water mass uptake with an increase in the amine concentration. The average mass uptake for samples containing 2.65 mol% DEA was 2.1% after 12 days and 6.0% after 4 months. This was expected as an increase in the concentration of the amine caused a decrease in the average functionality of the system and thus a decrease in the cross-link density of the material. Because the hydrophilic material was less cross-linked at higher amine concentrations, more water could interpenetrate the network causing an increase in the mass uptake over time. Even at the higher concentration of amine there was still very little mass increase at submersion times of ≤2 days. After 2 days of full submersion time, the material containing 2.65 mol% DEA experienced a mass increase of only 1.2%. Regardless of the amine concentration, there was little, if any, substantial water mass increase over the time period of interest for microfluidic applications using this native thiol-acrylate material.

3.5.14 Post Modification

In an attempt to alter the surface properties of the polymer product, specifically the contact angle, different surface modification methods were employed. The first method attempted was the modification of the surface of a previously prepared polymer sample. The premise behind this approach was to prepare a sample containing an excess of one of the two monomers (thiol or acrylate), and once polymerized, click on monofunctional surface modifiers containing the opposite functional group and some desired surface-altering side groups. The theory is illustrated in Scheme 3-6.

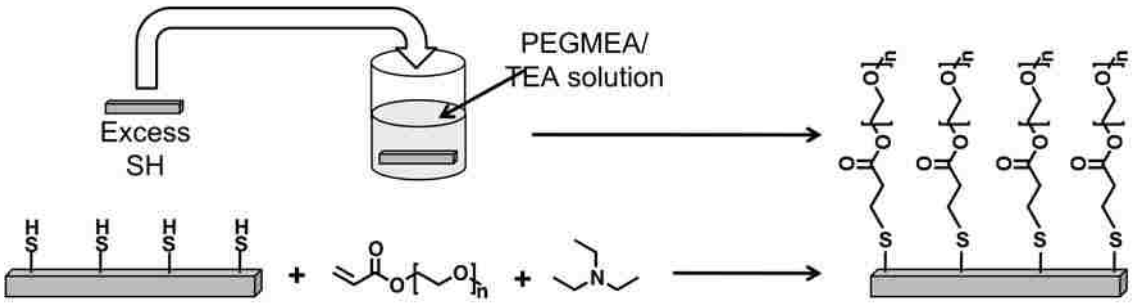

Scheme 3-6: Schematic illustrating the employed post-modification technique.

In this case, polymer samples were prepared containing 50% excess thiol by mole and functional group. The native contact angle did not depend on the thiol concentration as was shown in Figure 3-20 previously. Once the polymer samples were prepared containing excess thiol groups, the resulting films were submerged in a solution containing a triethylamine catalyst dissolved in a hydrophilic monofunctional surface modifier, poly(ethylene glycol) methyl ether acrylate, for various amounts of time. This resulted in the Michael addition of the excess thiol groups to the newly introduced monofunctional acrylate groups catalyzed by the triethylamine catalyst. Different samples were allowed to remain in the TEA/PEGMEA modifying solution for different amounts of time before being removed, washed and their contact angles determined. Figure 3-22 illustrates the contact angle for the post modification of the thiol-acrylate polymer films as a function of the excess thiol-containing sample's exposure time in the TEA/PEGMEA solution. The average contact angles decreased with an increase in the reaction time of the thiol-rich surface with the monofunctional surface modifying solution. This would be expected, as more time would correlate to a higher conversion of thiol and acrylate groups and thereby the attachment of more polyethylene glycol molecules causing the surface to be more hydrophilic. The surface was successfully altered using this post modification technique. It was concluded from

these data that a desired contact angle could be achieved by simply controlling the post modification reaction time.

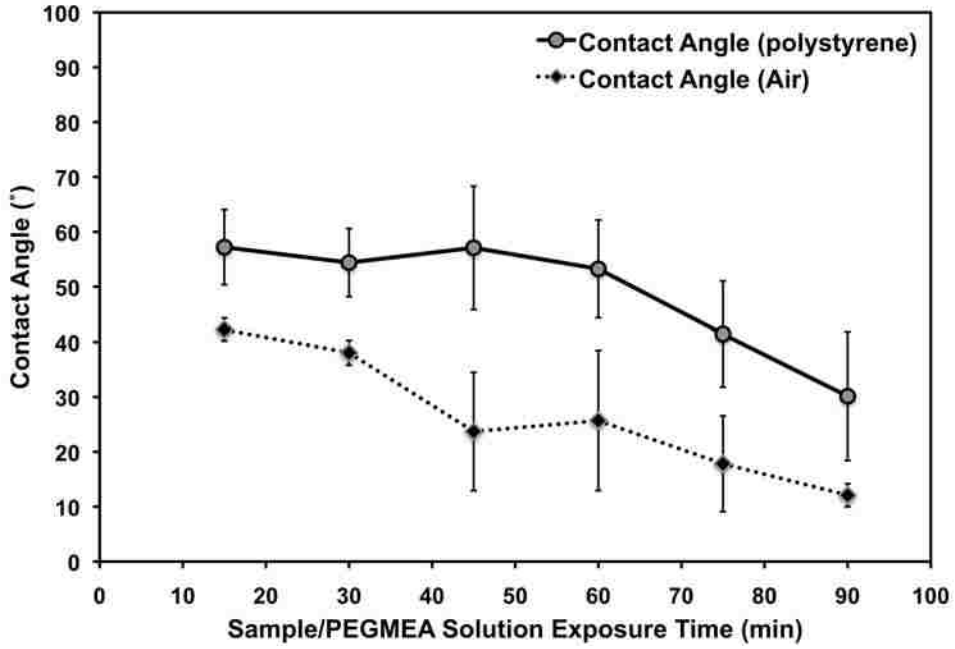

Figure 3-22: Post modification contact angles as a function of sample exposure time to PEGMEA/TEA solution. Both the angles for the surface exposed to air and the surface exposed to the polystyrene petri dish are shown.

Figure 3-22 also illustrates some differences in the contact angles of the surfaces that were exposed to air during initial polymerization and those surfaces that were exposed to the polystyrene petri dish during initial polymerization. Regardless of the post modification reaction time, the surfaces allowed to polymerize open to the atmosphere demonstrated lower contact angles. This can be attributed to the oxidation of the surface during and after polymerization causing the contact angle to be lower. Because the final application of these polymeric materials would be to prepare microfluidic chips, it is most beneficial to concentrate on the surfaces that were in contact with the petri dish and not exposed to air, as this would be the case when the monomer solution was poured onto a mold for a soft lithography process.

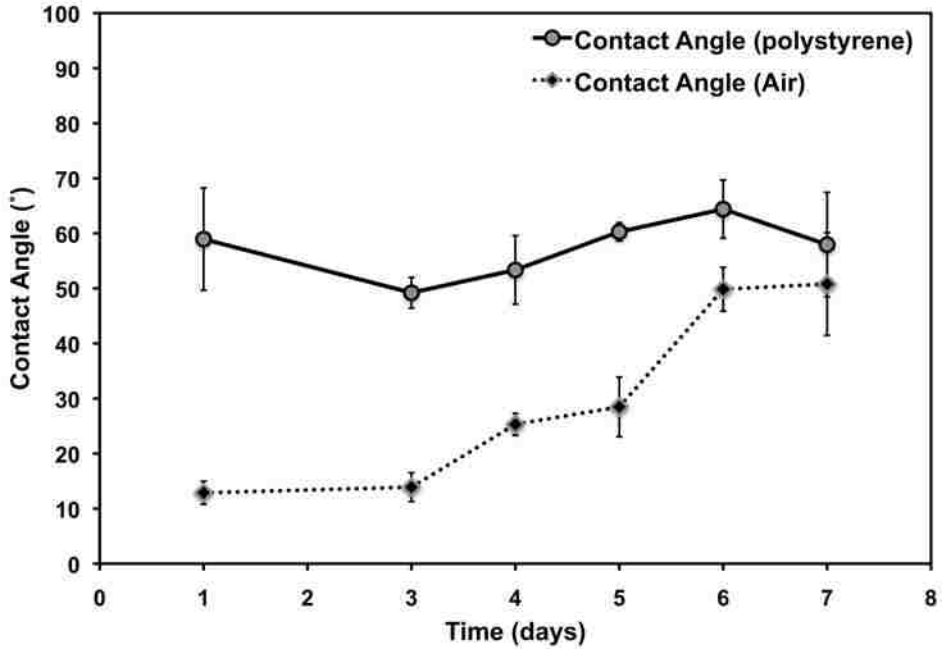

Figure 3-23: Post modification contact angles as a function of time after reaction. Both the angles for the surface exposed to air and the surface exposed to the polystyrene petri dish are shown.

Figure 3-23 illustrates the stability of the modified surface as a function of time. On average, a surface energy recovery was observed in association with these post-modified hydrophilic thiol-acrylate surfaces. The water contact angle was initially as low as ~13˚ but recovered back to ~50˚ after 1 week. This implied that the volatile monofunctional monomers were potentially not covalently bound via a Michael addition as was expected and that they were simply evaporating away over time, causing an increase in the average water contact angle as a function of time.

The mass uptake of these materials was monitored as a function of sample exposure time to the post-modification solution. The materials were weighed prior to being placed in the modifying solution and again once removed from the solution and dried. These data are illustrated in Figure 3-24.

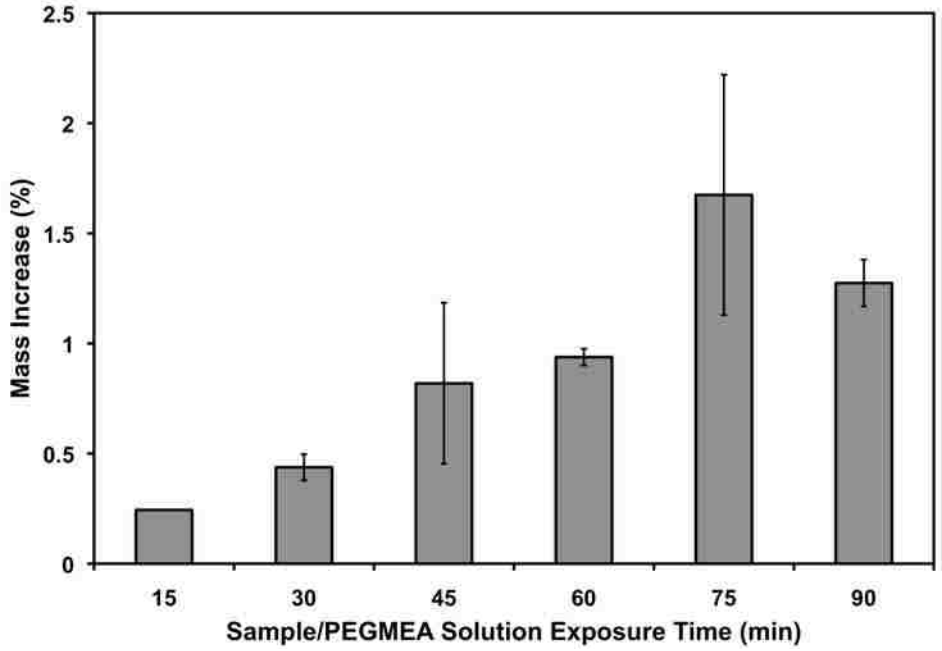

Figure 3-24: Mass increase of PETA-co-TMPTMP polymer as a function of sample exposure time to PEGMEA solution.

There was an average increase in the mass uptake as a function of exposure time. This increase in the mass can be attributed to two aspects of the process. As the monolayer is added to the surface of the material, an increase in the weight must physically occur due to an increase in the thickness of the layer. This would be expected, as there would be a correlation between the sample exposure time and the density of the added monofunctional modifier. As the density of the monolayer increased, the weight of the material increased. Secondly, there was likely some absorption/swelling of the material caused by the diffusion of the monofunctional acrylate into the similar trifunctional acrylate-containing sample.

Because of the irreproducibility (high standard deviations) and transient nature of these post-modified materials as shown in Figure 3-22 and 3-23, respectively, this method of modifying the surface was deemed rough and vague at best. Although, the surface of these thiol-acrylate materials could be modified using this technique to some

degree, other methods of surface modifications were explored in search of a more reliable technique.

3.5.15 Bulk Modification

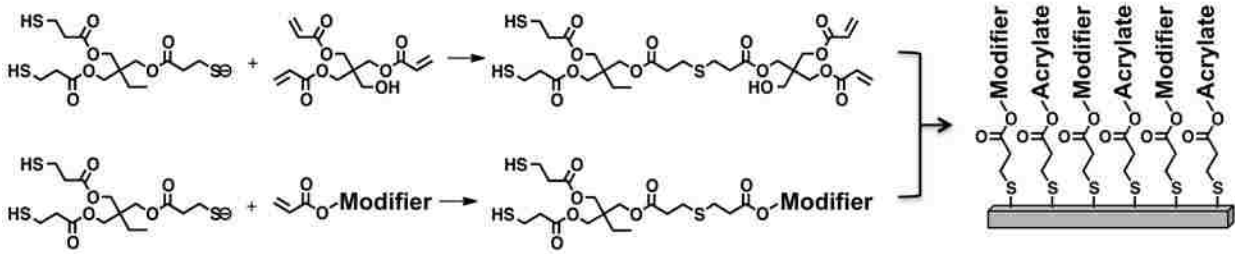

Scheme 3-7: Schematic illustration of the employed bulk-modification technique.

This technique involved the modification of the entire network as opposed to simply modifying the surface of the material via post modification. The theory behind this method was the covalent attachment of monofunctional modifying molecules within the network of the polymer during the initial reaction using the *in situ* amine catalyst. This provided more confidence in terms of the true covalent linkage of the modifying molecule. Scheme 3-7 illustrates this bulk modification technique. A monofunctional acrylate monomer molecule functionalized with the desired modifying functional group (either hydrophobic or hydrophilic) was incorporated into the original mixture in varying amounts. In this manner, the thiol anion had a choice to add to either the multifunctional acrylate molecule as usual or to the monofunctional molecule containing the modifying functional group. The monofunctional monomer was added in amounts that retained the 1:1 molar ratio of acrylate to thiol functional groups. Because of this stoichiometry and the high conversion associated with these thiol-acrylate reactions, the monofunctional acrylate containing the modifying molecule was well incorporated into

the polymer network regardless of the reactivity differences between the two competing acrylate molecules (mono- or multifunctional).

3.5.15a PEGMEA Bulk Modification

The first modifying molecule to be incorporated into the thiol-acrylate network via a bulk modification process was poly(ethylene glycol) methyl ether acrylate. The poly(ethylene glycol) pendant groups were used to introduce hydrophilicity into the material by producing a PEGylated surface. This modification attempt was thus fueled by the need for stable hydrophilic surfaces in the field of microfluidics. Various amounts of PEGMEA were added to the reaction mixture and the contact angles of these mixtures were determined. Figure 3-25 illustrates the contact angle as a function of PEGMEA concentration at day one and after two weeks. The contact angle was observed to decrease with an increase in the PEGMEA concentration. This was expected as an increase in the concentration of the monofunctional monomer caused an increase in the density of the pendant PEG groups throughout the network and thus the surface of the material. The water contact angles deviated very little from the native angles at low concentrations of PEGMEA but steadily decreased with an increase in PEGMEA concentration and reached a low of 11.2˚ at PEGMEA concentrations of 30 mol% by functionality (Figure 3-25). There was little hydrophobic recovery observed at relatively low concentrations of PEGMEA over a 14 day time period, however some deviation was observed at PEGMEA concentrations >20 mol% by functionality (Figure 3-25).

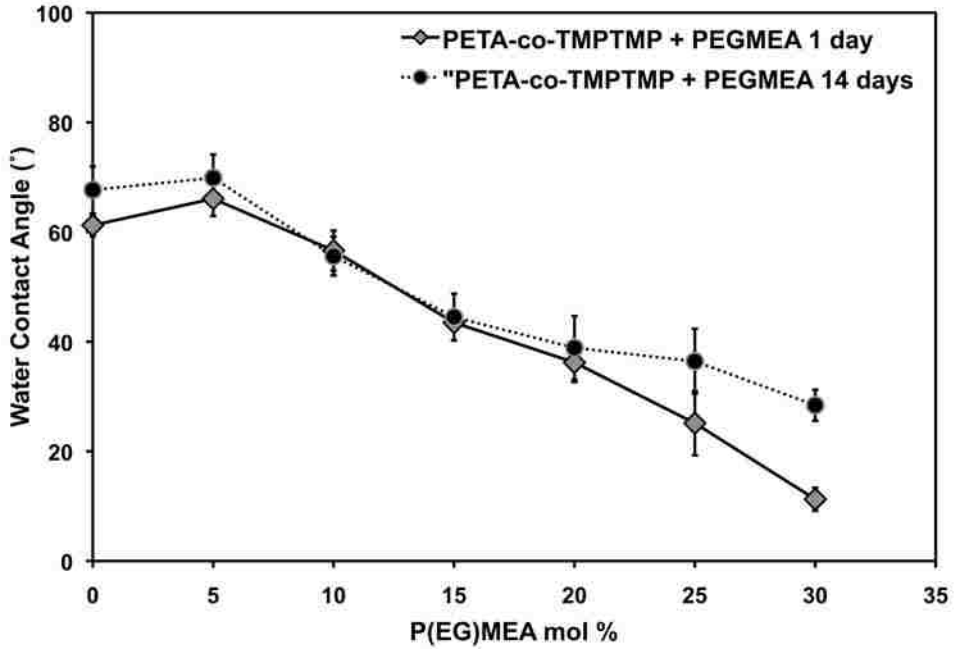

Figure 3-25: Contact angle as a function of poly(ethylene glycol) methyl ether acrylate molar concentration at 1 and 14 days.

This increase in the hydrophobic recovery at high PEGMEA concentrations is illustrated in Figure 3-26 showing the standard deviations of the average contact angles and the percent increase in the average water contact angles, both over a 14 day time period, as a function of PEGMEA molar concentration. An increase in the standard deviations of the average contact angles indicated an overall instability in the surface energy at high concentrations of PEGMEA. At PEGMEA concentrations of ≤20 mol% by functionality, the standard deviations over the 14-day time period were ≤2.1˚, while at PEGMEA molar concentrations of 25% and 30% the standard deviations over the 14-day time period were 5.1˚ and 8.6˚, respectively (Figure 3-26). At extremely high PEGMEA concentrations of ≥25 mol% by functionality, more variability was observed in terms of surface energy, mostly due to hydrophobic recovery. An increase in the percent increase of the water contact angle over the 14-day time period confirmed this hydrophobic recovery effect (Figure 3-26). At PEGMEA concentrations of ≤20 mol% by

functionality, the percent increases over the 14-day time period were ≤4.2%, while at PEGMEA molar concentrations of 25% and 30% the percent increases over the 14-day time period were 45.7% and 232.8%, respectively (Figure 3-26). At extremely high PEGMEA concentrations of ≥25 mol% by functionality, the high percent increase in the water contact angle over a 2-week time period illustrated the hydrophobic recovery of the materials. This recovery effect is likely caused by the lack of full incorporation of the monofunctional, modifying molecule into the polymer network allowing for the evaporation and natural removal of the small molecular weight and highly volatile PEGMEA molecule from the material. Nonetheless, moderately high PEGMEA concentrations were incorporated into the thiol-acrylate materials to produce low water contact angles with high levels of stability. Water contact angles as low as ~35˚ were obtained by bulk modification using PEGMEA and remained stable for at least 14 days.

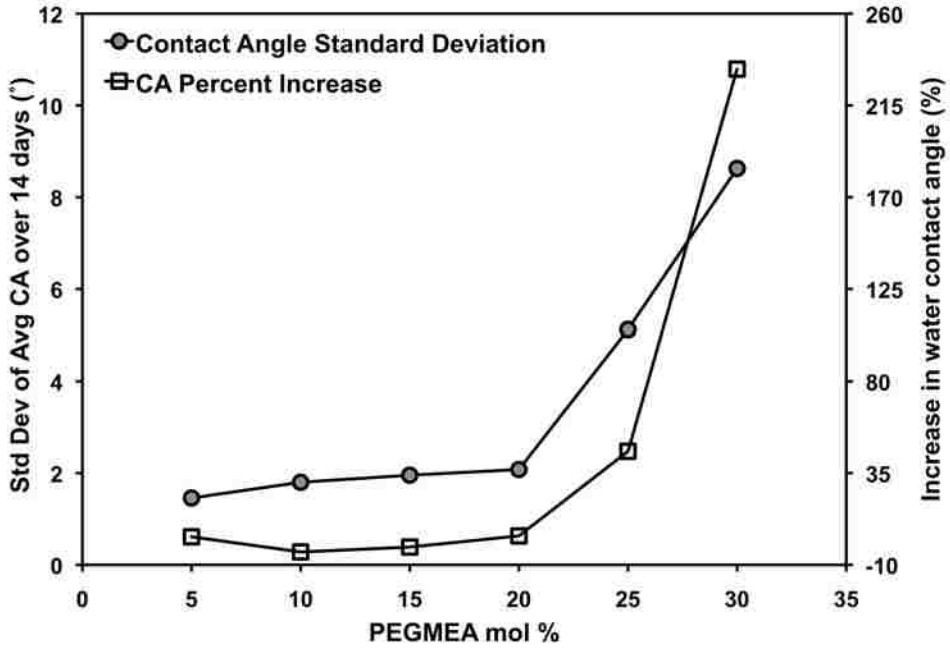

Figure 3-26: Standard deviations of average contact angles collected over a 14 day time period and the percent increase in the water contact angle over a 14 day time period, both as a function of PEGMEA molar concentration.

A more in-depth study of the contact angles as a function of the 14-day recovery time is illustrated in Figure 3-27 for samples containing ≤20 mol% by functional group PEGMEA modifier. Various hydrophilic contact angles can be achieved based on the concentration of the PEGMEA incorporated into the network via a bulk modification process. Average water contact angles of 68.1±1.5˚, 56.7±1.8˚, 43.7±2.0˚, and 35.6±2.1˚ were prepared by bulk modification of the thiol-acrylate materials with PEGMEA molar functionality concentrations of 5%, 10%, 15%, and 20%, respectively (Figure 3-27). Thus, thiol-acrylate materials can be prepared with stable hydrophilic water contact angles differing on average by only 10.8˚ using PEGMEA as a bulk modifier.

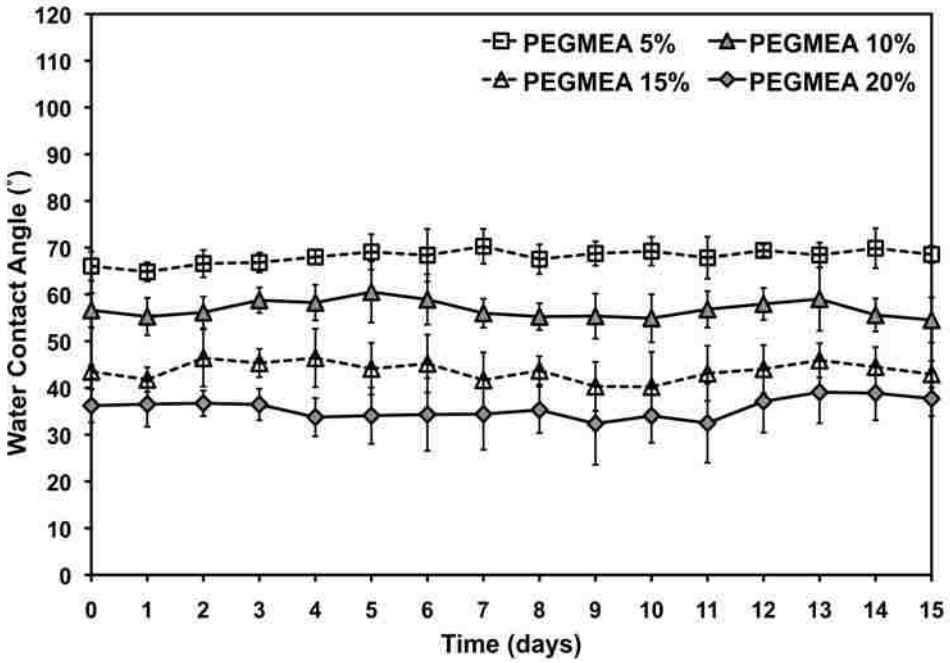

Figure 3-27: Contact angles as a function of time containing 5, 10, 15, and 20 mol% by functionality PEGMEA introduced via bulk modification.

The water mass increase as a function of PEGMEA mol% was determined at different time intervals and these data are illustrated in Figure 3-28. The average water

uptake percentage of the polymer materials increased with an increase in the PEGMEA molar concentration and with an increase in water exposure time. After 1 hour of water submersion time the mass uptake ranged from 0.33% at 10 mol% PEGMEA to 1.2% at 34 mol% PEGMEA. After 1 day of submersion time, the mass uptake ranged from 1.1% at 10 mol% PEGMEA to 6.7% at 34 mol% PEGMEA. After 3 days, the uptake ranged from 1.6% at 10 mol% PEGMEA to 8.6% at 34 mol% PEGMEA. Therefore, there was a correlation between the water contact angle and the water mass uptake as would be expected. A water mass uptake sacrifice is necessary to achieve lower water contact angles. Beyond 3 days, the mass stabilized or decreased indicating full saturation with water or degradation via hydrolysis, respectively. These results show that these bulk-modified thiol-acrylate materials, although hydrophilic in nature, do not swell excessively, especially at moderate concentrations of PEGMEA and shorter water submersion times.

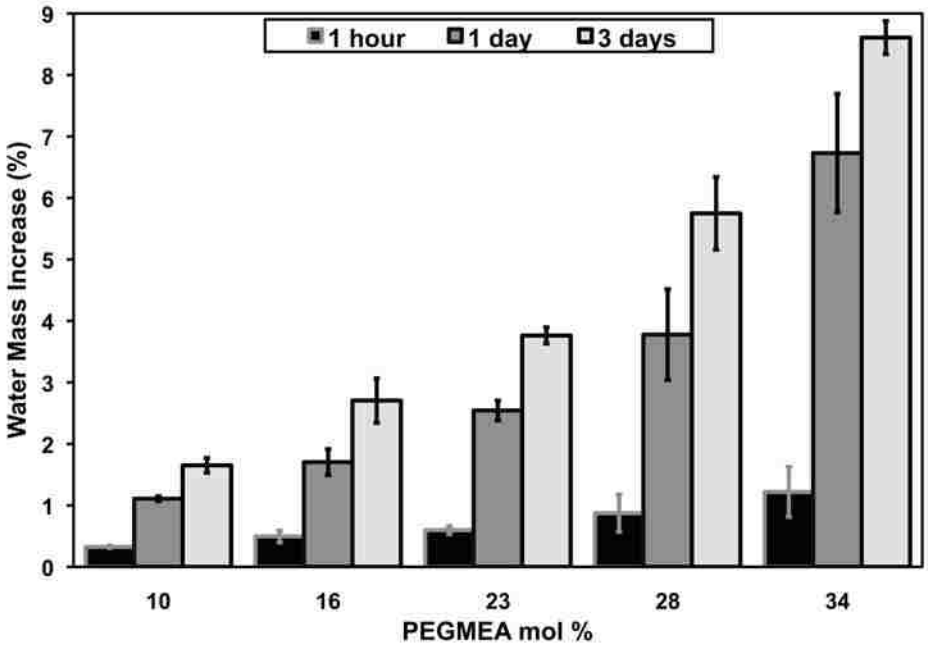

Figure 3-28: Water mass increase as a function of PEGMEA mol% for samples prepared via bulk modification.

3.5.15b Lauryl Acrylate Bulk Modification

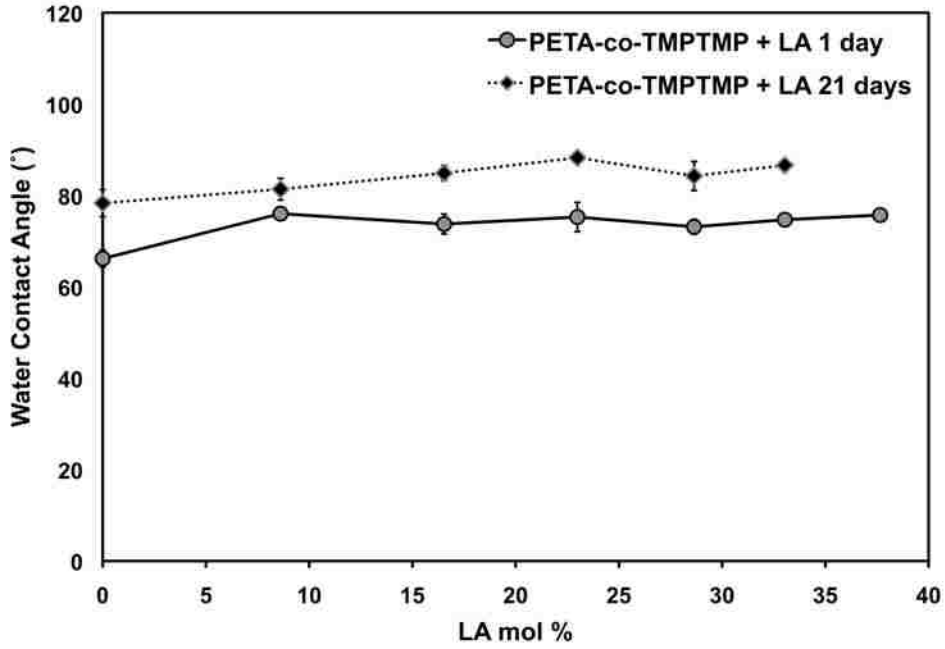

Figure 3-29: Contact angle as a function of lauryl acrylate molar concentration at 1 and 21 days introduced via bulk modification.

Hydrocarbons are known to be very hydrophobic in nature due in part to their negative entropies of aqueous solvation at room temperature. [241] In order to introduce a hydrophobic aspect to these versatile polymer materials, a monofunctional modifying acrylate functionalized with a long 12-member hydrocarbon chain was incorporated into the network. Various amounts of lauryl acrylate were added to the reaction mixture and the contact angles of these mixtures were determined. Figure 3-29 illustrates the contact angle as a function of LA molar concentration at day one and after three weeks. The presence of as little as 10 mol% LA increased the hydrophobicity of the surface to feature a water contact angle of ~75˚. There was no further increase in the contact angle with additional surplus of LA beyond 10 mol%, indicating that the density of the 12-membered carbon chains on the surface of the material did not play a major role in the surface energy. Beyond the critical amount, the excess chains were not a sufficient

enough source to further increase the hydrophobicity. The samples containing only 5 mol% LA were observed to remain stable throughout the 21 day time period, however samples containing >5 mol% LA were observed to increase in hydrophobicity during the 3 week time period (Figure 3-29).

A study was conducted on the water contact angles of samples containing 5 mol% LA as a function of a 14-day recovery time. These data are illustrated in Figure 3-30. Samples featuring an average water contact angle of 79.0±1.1 were prepared by bulk modification of the thiol-acrylate material with 5 mol% lauryl acrylate (Figure 3-30). These samples were found to be extremely stable over the 14-day recovery time.

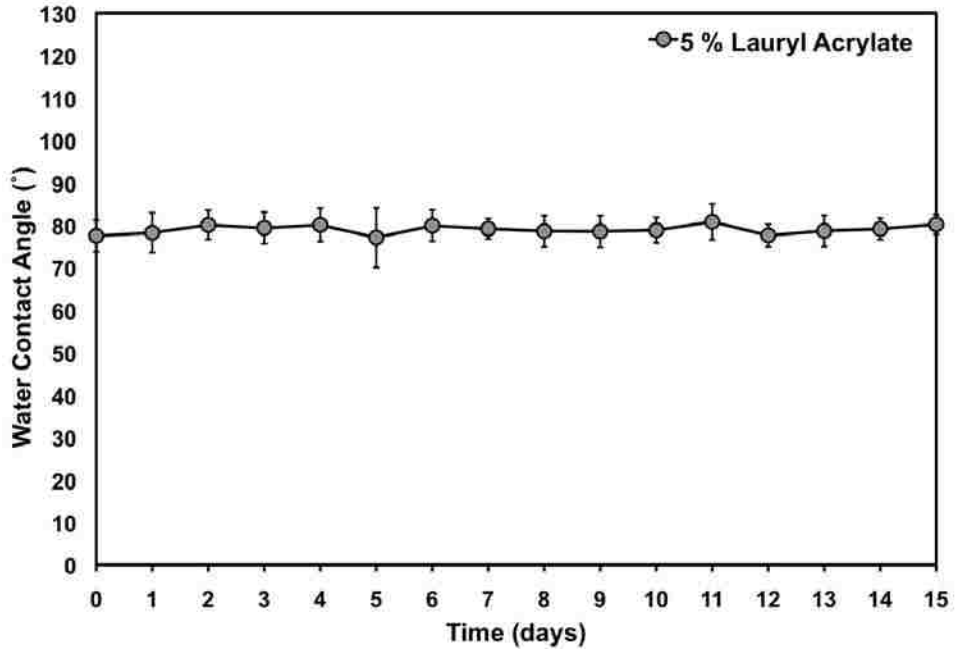

Figure 3-30: Contact angle as a function of time for samples containing 5 mol% lauryl acrylate introduced via bulk modification.

Optical clarity plays a critical role in the field of microfluidics as various types of microscopy are employed during microfluidic device analysis. The optical clarity of these lauryl acrylate bulk-modified thin films was subjectively investigated via the naked eye. Images are provided in Figure 3-32 for the reader's visual inspection.

Figure 3-31: Optical clearity of the films containing various concentrations of Lauryl Acrylate. From left to right and then top to bottom the lauryl acrylate concentration was 8.6, 16.5, 23.0, 28.6, 33.0, and 37.7 mol%.

The optical clarity of the polymer film was inversely related to the concentration of the lauryl acrylate. As the concentration of lauryl acrylate was increased, the film became more opaque until ~29 mol% LA at which point the opaqueness remained nearly constant. The opaque nature of this modified material at high concentrations of LA was attributed to the phase separation of the long hydrocarbon chain from the dissimilar hydrophilic native PETA-co-TMPTMP. This opaque feature of the material did not eliminate the use of LA as a modifying molecule as the optical clarity was affected only at high concentrations of LA, and high concentrations of LA were not required to cause a change in the surface energy of the material. Thus, low concentrations of LA were successful in the bulk modification of these thiol-acrylate materials, capable of increasing the water contact angle of the native material by ~10˚ and remaining constant for at least 14 days.

3.5.15c HFIPA Bulk Modification

Like hydrocarbons and potentially even to a larger extent, fluorinated compounds are very hydrophobic, again due partially to their negative entropies of solvation in aqueous solutions at room temperature. [241] In an attempt to harness the substantial hydrophobic potential of fluorinated compounds as modifying molecules, a monofunctional fluorinated acrylate molecule, hexafluoroisopropyl acrylate (HFIPA), was incorporated into the thiol-acrylate network via bulk modification. Various amounts of HFIPA were added to the reaction mixture and the contact angles of these mixtures were determined. Figure 3-32 illustrates the contact angle as a function of HFIPA concentration at day one and after two weeks.

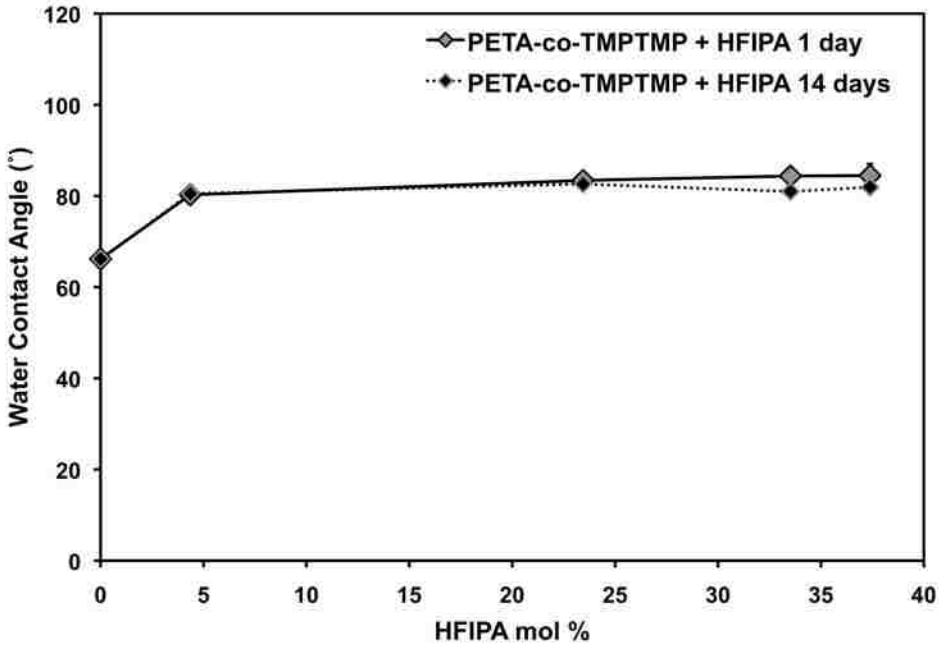

Figure 3-32: Contact angle as a function of hexafluoroisopropyl acrylate molar concentration at 1 and 14 days introduced via bulk modification.

The presence of as little as 5 mol% HFIPA resulted in an increase in the hydrophobicity of the surface to feature a water contact angle >80˚. There was a slight increase in the contact angle as a function of increasing HFIPA concentration. A water

contact angle near 85˚ was obtained when 40 mol% DEA was incorporated into the network. However, as with the lauryl acrylate, the density of the fluorinated pendant groups on the surface of the material did not play a significant role in the hydrophobicity of the material, increasing only ~5˚ with an increase in the HFIPA molar concentration from 5 mol% to 40 mol%. Unlike the lauryl acrylate-modified samples, an increase in the concentration of the HFIPA did not result in a loss in the optical clarity of the samples.

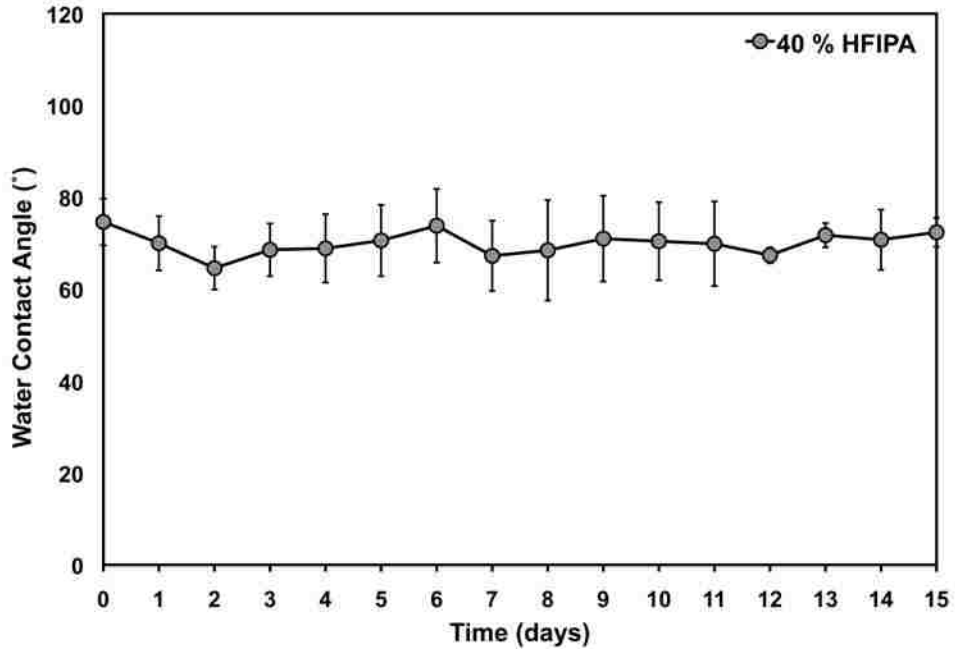

Figure 3-33: Contact angle as a function of time for samples containing 40 mol% hexafluoroisopropyl acrylate introduced via bulk modification.

An independent, detailed, collective study was conducted on the water contact angles of samples containing 40 mol% HFIPA as a function of a 14-day recovery time. These data are illustrated in Figure 3-33. These samples featured a sporadic average water contact angle of ~70˚ (Figure 3-33). The samples were found to be less stable than other samples containing other modifying molecules. The standard deviation of the average water contact angles was 2.5˚. The standard deviations for each individual

point indicated some irreproducibility in this fluorination method. The average standard deviation for individual points was ~6.5˚. Because of the high standard deviations and the irreproducibility of these samples, other fluorinated molecules were investigated as modifying molecules.

3.5.15d DFHA Bulk Modification

In an attempt to produce a more stable and reproducible fluorinated thiol-acrylate surface, a different fluorine-functionalized monofunctional acrylate was incorporated into the polymer network, 2,2,3,3,4,4,5,5,6,6,7,7-Dodecafluoroheptyl acrylate (DFHA). This material was chosen because it possessed multiple hydrophobic features, a 6-membered hydrocarbon chain and 12 pendant fluorine groups. As was predicted based on previous hydrophobic bulk modification experiments, there was basically no change in the hydrophobicity with an increase in the density of the modifying layer on the surface. The average water contact angle increased by only 0.1˚ with a 10 mol% increase in the DFHA concentration. Regardless of the hydrophobic modifier being incorporated, there was an upper limit where no more hydrophobicity could be obtained using this chemical modification technique. To introduce more hydrophobicity onto the surface, the physical morphology would likely need to be altered.

Figure 3-34 illustrates the narrowly distributed (lower standard deviations) water contact angles produced via the bulk modification of the thiol-acrylate materials using 10 mol% DFHA over a 14 day time period. The average water contact angle during this 14-day time period was 76.3˚. The standard deviation of the average water contact angles over the 2 week period was <1˚ indicating a high level of stability. The average standard deviation for the individual data points was <3˚ indicating a high level of

reproducibility. The use of DFHA was, therefore, successful in increasing the hydrophobicity of the thiol-acrylate copolymer materials, producing highly stable hydrophobic surfaces that could easily be reproduced.

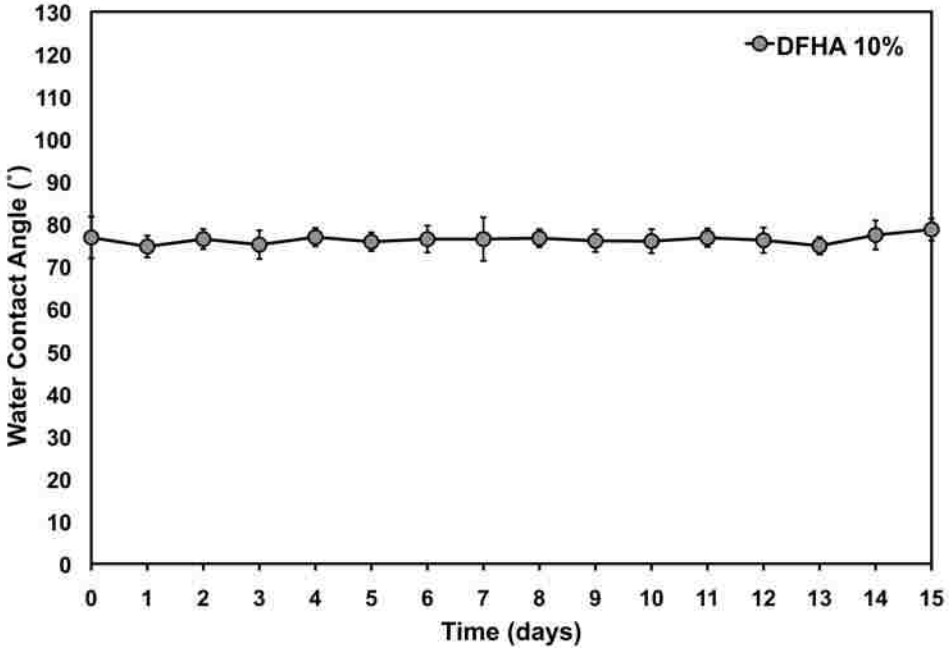

Figure 3-34: Contact angle as a function of time for samples containing 10mol% dodecafluoroheptyl acrylate introduced via bulk modification.

3.5.16 Construction of a Water Contact Angle Library

Using bulk modification to incorporate various monomers into the thiol-acrylate matrix, a stable water contact angle library was constructed. This library included bulk modifications utilizing both hydrophilic and hydrophobic modifying molecules. Figure 3-35 illustrates the average water contact angles as a function of recovery time for various native and modified materials. Native PDMS and PDMS samples exposed to oxygen plasma for 30 seconds are illustrated for comparison purposes. Native PDMS had a stable hydrophobic (undesirable for microfluidics) water contact angle of 116.1±1.5˚ and on average differed by 0.87˚ during the 2 week time period. The oxidized PDMS sample had a very transient hydrophilic water contact angle, initially of 17.2±3.4˚. After 1 day

the oxidized PDMS sample suffered a hydrophobic recovery to a contact angle of 70.6±4.1˚. After 1 week, the water contact angle of the oxidized PDMS sample recovered even more to 98.1±2.5˚. After the full 14 days, the water contact angle of the oxidized PDMS sample was 105.5±0.97˚, indicating a nearly full hydrophobic recovery. All of the PETA-co-TMPTMP samples illustrated a high level of stability in terms of their contact angles. Thiol-acrylate samples bulk modified with 10 mol% DFHA had an average water contact angle of 76.3±0.98˚ and differed on average by 2.9˚ during the 14 day time period. Thiol-acrylate samples bulk modified with 5 mol% PEGMEA had an average water contact angle of 68.1±1.5˚ and differed on average by 3.0˚ during the 14 day study. Thiol-acrylate samples bulk modified with 10 mol% PEGMEA had an average water contact angle of 56.9±1.8˚ and on average differed 4.2˚ during the 14 day time period. Thiol-acrylate samples bulk modified with 15 mol% PEGMEA had an average water contact angle of 43.7±2.0˚ and differed on average by 4.7˚ during the 14 day time period. Thiol-acrylate samples bulk modified with 20 mol% PEGMEA had an average water contact angle of 35.6±2.1˚ and on average differed by 5.7˚ during the 14 day time period. Overall, the thiol-acrylate materials were much more stable over the 2 week study compared to the transient nature of the activated PDMS. This was very important as stable hydrophilicity could be introduced into a microfluidic surface. The stability of these samples allowed for a substantial increase in the shelf life of microfluidic devices. Using this Boundless resin a microfluidic device could be prepared and confidently used at least fourteen days after production, having the same surface properties as it did on day one. The ease of modification also allowed for more specific binding of molecules. For example, a personalized microfluidic device could be

prepared for a consumer in need of analyzing a molecule that was known to interact most efficiently and effectively with a surface possessing a water contact angle near 45˚ by bulk modification of the material with 15 mol% PEGMEA. This simple bulk modification technique and thereby these easily modifiable surfaces allow for the production of a plethora of specifically personalized microfluidic devices.

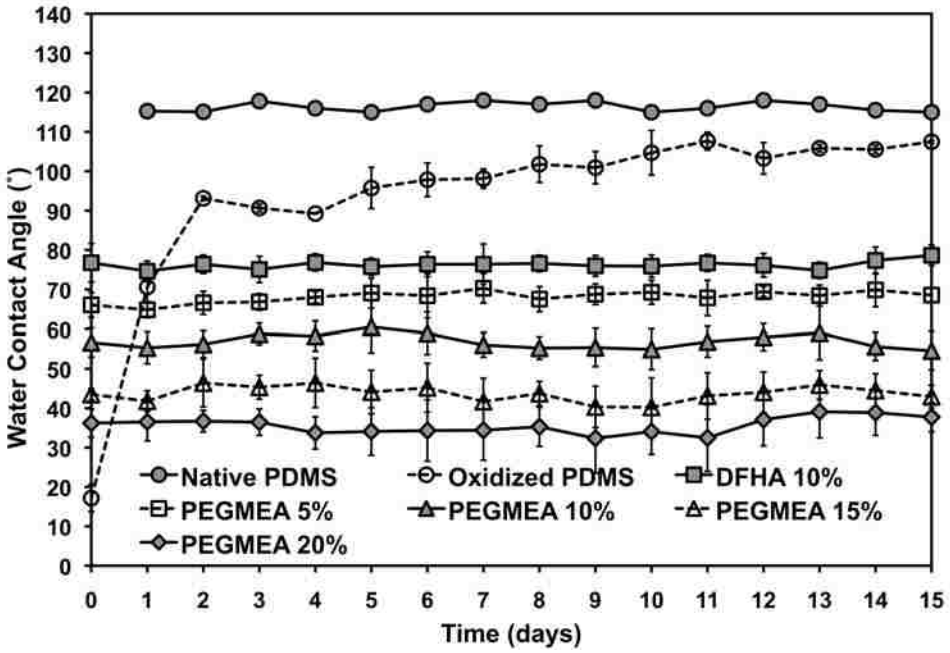

Figure 3-35: Stable water contact angle library showing native PDMS, PDMS exposed to an oxygen plasma generator for 30 seconds, and PETA-co-TMPTMP materials containing DFHA and various concentrations of PEGMEA as a function of recovery time.

3.5.17 Replication of Molds Via Soft Lithography

The accurate replication of a positive mold via a soft lithography technique was vital for the successful production of a stable hydrophilic thiol-acrylate microfluidic device. Poly (methyl methacrylate) (PMMA) positive molds were prepared via a hot embossing technique[179, 180, 184] with a copper plate micromilled[172, 178] to contain the desired microchannel patterns. The positive PMMA molds were used to prepare the thiol-acrylate microchannels via a simple soft lithography method. Figure 3-

36 illustrates the replication of the microchannels using this process where the positive PMMA mold microchannel had a measured channel width of 248.24 µm (Figure 3-36a) and the PETA-co-TMPTMP replica had a measured channel width of 247.82 µm. The replication process was very successful, showing that microstructures could easily be duplicated with a high level of certainty into a thiol acrylate material using a soft lithography technique.

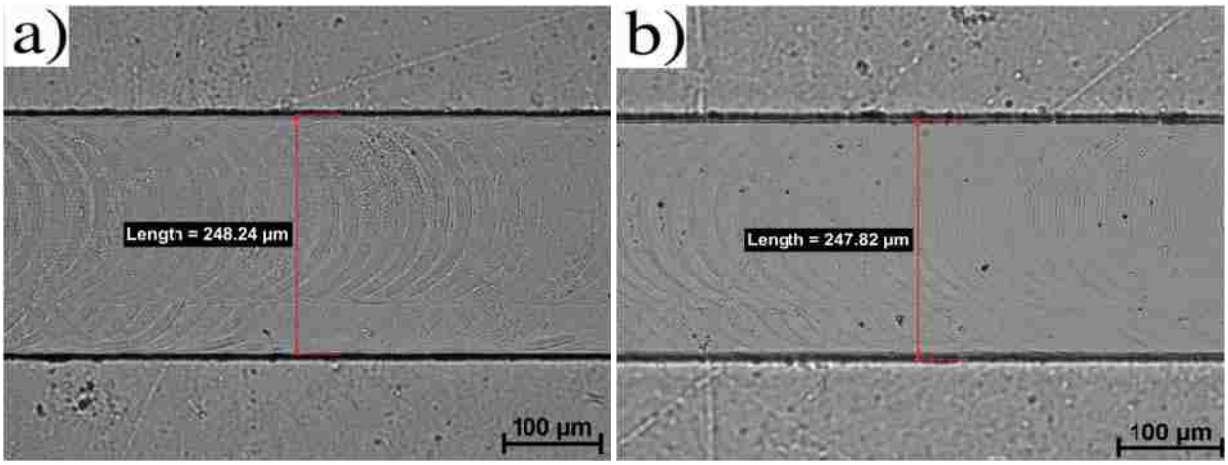

Figure 3-36: Optical microscopy illustrating the replication of a positive mold via a thiol-acrylate soft lithography process. a) PMMA positive mold with a measured microchannel width of 248.24 µm; b) replicated PETA-co-TMPTMP microchannel measuring 247.82 µm. The scale bar represents 100 µm.

The replication of smaller and more complex dimensions was also observed via the thiol-acrylate soft lithography method. Figure 3-37a illustrates small ring artifacts present on the PMMA positive mold introduced via micromilling and copied during the hot embossing process. These small ring dimensions were well reproduced into the thiol-acrylate material as shown in Figure 3-37b. This result denoted the potential for the introduction of microchannels with small dimensions, smaller than utilized for this research, into the thiol-acrylate material via soft lithography.

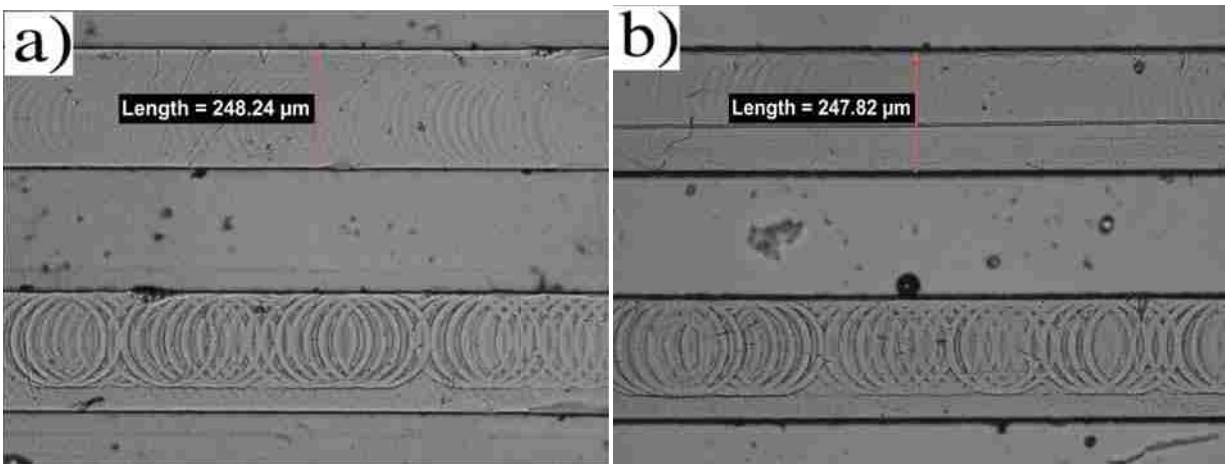

Figure 3-37: Optical microscopy illustrating the fine replication of a positive mold via a thiol-acrylate soft lithography process. a) PMMA positive mold ring artifacts within the channels; b) replicated PETA-co-TMPTMP microchannel also illustrating the ring structures.

3.5.18 Final, Annealed PETA-co-TMPTMP Microfluidic Devices

Multiple final microfluidic devices were prepared using the soft lithography technique coupled with the partial polymerization/excess monomer annealing technique. Some of these final devices are shown in Figure 3-38. Prior to the annealing process, holes were drilled in specific, predestined places on the half of the device containing the microchannels via a drill press and a small drill bit. This drilling step produced holes used to attach capillaries by which the fluid would be introduced to the microfluidic device. Blunt needles bent at 90˚ angles, over which rubber tubing was stretched, were inserted into the wholes, and a rapidly curing, two-part epoxy was used to append the needles and capillary tubing to the microfluidic device (Figure 3-38 top right). These capillaries were used to push aqueous fluids easily through the small hydrophilic microchannels. In some cases, polyether ether ketone (PEEK) flexible, thermoplastic tubing with an outside diameter (OD) approximately equal to the internal diameter (ID) of the predrilled holes was inserted directly, without the support of a blunt needle and

requiring no epoxy to append the tubing to the device (Figure 3-38 bottom). An aqueous methyl orange solution was easily flowed through these hydrophilic microchannels. Both the epoxy-bound rubber/blunt needle capillary microfluidic device and the PEEK tubing device showed no signs of leakage, which would be obvious around the perimeter of the microchannels or at the inlet junctions due to the use of a colored solution. These images in Figure 3-38 illustrate the successful production and application of proven, stable, hydrophilic thiol-acrylate microfluidic devices capable of flowing aqueous materials down small microchannels with no leakage of the aqueous solution from the microfluidic device.

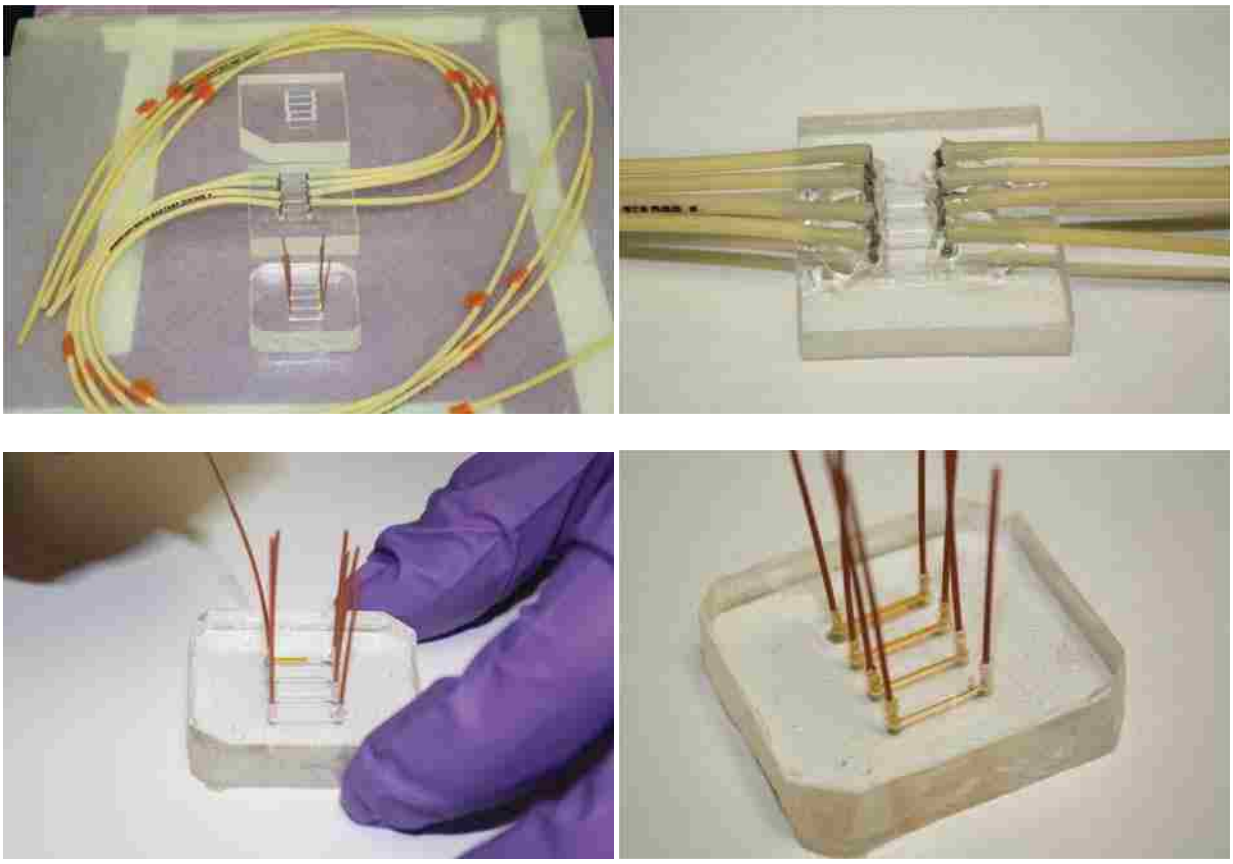

Figure 3-38: Photographic images of final, annealed PETA-co-TMPTMP microfluidic devices attached to inlet capillaries (top left and top right) and a aqueous methyl orange solution being pumped through a final, annealed PETA-co-TMPTMP microfluidic device (bottom left and bottom right).

3.5.19 Fluorescence Microscopy Potential and Capabilities

As fluorescence microscopy is an important tool in the field of microfluidics[242-246], it was nearly imperative that the thiol-acrylate materials have the potential to be used in such fluorescence experimentation. To prove their capabilities, an aqueous fluorescein isothiocyanate (FITC) solution was flowed through the microfluidic device and observed using simple photography and a fluorescence microscope.

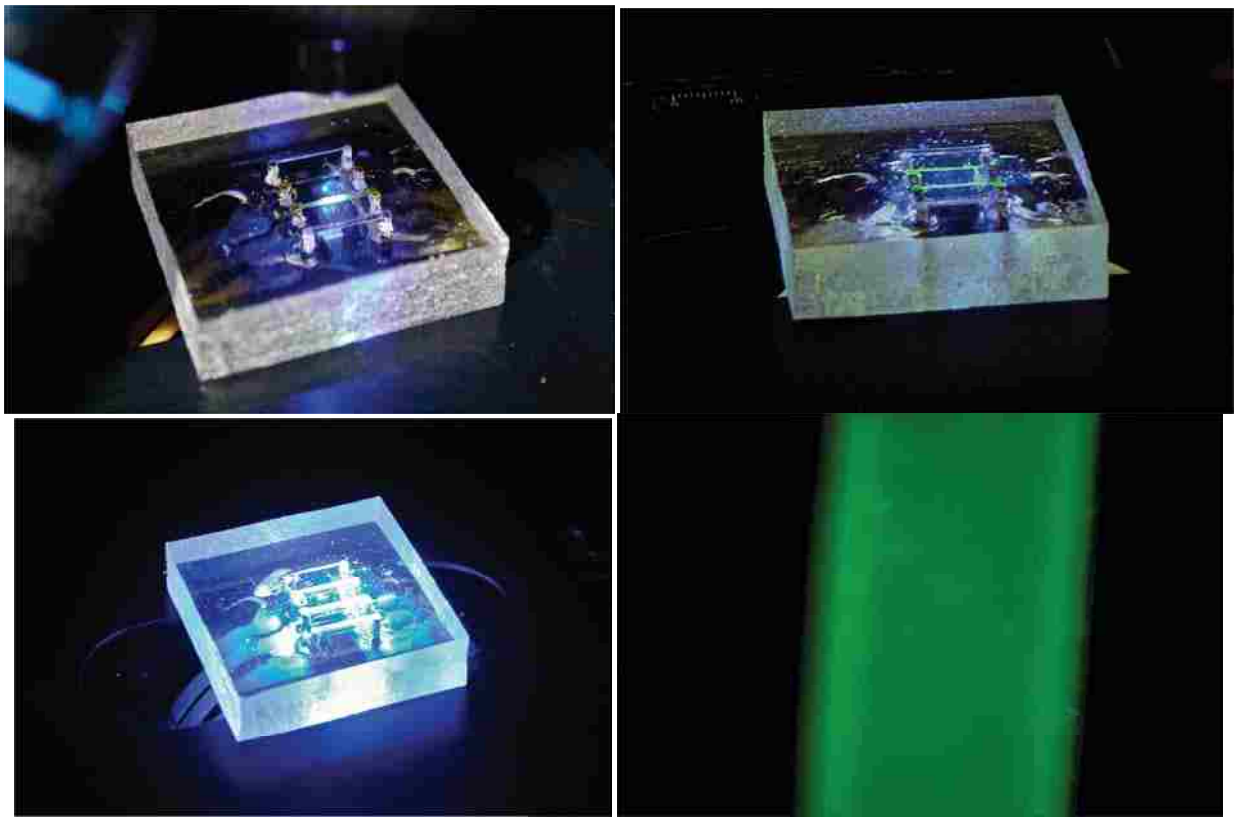

Figure 3-39: Fluorescent images of PETA-co-TMPTMP microfluidic devices containing an aqeous fluorescein isothiocyanate (FITC) solution. Photographic images of microchannels containing the FITC solution are shown on top and bottom left and top right, and a fluorescent microscopy image is shown on the bottom right.

Figure 3-39 illustrates multiple photographic images (top and bottom-left and top-right) of the microchannels fluorescing under the light source causing the green coloring effect. The bottom right picture in Figure 3-39 illustrates a fluorescent microscope image

showing the microchannel fluorescing on a microscopic scale. This indicates that fluorescence microscopy could be used to analyze aqueous specimens when flowed through these thiol-acrylate microfluidic devices.

3.6 TMPeTA-co-TMPTA

Other acrylic monomers were used to prepare novel thiol-acrylate materials with potential applications in the field of microfluidics. Specifically, a relatively large molecular weight, ethoxylated, and presumably hydrophilic trifunctional acrylate, trimethylolpropane ethoxylate triacrylate (TMPeTA), was employed along with DEA and TMPTMP in the same manner as discussed for the PETA. Two different TMPeTA monomers were exploited and studied, one with a typical M_n of 912 g/mol (TMPeTA 912) and the other with a typical M_n of 692 g/mol (TMPeTA 692). The increase in the molecular weight was due to additional ethoxylate groups incorporated between the trimethylolpropane moieties and the acrylate functional groups. The TMPeTA 692 thus typically had 7 ethoxylate groups per molecule, where as the TMPeTA 912 typically had 14 ethoxylate groups per molecule. It was hypothesized that the decrease in cross-link density facilitated by the increase in the length of the linkers between the acrylate functional groups would result in a more flexible material. Figure 3-40 illustrates the flexibility of the TMPeTA 912-co-TMPTMP (right) relative to the less flexible PETA-co-TMPTMP (left) on the microscopic level. The materials shown in Figure 3-40 were punctured using a hand-held biopsy punch, and the resulting holes were examined microscopically to determine the different effects on the materials. The PETA-co-TMPTMP (left) experienced a “spidering” effect when the biopsy bunch was forced through the material. The microscopic cracking indicated that the material had some

brittle properties. The TMPeTA 912-co-TMPTMP material, on the other hand, showed no signs of cracking or “spidering”, therefore the material with the relatively large molecular weight showed some improvements in terms of material flexibility.

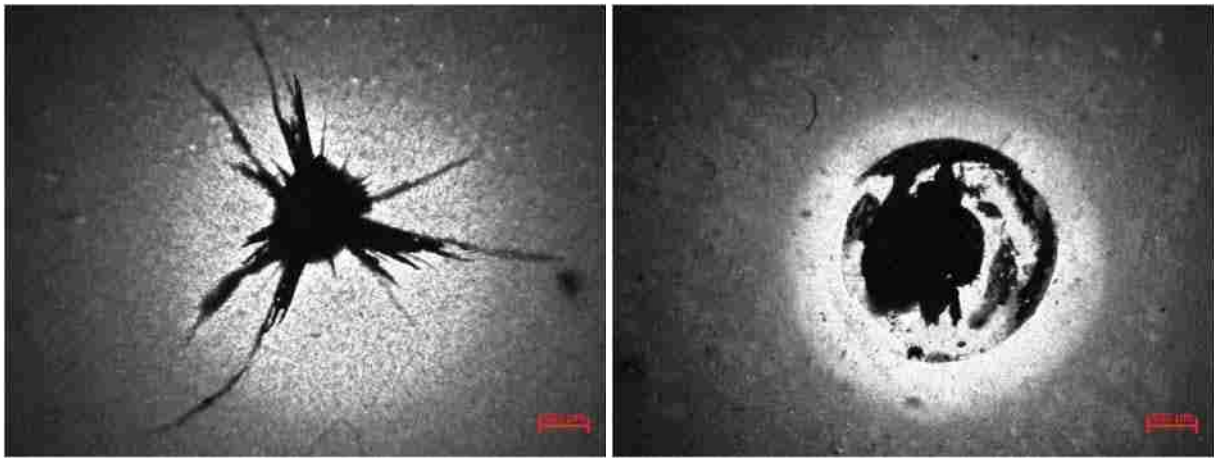

Figure 3-40: Optical microscopy images of holes punctured in PETA-co-TMPTMP material (left) and TMPeTA 912-co-TMPTMP material (right) using a biopsy punch.

3.6.1 TMPeTA 912 Gel Time Manipulation

The first ethoxylated triacrylate to be incorporated into a thiol-acrylate copolymer and studied was TMPeTA 912. As with its PETA competitor, the gel time was easily manipulated by changing the concentration of the diethylamine. Figure 3-41 illustrates the experimental gel time as a function of the DEA molar concentration. The manipulated gel times ranged from ~3 hours to <45 minutes within the amine concentration array examined in this study. As with PETA-co-TMPTMP, a parabola curve was again observed in associating with the gel time and amine concentration. The first half of this curve where the gel time decreased as a function of increasing amine concentration was attributed to the increase in the rate constant associated with an increase in the catalyst concentration as would normally be expected. The increase in the gel time at high amine concentrations shown in the second half of the curve was

accredited to the decrease in the crosslink density causing an increase in the critical conversion required for gelation of the copolymer material as shown by the Carothers[89] and Flory and Stockmeyer[89] gel time estimations discussed earlier.[89]

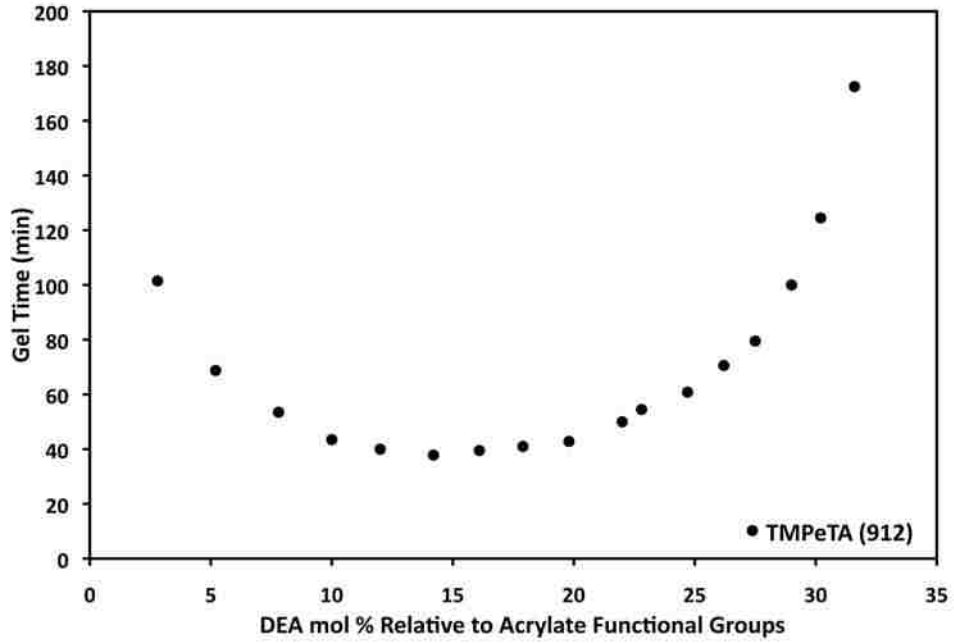

Figure 3-41: Gel time for TMPeTA 912 as a function of DEA mol% relative to acrylate functional groups.

3.6.2 TMPeTA 912 Water Contact Angles

The contact angles of the native TMPeTA 912-co-TMPTMP materials were determined as a function of time and the data are illustrated in Figure 3-42. These materials were found to be extremely hydrophilic and stable having an average water contact angle of 36.1±1.7˚ and differed on average by 1.9˚ during the 10-day study. As would be expected, the presence of the ethoxylate groups caused the material to be natively more hydrophilic than the PETA-co-TMPTMP material. This would be a beneficial property of the material in terms of a microfluidic application.

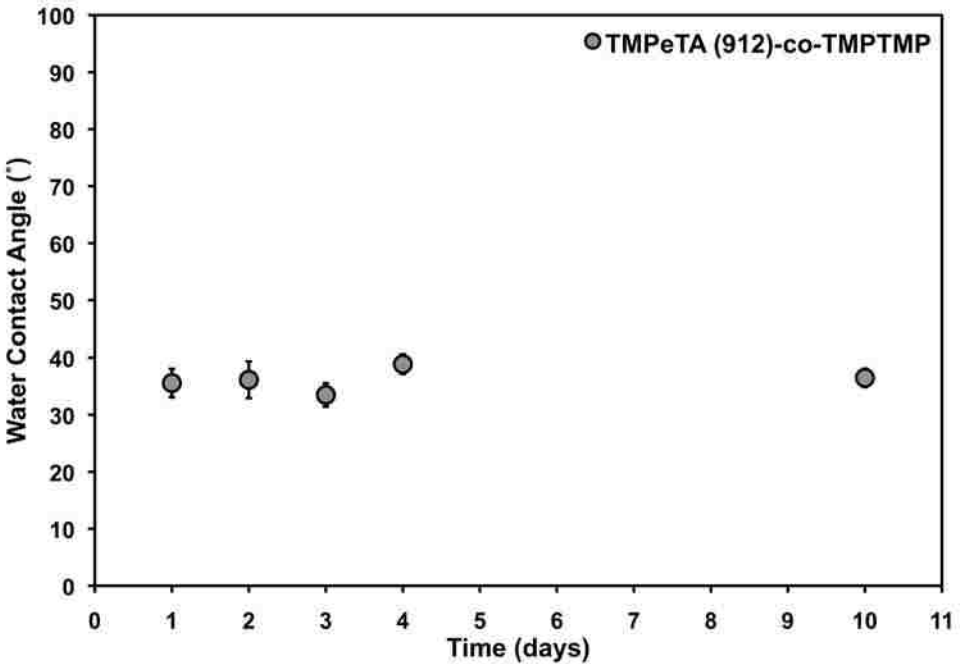

Figure 3-42: Water contact angle for TMPeTA 912 as a function of time. Showing data exposed to polystyrene petri dish.

3.6.3 TMPeTA 912 Water Mass Uptake

Due to the extremely hydrophilic nature of the TMPeTA 912-co-TMPTMP material and the relatively low crosslink density, it was expected to absorb water. This water uptake could be a negative property for a microfluidic application due to the likely chance that the material would swell causing a change in the dimensions of the microchannels. To determine the material bulk interactions with an aqueous environment, the water mass increase was determined as a function of amine concentration and time. These data are illustrated in Figures 3-43 and 3-44. The weight of the hydrophilic TMPeTA 912-co-TMPTMP copolymeric material was observed to increase as a function of DEA concentration when exposed to an aqueous environment. This was anticipated as an increase in the DEA concentration caused a decrease in the crosslink density and more void space in which the water could occupy. At a low amine

concentration of 3 mol% the weight of the material increased by only 1.2% after 20 minutes of being fully submerged in water and 3.3% after 2 hours, but at a high amine concentration of 34 mol% the material weight increased by 16.6% after 20 minutes and 55.8% after 2 hours. (Figure 3-43)

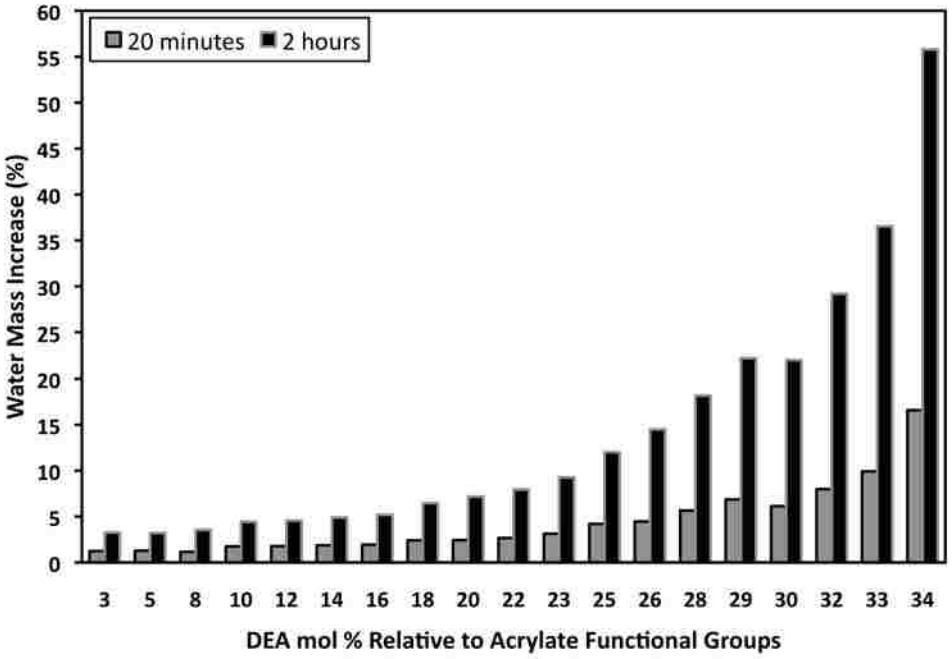

Figure 3-43: TMPeTA 912-co-TMPTMP water mass uptake as a function of diethylamine concentration illustrating the mass uptake as a function of a large range of DEA concentrations at 20 minutes and 2 hours.

The water mass uptake also increased as a function of time as would be expected. Figure 3-44 illustrates the water mass increase as a function of selected amine concentrations at various increments of time. At every amine concentration shown in Figure 3-44 the water mass uptake increased nearly linearly over the 2 hour time period. For example, a material containing a moderate concentration of DEA, 14.2 mol%, was observed to increase in mass by 7.4±2.2% after 20 minutes of full water submersion, 11.9±3.3% after 40 minutes, 14.3±3.2% after 60 minutes, 16.7±3.2% after 80 minutes, 19.5±3.7after 100 minutes, and 21.1±3.8% after 120 minutes. (Figure 3-44)

Even at moderate amine concentrations, this material experienced a high level of water mass increase when submerged in an aqueous environment. After 2 hours, an equilibrium water uptake had not been obtained implying that this material could potentially uptake even more water at longer submersion times. Due to this high level of water mass uptake and the high potential for swelling, this material could be limited in the areas of microfluidics that require precise, stable microchannel dimensions. However, there are some potential areas of microfluidics where water swelling could be beneficial. For example, these materials could be used to produce nanochannels using a swelling technique resulting in a decrease in the channel dimensions from the easily obtainable micro-size to the much more difficult nano-size using a simple soft lithography method.

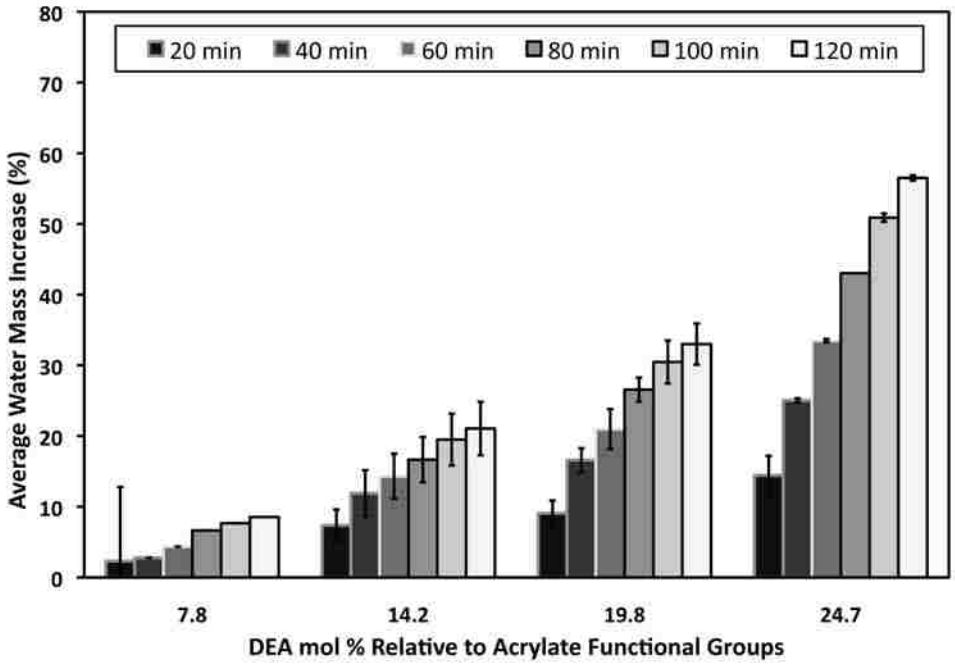

Figure 3-44: TMPeTA 912-co-TMPTMP water mass uptake as a function of diethylamine concentration illustrating selected concentrations at times ranging from 20 to 120 minutes.

3.6.4 TMPeTA 692 Gel Times

In an attempt to decrease the water uptake of the material but maintain the high flexibility, another TMPeTA material was investigated as the trifunctional acrylic monomer component. TMPeTA with an average M_n of 692 (TMPeTA 692) was used to prepare a highly hydrophilic compolymeric material in the same manner as discussed above. The gel times as a function of amine concentration for these TMPeTA 692-co-TMPTMP materials were determined. These data are shown in Figure 3-45. The manipulated gel times ranged from ~3.5 hours to <50 minutes within the amine concentration array examined in this study.

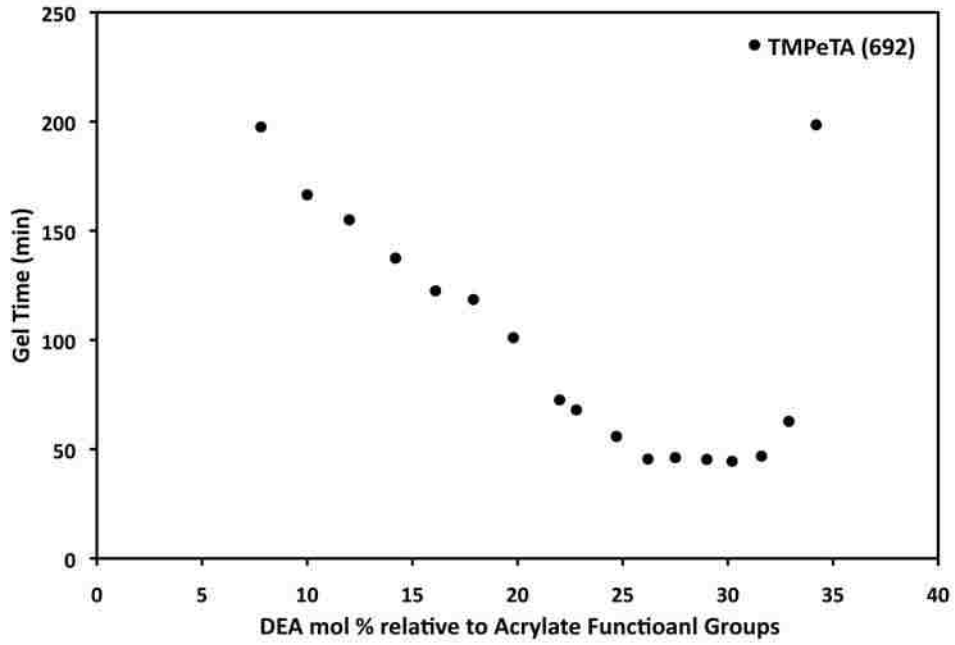

Figure 3-45: Gel time as a function of diethylamine mol% relative to acrylate functional groups.

Again, as with the other thiol-acrylate analogs, a parabola curve resulted when the gel times were plotted against the amine catalyst concentration. Figure 3-45 illustrates this parabola-type curve. The parabola produced by the data for TMPeTA 692-co-TMPTMP was not as symmetrical as that of the materials incorporating PETA or

TMPeTA 912 monomers, but the same trend held true. As would be expected, the gel time decreased from as a function of amine concentration at low amine concentration less than ~27 mol%. Beyond ~33 mol% DEA, the gel time was observed to sharply increase as a function of amine concentration which was explained again by the decrease in the crosslink density with an increase in amine concentration resulting in a increase in the critical conversion required fro gelation as described by the Carothers[89] and Flory and Stockmeyer[89] estimations.

The gel time was also monitored as a function of TMPeTA 692 and DEA reaction time. These data are shown in Figures 3-46 and 3-47. As with all of the thiol-acrylate systems studied here, the acrylate and amine were normally allowed to react for at least 24 hours prior to being utilized in the soft lithography process.

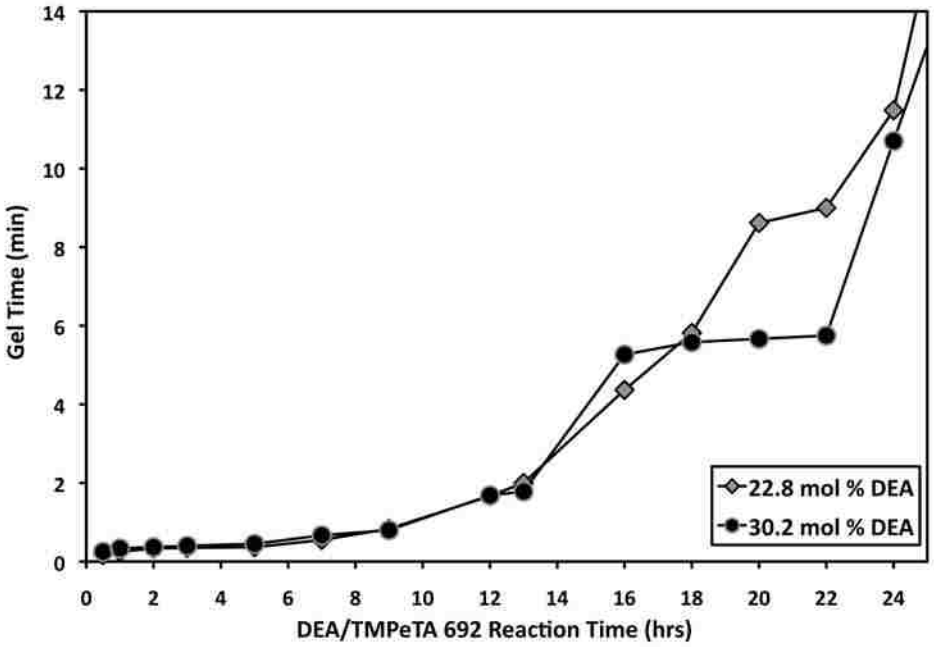

Figure 3-46: Gel time as a function of DEA-TMPeTA 692 reaction time for 24 hours.

The systems containing PETA were observed to reach a stable gel time after only 2 hours of PETA/DEA reaction time (Figure 3-8) implying the full conversion of the

secondary diethylamine to a large molecular weight tertiary amine/comonomer molecule. However as is seen in Figure 3-46, the gel time for the TMPeTA 692-containing systems had not reached equilibrium even after 24 hours, regardless of the amine concentration. For samples containing 22.8 mol% DEA the gel time ranged from ~10 seconds after 30 minutes of acrylate-amine reaction time to ~11 minutes after 24 hours of reaction time. (Figure 3-46)

When monitored for a longer period of time, up to 45 hours of TMPeTA 692-DEA reaction time, the gel time still had not reached a steady state. Figure 3-47 illustrates these data. For samples containing 22.8 mol% DEA, the gel time reached a high of 116 minutes after 45 hours of reaction time. These data indicated that much more time was required to convert the secondary amine to a tertiary amine when using TMPeTA 692 as the trifunctional acrylic comonomer component as opposed to PETA.

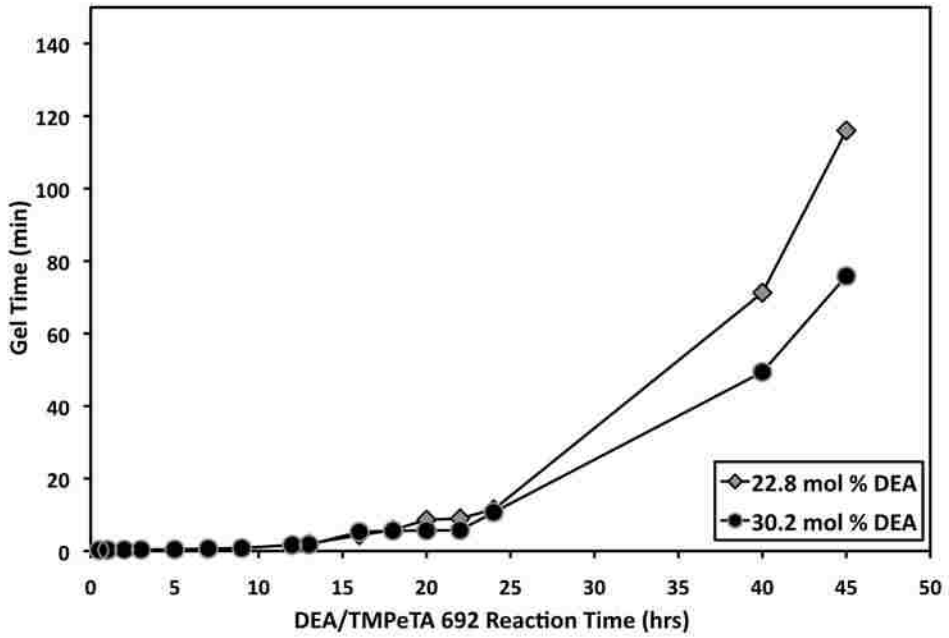

Figure 3-47: Gel time as a function of DEA-TMPeTA 692 reaction time for 50 hours.

3.6.5 TMPeTA 692 Water Contact Angles

The water contact angles of the native TMPeTA 692-co-TMPTMP materials were determined as a function of time and the data are illustrated in Figure 3-48. These native materials were found to be extremely hydrophilic having an initial water contact angle of 29.4±2.5˚. After the 14 day time period studied, the native water contact angle was observed to increase by ~10˚ (~40%) to 40.9±6.4, indicating that the surface of the material was only moderately stable. The average standard deviation during the 2 week studies was found to be ~4.1˚ demonstrating moderate reproducibility.

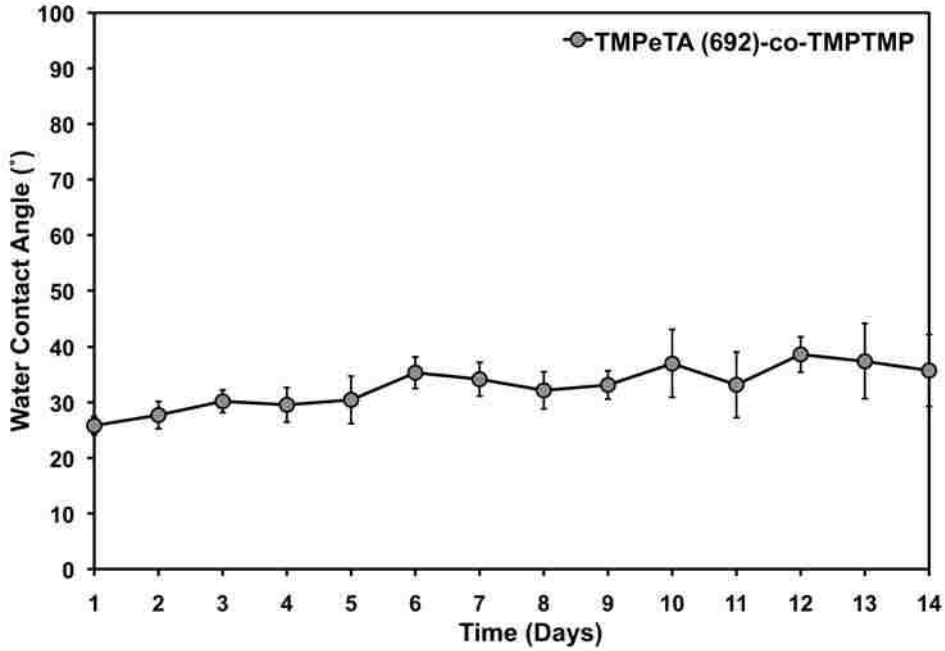

Figure 3-48: Water contact angle for native TMPeTA 692-co-TMPTMP as a function of time.

3.6.6 TMPeTA 692 Bulk Modifications

The TMPeTA 692-co-TMPTMP materials were bulk modified with various modifying molecules to determine the ease of manipulation of their surface energies. Figure 3-49 illustrates the initial water contact angles as a function of bulk modifier type. Unlike the PETA analogous systems, the contact angles of the TMPeTA 692 materials

were not greatly affected by the incorporation of small monofunctional modifying molecules. The contact angle was unchanged within the standard deviation when 5% lauryl acrylate or 10% hexafluoroisopropyl acrylate was incorporated into the network as a bulk-modifying molecule. This lack of surface energy manipulation demonstrated the difficulty of producing a hydrophobic surface using the extremely hydrophilic ethoxylated comonomer, TMPeTA 692. In an attempt to further decrease the water contact angle of the TMPeTA 692 material, polyethylene glycol methyl ether acrylate (PEGMEA) was incorporated into the network as a bulk-modifying molecule. The presence of 5 mol% PEGMEA caused a decrease in the initial water contact angle to 14.6±2.5˚, showing some potential for the hydrophilic bulk modification of these TMPeTA 692-co-TMPTMP materials.

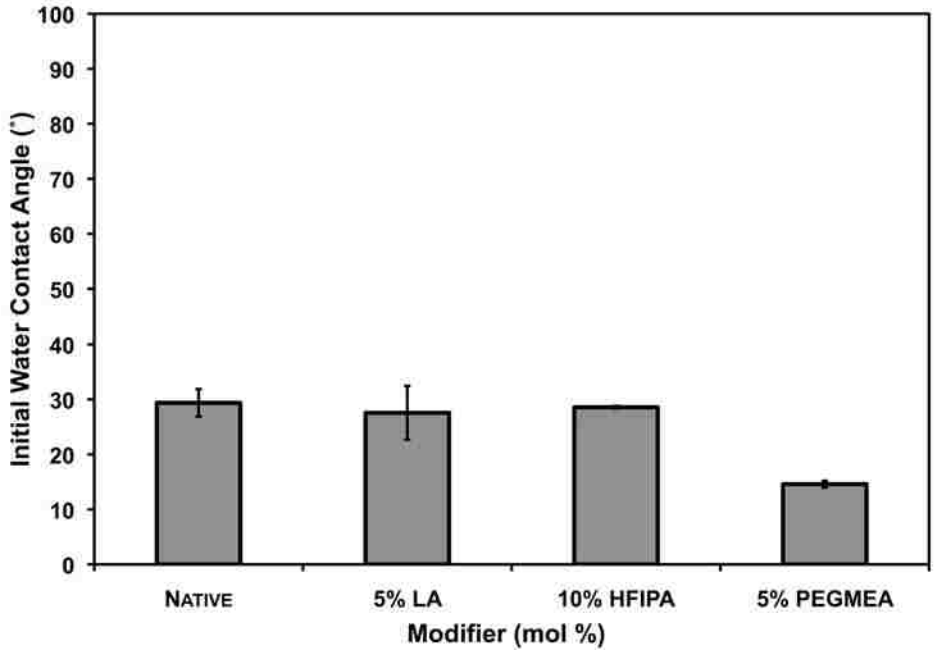

Figure 3-49: Water contact angle for TMPeTA 692-co-TMPTMP as a function various bulk modifiers.

The water contact angles were monitored as a function of time for TMPeTA 692-co-TMPTMP samples bulk modified with 5 mol% PEGMEA to determine the stability of

the material over a two week period of time. Figure 3-50 illustrates these data. The hydrophilic bulk modified materials were observed to suffer a hydrophobic recovery with the average water contact angles more than tripling during the 14-day study. The average water contact angle increased from 14.6±2.5˚ initially to 23.5±5.7˚ after 1 week and up to 46.1±16.9˚ after 2 weeks. The standard deviations of the contact angles were also observed to be very high, indicating reproducibility limitations. The average water contact angle standard deviation for the materials studied over 14 days was 5.6˚. Although an extremely low water contact angle could be achieved via the hydrophilic bulk modification of an already hydrophilic, ethoxylated triacrylate-containing material, the material was not stable, resulting in an increase in the water contact angle beyond that of even the native copolymer, and the results were not easily reproducible.

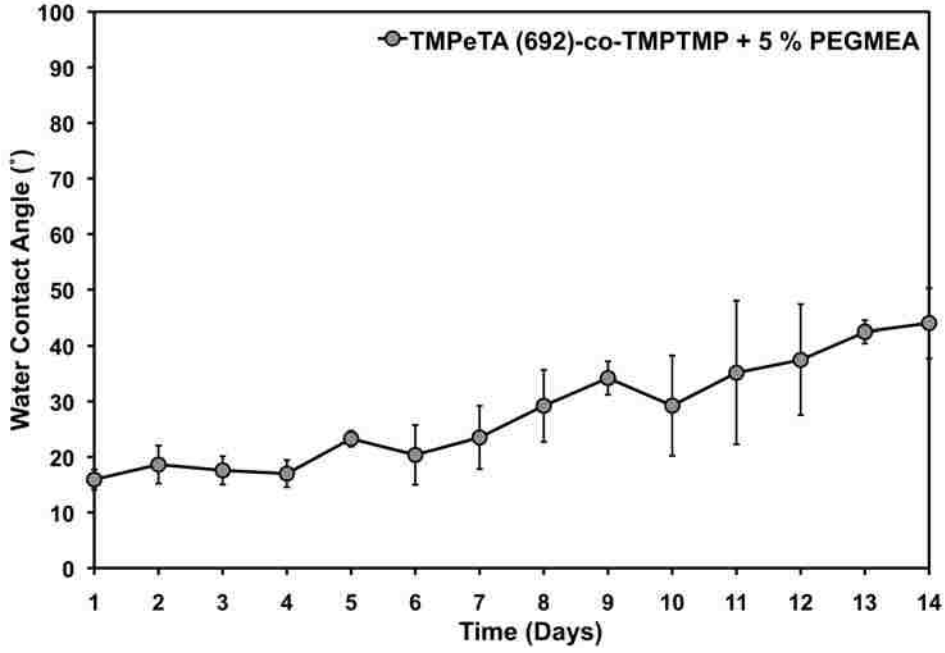

Figure 3-50: Water contact angle for TMPeTA 692-co-TMPTMP material containing 5 mol% diethylemaine relative to acrylate functional groups as a function of a 14 day time period.

3.6.7 TMPeTA 692 Water Mass Uptake

Like the previously studied materials containing TMPeTA 912, the TMPeTA 692-co-TMPTMP materials were expected to absorb water due to their extremely hydrophilic nature and relatively low crosslink density. In was hypothesized that these materials would uptake less water mass compared to the TMPeTA 912 materials as the TMPeTA 692 materials contained fewer hydrophilic ethoxylate groups and shorter linker groups, causing an increase the crosslink density and thereby a decrease the void space that could be occupied by water molecules. The water mass increase was determined as a function of amine concentration and time to determine the material bulk interactions in an aqueous environment. These data are illustrated in Figures 3-51 and 3-52.

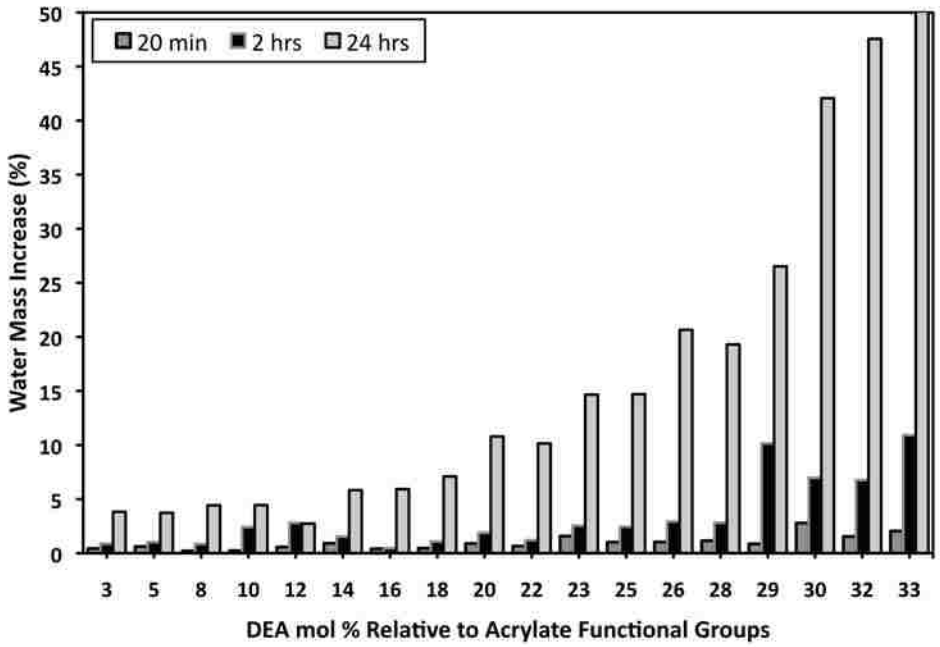

Figure 3-51: TMPeTA 692-co-TMPTMP water mass uptake as a function of diethylamine concentration illustrating the mass uptake as a function of a large range of DEA concentrations at 20 minutes, 2 hours and 24 hours.

Although somewhat sporadic, the weight of the hydrophilic TMPeTA 692-co-TMPTMP copolymeric material was observed to increase as a function of DEA

concentration. This was expected as an increase in the DEA concentration caused a decrease in the crosslink density and more void space in which the water could occupy. At a low amine concentration of 3 mol% the weight of the material increased by only 0.44% after 20 minutes of being fully submerged in water, 0.89% after 2 hours, and 3.8% in 24 hours. At a high amine concentration of 33 mol% the material weight increased by 2.1% after 20 minutes, 10.9% after 2 hours, and 74.11% after 24 hours. (Figure 3-51) For comparison purposes, the water mass uptake for the TMPeTA 912 materials containing 3 mol% and 34 mol% DEA were 3.3% after 2 hours and 55.8% after 2 hours, respectively.

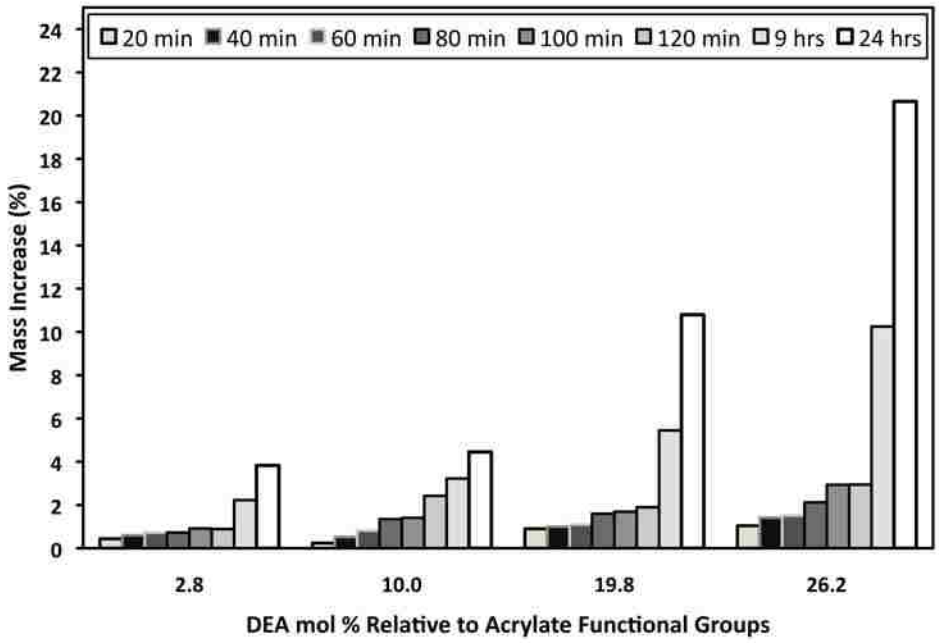

Figure 3-52: TMPeTA 692-co-TMPTMP water mass uptake as a function of diethylamine concentration illustrating selected concentrations at times ranging from 20 minutes to 24 hours.

The water mass uptake for the TMPeTA 692 materials also increased as a function of time. Figure 3-52 illustrates the water mass increase as a function of selected amine concentrations at various increments of time. At moderately low amine

concentrations, these materials were not observed to uptake an unacceptably large amount of water even after 24 hours. At a moderately low amine concentration of 10 mol%, the mass of the material was observed to increase by 0.24% after 20 minutes of full water submersion, 0.53% after 40 minutes, 0.82% after 60 minutes, 1.4% after 80 and 100 minutes, 2.4 after 2 hours, 3.2% after 9 hours, and 4.5% after 24 hours. (Figure 3-52) The use of this trifunctional acrylic monomer with shorter ethoxylated chains (692) was a great improvement over the longer TMPeTA 912 monomer in terms of water mass uptake.

Although these relatively long-chain, high-molecular weight TMPeTA trifunctional monomer components greatly increased the flexibility and initial contact angle of the thiol-acrylate microfluidic material, the limitations were not suitable for the application sought here. The combination of their extremely high aqueous uptakes and more volatile contact angles compared to those of PETA-co-TMPTMP proved these materials less useful in the production of simple, cost-efficient, stable hydrophilic microfluidic devices. These TMPeTA-co-TMPTMP materials could serve other purposes in the field of microfluidics in terms of “shrinking” easily reproducible microstructures to more difficult nanostructures.

3.7 Thiol-Acrylate Microfluidic Material Potential Forecast

As shown earlier, these PETA-co-TMPTMP surfaces can be successfully modified with small modifying molecules ranging from very hydrophilic molecules such as PEGylated acrylates (Figure 3-25) to very hydrophobic molecules such as those containing long hydrocarbon chains (Figure 3-30) or fluorinated compounds (Figures 3-32 and 3-34). The fact that these surfaces can be easily and robustly modified opens a

plethora of opportunities for further applications in the field of microfluidics even beyond the highly desirable stable hydrophilic nature of the material. Utilizing specific modifying molecules, these materials have the potential for bulk modification to produce a consumer-manipulatable microfluidic device via avidin-biotin interactions. Biotin is a critical vitamin found in all living cells that is used in a multitude of biological processes. [247] Avidin, a glycoprotein, specifically and stoichiometrically binds biotin with high affinity. [248] The avidin-biotin complex is one of the strongest non-covalent interactions known, boasting an equilibrium dissociation constant of 10^{-15} M. [248] Avidin molecules, including streptavidin, have four binding sites, therefore one avidin molecule can bind up to 4 independent biotin molecules. [249] A biotin molecule functionalized with a monofunctional acrylate component could be bound to the surface of these PETA-co-TMPTMP microfluidic devices via the bulk modification techniques described earlier. This biotinylated surface produced via bulk modification could then be used to bind functionalized avidin molecules resulting in a 2^{nd}-tier, consumer-controlled modification. A final consumer could attach specific active group molecules required for their unique analysis to biotin molecules and bind them in a stoichiometric fashion to avidin molecules, leaving one binding site open per avidin molecule. These then functionalized avidin molecules could be flowed in an aqueous solution down the previously prepared biotinylated microfluidic device, resulting in the attachment of the functionalized avidin molecules to biotin molecules covalently linked to the surface of the PETA-co-TMPTMP material. The premise for this potential forecasted technique is illustrated in Scheme 3-8. The realization of this 2-tier modification technique could be highly beneficial in the field of microfluidics. Multiple active groups could be attached o a

single avidin molecule and attached to the biotinylated microfluidic surface. This one device then could be used to separate multiple components, as each active group would have an affinity for a different molecule. Also, one type of biotinylated microfluidic device could be prepared and serve a multitude of specific final consumers as each surface could be manipulated depending on the individual needs of the final consumer.

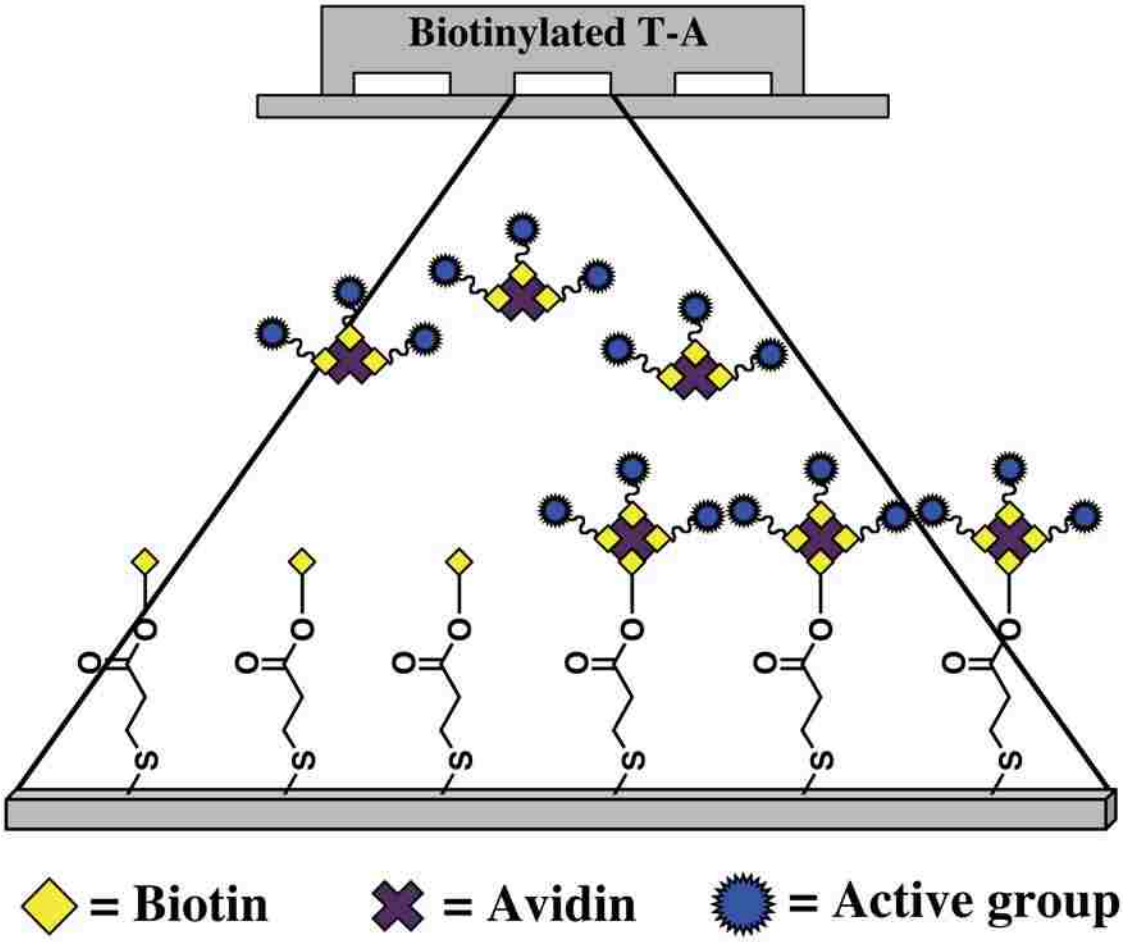

Scheme 3-8: Schematic illustration of a 2-tier consumer-modifiable microfluidic device.

3.8 Conclusions

Novel, cost-efficient thiol-acrylate microfluidic devices with native stable hydrophilic surfaces were prepared via a soft lithography technique in less than 24 hours at room temperature and ambient pressure with no complex or expensive

instrumentation. This research was fueled by the strong need for stable hydrophilic surfaces in a field of microfluidics that is dominated by other complicated and expensive techniques that require modification to achieve only transient surface energies. The chemistry employed to produce these polymeric materials involved two consecutive Michael additions. An *in situ* tertiary amine catalyst molecule was first prepared via the Michael addition of a secondary amine to a trifunctional acrylate. This molecule was then used as both a catalyst and a comonomer in an amine catalyzed thiol-acrylate Michael reaction. Because the catalyst molecule was incorporated into the polymer network, there was no need to remove it in the final steps of the reaction, making this reaction very beneficial for biological analysis. The kinetics of these reactions illustrated that the gel time of the systems could be manipulated depending on the amine concentration but only to a certain extent. The gel times for these materials ranged from 2 hours to <20 minutes. The kinetic studies provided here also proved that these reactions proceeded to extremely high conversion, which is a normal aspect of amine-catalyzed thiol-acrylate reactions. This high conversion is another beneficial facet of the reaction in terms of biological assays as high conversion translates into less small-molecular weight free monomer molecules capable of escaping and disrupting biological processes. It was found in this study that many of the properties of the material could be manipulated via a simple change in the amine concentration. Due to the *in situ* nature of the catalyst used in this system, an increase in the amine concentration resulted in a decrease in the crosslink density. The crosslink density affected many of the material properties such as strength, flexibility, and glass transition temperature. The strength and flexibility of the materials were found to be adequate, and the glass transition

temperatures indicated an applicable temperature range for microfluidic assays. These novel thiol-acrylate microfluidic materials were annealed via a partial polymerization technique utilizing excess monomers on opposing sides and the same versatile thiol-acrylate chemistry and *in situ* tertiary amine. This added another advantage, as other techniques require expensive equipment for annealing of microfluidic devices. The strength of annealing was investigated via orthogonal delamination analysis, and it was concluded that 40% excess monomer on either surface was adequate to produce a bond strength comparable to that of PDMS surfaces bound by a traditional oxygen plasma surface activation technique. These Hydrophilic PETA-co-TMPTMP microfluidic devices boasted native water contact angles between 60-65˚. These native high-energy surfaces were found to be extremely stable for at least 2.5 months. This is extremely beneficial for microfluidic applications as it allows for microfluidic devices with long shelf lives. The surface energies of these devices were also modified via both post- and a bulk-modification using various small molecule acrylic modifiers ranging from hydrophilic PEGylated acrylates to hydrophobic acrylates functionalized with long hydrocarbon chains or fluorinated compounds. It was concluded that the surface could be manipulated to have stable water contact angles ranging from very hydrophilic (<30˚) to mildly hydrophobic (>85˚) depending on the surface chemistry. From these modification results, a water contact angle library was generated illustrating the ability to formulate a material based on a desired level of hydrophilicity. The replication efficiency of these materials via soft lithography was found to be extremely high with capabilities of reaching structures even smaller that utilized in this study. Final devices were prepared and observed via fluorescence microscopy. It was concluded that these devices perform

very well when fluorescent dyes are flowed though the microchannels, and they are capable of being used in fluorescence microscopy studies, which are useful in the field of microfluidics. Other acrylic monomers were incorporated into the thiol-acrylate matrix as replacements for the PETA comonomer. TMPeTA monomers with longer intra-acrylate chains were incorporated to improve the flexibility of the final material. The flexibility of the material was improved, but the high level of water mass uptake and the inadequate surface modifications experienced by the material made it less appeasing in terms of a microfluidic device application. These thiol-acrylate microfluidic devices, specifically those prepared using the PETA-co-TMPTMP material, have high potential in the microfluidic industry. Future applications could involve the production of a specific biotinylated consumer-manipulatable microfluidic device exploiting a strong avidin-biotin interaction. These materials, coupled with a soft lithography technique, will certainly be beneficial as a simple, fast, tunable, and cost efficient method of producing a stable natively hydrophilic microfluidic device.

CHAPTER 4. CONCLUSIONS

The use of the very versatile and robust amine-catalyzed thiol-acrylate chemistry for novel applications was proven highly successful via the research provided here. Two completely new applications arose from this research, both fully utilizing the multitude of advantages associated with amine-catalyzed thiol-acrylate chemistry. Some of these advantages included low cost, simplicity of the reaction, high network uniformity, lack of oxygen inhibition, versatility in terms of monomers and catalysts, ease of modification, high strength, and the ability to reach extremely high conversion at room temperature and ambient pressure. These advantages were exploited in the preparation of novel core-containing microparticles and stable hydrophilic microfluidic devices. Various core materials were microencapsulated via the primary amine-catalyzed Michael addition of a trifunctional thiol to a trifunctional acrylate. The use of this chemistry facilitated the preparation of these microparticles via a simple dispersion polymerization using a minimum number of components, in less than one hour, at room temperature, and ambient pressure. These beneficial procedural aspects made this method of microencapsulation highly advantageous over typical methods of microencapsulation. It was determined that the size of these microparticles could be easily tuned via variations in energy input into the system via agitation. These microparticles could serve as either stimulated release or controlled release vesicles depending on core material incorporated. Benzoyl peroxide, Dimethyl-para-toluidine, a borontrifluoride-amine complex, a borontrichloride-amine complex, and carbon nanotubes were microencapsulated using this primary amine-catalyzed thiol-acrylate method and analyzed in various capacities, all showing some level of success.

Microparticles containing one particular initiator, a borontrichloride-amine complex, were extensively characterized and further analyzed in two multifunctional epoxy systems. These microparticles were observed to prevent the undesirable interaction between the Lewis acid initiator and fumed silica by separating the two components, hence improving the rheological properties of an epoxy system containing the initiator while maintaining the strength of the resulting polymer.

This versatile amine-catalyzed thiol-acrylate chemistry was also utilized in the preparation of novel hydrophilic microfluidic devices. Again, due to the multitude of advantages associated with this chemistry, these microfluidic devices were prepared via a simple, inexpensive soft-lithography technique in less than 24 hours at room temperature and ambient pressure with no complex or expensive instrumentation. An *in situ* tertiary amine catalyst/comonomer was prepared via an initial Michael addition of a secondary amine to a trifunctional hydrophilic acrylate. This hybrid molecule was then added to a trifunctional thiol where the tertiary amine portion functioned as a catalyst for the Michael addition of the trithiol to the remaining acrylate functional groups. A kinetic study illustrated that extremely high monomer conversions could be attained at room temperature in less than 24 hours, and the polymer gel times could be manipulated depending on the amine concentration to a lower limit of ~17 minutes. The concentration of the amine catalyst was found to play an enormous role in the manipulation of the material properties including gel times, flexibility, flexure strength, and glass transition temperatures. Due to the *in situ* nature of the catalyst, an increase in the amine concentration resulted in a decrease in the acrylate functionality and thereby a decrease in the average functionality of the system. The decrease in average

functionality caused an increase in the critical extent of conversion resulting in a gel-time parabola effect. This functionality decrease also caused a decrease in the crosslink density, which caused an increase in the flexibility of the material and a decrease in the flexure strength. The decrease in crosslink density caused an increase in the segmental mobility, which caused a decrease in the glass transition temperature. The annealing processed employed here utilized the step-growth nature of the thiol-acrylate reaction via a partial polymerization, excess monomer technique resulting in an annealing strength comparable to that of annealed PDMS. These novel microfluidic devices were produced with native contact angles of ~60˚ that were stable for at least 2.5 months. The surfaces of these materials were post- and bulk-modified with small monofunctional acrylate molecules containing modifying (hydrophilic or hydrophobic) functional groups. From these modifications, a water contact angle library was generated that could allow for the production of a microfluidic device based on a desired hydrophilicity. These materials were found to have astounding replication capabilities and high potential for fluorescence microscopy analysis. Various acrylic monomers were incorporated and observed to improve the mechanical properties of the polymer, but high levels of water uptake limited the use of these monomers. Future applications for these microfluidic devices could include the production of a fully consumer/non-scientist-manipulatable device, which could revolutionize the microfluidics industry. This thiol-acrylate chemistry allowed for the production of two novel products that have great advantages over current technologies. In both cases these products were observed to improve multiple aspects of the applications to which they were targeted. They decreased the cost of production, decreased the time required to complete the task,

simplified the process, eliminated the need for expensive instrumentation, allowed for production under ambient conditions, and solved at least one of the obvious problems associated with each respected application. These applications were examples of the large, untapped potential of the simple, highly useful, inexpensive, versatile, and robust amine-catalyzed thiol-acrylate chemistry, and there will certainly be many other applications utilizing this phenomenal chemistry in the near future as its potential unfolds.

REFERENCES

1. Goodyear, C., *Improvement in India-Rubber Fabrics*. 1844: U. S. Patent.

2. Posner, T., *Information on unsaturated compounds II The addition of mercaptan to unsaturated hydrocarbon.* Berichte Der Deutschen Chemischen Gesellschaft, 1905. **38**: p. 646-657.

3. Chan, J.W., et al., *The effects of primary amine catalyzed thio-acrylate Michael reaction on the kinetics, mechanical and physical properties of thio-acrylate networks.* Eur. Polym. J., 2009. **45**: p. 2717–2725.

4. Hoyle, C.E., T.Y. Lee, and T. Roper, *Thiol–Enes: Chemistry of the Past with a Promise for the Future.* J. Poly. Sci. Part A. Polym. Chem., 2004. **52**: p. 5301-5338.

5. Hoyle, C.E. and C.N. Bowman, *Thiol-Ene Click Chemistry.* Angewandte Chemie International Edition, 2009. **49**(9): p. 1540-1573.

6. Jacobine, A.F., *Thiol-Ene Photopolymers*, in *Radiation Curing in Polymer Science and Technology*, J.P. Fouassier, Editor. 1993, Elsevier: New York. p. 219-268.

7. Cramer, N.B., J.P. Scott, and C.N. Bowman, *Photopolymerization of Thiol-Ene Polymers without Photoinitiators.* Macromolecules, 2002. **35**: p. 5361-5365.

8. Roper, T.M., et al., *Photopolymerization of pigmented thiol-ene systems.* Polymer, 2004. **45**(4): p. 2921.

9. Wei, H., et al., *Photopolymerization of ternary thiol-ene/acrylate systems: Film and network properties.* J. Polym. Sci. Part A Polym. Chem., 2007. **45**: p. 822-829.

10. Cramer, N.B., et al., *Mechanism and Modeling of a Thiol-Ene Photopolymerization.* Macromolecules, 2003. **35**: p. 5361-5365.

11. Cramer, N.B., et al., *Initiation and Kinetics of Thiol-ene Photopolymerizations without Photoinitiators.* J. Polym. Sci. Part A Polym. Chem., 2004. **42**: p. 5817-5826.

12. Kade, M.J., D.J. Burke, and C.J. Hawker, *The Power of Thiol-ene Chemistry.* J. Polym. Sci. Part A: Polym. Chem., 2010. **48**: p. 743-750.

13. Hoyle, C.E., et al., *Photopolymerization of Systems Incorporating Thiol-Enes.* Polym. Preprints, 2001. **42**: p. 697-698.

14. Hoyle, C.E., M. Keel, and K.J. Kim, *Photopolymerization of 1,6 Hexanediol Diacrylate-The effect of Functionalized amines.* Polymer, 1988. **29**: p. 18-23.

15. Morgan, C.R., F. Magnotta, and A.D. Ketley, *Thiol/ene photocurable polymers.* J. Poly. Sci. Part A. Polym. Chem., 1977. **15**: p. 627.

16. Woods, J.G. and A.F. Jacobine. in *RadTech NA Tech Conf Proc*. 1992.

17. Gush, D.P. and A.D. Ketley, Mod. Paint Coatings, 1978. **68**: p. 61.

18. Chiou, B.S. and S.A. Khan, *Real-time FTIR and in situ rheological studies on the UV curing kinetics of thiol-ene polymers.* Macromolecules, 1997. **30**(23): p. 7322-7328.

19. Scranton, A.B., et al., *Photopolymerization: fundamentals and applications*. 1997: American Chemical Society.

20. Ash, M. and I. Ash, *Handbook of Preservatives*, Synapse Information Resources, Inc.

21. Mitrofanova, S., et al., *New oligomeric thioether antioxidants for polymers.* Russian Journal of Applied Chemistry, 2006. **79**(1): p. 137-141.

22. Macko, T., B. Furtner, and K. Lederer, *HPLC Quantification of Thioether Antioxidants in Polyethylene after Dissolution of the Polymer under Pressure in an Aliphatic Solvent.* International Journal of Polymer Analysis and Characterization, 1997. **3**(4): p. 369-379.

23. *Norland Optical Products Literature*. [cited 2012 June 21]; Available from: http://www.norlandproducts.com

.

24. Hoyle, C.E., et al., *Photoinitiated Polymerization of Selected Thiol-Ene Systems*, in *Photoinitiated Polymerization: ACS Symposium Series No. 793*, K.D. Belfield and J.V. Crivello, Editors. 2003, American Chemical Society: Washington, DC. p. 52-64.

25. Morgan, C.R. and A.D. Ketley, J. Polym. Sci. Polym. Lett. Edn., 1978. **16**: p. 75.

26. Hagberg, E.C., et al., *Effects of modulus and surface chemistry of thiol-ene photopolymers in nanoimprinting.* Nano Letters, 2007. **7**(2): p. 233-237.

27. Sebra, R.P., et al., *Controlled polymerization chemistry to graft architectures that influence cell-material interactions.* Acta Biomaterialia, 2007. **3**(2): p. 151-161.

28. Reddy, S.K., et al., *Living radical photopolymerization induced grafting on thiol-ene based substrates.* Journal of Polymer Science Part a-Polymer Chemistry, 2005. **43**(10): p. 2134-2144.

29. Jonkheijm, P., et al., *Photochemical surface patterning by the thiol-ene reaction.* Angewandte Chemie-International Edition, 2008. **47**(23): p. 4421-4424.

30. Besson, E., et al., *A novel and simplified procedure for patterning hydrophobic and hydrophilic SAMs for microfluidic devices by using UV photolithography.* Langmuir, 2006. **22**(20): p. 8346-8352.

31. Nilsson, C.M., E.; Johansson, M.; Trey, S. M. , *Methacrylated dendrimers in thiol-methacrylate networks and the effect of conversion on the thermoset properties.* J. Polym. Sci. Part A: Polym. Chem., 2009. **47**: p. 5815-5826.

32. Koo, S.P.S., et al., *Limitations of radical thiol-ene reactions for polymer–polymer conjugation.* J. Polym. Sci. Part A: Polym. Chem., 2010. **48**(8): p. 1699-1713.

33. Christmas, B.H., H. ; Ngo, T. ; Brenes, D. ; Hernandez, H. *UV Polymerization of Thiol-Acrylate Systems: An Initial Investigation of Shelf-Stability, Relative Reactivity, and Thermomechanical Properties*. in *RadTech UV/EB Conference*. 2002. Indianapolis, IN.

34. Zienty, F.B., A.A. Schleppnik, and B.D. Vineyard, *Base-catalyzed addition of thiols to alpha, beta-unsaturated anhydrides* Journal of Organic Chemistry, 1962. **27**(9): p. 3140-&.

35. Rim, C., et al., *Thiol-ene reactions of 1,3,5-triacryloylhexahydro-1,3,5-triazine (TAT): facile access to functional tripodal thioethers.* Tetrahedron Letters, 2009. **50**(7): p. 745-747.

36. Mather, B.D., et al., *Michael addition reactions in macromolecular design for emerging technologies.* Prog. Polym. Sci., 2006. **31**: p. 487-531.

37. Rizzi, S.C. and J.A. Hubbell, *Recombinant protein-co-PEG networks as cell-adhesive and proteolytically degradable hydrogel matrixes. Part 1: Development and physicochernical characteristics.* Biomacromolecules, 2005. **6**(3): p. 1226-1238.

38. Chan, J.W., et al., *Nucleophile-Initiated Thiol-Michael Reactions: Effect of Organocatalyst, Thiol, and Ene.* Macromolecules, 2010. **43**: p. 6381–6388.

39. Hu, G., et al., *Time-Lapse Thiol-Acrylate Polymerization Using a pH Clock Reaction.* J. Polym. Sci. Part A: Polym. Chem., 2010. **48**: p. 2955-2959.

40. Khire, V.S., T.Y. Lee, and C.N. Bowman, *Surface Modification Using Thiol-Acrylate Conjugate Addition Reactions.* Macromolecules, 2007. **40**: p. 5669-5677.

41. Lee, T., et al., *Synthesis and photopolymerization of novel multifunctional vinyl esters.* J. Polym. Sci. Part A Polym. Chem., 2004. **42**(17): p. 4424-4436.

42. Khire, V.S., et al., *Synthesis, Characterization and Cleavage of Linear Polymers Attached to Silica Nanoparticles Formed Using Thiol-Acrylate Conjugate Addition Reactions.* J. Polym. Sci. Part A: Polym. Chem., 2008. **46**(20): p. 6896-6906.

43. Clark, T., et al., *Photopolymerization of Thiol-Ene Systems Based on Oligomeric Thiols.* Journal of Polymer Science Part a-Polymer Chemistry, 2009. **47**(1): p. 14-24.

44. Sanui, K. and N. Ogata, Bull Chem. Soc. Jpn., 1967. **40**: p. 1727.

45. Shin, J., et al., *Segmented Polythiourethane Elastomers through Sequential Thiol-Ene and Thiol-Isocyanate Reactions.* Macromolecules, 2009. **42**(9): p. 3294-3301.

46. Chan, J.W., et al., *Convergent synthesis of 3-arm star polymers from RAFT-prepared poly(N,N-diethylacrylamide) via a thiol-ene click reaction.* Chemical Communications, 2008(40): p. 4959-4961.

47. Matsushima, H.S., J.; Bowman, C. N.; Hoyle, C. E. , *Thiol-isocyanate-acrylate ternary networks by selective thiol-click chemistry.* J. Polym. Sci. Part A: Polym. Chem., 2010. **48**: p. 3255-3264.

48. Dijk, J.T.M.V., *Composition comprising mercapto-functional compounds*. 2003, Akzo Nobel N.V.

49. Leake, J.S., *Coating adhesive and sealant compositions*. 2003.

50. Benita, S., ed. *Microencapsulation: Methods and Industrial Applications*. 1996, Marcel Dekker: New York.

51. Yow, H.N. and A.F. Routh, *Formation of liquid core-polymer shell microcapsules.* Soft Matter, 2006. **2**: p. 940-949.

52. Yang, C.-C. and I.-H. Pan, *Preparation of pesticide microcapsule*. 1996: U.S. Patent.

53. Hashemi, S.A. and M. Zandi, *Encapsulation Process in Synthesizing Polyurea Microcapsules Containing Pesticide.* Iranian Polym. J., 2001. **10**: p. 265-270.

54. Bodmeier, R. and J. Wang, *Microencapsulation of Drugs with Aqueous Colloidal Polymer Dispersions.* Journal of Pharmaceutical Sciences, 1993. **82**: p. 191-194.

55. Khopade, A.J. and F. Caruso, *Two Component Ultrathin Microcapsules Prepared by a Core Mediated Layer-by-Layer Approach.* Chem. Mater., 2004. **16**: p. 2107-2112.

56. Franjione, J. and N. Vasishtha, *The Art and Science of Microencapsulation.* Technology Today,, 1995.

57. Noda, A., et al., *Cosmetic containing fine soft microcapsule*. 2001: U. S. Patent.

58. Lew, C.W., *Encapsulated additives*. 2000: U. S. Patent.

59. Jason, M.E. and D.J. Kalota, *Microencapsulation process by coacervation*. 1996: U. S. Patent.

60. Washington, C., *Drug Release from Microparticulate Systems*, in *Microencapsulation: Methods and Industrial Applications*, S. Benita, Editor. 1996, Marcel Dekker: New York. p. 155-181.

61. White, S.R., et al., *Autonomic healing of polymer composites.* Nature, 2001. **409**: p. 794-797.

62. Kessler, M.R., N.R. Sottos, and S.R. White, *Self-healing structural composite materials.* Composites: Part A: applied science and manufacturing, 2003. **34**: p. 743-753.

63. Li, J., et al., *Polyurea Microcapsules: Surface Modification and Capsule Size Control.* Journal of Polymer Science Part a-Polymer Chemistry, 2011. **49**(14): p. 3038-3047.

64. Zhuo, L., C. Shuilin, and Z. Shizhou, *Factors affecting the particle size and size distribution of polyurea microcapsules by interfacial polymerization of polyisocyanates.* International Journal of Polymeric Materials, 2004. **53**: p. 21–31.

65. McFarland, B., *Investigations of Free-Radical Polymerization Systems Using Microencapsulated Initiators*. 2005.

66. McFarland, B., S. Popwell, and J.A. Pojman, *Free-Radical Frontal Polymerization with a Microencapsulated Initiator.* Macromolecules, 2004. **37**: p. 6670 - 6672.

67. McFarland, B., S. Popwell, and J.A. Pojman, *Free-Radical Frontal Polymerization with a Microencapsulated Initiator: Characterization of Microcapsules and their Effect on Pot Life, Front Velocity and Mechanical Properties.* Macromolecules, 2006. **39**: p. 53-63.

68. Yadav, S.K., A.K. Suresh, and K.C. Khilar, *Microencapsulation in polyurea shell by interfacial polycondensation.* AIChE J., 1990. **36**: p. 431-438.

69. Alzari, V., et al., *Stimuli Responsive Hydrogels Prepared by Frontal Polymerization.* Biomacromolecules, 2009. **10**(9): p. 2672-2677.

70. Shukla, P.G., Sivaram, Swaminathan, Rajagopalan, Natarajan , *Process for the preparation of polyurethane microcapsules containing monocrotophos*. 1999, Council of Scientific & Industrial Research (New Delhi, IN): United States.

71. Short, W.T., *Dual-walled microcapsules and a method of forming same*. 1978, General Motors Corp.: U.S. Patent.

72. Brow, E.N., et al., *In situ poly(urea-formaldehyde) microencapsulation of dicyclopentadiene.* J. Microencapsulation, 2003. **20**: p. 719-730.

73. Grochowicz, M., A. Bartnicki, and B. Gawdzik, *Preparation and Characterization of Porous Polymeric Microspheres Obtained from Multifunctional Methacrylate Monomers.* J. Polym. Sci. Part A: Polym. Chem., 2008. **46**: p. 6165–6174.

74. van Berkel, K.Y. and C.J. Hawker, *Tailored Composite Polymer-Metal Nanoparticles by Miniemulsion Polymerization and Thiol-ene Functionalization.* Journal of Polymer Science Part a-Polymer Chemistry, 2010. **48**(7): p. 1594-1606.

75. Gu, W.F., G.J. Chen, and M.H. Stenzel, *Synthesis of Glyco-Microspheres via a Thiol-Ene Coupling Reaction.* Journal of Polymer Science Part a-Polymer Chemistry, 2009. **47**(20): p. 5550-5556.

76. Costoyas, A., J. Ramos, and J. Forcada, *Encapsulation of Silica Nanoparticles by Miniemulsion Polymerization.* Journal of Polymer Science Part a-Polymer Chemistry, 2009. **47**(3): p. 935-948.

77. Vazquez, B., S. Deb, and W. Bonfield, *Optimization of benzoyl peroxide concentration in an experimental bone cement based on poly(methyl methacrylate).* Journal of Materials Science-Materials in Medicine, 1997. **8**(7): p. 455-460.

78. Horner, L. and E. Schwenk, **Uber die polymerisation von vinylverbindungen durch das system-diacrylperoxyD-tertiares amin.* Annalen Der Chemie-Justus Liebig, 1950. **566**(1): p. 69-84.

79. Imoto, M., T. Otsu, and K. Kimura, *Vinyl polymerization. 4. Influence of dimethylaniline on solution polymerization of vinyl chloride catalyzed by benzoyl peroxide.* Journal of Polymer Science, 1955. **15**(80): p. 475-484.

80. Walling, C. and N. Indictor, *Solvent effects and initiator efficiency in the benzoyl peroxide-dimethylaniline system.* Journal of the American Chemical Society, 1958. **80**(21): p. 5814-5818.

81. Meltzer, T.H. and A.V. Tobolsky, *Kinetics of polymerization of styrene initiated by the system benzoyl-peroxide dimethylaniline* Journal of the American Chemical Society, 1954. **76**(20): p. 5178-5180.

82. Nishimur.N, *Dead-end polymerization of styrene and methyl methacrylate in benzoyl peroxide-dimethylaniline redox system.* Journal of Polymer Science Part a-1-Polymer Chemistry, 1969. **7**(7PA1): p. 2015-&.

83. Imoto, M. and K. Takemoto, *Vinal polymerization. 6. Polymerization of acrylonitrile in the presence of substituted benzoyl peroxides and dimethylaniline.* Journal of Polymer Science, 1955. **18**(89): p. 377-387.

84. Odriscoll, K.F. and S.A. McArdle, *Dead-end polymerization with redox initiators.* Journal of Polymer Science, 1959. **40**(137): p. 557-561.

85. Odriscoll, K.F. and J.F. Schmidt, *Polymerization with redox initiators. 2. The system styrene-benzoyl peroxide-dimethylaniline at elevated temperatures* Journal of Polymer Science, 1960. **45**(145): p. 189-194.

86. Odriscoll, K.F. and E.N. Ricchezza, *Polymerizaiotn with redox initiators. 5. Substituent effects in the initiator system diethylaniline-benzoyl peroxide* Makromolekulare Chemie, 1961. **47**(1): p. 15-18.

87. Bartlett, P.D. and K. Nozaki, *The decomposition of benzoyl peroxide in solvents. 2. Ethers, alcohol, phenols and amines* Journal of the American Chemical Society, 1947. **69**(10): p. 2299-2306.

88. Rosato, D.V., *Reinforced Plastics Handbook*. 2004: Elsevier Advanced Technology.

89. Odian, G., *Principles of Polymerization, 4th Ed.* 3rd ed. ed. 2004, New York: Wiley.

90. Ullmann, F. and W. Gerhartz, *Ullmann's Encyclopedia of industrial chemistry*. 1995: VCH.

91. Brandrup, J. and E.H. Immergut, *Polymer handbook*. 1966: Interscience Publishers.

92. Bojar, R.A., W.J. Cunliffe, and K.T. Holland, *The short-term treatment of acne-vulgaris with benzoyl peroxide-effects on the surface and follicular cutaneous microflora.* British Journal of Dermatology, 1995. **132**(2): p. 204-208.

93. Fluhr, J.W. and K. Degitz, *Antibiotics, azelaic acid and benzoyl peroxide in topical acne therapy.* Journal Der Deutschen Dermatologischen Gesellschaft, 2010. **8**: p. S24-S30.

94. Sarquis, A.M., et al., *Investigating the Stability of Benzoyl Peroxide in Over-the-Counter Acne Medications.* Journal of Chemical Education, 2008. **85**(12): p. 1655.

95. Gruber, M.P. and R.W. Klein, *Determination of benzoyl peroxide stability in pharmaceuticals.* Journal of Pharmaceutical Sciences, 1967. **56**(11): p. 1505-1508.

96. Nokhodchi, A., et al., *Factors affecting the morphology of benzoyl peroxide microsponges.* Micron, 2007. **38**(8): p. 834-840.

97. Jelvehgari, M., et al., *The microsponge delivery system of benzoyl peroxide: Preparation, characterization and release studies.* International Journal of Pharmaceutics, 2006. **308**(1-2): p. 124-132.

98. Fuchigami, K., Y. Taguchi, and M. Tanaka, *Preparation of microcapsules containing reactive compound by the drying-in-liquid method using calcium carbonate as stabilizer.* Journal of Chemical Engineering of Japan, 2006. **39**(9): p. 994-999.

99. Wilson, G.O., et al., *Evaluation of Peroxide Initiators for Radical Polymerization-Based Self-Healing Applications.* Journal of Polymer Science Part a-Polymer Chemistry, 2010. **48**(12): p. 2698-2708.

100. Dalton, A.B., et al., *Super-tough carbon-nanotube fibres - These extraordinary composite fibres can be woven into electronic textiles.* Nature, 2003. **423**(6941): p. 703-703.

101. Yu, M.F., et al., *Tensile loading of ropes of single wall carbon nanotubes and their mechanical properties.* Physical Review Letters, 2000. **84**(24): p. 5552-5555.

102. Javey, A., et al., *Ballistic carbon nanotube field-effect transistors.* Nature, 2003. **424**(6949): p. 654-657.

103. Saito, R., et al., *Electronic-structure of graphene tubules based on C-60.* Physical Review B, 1992. **46**(3): p. 1804-1811.

104. Charlier, J.C. and J.P. Issi, *Electronic structure and quantum transport in carbon nanotubes.* Applied Physics a-Materials Science & Processing, 1998. **67**(1): p. 79-87.

105. Ausman, K.D., et al., *Organic solvent dispersions of single-walled carbon nanotubes: Toward solutions of pristine nanotubes.* Journal of Physical Chemistry B, 2000. **104**(38): p. 8911-8915.

106. Arnold, M.S., et al., *Encapsulation of carbon nanotubes by self-assembling peptide amphiphiles.* Langmuir, 2005. **21**(10): p. 4705-4709.

107. Hamerton, I., *Recent Developments in Epoxy Resins*. 1996: Smithers Rapra Technology.

108. Chabanne, P., L. Tighzert, and J.P. Pascault, *Monoepoxy polymerization initiated by BF(3)-amine complexes in bulk. 2. influence of water and by-products on polymer formation. .* Journal of Applied Polymer Science, 1994. **53**(6): p. 769-785.

109. Pfann, J.R., Kopacki, Adam F., *uring epoxy resins with boron trichloride-tertiary amine complexes*. 1968, Stauffer Chemical Co.: United States.

110. Harris, J.J. and S.C. Temin, *Proposed mechanism for curing of epoxy resins with amine-Lewis Acid complexes or salts.* Journal of Applied Polymer Science, 1966. **10**(4): p. 523-&.

111. Ghosh, N.N. and G.R. Palmese, *Electron-beam curing of epoxy resins: effect of alcohols on cationic polymerization.* Bulletin of Materials Science, 2005. **28**(6): p. 603-607.

112. Leepoxy Plastics, March 14, 2010; Available from: http://www.leepoxy.com/Docs/TB_Leecure_B.pdf.

113. Dong, H.T., H.B. Du, and X.H. Qian, *Theoretical Prediction of pK(a) Values for Methacrylic Acid Oligomers Using Combined Quantum Mechanical and Continuum Solvation Methods.* Journal of Physical Chemistry A, 2008. **112**(49): p. 12687-12694.

114. Raghavan, S.R. and S.A. Khan, *Shear-thickening response of fumed silica suspensions under steady and oscillatory shear.* Journal of Colloid and Interface Science, 1997. **185**(1): p. 57-67.

115. Bledzki, A.K., S. Reihmane, and J. Gassan, *Thermoplastics reinforced with wood fillers: A literature review.* Polymer-Plastics Technology and Engineering, 1998. **37**(4): p. 451-468.

116. Carioscia, J.A., J.W. Stansbury, and C.N. Bowman, *Evaluation and control of thiol-ene/thiol-epoxy hybrid networks.* Polymer, 2007. **48**(6): p. 1526-1532.

117. Séguin, C., et al., *Surface modification of poly(dimethylsiloxane) for microfluidic assay applications.* Applied Surface Science, 2010. **256**: p. 2524-2531.

118. de Menezes Atayde, C. and I. Doi, *Highly stable hydrophilic surfaces of PDMS thin layer obtained by UV radiation and oxygen plasma treatments.* physica status solidi (c), 2010. **7**(2): p. 189-192.

119. Whitesides, G.M., *The origins and the future of microfluidics.* Nature, 2006. **442**(7101): p. 368-373.

120. Lin, C.C., et al., *Microfluidic Immunoassays.* Jala, 2010. **15**(3): p. 253-274.

121. Sia, S.K. and G.M. Whitesides, *Microfluidic devices fabricated in poly(dimethylsiloxane) for biological studies.* Electrophoresis, 2003. **24**(21): p. 3563-3576.

122. Lenigk, R., et al., *Plastic biochannel hybridization devices: a new concept for microfluidic DNA arrays.* Analytical Biochemistry, 2002. **311**(1): p. 40-49.

123. Dimalanta, E.T., et al., *A microfluidic system for large DNA molecule arrays.* Analytical Chemistry, 2004. **76**(18): p. 5293-5301.

124. Chiem, N.H. and D.J. Harrison, *Monoclonal antibody binding affinity determined by microchip-based capillary electrophoresis.* Electrophoresis, 1998. **19**(16-17): p. 3040-3044.

125. Badal, M.Y., et al., *Protein separation and surfactant control of electroosmotic flow in poly(dimethylsiloxane)-coated capillaries and microchips.* Journal of Chromatography A, 2002. **947**(2): p. 277-286.

126. Chang, W., T. Komazu, and T. Korenaga, *Fabrication of monolithic silica in microchannel as an adsorbent for preconcentration of VOCs.* Analytical Letters, 2008. **41**(8): p. 1468-1476.

127. Reyes, D.R., et al., *Micro total analysis systems. 1. Introduction, theory, and technology.* Analytical Chemistry, 2002. **74**(12): p. 2623-2636.

128. Auroux, P.A., et al., *Micro total analysis systems. 2. Analytical standard operations and applications.* Analytical Chemistry, 2002. **74**(12): p. 2637-2652.

129. Manz, A., et al., *Planar chips technology for miiturazation and integration of separation techniques into monitoring systmes-capillary electrophoresis. .* Journal of Chromatography, 1992. **593**(1-2): p. 253-258.

130. Henares, T.G., F. Mizutani, and H. Hisamoto, *Current development in microfluidic immunosensing chip.* Analytica Chimica Acta, 2008. **611**(1): p. 17-30.

131. Lee, S.J.J. and N. Sundararajan, *Microfabrication for Microfluidics*. 2010: Artech House.

132. Kim, J.Y., et al., *Thermoset polyester droplet-based microfluidic devices for high frequency generation.* Lab on a Chip, 2011. **11**(23): p. 4108-4112.

133. Vickers, J.A., et al., *Thermoset polyester as an alternative material for microchip electrophoresis/electrochemistry.* Electrophoresis, 2007. **28**(7): p. 1123-1129.

134. Dobrzynska, J.A., et al., *Polyimide foam-like microstructures: technology and mechanical properties.* Journal of Micromechanics and Microengineering, 2011. **21**(10).

135. Zhu, K.Y., et al., *Microfluidic chip based nano liquid chromatography coupled to tandem mass spectrometry for the determination of abused drugs and metabolites in human hair.* Analytical and Bioanalytical Chemistry, 2012. **402**(9): p. 2805-2815.

136. Madou, M.J., *Fundamentals of Microfabrication: The Science of Miniaturization*. 2002: CRC Press.

137. Becker, H. and C. Gartner, *Polymer microfabrication technologies for microfluidic systems.* Analytical and Bioanalytical Chemistry, 2008. **390**(1): p. 89-111.

138. Liu, Y.J. and C.B. Rauch, *DNA probe attachment on plastic surfaces and microfluidic hybridization array channel devices with sample oscillation.* Analytical Biochemistry, 2003. **317**(1): p. 76-84.

139. Swickrath, M.J., et al., *The design and fabrication of autonomous polymer-based surface tension-confined microfluidic platforms.* Microfluidics and Nanofluidics, 2008. **4**(6): p. 601-611.

140. Hashimoto, M., F. Barany, and S.A. Soper, *Polymerase chain reaction/ligase detection reaction/hybridization assays using flow-through microfluidic devices for the detection of low-abundant DNA point mutations.* Biosensors & Bioelectronics, 2006. **21**(10): p. 1915-1923.

141. Kempitiya, A., et al., *Localized microwave heating in microwells for parallel DNA amplification applications.* Applied Physics Letters, 2009. **94**(6).

142. Lee, G.B., et al., *Microfabricated plastic chips by hot embossing methods and their applications for DNA separation and detection.* Sensors and Actuators B-Chemical, 2001. **75**(1-2): p. 142-148.

143. Wang, Y., et al., *Microarrays assembled in microfluidic chips fabricated from poly(methyl methacrylate) for the detection of low-abundant DNA mutations.* Analytical Chemistry, 2003. **75**(5): p. 1130-1140.

144. Emory, J.M., et al., *Design and development of a field-deployable single-molecule detector (SMD) for the analysis of molecular markers.* Analyst, 2012. **137**(1): p. 87-97.

145. Kotani, A., et al., *EndoV/DNA ligase mutation scanning assay using microchip capillary electrophoresis and dual-color laser-induced fluorescence detection.* Analytical Methods, 2012. **4**(1): p. 58-64.

146. Nesterova, I.V., et al., *Hydrodynamic shearing of DNA in a polymeric microfluidic device.* Lab on a Chip, 2012. **12**(6): p. 1044-1047.

147. Wang, H., et al., *Fully Integrated Thermoplastic Genosensor for the Highly Sensitive Detection and Identification of Multi-Drug-Resistant Tuberculosis.* Angewandte Chemie-International Edition, 2012. **51**(18): p. 4349-4353.

148. Le, N.C.H., et al., *Total internal reflection ellipsometry as a label-free assessment method for optimization of the reactive surface of bioassay devices based on a functionalized cycloolefin polymer.* Analytical and Bioanalytical Chemistry, 2010. **398**(5): p. 1927-1936.

149. Miserere, S., et al., *Fabrication of thermoplastics chips through lamination based techniques.* Lab on a Chip, 2012. **12**(10): p. 1849-1856.

150. Hu, S.W., et al., *Surface modification of poly(dimethylsiloxane) microfluidic devices by ultraviolet polymer grafting.* Analytical Chemistry, 2002. **74**(16): p. 4117-4123.

151. Wang, B., et al., *Surface characterization using chemical force microscopy and the flow performance of modified polydimethylsiloxane for microfluidic device applications.* Electrophoresis, 2003. **24**(9): p. 1442-1450.

152. Leclerc, E., Y. Sakai, and T. Fujii, *Microfluidic PDMS (polydimethylsiloxane) bioreactor for large-scale culture of hepatocytes.* Biotechnology Progress, 2004. **20**(3): p. 750-755.

153. Garcia, C.D., et al., *Comparison of surfactants for dynamic surface modification of poly(dimethylsiloxane) microchips.* Electrophoresis, 2005. **26**(3): p. 703-709.

154. Mehta, G., et al., *Polyelectrolyte-clay-protein layer films on microfluidic PDMS bioreactor surfaces for primary murine bone marrow culture.* Advanced Functional Materials, 2007. **17**(15): p. 2701-2709.

155. Wu, M.H., *Simple poly(dimethylsiloxane) surface modification to control cell adhesion.* Surface and Interface Analysis, 2009. **41**(1): p. 11-16.

156. Waldbaur, A., et al., *Let there be chip-towards rapid prototyping of microfluidic devices: one-step manufacturing processes.* Analytical Methods, 2011. **3**(12): p. 2681-2716.

157. Hou, H.H., et al., *Experimental and numerical investigation into micro-flow cytometer with 3-D hydrodynamic focusing effect and micro-weir structure.* Electrophoresis, 2009. **30**(14): p. 2507-2515.

158. Bahadorimehr, A. and B.Y. Majlis, *Fabrication of glass-based microfluidic devices with photoresist as mask* Informacije Midem-Journal of Microelectronics Electronic Components and Materials, 2011. **41**(3): p. 193-196.

159. Henley, W.H., P.J. Dennis, and J.M. Ramsey, *Fabrication of Microfluidic Devices Containing Patterned Microwell Arrays.* Analytical Chemistry, 2012. **84**(3): p. 1776-1780.

160. Kohler, F., et al., *Gradient etching of silicon-based thin films for depth-resolved measurements: The example of Raman crystallinity.* Thin Solid Films, 2012. **520**(7): p. 2605-2608.

161. Queste, S., et al., *Manufacture of microfluidic glass chips by deep plasma etching, femtosecond laser ablation, and anodic bonding.* Microsystem Technologies-Micro-and Nanosystems-Information Storage and Processing Systems, 2010. **16**(8-9): p. 1485-1493.

162. De Marco, C., et al., *Femtosecond laser fabrication and characterization of microchannels and waveguides in methacrylate-based polymers.* Microsystem Technologies-Micro-and Nanosystems-Information Storage and Processing Systems, 2012. **18**(2): p. 183-190.

163. Li, M., et al., *A simple and cost-effective method for fabrication of integrated electronic-microfluidic devices using a laser-patterned PDMS layer.* Microfluidics and Nanofluidics, 2012. **12**(5): p. 751-760.

164. Li, Y. and S.L. Qu, *The effects of heat treatment on microfluidic devices fabricated in silica glass by femtosecond lasers.* Chinese Physics B, 2012. **21**(3).

165. Burns, M.A., et al., *An integrated nanoliter DNA analysis device.* Science, 1998. **282**(5388): p. 484-487.

166. Harrison, C., et al., *A rapid prototyping technique for the fabrication of solvent-resistant structures.* Journal of Micromechanics and Microengineering, 2004. **14**(1): p. 153-158.

167. Sikanen, T., et al., *Characterization of SU-8 for electrokinetic microfluidic applications.* Lab on a Chip, 2005. **5**(8): p. 888-896.

168. Tuomikoski, S., et al., *Fabrication of enclosed SU-8 tips for electrospray ionization-mass spectrometry.* Electrophoresis, 2005. **26**(24): p. 4691-4702.

169. Gadre, A.P., et al., *Fabrication of a fluid encapsulated dermal patch using multilayered SU-8.* Sensors and Actuators a-Physical, 2004. **114**(2-3): p. 478-485.

170. Nijdam, A.J., et al., *Fluidic encapsulation in SU-8 mu-reservoirs with mu-fluidic through-chip channels.* Sensors and Actuators a-Physical, 2005. **120**(1): p. 172-183.

171. Lee, D.E., S. Soper, and W.J. Wang, *Design and fabrication of an electrochemically actuated microvalve.* Microsystem Technologies-Micro-and Nanosystems-Information Storage and Processing Systems, 2008. **14**(9-11): p. 1751-1756.

172. Park, D.S.W., et al., *A titer plate-based polymer microfluidic platform for high throughput nucleic acid purification.* Biomedical Microdevices, 2008. **10**(1): p. 21-33.

173. Husny, J., et al., *The creation of drops in T-shaped microfluidic devices with the 'modified' laser-LIGA technique: I. Fabrication.* Smart Materials & Structures, 2006. **15**(1): p. S117-S123.

174. Malek, C.G.K., *Laser processing for bio-microfluidics applications (part I).* Analytical and Bioanalytical Chemistry, 2006. **385**(8): p. 1351-1361.

175. Malek, C.G.K., *Laser processing for bio-microfluidics applications (part II).* Analytical and Bioanalytical Chemistry, 2006. **385**(8): p. 1362-1369.

176. Heckele, M. and W.K. Schomburg, *Review on micro molding of thermoplastic polymers.* Journal of Micromechanics and Microengineering, 2004. **14**(3): p. R1-R14.

177. Kukharenka, E., et al., *Electroplating moulds using dry film thick negative photoresist.* Journal of Micromechanics and Microengineering, 2003. **13**(4): p. S67-S74.

178. Hupert, M.L., et al., *Evaluation of micromilled metal mold masters for the replication of microchip electrophoresis devices.* Microfluidics and Nanofluidics, 2007. **3**(1): p. 1-11.

179. Juang, Y.J., L.J. Lee, and K.W. Koelling, *Hot embossing in microfabrication. Part I: Experimental.* Polymer Engineering and Science, 2002. **42**(3): p. 539-550.

180. Juang, Y.J., L.J. Lee, and K.W. Koelling, *Hot embossing in microfabrication. Part II: Rheological characterization and process analysis.* Polymer Engineering and Science, 2002. **42**(3): p. 551-566.

181. Scheer, H.C. and H. Schulz, *A contribution to the flow behaviour of thin polymer films during hot embossing lithography.* Microelectronic Engineering, 2001. **56**(3-4): p. 311-332.

182. Schulz, H., M. Wissen, and H.C. Scheer, *Local mass transport and its effect on global pattern replication during hot embossing.* Microelectronic Engineering, 2003. **67-8**: p. 657-663.

183. Young, W.B., *Analysis of the nanoimprint lithography with a viscous model.* Microelectronic Engineering, 2005. **77**(3-4): p. 405-411.

184. Okagbare, P.I. and S.A. Soper, *Polymer-based dense fluidic networks for high throughput screening with ultrasensitive fluorescence detection.* Electrophoresis, 2010. **31**(18): p. 3074-3082.

185. Truckenmuller, R., et al., *Flexible fluidic microchips based on thermoformed and locally modified thin polymer films.* Lab on a Chip, 2008. **8**(9): p. 1570-1579.

186. Focke, M., et al., *Microstructuring of polymer films for sensitive genotyping by real-time PCR on a centrifugal microfluidic platform.* Lab on a Chip, 2010. **10**(19): p. 2519-2526.

187. Heilig, M., et al., *Microthermoforming of nanostructured polymer films: a new bonding method for the integration of nanostructures in 3-dimensional cavities.* Microsystem Technologies-Micro-and Nanosystems-Information Storage and Processing Systems, 2010. **16**(7): p. 1221-1231.

188. Heilig, M., et al., *Technology of microthermoforming of complex three-dimensional parts with multiscale features.* Microsystem Technologies-Micro-and Nanosystems-Information Storage and Processing Systems, 2011. **17**(4): p. 593-600.

189. Truckenmuller, R., et al., *Thermoforming of Film-Based Biomedical Microdevices.* Advanced Materials, 2011. **23**(11): p. 1311-1329.

190. Giselbrecht, S., et al., *3D tissue culture substrates produced by microthermoforming of pre-processed polymer films.* Biomedical Microdevices, 2006. **8**(3): p. 191-199.

191. Fu, G., et al., *Effects of processing parameters on the micro-channels replication in microfluidic devices fabricated by micro injection molding.* Microsystem Technologies-Micro-and Nanosystems-Information Storage and Processing Systems, 2011. **17**(12): p. 1791-1798.

192. Giboz, J., T. Copponnex, and P. Mele, *Microinjection molding of thermoplastic polymers: a review.* Journal of Micromechanics and Microengineering, 2007. **17**(6): p. R96-R109.

193. Giboz, J., T. Copponnex, and P. Mele, *Microinjection molding of thermoplastic polymers: morphological comparison with conventional injection molding.* Journal of Micromechanics and Microengineering, 2009. **19**(2).

194. Giboz, J., et al., *On the Origin of the "Core-Free" Morphology in Microinjection-Molded HDPE.* Journal of Polymer Science Part B-Polymer Physics, 2011. **49**(20): p. 1470-1478.

195. Tosello, G., F. Marinello, and H.N. Hansen, *Characterisation and analysis of microchannels and submicrometre surface roughness of injection moulded*

microfluidic systems using optical metrology. Plastics Rubber and Composites, 2012. **41**(1): p. 29-39.

196. Danz, N., et al., *Surface plasmon resonance platform technology for multi-parameter analyses on polymer chips.* Engineering in Life Sciences, 2011. **11**(6): p. 566-572.

197. Senousy, Y.M. and C.K. Harnett, *Fast three dimensional ac electro-osmotic pumps with nonphotolithographic electrode patterning.* Biomicrofluidics, 2010. **4**(3).

198. Lam, M.H.C., et al., *Sub-nanoliter nuclear magnetic resonance coils fabricated with multilayer soft lithography.* Journal of Micromechanics and Microengineering, 2009. **19**(9).

199. Yoon, T.H., et al., *Fabrication of SiC-based ceramic microstructures from preceramic polymers with sacrificial templates and lithographic techniques - A review.* Journal of the Ceramic Society of Japan, 2006. **114**(1330): p. 473-479.

200. Becker, H. and C. Gartner, *Polymer microfabrication methods for microfluidic analytical applications.* Electrophoresis, 2000. **21**(1): p. 12-26.

201. Lee, S., H.S. Kang, and J.K. Park, *Directional Photofluidization Lithography: Micro/Nanostructural Evolution by Photofluidic Motions of Azobenzene Materials.* Advanced Materials, 2012. **24**(16): p. 2069-2103.

202. Zorlutuna, P., et al., *Microfabricated Biomaterials for Engineering 3D Tissues.* Advanced Materials, 2012. **24**(14): p. 1782-1804.

203. Valiokas, R., *Nanobiochips.* Cellular and Molecular Life Sciences, 2012. **69**(3): p. 347-356.

204. Xue, L.J., J.L. Zhang, and Y.C. Han, *Phase separation induced ordered patterns in thin polymer blend films.* Progress in Polymer Science, 2012. **37**(4): p. 564-594.

205. Huh, D., G.A. Hamilton, and D.E. Ingber, *From 3D cell culture to organs-on-chips.* Trends in Cell Biology, 2011. **21**(12): p. 745-754.

206. Pan, J., et al., *Microfabricated particulate drug-delivery systems.* Biotechnology Journal, 2011. **6**(12): p. 1477-1487.

207. Hahm, J.I., *Polymeric Surface-Mediated, High-Density Nano-Assembly of Functional Protein Arrays.* Journal of Biomedical Nanotechnology, 2011. **7**(6): p. 731-742.

208. Ng, J.M.K., et al., *Components for integrated poly(dimethylsiloxane) microfluidic systems.* Electrophoresis, 2002. **23**(20): p. 3461-3473.

209. Grover, W.H., et al., *Monolithic membrane valves and diaphragm pumps for practical large-scale integration into glass microfluidic devices.* Sensors and Actuators B-Chemical, 2003. **89**(3): p. 315-323.

210. Eddings, M.A. and B.K. Gale, *A PDMS-based gas permeation pump for on-chip fluid handling in microfluidic devices.* Journal of Micromechanics and Microengineering, 2006. **16**(11): p. 2396-2402.

211. Johnson, M., et al., *Bubble inclusion and removal using PDMS membrane-based gas permeation for applications in pumping, valving and mixing in microfluidic devices.* Journal of Micromechanics and Microengineering, 2009. **19**(9).

212. Zhou, J.W., A.V. Ellis, and N.H. Voelcker, *Recent developments in PDMS surface modification for microfluidic devices.* Electrophoresis, 2010. **31**(1): p. 2-16.

213. van Poll, M.L., et al., *A self-assembly approach to chemical micropatterning of poly(dimethylsiloxane).* Angewandte Chemie-International Edition, 2007. **46**(35): p. 6634-6637.

214. Mata, A., A.J. Fleischman, and S. Roy, *Characterization of polydimethylsiloxane (PDMS) properties for biomedical micro/nanosystems.* Biomedical Microdevices, 2005. **7**(4): p. 281-293.

215. Patrito, N., et al., *Spatially controlled cell adhesion via micropatterned surface modification of poly(dimethylsiloxane).* Langmuir, 2007. **23**(2): p. 715-719.

216. Hu, S.W., et al., *Tailoring the surface properties of poly(dimethylsiloxane) microfluidic devices.* Langmuir, 2004. **20**(13): p. 5569-5574.

217. Lahann, J., et al., *Reactive polymer coatings: A first step toward surface engineering of microfluidic devices.* Analytical Chemistry, 2003. **75**(9): p. 2117-2122.

218. Phillips, K.S. and Q. Cheng, *Microfluidic immunoassay for bacterial toxins with supported phospholipid bilayer membranes on poly(dimethylsiloxane).* Analytical Chemistry, 2005. **77**(1): p. 327-334.

219. Rolland, J.P., et al., *Solvent-resistant photocurable "liquid teflon" for microfluidic device fabrication.* Journal of the American Chemical Society, 2004. **126**(8): p. 2322-2323.

220. Bodas, D. and C. Khan-Malek, *Formation of more stable hydrophilic surfaces of PDMS by plasma and chemical treatments.* Microelectronic Engineering, 2006. **83**(4-9): p. 1277-1279.

221. Bodas, D., J.Y. Rauch, and C. Khan-Malek, *Creation of a Stable Hydrophilic Poly(dimethyl siloxane) Surface by the Plasma-Induced Cross linking of Monomers.* Journal of Applied Polymer Science, 2011. **120**(3): p. 1426-1430.

222. Bodas, D.S. and C. Khan-Malek, *Fabrication of long-term hydrophilic surfaces of poly(dimethyl siloxane) using 2-hydroxy ethyl methacrylate.* Sensors and Actuators B-Chemical, 2007. **120**(2): p. 719-723.

223. Gao, C.Y., et al., *L-3,4-dihydroxyphenylalanine-collagen modified PDMS surface for controlled cell culture.* Journal of Materials Chemistry, 2012. **22**(21): p. 10763-10770.

224. Lee, D. and S. Yang, *Surface modification of PDMS by atmospheric-pressure plasma-enhanced chemical vapor deposition and analysis of long-lasting surface hydrophilicity.* Sensors and Actuators B-Chemical, 2012. **162**(1): p. 425-434.

225. Li, J.Y., M. Wang, and Y.B. Shen, *Chemical modification on top of nanotopography to enhance surface properties of PDMS.* Surface & Coatings Technology, 2012. **206**(8-9): p. 2161-2167.

226. Wu, Z.Q., et al., *Poly(N-vinylpyrrolidone)-modified poly(dimethylsiloxane) elastomers as anti-biofouling materials.* Colloids and Surfaces B-Biointerfaces, 2012. **96**: p. 37-43.

227. Yao, M.J. and J. Fang, *Hydrophilic PEO-PDMS for microfluidic applications.* Journal of Micromechanics and Microengineering, 2012. **22**(2).

228. Brigo, L., et al., *An optical sensor for pH supported onto tentagel resin beads.* Sensors and Actuators B-Chemical, 2008. **130**(1): p. 477-482.

229. Cygan, Z.T., et al., *Microfluidic platform for the generation of organic-phase microreactors.* Langmuir, 2005. **21**(8): p. 3629-3634.

230. Natali, M., et al., *Rapid prototyping of multilayer thiolene microfluidic chips by photopolymerization and transfer lamination.* Lab on a Chip, 2008. **8**(3): p. 492-494.

231. Cabral, J.T., et al., *Frontal Photopolymerization for Microfluidic Applications.* Langmuir, 2004. **20**: p. 10020-10029.

232. Good, B.T., C.N. Bowman, and R.H. Davis, *An effervescent reaction micropump for portable microfluidic systems.* Lab on a Chip, 2006. **6**(5): p. 659-666.

233. Ashley, J.F., et al., *Soft-lithography fabrication of microfluidic features using thiol-ene formulations.* Lab on a Chip, 2011. **11**(16): p. 2772-2778.

234. Dickey, M.D., et al., *Photocurable pillar arrays formed via electrohydrodynamic instabilities.* Chemistry of Materials, 2006. **18**(8): p. 2043-2049.

235. Crowe, J.A. and J. Genzer, *Creating responsive surfaces with tailored wettability switching kinetics and reconstruction reversibility.* Journal of the American Chemical Society, 2005. **127**(50): p. 17610-17611.

236. Pojman, J.A., et al., *Frontal Polymerization with Thiol-Ene Systems.* Macromolecules, 2004. **37**: p. 691-693.

237. Bounds, C.O., et al., *Preparation and Application of Microparticles Prepared Via the Primary Amine-catalyzed Michael Addition of a Trithiol to a Triacrylate.* J. Polym. Sci. Part A: Polym. Chem., 2012. **50**: p. 409–422.

238. Shin, J., S. Nazarenko, and C.E. Hoyle, *Effects of Chemical Modification of Thiol-Ene Networks on Enthalpy Relaxation.* Macromolecules, 2009. **42**(17): p. 6549-6557.

239. Carioscia, J.A., et al., *Thiol-ene oligomers as dental restorative materials.* Dental Materials, 2005. **21**(12): p. 1137-1143.

240. Cramer, N.B., et al., *Thiol-ene photopolymerization mechanism and rate limiting step changes for various vinyl functional group chemistries.* Macromolecules, 2003. **36**(21): p. 7964-7969.

241. Biffinger, J.C., H.W. Kim, and S.G. DiMagno, *The polar hydrophobicity of fluorinated compounds.* Chembiochem, 2004. **5**(5): p. 622-627.

242. Luo, Y., et al., *Towards single-cell analysis for pharmacokinetics.* Bioanalysis, 2012. **4**(4): p. 453-463.

243. Jiang, L.G., et al., *Visualizing millisecond chaotic mixing dynamics in microdroplets: A direct comparison of experiment and simulation.* Biomicrofluidics, 2012. **6**(1).

244. Foley, C.P., et al., *Real-Time Imaging of Perivascular Transport of Nanoparticles During Convection-Enhanced Delivery in the Rat Cortex.* Annals of Biomedical Engineering, 2012. **40**(2): p. 292-303.

245. Burgess, J.G., *New and emerging analytical techniques for marine biotechnology.* Current Opinion in Biotechnology, 2012. **23**(1): p. 29-33.

246. Batabyal, S., et al., *An improved microfluidics approach for monitoring real-time interaction profiles of ultrafast molecular recognition.* Review of Scientific Instruments, 2012. **83**(4).

247. Livaniou, E., et al., *Analytical techniques for determining biotin.* Journal of Chromatography A, 2000. **881**(1-2): p. 331-343.

248. Green, N.M., *AVIDIN AND STREPTAVIDIN.* Methods in Enzymology, 1990. **184**: p. 51-67.

249. Wilchek, M., E.A. Bayer, and O. Livnah, *Essentials of biorecognition: The (strept)avidin-biotin system as a model for protein-protein and protein-ligand interaction.* Immunology Letters, 2006. **103**(1): p. 27-32.

Appendix. Permission for Chapter 2

JOHN WILEY AND SONS LICENSE
TERMS AND CONDITIONS

Aug 09, 2012

This is a License Agreement between Christopher O Bounds ("You") and John Wiley and Sons ("John Wiley and Sons") provided by Copyright Clearance Center ("CCC"). The license consists of your order details, the terms and conditions provided by John Wiley and Sons, and the payment terms and conditions.

All payments must be made in full to CCC. For payment instructions, please see information listed at the bottom of this form.

License Number	2965010272037
License date	Aug 09, 2012
Licensed content publisher	John Wiley and Sons
Licensed content publication	Journal of Polymer Science Part A: Polymer Chemistry
Licensed content title	Preparation and application of microparticles prepared via the primary amine-catalyzed michael addition of a trithiol to a triacrylate
Licensed content author	Christopher O. Bounds,Ronald Goetter,John A. Pojman,Max Vandersall
Licensed content date	Oct 14, 2011
Start page	409
End page	422
Type of use	Dissertation/Thesis
Requestor type	Author of this Wiley article
Format	Print and electronic
Portion	Full article
Will you be translating?	No
Order reference number	
Total	0.00 USD

Terms and Conditions

TERMS AND CONDITIONS

This copyrighted material is owned by or exclusively licensed to John Wiley & Sons, Inc. or one of its group companies (each a "Wiley Company") or a society for whom a Wiley Company has exclusive publishing rights in relation to a particular journal (collectively WILEY"). By clicking "accept" in connection with completing this licensing transaction, you agree that the following terms and conditions apply to this transaction (along with the billing and payment terms and conditions established by the Copyright Clearance Center Inc., ("CCC's Billing and Payment terms

and conditions"), at the time that you opened your Rightslink account (these are available at any time at http://myaccount.copyright.com)

Terms and Conditions

1. The materials you have requested permission to reproduce (the "Materials") are protected by copyright.

2. You are hereby granted a personal, non-exclusive, non-sublicensable, non-transferable, worldwide, limited license to reproduce the Materials for the purpose specified in the licensing process. This license is for a one-time use only with a maximum distribution equal to the number that you identified in the licensing process. Any form of republication granted by this licence must be completed within two years of the date of the grant of this licence (although copies prepared before may be distributed thereafter). The Materials shall not be used in any other manner or for any other purpose. Permission is granted subject to an appropriate acknowledgement given to the author, title of the material/book/journal and the publisher. You shall also duplicate the copyright notice that appears in the Wiley publication in your use of the Material. Permission is also granted on the understanding that nowhere in the text is a previously published source acknowledged for all or part of this Material. Any third party material is expressly excluded from this permission.

3. With respect to the Materials, all rights are reserved. Except as expressly granted by the terms of the license, no part of the Materials may be copied, modified, adapted (except for minor reformatting required by the new Publication), translated, reproduced, transferred or distributed, in any form or by any means, and no derivative works may be made based on the Materials without the prior permission of the respective copyright owner. You may not alter, remove or suppress in any manner any copyright, trademark or other notices displayed by the Materials. You may not license, rent, sell, loan, lease, pledge, offer as security, transfer or assign the Materials, or any of the rights granted to you hereunder to any other person.

4. The Materials and all of the intellectual property rights therein shall at all times remain the exclusive property of John Wiley & Sons Inc or one of its related companies (WILEY) or their respective licensors, and your interest therein is only that of having possession of and the right to reproduce the Materials pursuant to Section 2 herein during the continuance of this Agreement. You agree that you own no right, title or interest in or to the Materials or any of the intellectual property rights therein. You shall have no rights hereunder other than the license as provided for above in Section 2. No right, license or interest to any trademark, trade name, service mark or other branding ("Marks") of WILEY or its licensors is granted hereunder, and you agree that you shall not assert any such right, license or interest with respect thereto.

5. NEITHER WILEY NOR ITS LICENSORS MAKES ANY WARRANTY OR REPRESENTATION OF ANY KIND TO YOU OR ANY THIRD PARTY, EXPRESS, IMPLIED OR STATUTORY, WITH RESPECT TO THE MATERIALS OR THE ACCURACY OF ANY INFORMATION CONTAINED IN THE MATERIALS, INCLUDING, WITHOUT LIMITATION, ANY IMPLIED WARRANTY OF MERCHANTABILITY, ACCURACY, SATISFACTORY QUALITY, FITNESS FOR A PARTICULAR PURPOSE, USABILITY, INTEGRATION OR NON-INFRINGEMENT AND ALL SUCH WARRANTIES ARE HEREBY EXCLUDED BY WILEY AND ITS LICENSORS AND WAIVED BY YOU.

6. WILEY shall have the right to terminate this Agreement immediately upon breach of this Agreement by you.

7. You shall indemnify, defend and hold harmless WILEY, its Licensors and their respective directors, officers, agents and employees, from and against any actual or threatened claims, demands, causes of action or proceedings arising from any breach of this Agreement by you.

8. IN NO EVENT SHALL WILEY OR ITS LICENSORS BE LIABLE TO YOU OR ANY OTHER PARTY OR ANY OTHER PERSON OR ENTITY FOR ANY SPECIAL, CONSEQUENTIAL, INCIDENTAL, INDIRECT, EXEMPLARY OR PUNITIVE DAMAGES, HOWEVER CAUSED, ARISING OUT OF OR IN CONNECTION WITH THE DOWNLOADING, PROVISIONING, VIEWING OR USE OF THE MATERIALS REGARDLESS OF THE FORM OF ACTION, WHETHER FOR BREACH OF CONTRACT, BREACH OF WARRANTY, TORT, NEGLIGENCE, INFRINGEMENT OR OTHERWISE (INCLUDING, WITHOUT LIMITATION, DAMAGES BASED ON LOSS OF PROFITS, DATA, FILES, USE, BUSINESS OPPORTUNITY OR CLAIMS OF THIRD PARTIES), AND WHETHER OR NOT THE PARTY HAS BEEN ADVISED OF THE POSSIBILITY OF SUCH DAMAGES. THIS LIMITATION SHALL APPLY NOTWITHSTANDING ANY FAILURE OF ESSENTIAL PURPOSE OF ANY LIMITED REMEDY PROVIDED HEREIN.

9. Should any provision of this Agreement be held by a court of competent jurisdiction to be illegal, invalid, or unenforceable, that provision shall be deemed amended to achieve as nearly as possible the same economic effect as the original provision, and the legality, validity and enforceability of the remaining provisions of this Agreement shall not be affected or impaired thereby.

10. The failure of either party to enforce any term or condition of this Agreement shall not constitute a waiver of either party's right to enforce each and every term and condition of this Agreement. No breach under this agreement shall be deemed waived or excused by either party unless such waiver or consent is in writing signed by the party granting such waiver or consent. The waiver by or consent of a party to a breach of any provision of this Agreement shall not operate or be construed as a waiver of or consent to any other or subsequent breach by such other party.

11. This Agreement may not be assigned (including by operation of law or otherwise) by you without WILEY's prior written consent.

12. Any fee required for this permission shall be non-refundable after thirty (30) days from receipt.

13. These terms and conditions together with CCC's Billing and Payment terms and conditions (which are incorporated herein) form the entire agreement between you and WILEY concerning this licensing transaction and (in the absence of fraud) supersedes all prior agreements and representations of the parties, oral or written. This Agreement may not be amended except in writing signed by both parties. This Agreement shall be binding upon and inure to the benefit of the parties' successors, legal representatives, and authorized assigns.

14. In the event of any conflict between your obligations established by these terms and conditions and those established by CCC's Billing and Payment terms and conditions, these terms and conditions shall prevail.

15. WILEY expressly reserves all rights not specifically granted in the combination of (i) the license details provided by you and accepted in the course of this licensing transaction, (ii) these terms and conditions and (iii) CCC's Billing and Payment terms and conditions.

16. This Agreement will be void if the Type of Use, Format, Circulation, or Requestor Type was misrepresented during the licensing process.

17. This Agreement shall be governed by and construed in accordance with the laws of the State of New York, USA, without regards to such state's conflict of law rules. Any legal action, suit or proceeding arising out of or relating to these Terms and Conditions or the breach thereof shall be instituted in a court of competent jurisdiction in New York County in the State of New York in the United States of America and each party hereby consents and submits to the personal jurisdiction

• Copying, downloading or posting by a site or service that incorporates advertising with such content;
• The inclusion or incorporation of article content in other works or services (other than normal quotations with an appropriate citation) that is then available for sale or licensing, for a fee (for example, a compilation produced for marketing purposes, inclusion in a sales pack)
• Use of article content (other than normal quotations with appropriate citation) by for-profit organisations for promotional purposes
• Linking to article content in e-mails redistributed for promotional, marketing or educational purposes;
• Use for the purposes of monetary reward by means of sale, resale, licence, loan, transfer or other form of commercial exploitation such as marketing products
• Print reprints of Wiley Open Access articles can be purchased from: corporatesales@wiley.com

Other Terms and Conditions:

BY CLICKING ON THE "I AGREE..." BOX, YOU ACKNOWLEDGE THAT YOU HAVE READ AND FULLY UNDERSTAND EACH OF THE SECTIONS OF AND PROVISIONS SET FORTH IN THIS AGREEMENT AND THAT YOU ARE IN AGREEMENT WITH AND ARE WILLING TO ACCEPT ALL OF YOUR OBLIGATIONS AS SET FORTH IN THIS AGREEMENT.

v1.7

If you would like to pay for this license now, please remit this license along with your payment made payable to "COPYRIGHT CLEARANCE CENTER" otherwise you will be invoiced within 48 hours of the license date. Payment should be in the form of a check or money order referencing your account number and this invoice number RLNK500835920.
Once you receive your invoice for this order, you may pay your invoice by credit card. Please follow instructions provided at that time.

Make Payment To:
Copyright Clearance Center
Dept 001
P.O. Box 843006
Boston, MA 02284-3006

For suggestions or comments regarding this order, contact RightsLink Customer Support: customercare@copyright.com or +1-877-622-5543 (toll free in the US) or +1-978-646-2777.

Gratis licenses (referencing $0 in the Total field) are free. Please retain this printable license for your reference. No payment is required.

of such court, waives any objection to venue in such court and consents to service of process by registered or certified mail, return receipt requested, at the last known address of such party.

Wiley Open Access Terms and Conditions

All research articles published in Wiley Open Access journals are fully open access: immediately freely available to read, download and share. Articles are published under the terms of the Creative Commons Attribution Non Commercial License, which permits use, distribution and reproduction in any medium, provided the original work is properly cited and is not used for commercial purposes. The license is subject to the Wiley Open Access terms and conditions: Wiley Open Access articles are protected by copyright and are posted to repositories and websites in accordance with the terms of the Creative Commons Attribution Non Commercial License. At the time of deposit, Wiley Open Access articles include all changes made during peer review, copyediting, and publishing. Repositories and websites that host the article are responsible for incorporating any publisher-supplied amendments or retractions issued subsequently. Wiley Open Access articles are also available without charge on Wiley's publishing platform, **Wiley Online Library** or any successor sites.

Use by non-commercial users

For non-commercial and non-promotional purposes individual users may access, download, copy, display and redistribute to colleagues Wiley Open Access articles, as well as adapt, translate, text- and data-mine the content subject to the following conditions:

- The authors' moral rights are not compromised. These rights include the right of "paternity" (also known as "attribution" - the right for the author to be identified as such) and "integrity" (the right for the author not to have the work altered in such a way that the author's reputation or integrity may be impugned).
- Where content in the article is identified as belonging to a third party, it is the obligation of the user to ensure that any reuse complies with the copyright policies of the owner of that content.
- If article content is copied, downloaded or otherwise reused for non-commercial research and education purposes, a link to the appropriate bibliographic citation (authors, journal, article title, volume, issue, page numbers, DOI and the link to the definitive published version on Wiley Online Library) should be maintained. Copyright notices and disclaimers must not be deleted.
- Any translations, for which a prior translation agreement with Wiley has not been agreed, must prominently display the statement: "This is an unofficial translation of an article that appeared in a Wiley publication. The publisher has not endorsed this translation."

Use by commercial "for-profit" organisations

Use of Wiley Open Access articles for commercial, promotional, or marketing purposes requires further explicit permission from Wiley and will be subject to a fee. Commercial purposes include:

- Copying or downloading of articles, or linking to such articles for further redistribution, sale or licensing:

VITA

Christopher O'neil Bounds was born in McComb, Mississippi in April of 1984. Shortly thereafter, his family relocated to Newton, Mississippi, and he was raised in this small rural town with a total population of less than 4000 citizens. Chris attended Newton County academy for 14 years from age 4 until age 18. He graduated from Newton County Academy in 2002 at the top of this class and was named Valedictorian. Chris attended East Central Community College from 2002-2004, earning an Associate of Science degree. He then moved to Hattiesburg, Mississippi and attended The University of Southern Mississippi, earning a Bachelor of Science in Chemistry with an emphasis on Biochemistry in May 2007. Prior to- and after graduation, he worked as a research associate and lab manager at The University of Southern Mississippi. In the fall of 2008, Chris started graduate work toward his Doctorate of Philosophy in Chemistry, specializing in Macromolecular Chemistry at Louisiana State University and will complete his degree in 2012.